Generation and Characterization of BACHD Rats expressing full-length human mutant Huntingtin

Dissertation

zur Erlangung des Grades eines
Doktors der Naturwissenschaften

der Mathematisch-Naturwissenschaftlichen Fakultät
und
der Medizinischen Fakultät
der Eberhard-Karls-Universität Tübingen

vorgelegt

von

Libo Yu-Täger

aus Heilongjiang, China

Januar 2013

Tag der mündlichen Prüfung: 03.06.2013

Dekan der Math.-Nat. Fakultät:	Prof. Dr. W. Rosenstiel
Dekan der Medizinischen Fakultät:	Prof. Dr. I. B. Autenrieth
1. Berichterstatter:	Prof. Dr. Olaf Riess
2. Berichterstatter:	Prof. Dr. Mathias Jucker
Prüfungskommission:	Prof. Dr. Olaf Riess
	Prof. Dr. Mathias Jucker
	Prof. Dr. Ludger Schöls
	Prof. Dr. Robert Feil

I hereby declare that I have produced the work entitled: "*Generation and Characterization of BACHD Rats expressing full-length human mutant Huntingtin*", submitted for the award of a doctorate, on my own (without external help), have used only the sources and aids indicated and have marked passages included from other works, whether verbatim or in content, as such. I swear upon oath that these statements are true and that I have not concealed anything. I am aware that making a false declaration under oath is punishable by a term of imprisonment of up to three years or by a fine.

Tübingen, _____ _____

Date Signature

DEDICATION

To my grandfather who taught me by personal example the value of honesty and altruism in life

Publication and posters from work in this thesis

Publication

Yu-Taeger L, Petrasch-Parwez E, Osmand AP, Redensek A, Metzger S, Clemens LE, Park L, Howland D, Calaminus C, Gu X, Pichler B, Yang XW, Riess O, Nguyen HP (2012) **A Novel BACHD Transgenic Rat Exhibits Characteristic Neuropathological Features of Huntington Disease.** J Neurosci 32:15426-38

Posters

Libo Yu, Silke Metzger, Alexandra Schwienbacher, Claudia Bauer, Thomas Ott, Xiaofeng Gu, Michelle Gray, William Yang, Olaf Riess and Huu Phuc Nguyen
Generation and expression characterization of BAC-HD transgenic rats with full-length mutant huntingtin
European Huntinton Disease Network 2008, Lisbon, September 2008

Libo Yu, Silke Metzger, Jasmin Ehrismann, Thomas Ott, Xiaofeng Gu, Michelle Gray, William Yang, Andeas Weiss, Paolo Paganetti, Olaf Riess and Huu Phuc Nguyen
Generation and characterization of BAC-HD transgenic rats with full-length mutant human huntingtin
Wold congress on Huntington Disease 2009, Vancouver, September 2009

Libo Yu, Silke Metzger, Laura Clemens, Jasmin Ehrismann, Thomas Ott, Xiaofeng Gu, Michelle Gray, William Yang, Alexander P. Osmand, Olaf Riess and Huu Phuc Nguyen
Accumulation and Aggregation of human mutant huntingtin and neuron atrophy in BAC-HD transgenic rat
European Huntington Disease Network 2010, Prague, September 2010

Libo Yu-Taeger, Elisabeth Petrasch-Parwez, Alexander P. Osmand, Adriana Redensek, Silker Metzger, Laura Clemens, Larry Park, David Howland, Carsten Calaminus, XiaoFeng Gu, Bernd Pichler, X. William Yang, Olaf Riess, Huu Phuc Nguyen
A Novel BACHD Transgenic Rat Exhibits Characteristic Neuropathological Features of Huntington Disease
European Huntington Disease Network 2012, Stockholm, September 2012

Acknowledgements

The present Ph.D thesis was financially supported by the CHDI Foundation.

I would like to thank my supervisors Prof. Olaf Riess and Dr. Huu Phuc Nguyen, for providing an excellent research environment and project, for giving me the freedom to independently design and carry out the experiments and for their constructive criticism and advice to my thesis. I would like to thank especially Dr. Huu Phuc Nguyen for detailed correction of my manuscripts including the written language. I would also like to thank the other advisory board members of my thesis, Prof. Ludger Schöls and Prof. Thomas Gasser for their advice and guidance along the way. I am grateful to Dr. Alexander P. Osmand for the technical supervision on immunohistochemical staining methods. I thank Dr. Elisabeth Petrasch-Parwez for the many discussions on neuron pathology.

I would like to thank the people who helped me during my thesis. I would like to thank the brilliant research assistant Adriana Redensek for taking care of a lot of experiments and organizational work. I would also like to thank the two super technicians Patrycja Bambynek-Dziuk and Celina Tomczak for their assistance with consistent quality, and especially Patrycja Bambynek-Dziuk for leading the other technicians. I would like to thank Dr. Jasmin Ehrismann for performing half of the PhenoMaster experiments. I would also like to thank my master student Erik Jassion for his excellent work with cognitive behaviour tests. I am grateful to Laura Emily Clemens for discussion on all behavioural tests and Esteban Portal for his technical support on data analysis for the PhenoMaster experiments. I would like to thank Dr. Silker Metzger for purifying the BACHD construct before the generation of the BACHD rat model. I would also like to thank Dr. Karina Haebig, Dr. Thorsten Schmidt, Dr. Yu-Chun Tsai, Dr. Jeanette Hübener and Dr. Silker Nuber for teaching me general lab techniques at the beginning of my thesis. I thank Nicolas Casadei for discussion and IT support. I am also grateful to everybody else in the department of Medical Genetics, University of Tuebingen, for the great team work and for making my time in the lab more pleasant.

Finally, I wish to thank my parents, my brothers and their families for the understanding and encouragement along the way. I wish also to thank all of my friends for the joy they gave me during my leisure time.

Special thanks I want to give Joachim, my husband. He gave me not only love, happiness, understanding and encouragement, but also provided me constructive

criticism, great ideas, computer support and was correcting my language throughout the whole thesis.

Abstract

Huntington disease (HD) is an inherited progressive neurodegenerative disorder, characterized by motor, cognitive and psychiatric deficits as well as neurodegeneration and brain atrophy beginning in the striatum and the cortex and extending to other subcortical brain regions. A number of mouse models expressing full-length mutant htt (mhtt) or truncated mhtt fragments were developed for therapeutic studies and to better understand the pathogenesis of HD. However, mouse models are limited for studying certain functional and behavioural aspects of the disease, which are better mirrored in rats. Therefore, rat models have made substantial contributions to our understanding of biological function and behaviour.

The major objectives of this thesis were:

- To generate and characterize two HD transgenic rat lines that express fl-mhtt (BACHD rats) with different protein expression levels.
- To determine whether BACHD rats recapitulate symptoms and pathological changes as seen in HD patients.
- To develop a standard protocol for subsequent preclinical therapy trials in these rats.
- To potentially uncover yet unknown neuropathological abnormalities in HD using these rat models.
- To provide further disease-relevant insights allowing new strategies for therapeutical approaches.

The findings demonstrate that BACHD transgenic rats display a robust, early-onset and progressive HD-like phenotype including motor deficits, impaired cognitive function and anxiety-related symptoms as well as metabolic changes. Neuropathologically, the distribution of neuropil aggregates and nuclear accumulations of N-terminal mutant huntingtin in BACHD rats is similar to that seen in HD patients. Neuropil aggregates in the sensorimotor circuitry may be associated with motor dysfunction and aggregates in the limbic-based circuitries could be related to anxiety changes and thus render this model suitable for the ongoing research in how these circuitries are affected in HD. In addition, dark neurons and dark axons accompanied by a brain volume reduction in advanced ages reflecting neuronal degeneration were observed in BACHD rats. BDNF transcription was down-regulated in our BACHD rats, rendering them valuable for understanding mhtt- associated transcriptional dysregulations as well as BDNF- mediated treatment of HD.

An imbalance in the striosome and matrix compartments in early stages of the disease, as well as a reduction of some pre-synaptic proteins and a relative increase in the post-synaptic marker PSD-95 in BACHD rats provide new insights into disease pathogenesis and may give a new approach to the treatment of HD.

Overall, the data in this thesis demonstrate robust neuropathological changes in addition to the early HD-like phenotype in BACHD rats. Therefore BACHD rats may be a valuable model for further understanding the disease mechanism and for preclinical pharmacological studies.

Table of contents

List of figures

List of tables

List of abbreviations

8OH2´dG	8-hydroxy-2'deoxy-guanosine
24-OHC	24-hydroxycholesterol
Ac	anterior commissure
Acb	nucleus accumbens
AbcC	nucleus accumbens core
ADP	adenosine diphosphate
Amg	amygdala
ANOVA	analysis of variance
APP	amyloid precursor protein
ATP	adenosine triphosphate
BAC	bacterial artificial chromosome
BBB	brain-blood barrier
BDNF	Brain-derived neurotrophic factor
BNST	stria terminalis
BP	binding potential
BSTpi	posterointermediate bed nucleus of stria terminals
BT	biotinylated tyramine
CBP	CREB binding protein
CMC	cingulate motor cortex
CPu	caudate putamen
Crb	cerebellum
CSF	cerebrospinal fluid
Ctx	cortex
DAB	3,3'-diaminobenzidine
DAPI	4' 6-diamidino-2-phenylindole
DARPP-32	Dopamine- and cyclic-AMP-regulated phosphoprotein of molecular weight 32,000
DA	dark degenerated neurons
De	neuronal dendrites
DG	dentate gyrus
DNA	Deoxyribonucleic *Acid*
DRP1	dynamin-related protein-1
DT	dark terminals
ELISA	Enzyme-linked immunosorbent assay
ER	endoplasmic reticulum
FDG	Fluor-18-Deoxyglucose: glucose metabolism
FeS	iron-sulphur
GAPHD	glyceraldehydes-3-phosphate dehydrogenase
GP	globus pallidus
GPe	gloubus pallidus external segments
GPi	gloubus pallidus internal segments
GTP	Guanosintriphosphat
HAP1	Huntingtin-associated protein 1

Hc	hippocampus
HD	Huntington disease
HIP1	Huntingtin interacting protein 1
HIPP1	HIP1 protein interactor
HMG-CoAR	3-hydroxy-3-methyl-glutaryl-CoA reductase
HTT	gene encoding htt
htt	huntingtin
HRP	*Horseradish peroxidase*
IGF-1	Insulin-like *growth factor 1*
IF	immunoflorescence
IHC	immunohistochemistry
IHD	infantile HD
JHD	juvenile HD
InsP3R1	type 1 inositol (1,4,5)-trisphosphate receptor
i.p.	Intraperitoneal injection
kb	kilobase
kDa	kilodalton
KI	knock in
KO	knock out
LS	lateral septum
LTP	long-term potentiation
M1	primary motor cortex
MBP	Myelin Basic Protein
MEF	mouse embryonic fibroblast
MF	mossy fiber
Mhtt	mutant huntingtin
MRI	*Magnetic resonance imaging*
MRS	*magnetic resonance spectroscopy*
MSNs	medium spiny neurons
NIIs	nuclear inclusions
NMDA	N-methyl-D-aspartate
NMDAR2	NMDA type 2 receptor
NMDAR2B	NMDA type 2B receptor
NES	nuclear export signal
NLS	nuclear localization signal
NRSF	neuronal restrictive silencing factor
PARP	poly (ADP-ribose) polymerase
PCA	principal component analysis
PCR	*Polymerase Chain Reaction*
PD	Parkinson disease
PDe	pallidal dendrites
PET	positron emission tomography
PGC-1α	PPARγ coactivator-1α
PI3K	phosphoinositide 3-kinase
PMC	premotor cortex

PPARγ	proliferator activated receptor-γ
PSD-95	postsynaptic density protein 95
Q	glutamine
RNA	Ribonucleic *acid*
PARP	anti-poly (ADP-ribose) polymerase
ROI	region of interest
RH	humidity
RER	respiratory exchange ratio
REST	repressor element-1 transcription factor
SCA	spinocerebellar Ataxia
SEM	standard error of the mean
SLu	stratum lucidum
SMA	supplementary motor area
SNr	substantia nigra pars reticulate
SNc	substantia nigra pars compacta
SOD	superoxide dismutase
SP1	specific protein 1
SPRD	Sprague-Dawley
STN	subthalamic nucleus
SUV	standard uptake volume
TBP	TATA-binding protein
TAFII	TBP-associated factor
TG5	transgenic line 5
TG9	transgenic line 9
TUNEL	terminal deoxynucleotidyl transferase-mediated dUTP nick end-labeling
UPS	ubiquitin-proteasome system
WB	western blot
WT	wild type
YAC	yeast artificial chromosome

1. Introduction

Huntington disease (HD) is an autosomal dominant inherited, progressive neurodegenerative disorder caused by an expansion of CAG triplet repeats in the gene encoding the huntingtin (htt) protein (Harper, 1991). HD commonly manifests in adulthood with usually an onset between ages of 35 and 55 years (Huntington 1872).

Despite of the world wide distribution, the prevalence of HD differs geographically accounting for 5 per 100 000 in the western population including Europe and America and 0.1-0.5 per 100 000 in Asian populations including China and Japan (al-Jader *et al.*, 1992; Leung *et al.*, 1992; Chang *et al.*, 1994; Al-Jader *et al.*, 2001).

1.1 Genetic aspects of HD

1.1.1 Inverse correlation between expanded CAG repeat size and age at onset

HD is an autosomal dominant inherited disease. Expansions of the CAG repeat (>38) in exon 1 of the gene encoding htt (*HTT*) were first discovered in 1993 and represent to date the sole genetic cause of the disease (The Huntington's Disease Collaborative Research Group, 1993). The *HTT* gene comprises of 67 exons and is located on the short arm of chromosome 4 at position 4p16.3. Two of 13 splice variants encode proteins with a size of 3,142 and 112 amino acids, respectively. The 350 kDa isoform is ubiquitously expressed with higher levels in brain tissue and testis (Sharp *et al.*, 1995). The small isoform lacking the polyQ stretch was not well studied. Interestingly, the majority of HD pathological changes have been found in the central neuron system, especially the selective vulnerability in the striatum.

The expansion of CAG repeats has been clearly identified as genetic cause of HD in 1993. However, the upper range of normal alleles is reported to vary from 30 to 39 repeats (Andrew *et al.*, 1993; Myers *et al.*, 1993; Zuhlke *et al.*, 1993). Alleles with 30-38 CAG repeats have been termed intermediate alleles, which possess a CAG repeat range between that observed in general population and HD patients without HD expression (Goldberg *et al.*, 1993; Myers *et al.*, 1993). Alleles with 36-39 CAG repeats show a reduced penetrance in comparison to those with 40 or more repeats (McNeil *et al.*, 1997). Nervertherless, numerous studies focused on the influence of CAG repeat length on disease phenotype. One major outcome is the strong inverse correlation between CAG repeat length and the age of onset (Figure 1.1), patients with juvenile Huntington disease (JHD), or early-onset HD usually carry a large

number of CAG repeats than individuals with adult-onset HD (Andrew *et al.*, 1993; Norremolle *et al.*, 1993). The correlation of CAG repeat length and the severity of symptoms was studied as well. It seems that the CAG length influences the severity of symptoms only in the early stages of the disease but not at later stages (Foroud *et al.*, 1995; Siemers *et al.*, 1996). No correlation of CAG repeat length and disease progression have been reported, while a clear relation between CAG length and the degree of pathology was revealed in several studies (Penney *et al.*, 1997; Becher *et al.*, 1998).

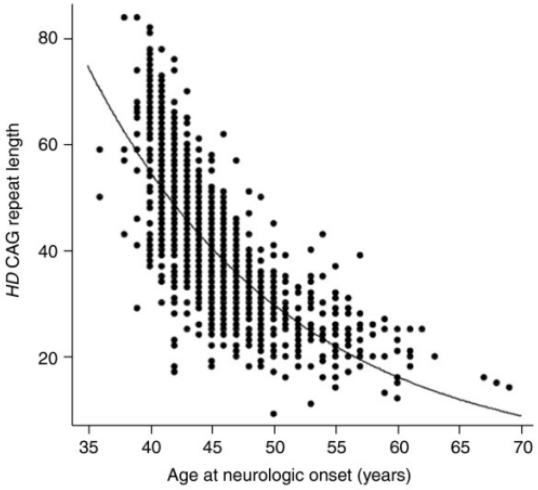

Figure 1.1: Reverse correlation of age at onset and CAG repeat length. The plot shows data points from 1,200 HD subjects of known age at neurologic onset. For each individual, the measured CAG repeat length in blood DNA (*x*-axis) is plotted against age at neurologic onset (*y*-axis). The line represents the best-fit simple logarithmic regression to the data. The CAG repeat length accounts for approximately 67% of the overall variation in age at neurologic onset, and the remaining variation shows a heritability of approximately 0.56. (from James F Gusella and Marcy E MacDonald, 2009)

1.1.2 Paternal origin and juvenile HD

Although HD is autosomal inherited, parental transmission shows an effect on age at onset. The first observation was reported by Bruyn that most juvenile and patients with early-onset were descendents of an affected father (GW, 1968). Further detailed analysis revealed that affected children displayed an 8-year earlier age at onset in paternally transmitted cases. In contrast, only an approximately 1.4-years earlier age at onset in maternally transmitted cases was observed (Conneally, 1984). A later study with 254 parent-child pairs of HD patients showed a similar proportion of small increase in CAG repeat number (<7 repeats) in transmission by both sexes, however a huge difference in frequency of large increase (> 7 repeats, 21.0% in paternal transmission, 0.7% in maternal transmission) (Kremer *et al.*, 1995).

1.1.3 HD homozygotes

The clinical features and age at onset were also compared between homozygotes and heterozygotes in the affected families. There was no difference in these between siblings with one or two affected alleles (Wexler *et al.*, 1987; Durr *et al.*, 1999). In transgenic mice carrying 150 CAG repeats, earlier onset of symptoms and pathological changes were found in homozygous animals compared to heterozygous littermates (Lin *et al.*, 2001). However a recent report shows no difference in the onset of the disease in *Htt* knock-in mice with 140 CAG having one or two copies of the mutant gene (Rising *et al.*, 2011).

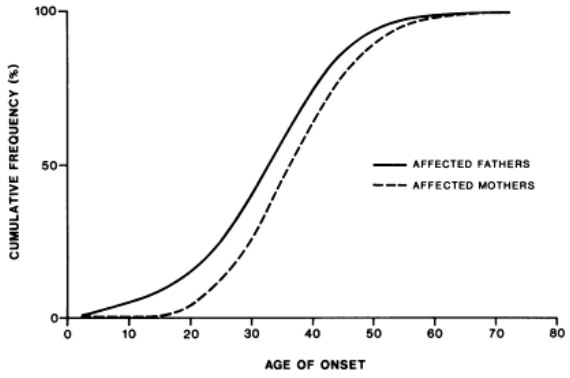

Figure 1.2: Cumulative frequency of age at onset in offspring of affected mothers compared with offspring of affected fathers. (from Conneally et al., 1984)

1.1.4 Mosaicism in HD

Mosaicism is another genetic aspect in CAG repeat diseases including HD. During DNA replication, hairpin structure formation by DNA polymerase slippage at CAG repeat either thenascent strand or the template strand results in an expansion or contraction of CAG stretches (Mirkin, 2006; Mirkin, 2007). This mechanism explains the basis of germline instability in trinucleotide repeats (TNR). In contrast, somatic instability is generally related to the operations of other processes on the level of the DNA. One remarkable study has reported that the lacking of the mismatch repair gene *Msh2* caused a reduction of trinucleotide expansion in mutant *HTT* exon1 transgenic mice. This suggested that the expansion of CAG stretch takes place during gap-filling synthesis when DNA loops formed by the CAG repeats sequence are sealed into the DNA strand (Manley *et al.*, 1999). In both HD patients and transgenic mice, the greatest somatic instability has been found in the striatum (Telenius *et al.*, 1993; Aronin *et al.*, 1995; Kennedy and Shelbourne, 2000).

1.1.5 Modifier genes in HD

Although several studies revealed an inverse correlation between the number of CAG repeats and the age at onset, it remains unclear, why HD patients carrying the same repeat length sometimes have a huge variation in the age at onset. Thus, other modifying factors, especially genetic modifiers influencing the age at onset of HD symptoms evoked the scientists' attention. Several studies have focused on genes encoding proteins, which are involved in HD pathogenesis. Positive results have been reported in processes and/or pathways of glutamate transmission (MacDonald *et al.*, 1999; Cannella *et al.*, 2004), protein degradation (Naze *et al.*, 2002; Metzger *et al.*, 2010), gene transcription (Holbert *et al.*, 2001; Chattopadhyay *et al.*, 2005) as well as energy metabolism (Taherzadeh-Fard *et al.*, 2010; Che *et al.*, 2011). These studies will be extended in the coming years and potentially contribute to uncovering the HD pathogenesis.

1.2 Clinical description of Huntington disease

Clinical features of HD can be divided in three major subgroups: motor deficits, cognitive decline and psychiatric disturbances (Vonsattel and DiFiglia, 1998).

The most prominent aspect in loss of motor function is the development of chorea, which gave the disease its initial name "Huntington's chorea". Chorea is defined by excessive spontaneous movements, which occur abrupt and in a random temporal pattern. They cannot be suppressed voluntarily. Chorea occurs in over 90 percent of HD patients, increasing at early stages of the disease but tending to disappear in progressed stages. A further component adding to the movement defects observed in patients is the progressive decline of voluntary movements, which appear gradually at the beginning and dominant in advanced stages of the illness. The prominent features are bradykinesia (slowness of movement), all patients develop hypokinesia, akinesia, and rigidity. Dystonia, characterized by slow abnormal movements and posturing with increased muscle tone, may be the first sign of HD patients passing on towards advanced stages of the disease. During the course of disease, some patients display speech (dysarthria) and swallowing (dysphagia) abnormalities. Gait disturbances and oculomotor disturbances (eye movements) are also present in HD patients, specifically on the early onset HD which do not manifest with chorea but rather spasticity.

Cognitive decline is a further major sign observed in HD. It can appear prior to the onset of motor symptoms or mild in advanced stages of the illness. Many studies have revealed that HD patients have difficulties in the performance in tasks involving multiple cognitive domains such as strategy shifting (Lawrence *et al.*, 1999), episodic memory (Caine *et al.*, 1977; Butters *et al.*, 1978; Moses *et al.*, 1981), as well as executive functions (organization, regulation and perception) and mental flexibilities (Norton, 1975; Josiassen *et al.*, 1983; Butters *et al.*, 1985). The most common cognitive impairment is a difficulty in performing tasks requiring a shift in strategy, which is typically involved in the hierarchy of inhibitory and attentional mechanisms, which is controlled by the striatum (Sutherland and Mackintosh, 1971).

HD patients also exhibit psychiatric disturbances, frequently observed in early disease stages, often prior to the onset of motor symptoms. The most frequent neuropsychiatric feature is depression followed by secondary symptoms comprising anxiety, guilt feelings and apathy. Apathy is related to the disease stage, depression and anxiety are not. It seems that non-neurological factors play a prominent role in depression and anxiety symptoms rather than in the pathophysiology of motor and cognitive disorder. Compulsion leading to irritability and aggression, psychosis as well as hyper-sexuality in early stages and hypo-sexuality in later stages is also present in HD patients (Craufurd and Snowden 2002).
Weight loss has been reported as an additional secondary symptom in all patients being not associated with the movement disorder. This suggests a connection of the disease with metabolism defects throughout the body or loss of neurons in the hypothalamus regulating metabolism (van der Burg *et al.*, 2008). Furthermore, sleep- and circadian rhythm disturbances as well as autonomic disturbances have also been observed in HD patients (Morton *et al.*, 2005).

1.3 Neuropathology of Huntington disease

1.3.1 Selective neuronal loss in HD brain

The hallmark of HD neuropathology is initial striatal atrophy, which expands at later stages to the cerebral cortex and other subcortical brain regions (Bruyn, 1979; Vonsattel *et al.*, 1985). Interestingly, neuropil and nuclear huntingtin (htt) aggregates are abundantly observed in the cortex, but only sparsely seen in the striatum of HD affected brains (Gutekunst *et al.*, 1999; Kuemmerle *et al.*, 1999).

Gross pathology shows a reduction of size and weight in HD patient brains, occurring in both gray and white matter in the cerebral hemispheres, the diencephalon, the cerebellum, and also the brainstem and spinal cord. Especially in the neostriatum, gross atrophy arises in caudate nucleus and putamen with the caudate nucleus shrinking to a thin rim of tissue (Figure 1.3).

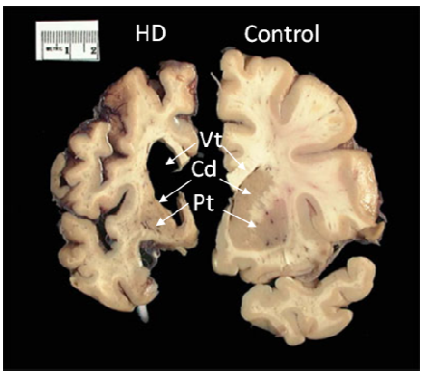

Figure 1.3: Gross pathology of HD. Macroscopic image of HD brain (left) and an age-matched normal control (right). Note the marked atrophy in caudate nucleus (Cd), and putamen (Pt) resulting in an enlarged lateral ventricle (Vt), cortical atrophy and white mater loss in HD brain. (modified according to http://naota.medgen.iupui.edu/hdrosternew/AboutHD/brainAndHD.asp)

Table 1.1: Neurodegeneration observed in HD patients

Brain region	Neuron loss observed	Reference
neostriatum	more than 90% in grade 4	(Vonsattel et al., 1985, Bots and Bruyn, 1981)
globus pallidus	40%	(Lange *et al.*, 1976)
subthalamus	25%	(Lange *et al.*, 1976)
Substantia nigra	45%	(Ferrante *et al.*, 1987; Oyanagi *et al.*, 1989)
neocortex	10-55% within various regions	(Macdonald *et al.*, 1997; Thu *et al.*, 2010)
hypothalamus	up to 90% in lateral tuberal nucleus, 45% in oxytocin-expressing neuron, 24% in vasopressin-expressing neurons	(Kremer, 1992; Gabery *et al.*, 2010)
thalamus	55% in the centromedial-perafasicular (TCP) complex	(Heinsen *et al.*, 1996)
hippocampus	35% in CA1	(Spargo *et al.*, 1993)
cerebellum		(Jeste *et al.*, 1984)
brainstem		(Roos *et al.*, 1986)

By using quantitative microscopy, neuron cell death was observed in many different brain regions starting in the neostriatum (Heinsen *et al.*, 1994), and spreading to cortex and other basal ganglia region. The severity of HD pathology is divided into 5 grades (0-4) correlating with clinical stages, up to 50% neuron loss has been

detected in HD brains of grade 1. In the most severe grade 4, a depletion of more than 90% of the striatal neurons is observed (Bots and Bruyn, 1981; Roos *et al.*, 1985). Numerous studies have reported neurodegeneration in other brain regions in HD patients including globus pallidus, subthalamus, substantia nigra as well as neocortex, hypothalamus, thalamus and hippocampurs. Neuronal loss has also been reported in Purkinje cells in the cerebellum and brainstem (Table1.1).

In summary, neuron loss occurs predominantly in the basal ganglia, which is strongly connected with the cortex and thalamus. Basal ganglia are a group of interconnected subcortical nuclei consisting of the striatum (caudate and putamen), globus pallidus (internal (GPi) and external (GPe) segments), the substantia nigra (pars reticulate (SNr), and pars compacta (SNc)), and the subthalamic nucleus (STN). The major excitatory input to the basal ganglia comes from the cerebral cortex, which receives its input from the thalamus. Two populations of striatal spiny neurons containing either D1-type receptor or D2-type receptor convey the output signal through a direct (D1 receptor expressed neuron) or indirect (D2 receptor expressed neuron) pathway into GPi and SNr. The bulk arises from GPi and SNr projecting to the thalamus, where the signal will be forwarded to the cerebral cortex, the originating region of the basal ganglia input. The dopaminergic projection from SNc is the extrinsic modulating input to the striatum, which reacts on the striatal output. The direct pathway consists of 2 cascades of inhibitory signals, the excitatory signaling of D1 neurons leads to an increase of thalamic activity. However the indirect pathway contains 3 cascades of inhibitory signals, three times negative effect results in a decrease of activity in the thalamus after excitation of D2 neurons in the striatum. The balance of the direct and indirect pathway plays an essential role in the striatum-thalamus-cortex circuit. In the case of HD, it was suggested that the preferential loss of D2 neuron in the striatum results in excitatoxicity affecting the signiling of the whole pathway.

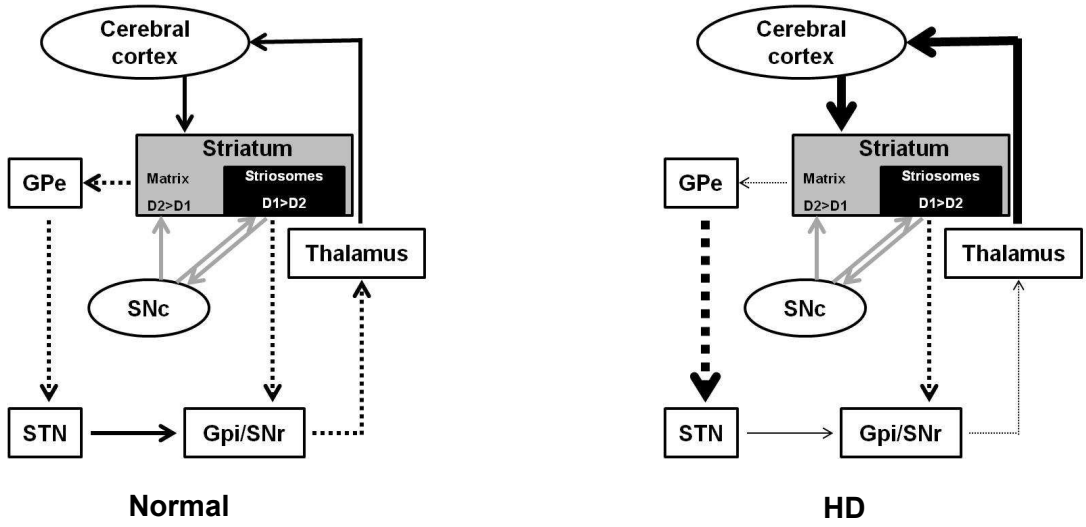

Figure 1.4: Schematic representation of basal ganglia pathway under normal condition and in HD pathogenesis. Continued line and dotted line represent excitatory and inbitory signal. The width of each line indicates the strength of each signal. Gpe, Globus pallidus external segment; Gpi, globus pallidus internal segment; STN, subthalamic nucleus; SNr, substantia nigra pars reticulata; SNc, substantia nigra pars compacta. Modified according to (Gutekunst, 2002).

Notably, GABAergic medium spiny neurons (MSNs) are most affected in the striatum. Neuronal cell death has been shown to be driven by both apoptosis and necrosis dependent pathways. Structural and ultra-structural observations revealed a dendritic remodeling in MSNs (Ferrante *et al.*, 1991), as well as recurving and branching of distal dendritic segments and an increase of dendritic spines. Moreover, non-phosphorylated axonal neurofilaments have been reported to show morphology abnormalities and the number of non-phosphorylated neurofilaments is significantly reduced in HD brains (Goto and Hirano, 1990).

In addition to cell loss, neuroinflammation has been observed in HD brain since 1991. Later reports described the activation of microglia cells in HD in more detail. Activation of microglia cells occurs in HD brains in grade 1-4 (Sapp *et al.*, 2001), and activated microglia are distributed throughout the neostriatum, neocortex, globus palidus, and also in the subcortical white mater. Numbers of microglia cells increase with the grade of the pathology. Activated microglia has been observed frequently in close proximity to neuron cell bodies containing nuclear aggregates (Sapp et al., 2001). Several recent studies indicated an activation of microglia in brains of presymptomatic HD gene carriers (Tai YF, 2007) and immune activation in plasma before clinical onset of HD (Bjorkqvist *et al.*, 2008).

Recently, astrocytes have been implicated in contributing to the neurodegeneration in HD via changing the extracellular environment. Earlier analysis of the function of

astrocytes revealed that expression of mutant htt in mouse astrocytes induced age-dependent neurological symptoms (Bradford *et al.*, 2009; Bradford *et al.*, 2010), while double transgenic mice expressing mhtt in both astrocytes and neurons displayed more severe neurological symptoms and earlier death (Bradford *et al.*, 2010). In 2012, Wang and colleagues could show, that an *in vivo* expression of a N-terminal fragment of mhtt in astrocytes suppresses BDNF transcription and secretion (Wang *et al.*, 2012).

1.3.2 Aggregates of N-terminal htt in HD brain

Another hallmark of HD pathogenesis is the deposition of mhtt containing nuclear inclusions (NIIs) and cytoplasmic aggregates of N-terminal mhtt. After cleavage of full-length mhtt the N-terminal fragment of mhtt is released, which interacts with and recruits hundreds of other proteins, subsequently forming aggregates in different neuronal compartments. These aggregates can be found in every subcellular compartment of neurons including the nucleus, perikaryon, dendrites, axons, and also the synaptic terminal. The Cortex is the brain region showing aggregates most abundantly, especially in layer V and VI (Gutekunst et al., 1999). Less abundance of aggregates has been observed in the hypothalamus, thalamus, hippocampus, and substantia nigra. Interestingly, aggregates are less common in the striatum where the highest degree of neurodegeneration occurs. A lower number of aggregates is also present in the molecular and granule cell layers of the cerebellum (Gutekunst et al., 1999). Nearly all transgenic animal models of HD exhibit aggregates of mhtt. For example the R6/2 mice carrying exon 1 of mhtt display predominantly NIIs and the YAC mice expressing full-length mhtt present both NII and neuropil aggregates in different brain regions (Kosinski *et al.*, 1999; Wang *et al.*, 2008). Numerous experiments have been performed to answer the question whether aggregate formation correlates with neuron death; however, the answer remains still elusive.

1.4 Biological function of the huntingtin protein

Huntingtin is a soluble cytoplasmic protein consisting of 3144 amino acids, which is associated with various organelles including the nucleus, Golgi complex, endoplasmic reticulum (DiFiglia *et al.*, 1995; Hilditch-Maguire *et al.*, 2000), as well as vesicular structures in neurites and the synapse (Li *et al.*, 2003).

Huntington disease is an autosomal dominantly inherited disease suggesting a toxic gain of function of mhtt. Several experimental evidences have supported this idea

(Sipione and Cattaneo, 2001) and shown that mhtt initiates the disease with a reverse correlation between the number of CAG repeats and the age of onset of HD (Andrew *et al.*, 1993; Snell *et al.*, 1993). In contrast, it was also demonstrated that a depletion of htt is lethal in the embryonic stage of mice whereas in heterozygous htt knock-out (KO) mice, abnormalities in brain development and morphology as well as behavioural deficits have been observed (Nasir *et al.*, 1995; Zeitlin *et al.*, 1995). Subsequent studies revealed that an increase of wild-type htt in mice leads to neuroprotection from apoptosis and excitotoxicity and increased the transcription of BDNF (Zuccato *et al.*, 2001). Notably, mhtt is able to rescue wild-type htt KO mice from embryonic lethality, indicating an essential function of wild-type htt.

1.4.1 Huntingtin influences neuronal gene transcription

In both HD patients and HD animal models, it has been observed that a large number of genes are dysregulated in striatum and cortex with the majority of them being down-regulated (Hodges *et al.*, 2006; Kuhn *et al.*, 2007; Nguyen *et al.*, 2008). Huntingtin is suggested to interact with several proteins involved in the transcription process. Mutant htt is able to impair the chromatin folding via interacting with chromatin regulation proteins, subsequently interfering transcription (Faber *et al.*, 1998; Boutell *et al.*, 1999; Steffan *et al.*, 2000). Mutant htt can also dysregulate transcription through direct interaction with transcription factors and co-activators, this has been particularly well studied with factors such as TBP, CBP, SP1 and TAFII (Steffan *et al.*, 2000; Pelton *et al.*, 2002; Goehler *et al.*, 2004). Furthermore, the abnormal interaction of mhtt with members of the transcription machinery can also affect the transcription process (Steffan *et al.*, 2000; Zhai *et al.*, 2005).

The most explicit determination of gene dysregulation is in BDNF transcription. Down-regulation of BNDF by mhtt has been demonstrated both in vitro and in vivo (Zuccato *et al.*, 2005), while the over-expression of wild-type htt enhanced BDNF level in mice (Zuccato, 2001). The proposed underlying mechanism is that wild-type htt maintains the REST/NRSF (repressor element-1 transcription factor/neuronal restrictive silencing factor) in the cytoplasm, whereas the expression of mhtt results in a translocation of REST/NRSF into the nucleus forming a repressor complex, thus suppressing the transcription of severall genes including BDNF (Zuccato *et al.*, 2003).

1.4.2 Huntingtin as an essential integrator of intracellular vesicular transport

It is widely accepted that an altered intracellular axonal transport contributes to HD pathologenesis. Wild-type htt plays a role in the intracellular transport by interacting with proteins that are involved in protein trafficking, secretory and endocytic pathways.

Huntingtin associated protein 1 (HAP1) was first identified to interact with htt (Li *et al.*, 1995). HAP1 and htt were shown to bind to the large domain of dynactin P150 forming a protein complex, which through coupling with the dynein-dynactin complex facilitates intracellular trafficking (Li *et al.*, 1998). Increased binding affinity of mhtt to HAP1 and P150 compared to wt htt leads to a dissociation of the dynein-dynactin microtubule motor complex, eventually impairing axonal transport (Trushina *et al.*, 2004). Compelling evidence for wild-type htt function in axonal transport was shown using striatal neurons of embryonic *Htt*$^{-/-}$ mice. A dose-dependent effect of wildtype htt was observed by comparing homozygous and heterozygous KO animals, which revealed a worsening of intracellular trafficking after complete loss of wildtype htt (Trushina, 2004). Another example is the transport of BDNF, which has been described to be associated with htt during anterograde and retrograde transport. Both, *in vitro* and *in vivo* analysis showed that modulating wildtype htt levels affects the transport of BDNF along axons (Gauthier *et al.*, 2004; Trushina *et al.*, 2004). The defective trafficking of other organelles such as mitochondria and the amyloid precursor protein (APP) vesicles has also been demonstrated in HD (Li *et al.*, 2001; Rong *et al.*, 2006).

N-terminal htt forms aggregates in the nucleus as well as in the cytoplasm, mainly located in axon processes and synaptic terminals. This results in a recruitment of soluble htt as well as its interaction partners such as HAP1 and P150, which are the keys protein for the axonal transport. In addition, the aggregates in the axon processes may cause a mechanic block of vesicle and organelle circulation in neurons leading to axonal neurodegeneration (Li *et al.*, 2001).

1.4.3 Function of huntingtin at the synapse

Huntingtin also interacts with several proteins implicated in synaptic function. Especially the interaction of htt with Huntingtin interacting protein 1 (HIP1) and postsynaptic density protein 95 (PSD-95) were studied in more detail. HIP1 and clathrin are essential for the clathrin-mediated coating of vesicles therefore playing

an important role in clathrin-mediated endocytosis (Engqvist-Goldstein *et al.*, 1999; Mishra *et al.*, 2001; Waelter *et al.*, 2001b). This raised the hypothesis that mhtt influences endocytosis via an interaction with HIP1, potentially impairing the recycling of synaptic vesicles and trafficking of neurotransmitter receptors. PSD-95 has been reported to be associated with htt via an SH3 domain, as well as to interact with the NR2 subunit of the NMDA receptor (Sun *et al.*, 2001). An important finding came from a mutant mouse model lacking PSD-95. This model displayed an increased NMDA dependent long-term potentiation (LTP) accompanied with spatial learning abnormalities (Garcia *et al.*, 1998) indicating a key role of PSD-95 in coupling to the NMDA receptor in synaptic plasticity and spatial learning. In the presence of mutant huntingtin with a prolonged polyQ tract, PSD-95 is less associated with mhtt leading to an increased interaction with NMDA2B and subsequent signaling and cell death (Sun *et al.*, 2001). Fan and colleagues could verify an enhanced interaction of PSD-95 and NMDAR2 with increased polyQ length in YAC transgenic mice *in vitro*. Either blocking the binding of PSD-95 to NMDA2B or knock-down of PSD-95 by siRNA resulted in a reduction of NMDA expression on the cell surface and reduced susceptibility to excitotoxicity (Fan *et al.*, 2009).

1.4.4 Neuroprotective properties of wild-type htt

The first observation that wildtype htt protects neurons from cell death originated from a study indicating that an increased apoptosis and embryonic lethality occurs in htt KO mice (Zeitlin et al., 1995). Another important finding was reported by White and colleagues. The experiment used Hdh^{neoQ50} and Hdh^{Q50} homozygous mice. Hdh^{neoQ50} homozygous mice carring hypomorphic alleles (Hdh^{neoQ50}) possessed only reduced expression of mhtt at one-third the level of endogen as in WT controls, while Hdh^{Q50} homozygous mice only expressed mhtt at a comparable level as Htt in WT mice.Mice with reduced mhtt expression level exhibited a characteristic aberration of brain development and perinatal lethality. In comparison, mice with normal levels of mhtt do not exhibit these abnormalities (White *et al.*, 1997). A subsequent study was done by creating a targeted disruption in exon 5 of *HTT* homologue mouse *Htt* (Httex5), homozygotes mice for the Httex5 mutation displayed embryolethality, while the heterozygotes exhibited neurodegeneration in basal ganglia and behavior abnormalities as well as impaired synaptic plasticity (O'Kusky *et al.*, 1999). Other studies have assessed normal htt function in adult animals. For this purpose a conditional KO mouse model using the Cre/loxP site-specific

recombination strategy was used to enable the inactivation of endogenous *Htt* expression in forebrain and testis. The Htt KO mice developed a progressive neurodegeneration phenotype and sterility (Dragatsis *et al.*, 1998). These studies imply an essential role of htt in neuronal function not only during development and but also at later stages.

The neuroprotective properties of wild-type htt were confirmed by a series of experiments using immortalized striatal neurons over-expressing human wild-type htt. The level of apoptosis was measured after treatment of the cells with mitochondrial toxins, serum deprivation and over-expression of proteins involved in cell death pathways (Rigamonti *et al.*, 2000). These experiments showed a protective role of wildtype htt against polyglutamine toxicity. Ho and colleagues observed that over-expression of wild-type htt was able to prevent apoptosis caused by expression of CAG repeat in N-terminal mutant htt (Ho *et al.*, 2001). Recently, a study investigating cell fate after depletion of wild-type htt was carried out utilizing neuroepithelial cells from various brain regions. KO of htt resulted in a disturbed cell migration and reduced proliferation in neuroepithelial cells isolated from the neocortex but not in neuroepithelial cells isolated from cerebellum. This experiment indicated a spatial and temporal influence of htt expression in neural development (Tong *et al.*, 2011).

The mechanisms underlying anti-apoptotic effects of htt have been investigated in several pathways. Wildtype htt is involved in transcription of several genes including BDNF, and is also able to facilitate BDNF transport along axons to the pre-synapse thus supporting neuronal survival by enriching neurotrophic factors. Furthermore, it has been shown that htt prevents activation of caspase-3 through inhibiting the cleavage of pro-caspase-9, therefore suppressing the caspase cascade, which induces apoptotic processes (Rigamonti *et al.*, 2001).

Another pathway of htt exerting its anti-apoptotic function is by interacting with HIP1, which is involved in the initiation of pro-apoptotic proteins through interaction with HIP1 protein interactor (HIPP1) and activation of caspase-8. Mutant htt has a reduced binding affinity to HIP1, which results in an increase of free HIP1, subsequently leading to apoptosis (Hackam *et al.*, 2000). Furthermore, overexpressing wildtype htt in transgenic mice protected against excitotoxicity induced by increased NMDA receptor signaling (Van Raamsdonk *et al.*, 2005; Leavitt *et al.*, 2006). Phosphorylation of htt by Akt (a serine/ threonine kinase) also plays an important role in neuroprotection. Huntingtin has been implicated in the

phosphoinositide 3-kinase (PI3K)-Akt pathway by stimulating the expression of pro-survival genes (Humbert *et al.*, 2002; Rangone *et al.*, 2004). Recently, it has been reported that the ganglioside GM1 promotor activity of Akt leads to an increase of htt phosphorylation and reduces neurodegeneration in HD mice (Maglione *et al.*, 2010).

The role of htt in calcium signaling pathways was revealed using a mouse embryonic fibroblast (MEF) cell line from htt KO mice. The inositol 1,4,5-trisphosphate receptor signaling pathway possesses a reduced sensitivity to stimulation in the absence of htt leading to an abnormal ER-mitochondrial calcium coupling and ATP-induced calcium mobilization (Zhang *et al.*, 2008). These results support the hypothesis that htt expression induces a calcium overload in cytosol and mitochondria resulting from sensitization of IP3R1 in MSN (Zhang *et al.*, 2008). Moreover, numerous genes related to calcium homeostasis are down-regulated in HD patients and HD animals supporting the important role of htt in calcium signaling pathways (Kuhn *et al.*, 2007).

1.5 Proteolysis, aggregation and degradation of mutant huntingtin

1.5.1 Proteolysis of huntingtin

Formation of both nuclear and cytoplasmic aggregates is a hallmark of HD pathology. N-terminal fragments of mutant huntingtin are the major component of these aggregates raising the question whether the proteolysis of huntingtin affects aggregate formation. Both, wildtype and mutant htt are substrates of caspase-3, caspase-6, calpain as well as aspartyl proteases indicating that cleavage of htt may be a normal physiological process (Kim *et al.*, 2001; Wellington *et al.*, 2002; Graham *et al.*, 2006). However, cleavage of mhtt is dependent on the length of the polyQ tract suggesting that the proteolytic process of htt is involved in htt pathogenesis. It was demonstrated that inhibition of calpain activity in mhtt expressing cells resulted in a reduction of aggregated N-terminal htt in the nucleus (Gafni *et al.*, 2004). Caspase-3 and -6 were studied more extensively in *in vivo* experiments. The caspase-3 htt cleavage product comprising of 552 amino acids was found at early ages in YAC72 transgenic mice but not in the wildtype littermates, suggesting a role of the cleaved mutant htt in initiating HD pathology (Wellington *et al.*, 2002). A remarkable finding was yielded in HD transgenic mice carrying modulated caspase-3 and caspase-6 cleavage sites. Inhibition of htt cleavage at a specific caspase-3 site did not prevent the behavior abnormalities and neuropathological findings associated with HD. In contrast, caspase-6-resistant mutant htt mice displayed a statistically significant

reduction in neurodegeneration as well as ameliorated behavioral abnormalities and resistance to exitotoxicity (Graham *et al.*, 2006). Furthermore, several studies showed that N-terminal fragments of htt produced by caspase-3 and caspase-6 are localized in different subcellular regions. The fragment generated by caspase-6 is present in the nucleus, while those generated by caspse-3 show a perinuclear localization in the cytoplasm (Warby *et al.*, 2008). Most of the caspase activity occurs in cortical projections of neurons (Wellington *et al*., 2002).

1.5.2 Aggregation of mutant huntingtin

Aggregates have been well characterized in different transgenic HD mice, showing a predominant nuclear localization of aggregates in transgenic HD model carrying a truncated huntingtin fragment, while full-length transgenic models presented both, nuclear and neuropil aggregates (Wang *et al*., 2008). It was suggested that htt is cleaved by caspase-3 in the cytosol, whereas the primary location of the fragment generated by caspase-6 is in the nucleus. Both mutant and wild-type htt contain a highly conserved nuclear export signal in the carboxy-terminus (Xia *et al.*, 2003). Transgenic fragments and those generated by cleavage of caspases are prevented from being transported back into cytoplasm as the export signal has been removed through cleavage and release of the c-terminal fragment (Warby *et al*., 2008).

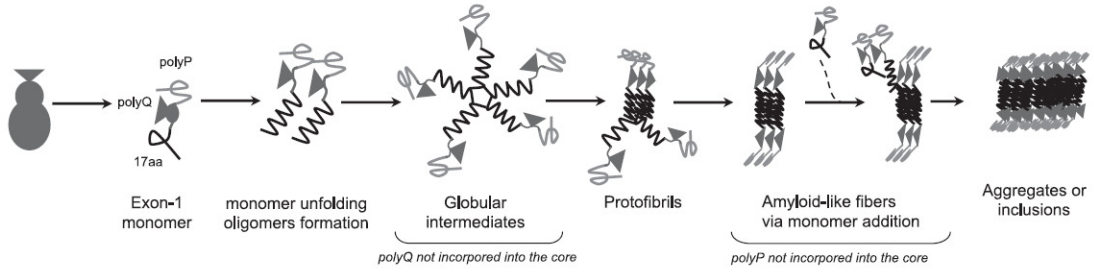

Figure 1.5: Model of huntingtin aggregation described by Thakur and colleagues. N-terminal fragments of htt oligomerize and form micelle-like structures with the first 17 amino acids forming a coil in the core and polyQ sequence positioned peripherally. With increasing number of htt fragments, the oligomers or protofibrils rearrange into amyloid-like seeds rapididly growing into aggregates (Zuccato *et al.*, 2010).

Two models of htt aggregation have been described. In the first one, aggregation of mhtt is thought to arise through a nucleation-dependent fibrillation (Scherzinger *et al.*, 1999), similar to ß-amyloid and α-synuclein aggregates (Harper and Lansbury, 1997; Wood *et al.*, 1999). The random coil structure of mhtt may change into a hair-pin structure, and when the polyglutamine stretch exceeds a critical length, the hair-pin

structure is further stabilized. Once the intermediate structures (seeds) are formed, in the presence of a high concentration of mhtt, they will grow very quickly into high-molecular-weight fibrillar structures. Thakur and colleagues observed ten years later that during the initial aggregation process micelle-like structure are formed with the first 17 amino acids of htt in the core and polyQ sequences being present on the surface of the micelle-like structures. As more monomer fragments involve in this loosely packed structure, it is rearranged into amyloid nuclei followed by a rapid fibril elongation process (Figure 1.3) (Thakur *et al.*, 2009). Nevertheless, cleavage of mhtt by caspases or calpains and/or interaction with other cellular proteins could accelerate the aggregation process (Sittler *et al.*, 1998; Welch and Gambetti, 1998). In contrast, increased proteasomal or lysosomal clearance can slow down or inhibit the formation of aggregates (Chen, 1977; Carmichael *et al.*, 2000).

1.5.3 Degradation of mutant huntingtin

The ubiquitin-proteasome system (UPS) and the lysosome system are two pathways responsible for protein degradation in cells. The contribution of the UPS in degrading htt was studied by two approaches using either an N-terminal htt fragment resistant to proteasomal degradation or a selective inhibition of the UPS. After cleavage of htt by caspases or calpain, the released N-termini form into cores (as described above), which are resistant to proteasomal degradation (Holmberg *et al.*, 2004). Since the mhtt seeds cannot be degraded by the UPS, which on the other hand is occupied and therefore blocked by mhtt, the degradation of other protein substrates is inhibited. This idea is supported by a recent study, which showed that the purified fibrillar structure of htt aggregates isolated from HD animals and human HD post mortem brains was able to reduce UPS activity in vitro (Diaz-Hernandez *et al.*, 2006). The second mechanism is that UPS is impaired in the presence of mhtt. Immunocytochemical analysis of cells isolated from brains of HD animal models or HD post mortem brains have revealed a sequestration and altered subcellular localization of UPS components, suggesting an impairment of UPS function (Davies *et al.*, 1997; DiFiglia *et al.*, 1997).

The UPS has only capacity to degrade soluble mhtt, once aggregates are formed, they are no longer degraded by the UPS. In contrast, the lysosomal pathway can degrade misfolded proteins, protein aggregates as well as organelles. Inhibiting autophagy increased the accumulation of mutant huntingtin and the formation of

aggregates, whereas a stimulation of lysosomal activity caused its reduction (Qin *et al.*, 2003).

The formation of huntingtin aggregates is toxic for neuronal cells, especially when it is localized in the nucleus (Waelter *et al.*, 2001a; Bates, 2003). This can be explained by *per se* toxicity of aggregates in neuronal cell and recruitment of proteins into aggregates, which are essential for cell viability. However, there is a conflicting hypothesis that aggregates might protect neuronal cells since aggregates can remove misfolded mhtt monomers and oligomers, which may be more toxic (Bence *et al.*, 2001). Nevertheless, inhibition of huntingtin aggregation as a therapeutic approach has been extensively studied in the last decade. Chemical compounds have been screened and selected for further testing their ability to prevent htt aggregation. Notably, small peptides and antibodies against either full-lenth huntingtin or the polyQ tract itself have also been analyzed. The reports showed that the antibody 1C2 is able to bind to the polyQ stretch of mhtt and prevents aggregates formation *in vitro* (Trottier *et al.*, 1995). A further study demonstrated that a single-chain Fv antibody from a phage display library, which recognizes the first 17 amino acids of htt, inhibits mhtt aggregation *in vitro* (Lecerf *et al.*, 2001). Additionally, antisense oligodeoxynucleotides and antisense oligonucleutides were also used to down-regulate mhtt expression thereby preventing its aggregation (Boado *et al.*, 2000; Nellemann *et al.*, 2000; DiFiglia *et al.*, 2007).

1.6 Excitotoxicity in HD

Excitotoxicity is defined as a pathological process, which is induced by overstimulation of receptors thus releasing large quantities of excitatory neurotransmitters causing neuronal damage or death. The main excitatory neurotransmitter is glutamate, which stimulates the N-methyl-D-aspartate (NMDA) receptor and non-NMDA receptors such as the AMPA receptor, which may induce excitotoxicity by allowing high levels of calcium ions to enter the cell.

Excitotoxicity has been proposed as a major mechanism of pathogenesis in HD based on predominant degeneration of MSNs in the striatum, which mainly receives signals from glutamatergic neurons of the cortex. Overstimulation of glutamate receptors in MSNs by high levels of extracellular glutamate induces excitotoxicity (Coyle and Schwarcz, 1976; Beal *et al.*, 1994). A reduction of glutamate receptors has been observed in HD brains, in particular a reduction of the mGluR2 receptor

(Cha *et al.*, 1999). Furthermore, this hypothesis was supported by manipulating NMDA receptor output by agonists and antagonists applied to striatum of animals resulting in a selective loss of MSNs accompanied with neurological symptoms and a reduced excitotoxicity, respectively (Greene *et al.*, 1993). Most HD animal models present an increased NMDA receptor activity (Levine *et al.*, 1999; Zeron *et al.*, 2002).

The mechanism for the increased excitotoxicity in HD is based on an altered mhtt interaction with PSD-95 resulting in an increased level of free PSD-95, which can interact with the NMDA receptor and influence excitotoxicity (Fan *et al.*, 2009). Several studies have indicated that the cause for cell death is rather an increased susceptibility to excitotoxicity than an increase of excitotoxicity in HD animal models. Heng and colleagues crossed *Htt* knock-in (KI) mice with a transgenic mouse line overexpressing NMDA2B. This double transgenic mice exhibited a exacerbation of selective degeneration of striatal neurons (Heng *et al.*, 2009). A recent study revealed that PGC-1a, which has been observed to be downregulated in HD brains, displayed a negative regulation of extrasynaptic NMDA activity in a rat model (Puddifoot *et al.*, 2012). Another experiment in HD mice showed an impaired trafficking of GABAA receptor leading to a diminished inhibitory synaptic efficacy, which could contribute to the increase of neuronal excitotoxicity in HD (Puddifoot *et al.*, 2012).

1.7 Energy metabolism in Huntington disease

Recently, an impaired cholesterol metabolism has been found to play a role in the pathogenesis of neurodegenerative diseases. Several studies reported that cholesterol synthesis and metabolism are impaired in HD patients as well as in cell culture and animals models. Plasma cholesterol level was reduced in manifest HD patients and a reduced cholesterol synthesis was detected in HD brains (del Toro *et al.*, 2010; Leoni *et al.*, 2011). The findings of an impaired cholesterol homeostasis in HD were supported by numerous studies in cell culture and animal models. Decreased cholesterol levels in brain were detected in R6/2 and YAC128 transgenic mice, which carry exon 1 of the mutant human HD gene and full-length *Htt* genomic DNA, respectively (Valenza *et al.*, 2005; Valenza *et al.*, 2007a). Symptomatic R6/2 mice exhibited a reduced expression of cholesterol mRNA as well as a reduced activity of the enzyme HMG-CoAR, which is involved in the synthesis of cholesterol. This results in decreased levels of cholesterol precursors, however the level of cholesterol does not change until later stages of the disease (Valenza *et al.*, 2005,

Valenza *et al.*, 2007). In YAC128 mice, reduced levels of cholesterol were found starting with the symptomatic stage corresponding to reduced HMG-CoAR activity, as well as reduced levels of cholesterol precursors and the cholesterol metabolite 24-OHC (24-hydroxycholesterol) (Valenza *et al.*, 2007). Cholesterol and 24-OHC were also found to be reduced in HD KI mice carrying a CAG expansion and HD transgenic rats expressing truncated mutant *Htt* with 51 CAG repeats (Valenza *et al.*, 2010).

However, accumulations of free cholesterol at the plasma membrane have been observed in isolated and cultured neurons expressing mutant htt (Trushina *et al.*, 2006; Luthi-Carter *et al.*, 2010). These can lead to an increased excitotoxicity because the elevated cholesterol content in the plasma membrane clusters the distribution of neurotransmitter receptors, thereby creating signaling platforms that contribute to intercellular transmission. These accumulations of cholesterol at the plasma membrane is in contrast to the reduction of cholesterol found in plasma, maybe could be explained by a decreased conversion of cholesterol into 24-OHC to compensate for an impaired cholesterol synthesis.

Two mechanisms could contribute to the cholesterol changes observed in HD: 1. loss of neurons, which control cholesterol synthesis and metabolism; 2. direct effects of mutant htt on cholesterol homeostasis. Several reports suggest that an impairment of cholesterol metabolism is related to an abnormal interaction of mutant htt with the specific transcription factor Sp1, which cooperates with the sterol regulatory element-binding protein (Harjes and Wanker, 2003).

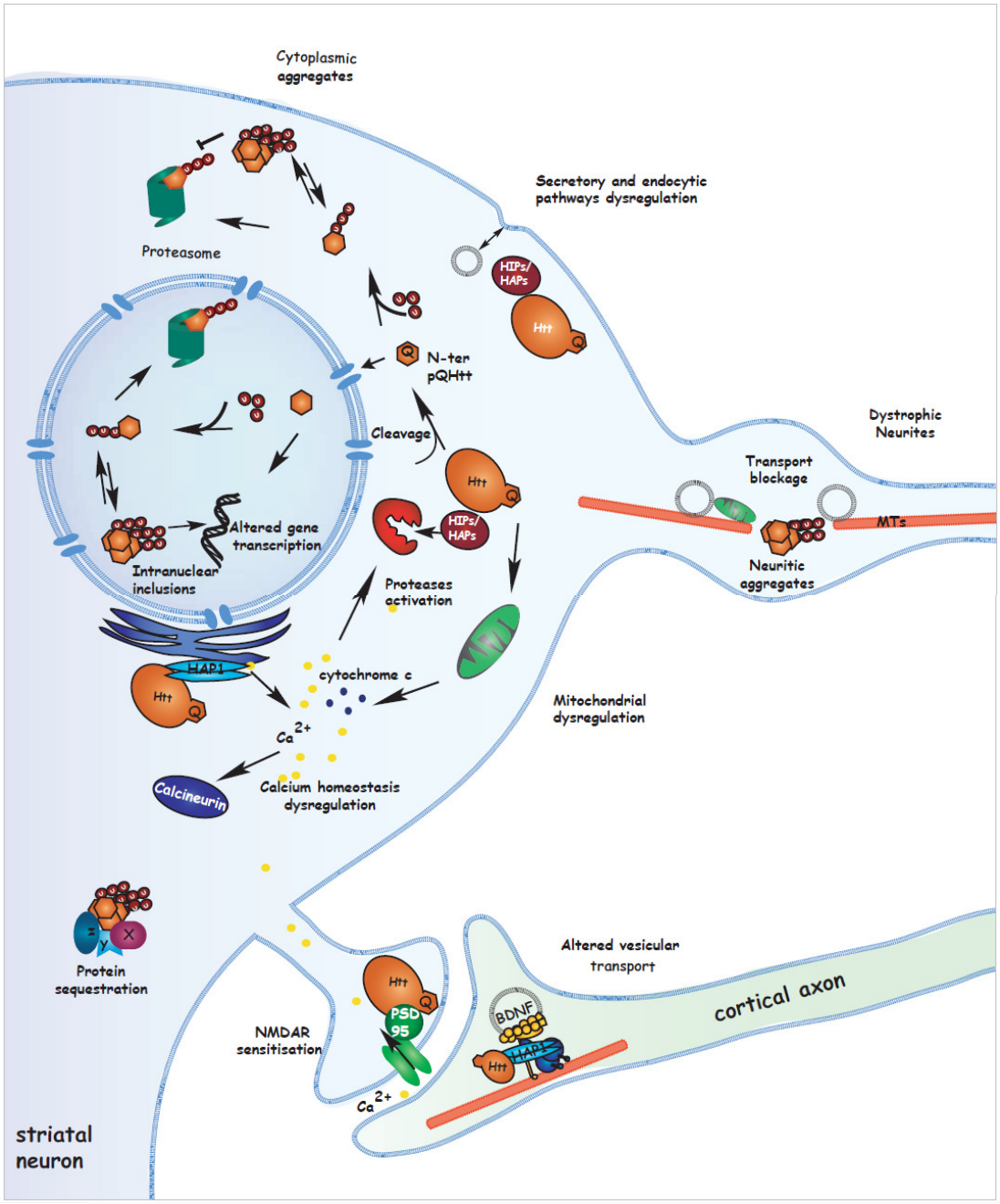

Figure 1.6: Toxic function of mhtt. Mutant huntingtin is cleaved by caspases or calpains in the cytoplasma. The translocation of N-terminal fragments of htt into the nucleus leads to an altered transcription. Mutant huntingtin also impairs calcium homeostasis in the cytoplasm. An Altered interaction with HAP1 and motor protein impairs the axonal transport, e.g. in the case of BDNF. Furthermore, the formed aggregates in axons can also mechanically block intracellular transport. In synaptic terminals, abnormal interaction of mutant huntingtin with HIP1 and other synaptic proteins leads to an impaired endocytosis and exocytosis. Additionally, decreased interaction between mutant htt and PSD-95 results in an increased interaction between PSD-95 and NMDA2R leading to excitotoxicity. Increased levels of N-terminal mhtt fragments result in aggregate formation, which can not be degraded by the proteasome, thereby inhibiting proteasome activity. (adapted from (Borrell-Pages *et al.*, 2006)).

As result of an reduced cholesterol synthesis in HD synapse maturation, neurotransmitter vesicle generation and fusion with the synaptic membrane as well

as signal transduction in cell membrane due to fluidity could be impaired (Pfrieger, 2003).

The defective energy metabolism in HD brains was first found in 1982 via positron emission tomography (PET) with FDG (Fluor-18-Deoxyglucose: glucose metabolism) was decreased in striatal regions in symptomatic patients and correlated with disease severity (Kuhl *et al.*, 1982; Young *et al.*, 1986). Several follow-up studies have verified the impaired glucose metabolism in cerebral cortex and striatum, but not in thalamus and cerebellum (Kuwert *et al.*, 1990; Martin *et al.*, 1992). Using (1)H-MRS, elevated lactate has been observed in optical cortex, frontal and parietal cortices as well as in striatum. Interestingly, it was also revealed that striatal lactate levels correlated with the length of CAG repeats, especially when these were more than 45 (Harms *et al.*, 1997; Jenkins *et al.*, 1998). Similarly, a reduced glucose metabolism has also been found in HD transgenic rats (von Hörsten S). The reduction of muscle adenosine triphosphate (ATP) in most symptomatic and presymptomatic patients was demonstrated by utilizing (31)P-MRS supporting the hypothesis of a mitochondrial dysfunction in HD. Moreover, the decreased ATP level in muscle is also correlated with CAG length (Lodi *et al.*, 2000).

1.8 Mitochondrial dysfunction and oxidative stress in Huntington disease

Since the respiratory chain in the mitochondria is the main source of energy in eukaryotic cells, defects in the energy metabolism are closely associated with mitochondrial dysfunction in neurodegenerative diseases. The mitochondrial respiratory chain is composed of five multisubunit protein complexes (I, II, III, IV and V), embedded in the inner membrane. Early studies have demonstrated a decrease in complex II/III activity in caudate and putamen but not in cortex and cerebellum of HD brains (Mann *et al.*, 1990; Browne *et al.*, 1997), A defect in complex IV was also observed in putamen but nowhere else (Brownw, 1997). The generation of free radicals analyzed with the marker 8-hydroxy-2'deoxy-guanosine (8OH2´dG) was also observed to be increased in caudate nuclear NDA, but no change in superoxide dismutase (SOD) or glyceraldehyde-3-phosphate dehydrogenase (GAPDH) in either caudate or putamen (Tabrizi *et al.*, 1999). In addition, aconitas was shown to be deceased in activity by 92% in HD caudate, 73% in putamen and 48% in cortex, whereas no changes was observed in the cerebellum (Tabrizi *et al.*, 1999). Both aconitas and complex II/III are iron-sulphur (FeS)-containing enzymes, and are in consequence especially susceptible when exposed to free oxygen radicals

suggesting an important role of oxidative stress and excitotoxicity in HD pathogenesis with mitochondrial dysfunction. A later study has shown a considerable increase in depolarization of mitochondria isolated from lymphoblasts of HD patients when treated with a complex IV inhibitor. Again, this effect correlated with the length of CAG repeats (Sawa *et al.*, 1999).

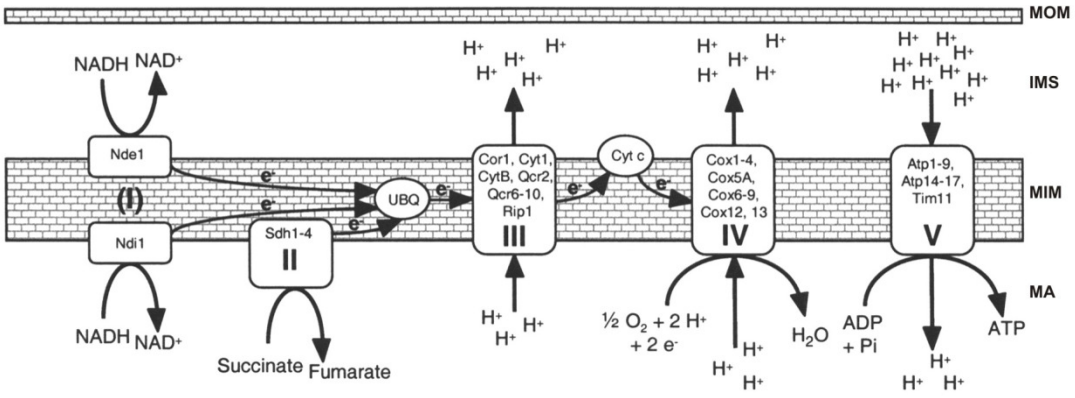

Figure 1.7: A schematic diagram of the mitochondrial respiratory chain with its subcomplexes. According to Joseph-Horne et al., 2001.

In follow-up studies, a decreased cell basal calcium level and increased calcium sensitivity of the permeability transition pore in mitochondria have been demonstrated in various HD cell lines as well as HD animal models indicating an impairment in mitochondrial calcium handling in the presence of mutant htt (Panov *et al.*, 1999; Gizatullina *et al.*, 2006; Lim *et al.*, 2008). Isolated cells from *Htt*$^{150Q/150Q}$ KI mice displayed an increased sensitivity in response to NMDA undergoing calcium deregulation (Oliveira *et al.*, 2007). Moreover, the decreased activities of enzyme aconitas and complex IV have been demonstrated in R6/2 mice (Tabrizi *et al.*, 2000) as well as an abnormal morphology of mitochondria (Mihm *et al.*, 2007).

Recent studies have further elucidated the mechanisms underlying mitochondrial dysfunction. The dearrangement of cytosolic calcium signaling in HD can be explained by association of htt and HAP1 with the type 1 inositol (1,4,5)-trisphosphate receptor (InsP3R1) forming a functional protein complex, which can be activated by InsP3. This protein complex is only sensitized in presence of mutant htt but not normal htt facilitating calcium release in response to NMDAR stimulation (Tang *et al.*, 2003). PGC-1α is a member of a family of transcription coactivators, which regulate transcription of numerous proteins involved in mitochondrial biogenesis and respiration. Abnormal interaction between mutant htt and PGC-1α

causes a repression of PGC-1α dependent gene expression. It has been reported that depletion of PGC-1α in HD KI mice resulted in increased neurodegeneration and neuronal symptoms. In contrast overexpression of PGC-1α reversed the toxic effect in cultured HD striatal cells (Cui *et al.*, 2006). Another study showed that overexpression of PGC-1α could reverse mitochondrial loss in HD neurons (Wareski *et al.*, 2009). The finding of an impaired dynamic and fragmentation of mitochondria came from several *in vitro* and *in vivo* studies. Abnormal interaction between mhtt and mitochondrial fission GTPase dynamin-related protein-1 (DRP1) subsequently stimulate GTPase activity leading to an impairment of the fission-fusion balance, thereby affecting mitochondrial axonal transport (Bossy-Wetzel *et al.*, 2008; Song *et al.*, 2011).

1.9 Therapeutic strategies

Therapeutic strategies in HD have been focused on symptomatic therapy using motor sedatives, cognition enhancers and agents against psychiatric disturbances. However, there have been little benefits reported after treatment with these drugs (Goety *et al.*, 1990; Peyser *et al.*, 1995). As mentioned before HD is affected by multiple pathogenic mechanisms based on loss-of-function and gain-of-function of htt. Recently, the therapeutic strategies point to neuroprotective and preventive therapies. The drugs against exitotoxicity, which inhibit glutamate release and/or reduce the reactivity of glutamate receptors as well as dopamine signaling pathway inhibitors, might play a neuroprotective role in HD (Zeron *et al.*, 2002; Cyr *et al.*, 2006). Increasing BDNF via gene therapy of infusion of recombinant BDNF is another approach to protect striatal cells. It is even considered to design the BDNF minetics molecularly, which are able to bind to the BDNF receptor and mimic the function of BDNF (Fletcher and Hughes, 2009). Furthermore, improving mitochondrial function or modulating the levels of cholesterol and its' derivatives is a further neuroprotective approach for HD (Beckman and Clements, et al., submitted, (Tabrizi *et al.*, 2005). Another promising strategy is the use of stem cells, which are introduced into the striatum and are able to differentiate into neurons thus replacing the damaged MSNs. Allele specific targeting of mutant htt transcription via siRNA and also targeting of its general transcription can reduce htt gain-of function (Hu *et al.*, 2009). Inhibiting caspase-6 activity leads to a reduction of proteolysis and release of potentially toxic fragments in HD (Graham *et al.*, 2010). In addition, targeting htt aggregation via anti-aggregation compounds and enhancing htt clearance have been

considered for HD therapy to postpone the onset of the disease (Tanaka *et al.*, 2004).

1.10 Animal models of Huntington disease

The discovery of the sole genetic cause - the expansion of CAG repeats – allowed the generation of animal models resembling many features of HD. In the past 17 years, a number of rodent and large animal models expressing full-length mhtt or truncated mhtt fragments were developed for therapeutic studies and to better understand the pathogenesis of the disease (Menalled and Chesselet, 2002; Ehrnhoefer *et al.*, 2009; Crook and Housman, 2011; Munoz-Sanjuan and Bates, 2011). The majority of HD animal models are mouse models, which can be divided in 4 groups, KO models, KI models, fragment transgenic mice and full-length transgenic mice.

1.10.1 Knock-out HD models

To assess the wildtype function of htt protein, *Htt* KO mice were generated by targeted ablation of the homologous mouse gene (Duyao *et al.*, 1995; Zeitlin *et al.*, 1995). Nullizygous mouse embryos show an increased apoptosis and lethality indicating an essential role of htt in development. Further experiments were done in the heterozygous *Htt* KO mice and revealed a decreased mRNA level of BDNF (Zuccato *et al.*, 2003), as well as neuron loss in the subthalamic nuclei and the globus pallidus, which is accompanied by an abnormal motor and cognitive behavior implying an anti-apoptotic function of htt (Nasir *et al.*, 1995).

1.10.2 Huntington knock-in mouse models

KI mice were generated by introducing an expanded CAG repeat stretch into the mouse *Htt* using a homologous strategy, thereby carrying the mutation in its appropriate genomic context as in HD patients. Five different KI mouse models were created expressing mouse htt with an expansion of polyQ repeats ranging from 50Q to 150Q (Shelbourne *et al.*, 1999; Wheeler *et al.*, 2000; Lin *et al.*, 2001), with 50Q leading to an adult age of onset in humans and 150Q being larger than the repeat size that would cause juvenile HD. These KI mouse models display a more severe neurological phenotype with increasing length of CAG repeats. However, even in the homozygous state of *htt*140CAG only mild abnormalities were observed including impaired motor function, reduced activity as well as aggregation of htt and increased

sensitivity towards NMDA (Menalled *et al.*, 2003), while the KI mice with 50Q present no distinguishable phenotype in comparison to wildtype mice (White *et al.*, 1997) mice present slowly progressive, mild behavioral changes and neuronal pathology, making them suitable to understand the early pathological events occuring in HD and to develop a strategy for delaying the onset of the disease. However with this mild phenotype, therapy studies using KI mice seem to be less suitable requiring a higher number of animals and might need a longer period of testing.

1.10.3 HD mouse models expressing truncated fragments of mhtt

Several HD mouse models expressing a truncated N-terminal fragment of htt with expanded polyQ stretches were created. The R6 lines were the first generated fragment HD transgenic mice, which carry exon 1 with 115-150 CAG repeats (Mangiarini *et al.*, 1996). These mice develop a robust progressive neurological phenotype of HD, especially the R6/2 mice carrying approximately 150 CAG repeats. R6/2 mice show a reduce life span, weight loss starting at 5 weeks of age, cognitive decline starting at 3-4 weeks of age and an impaired rotarod performance beginning at 4-8 weeks. Furthermore, striatal neuron loss and volume reduction were observed as well as predominantly nuclear aggregates is another crucial pathologic change in R6/2 mice (Mangiarini *et al*. 1996; Wang *et al.*, 2008; Menalled *et al.*, 2009).

A mouse line expressing a slightly larger htt fragment than R6/2 mice was generated by Schiling and coworkers. This mouse expresses the first 171 amino acids of htt under the control of the prion promoter showing a less abundant expression than endogenous htt (Schilling *et al.*, 1999). The transgenic line N171-82Q (carrying 82 glutamines) developed a neuronal pathology starting at 2 months of age. N171-82Q mice have a very short life span during which they suffer from a body weight loss, behavioral abnormalities including clasping, hyperactivity and gait changes. Neuropil and nuclear aggregates with accumulations of htt in the nucleus were found after immunohistochemical stainings (Schilling *et al.*, 1999). In a further study, a nuclear localization signal (NLS) was fused to the N171-82Q construct, resulting in a solely expression of the N-terminal mhtt fragment in the nucleus. Interestingly, this relocation of mhtt did not show any effect on NLS-N171-82Q mice, with the pathological phenotype in these mice being identical as in N171-82Q mice (Schilling *et al.*, 2004).

Mouse lines expressing the first 1 kb of human htt with normal (CD18) or expanded (HD46, HD100) polyglutamine tract were generated later. The line CD18 carrying 18 CAG repeats displayed a phenotype similar to wildtype littermates, while the other two lines HD46 and HD100 carrying 46 and 100 CAG, respectively, presented a progressive HD-like phenotype. HD100 mice exhibited abnormal behavior including clasping, hypoactivity, and a worsening in the performance on the rotarod. Pathological examinations revealed mhtt accumulation in the nucleus and cytoplasm accompanied by a formation of nuclear aggregates and striatal atrophy. HD100 mice also show an altered response to cortical stimulation and increased intracellular calcium levels after activation of NMDA receptors. In comparison, HD46 mice display a less severe change in behavioral abnormalities and neuronal pathology (Laforet *et al.*, 2001).

Overall, the mouse model expressing a htt fragment shorter than the fragment generated after caspase cleavage show a rapid early-onset of behavioral deficits, abundant htt accumulation and aggregation and a reduced life span. In contrast, the age of onset in mice expressing fragments with a size of one third of full-length htt is similar to the mice carrying full-length htt with the same CAG repeat number. These mice develop a relatively mild phenotype and normal life span. Notably, neurodegeneration was found in none of the fragment models.

1.10.4 HD models expressing full-length mhtt

The first mouse model expressing full-length human htt was generated using the htt cDNA (Reddy, 1998). With widespread expression of the transgenic htt in all brain regions, these mice presented a selective neuronal loss in striatum, cortex, thalamus and hippocampus, which is consistent with findings in HD patients. In all the transgenic lines carrying either 18 (HD18), 48 (HD48) or 89 (HD89) CAG repeats, both HD48 and HD89 lines developed a progressive neuronal phenotype, while HD18 preserved a normal phenotype similar to the wildtype situation. HD48 and HD89 develop progressive motor dysfunction, aggregation of htt, neurodegeneration and gliosis. Unfortunately, these lines are no longer available for research.

Michael Hayden's group has used artificial yeast chromosomes (YAC) to generate transgenic mice carrying the human genomic DNA sequence encoding for the full-length *HTT* (Hodgson *et al.*, 1999). One mouse line carrying 72Q expressed lower mhtt levels in comparison to the endogenous wild-type protein and developed a mild

neurological phenotype including hyperactivity, nuclear accumulation of mhtt, dark neurons as well as an altered electrophysiology in the hippocampus. Another YAC mice line expressing full-length mhtt was generated carrying 128 polyglutamines (Slow *et al.*, 2003). These mice presented an increased body weight, hyperkinesis at younger age followed by a hypokinesis at later stages of the disease, abnormal but not progressive performance on rotarod starting at 3 months of age (Menalled, 2010), abundant mhtt aggregates in the striatum and cortex as well as selective brain atrophy and neuron loss in striatum and cortex (Wang *et al.*, 2008). Remarkably, motor deficits in YAC mice were highly correlated with neuropathology (Slow *et al*., 2003). Additionally, Increased NMDA and NMPA were observed in YAC128 mice (Fan *et al.*, 2007; Fernandes *et al.*, 2007).

BACHD mice is another transgenic line expressing full-length human mutant htt. These mice were generated using a human bacterial artificial chromosome (BAC), which contains the full-length *HTT* genomic sequence with 97 CAG/CAA repeats and all regulatory elements (Gray *et al.*, 2008). BACHD mice exhibited an equal expression of mhtt in the striatum, cortex and cerebellum with a level of approximately 2.5 folds higher compared to endogenous mouse htt, and a selective brain atrophy and neuron loss in striatum and cortex. These mice showed an increased body weight, hypoactivity at later stage of the disease as well as a highly significant progressive motor decline starting at 4 weeks of age (Menalled *et al.*, 2010). A depressive-like and anxiety-like behavior was observed in a further study (Hult, 2010). A widespread formation of aggregates with selective neuronal loss and a reduction of synaptic activity in the striatum were observed in this model (Gray *et al.*, 2008,). Recent studies have shown reduced cortical excitatory output and thus a loss of inhibition onto pyramid cell signaling as well as synaptic degeneration in BACHD mice (Spampanato *et al.*, 2008; Shirendeb *et al.*, 2012).

In summary, mice expressing full-length htt possess increased body weight, hypoactivity as well as neurodegeneration, which is lacking in fragment models. Mild and progressive neuronal phenotypes in context of accurate replication of the human condition make them suitable for the understanding of pathogenesis in HD.

1.10.5 Large-animal HD transgenic models

Very recently, an ovine transgenic model was created by pronuclear injection of *HTT* cDNA with 73 CAG repeats under the control of the human huntingtin promoter

(Jacobsen *et al.*, 2010). Widespread expression was found in CNS and non-CNS tissues, but no information about the expression levels is available. Immunohistological investigations revealed a reduction in DARPP-32 (Dopamine- and cyclic-AMP-regulated phosphoprotein of molecular weight 32,000) positive cells in the caudate nucleus at 7 months of age. In the same year a miniature pig model carrying the first 208 amino acids of human htt with 105 polyQ repeats (N208-105Q) was published (Yang *et al.*, 2010). The transgene is expressed under the control of the cytomegalovirus enhancer and chicken beta-actin (CAG) promoter. Three of five newborn pigs died within 53 hours, while one lived for 25 days. The last animal did not show any abnormalities with up to four months of age, later time points have not been investigated so far. Typically, cell apoptosis and an increased number of caspase-3 positive cells were observed in the brains of N208-105Q pigs, while no aggregates were found.

Notable, one non-human primate HD model was developed carrying exon 1 of human htt (first 67 amino acids) by (Information einfügen), yielding five transgenic monkeys. One animal carried wildtype human htt with 29 CAG repeats, four monkeys expressed mutant human htt with 69-88 CAG repeats. Similar to the transgenic pigs, three out of four transgenic mhtt monkeys showed an early postnatal death, only the monkey expressing wildtype human htt and another one carrying mutant htt survived. The transgenic monkeys expressing mutant htt exhibited dystonia and chorea at young age, while the transgenic monkey with wild type htt displayed no disease-related phenotype. Abundant aggregates and nuclear accumulation of htt were demonstrated in striatum and cortex of monkeys that died postnatally and expressed mutant htt. However, no neurodegeneration was observed.

1.10.6 Transgenic rat model for HD

All the mendtioned HD animals including the HD transgenic mice and large animal models have made a great contribution to therapeutic studies and better understanding of the pathogenesis of HD. However, the suitablitity of mouse models is in general limited for studying certain functional and behavioural aspects, especially related to cognition. Large animals share the disadvantage of high cost in contrast to low reproductive output due to the difficulty for maintaining large colonies, as well as a long developmental period.

Rat models have made substantial contributions to our understanding of biological function and behaviour. Numerous rat disease models have successfully proven their utility for modelling the human condition (Hammer *et al.*, 1990; von Horsten *et al.*, 2003; Yamada *et al.*, 2004; Liu *et al.*, 2008). Although learning and memory can be studied with some restrictions in mice, the current scientific knowledge concerning the complexity of learning and memory, as well as the multiplicity of brain systems supporting it, has come largely from behavioural research using rats. Compared to mice (Report of the NIH rat Model Priority Meeting, 1999, http://www.nhibi.nih.gov/resources/docs/ratmtg.pdf), rats show excellent learning abilities, a mandatory requirement for the identification of the subtle cognitive deficits that may be present in the early stages of HD. Another practical advantage of rats is their larger brain size, which facilitates direct invasive procedures. In addition, miniaturized physiological *in vivo* approaches, such as structural and functional imaging of small brain structures, are more difficult in mouse models due to size limitations.

We have previously generated an HD transgenic rat line, which expresses a fragment of mutant human htt with 51 polyQ under control of a rat htt promoter (von Horsten *et al.*, 2003). These transgenic rats developed an abnormal performance on the rotarod, cognitive decline, as well as reduced anxiety behaviour. Aggregates of mhtt are abundantly distributed in striatum, amygdala, nucleus accumbens, the substantia nigra and the midbrain nuclei of optic and auditory pathways, but there was no direct sign of neurodegeneration found in this model (Nguyen *et al.*, 2006). This rat model mirrored many aspects of HD, but because of the lack of the full-length mutant htt (fl-mhtt) protein, certain aspects of the human disease would be imperfectlyreplicated.

Table 1.2: Advantages and disadvantages in different HD animal models

Model	Gene expression	Advantage		Disadvantage		Example
Knock-in mouse	Target insertion of CAG repeat into mouse *Htt*	appropriate genomic and protein context	Lower costs, short generation time	Mild phenotype, slow disease progression, therapy studies less feasible	small body size, aggressive behavior, not well suited for cognitive tests	HdhQ50 (White *et al*., 1997); HdhQ111 (Wheeler *et al*., 2000); Hdh150 (Lin *et al*., 2001); HdhQ140 (Manelled *et al*., 2003)
Fragment mouse	Transgenic expression of N-terminal fragment of human mutant *HTT* in mouse	clear and early onset of behavioural abnormalities, fast progression, premature death		unspecific neuronpathology, no neuron loss		R6/2, R6/1 (Mangiarini *et al*., 1996); N-171-82Q (Schilling *et al*., 1999);
Full-length mouse	Transgenic expression of full-length human mutant *HTT* in mouse	present both altered behaviour and neuropathological changes including cell death				YAC 72 (Hodgson *et al*., 1999); YAC128 (Slow *et al*., 2003)
Ovine	Transgenic expression of mutant *HTT* in mouse	anatomically closer to human brain	Large body size make them suitable for imaging measurement	Working methods need to be established	Long life span, higher living costs, lower reproductivity, and ethical concerns	HTT-73Q (Jessie *et al*., 2010)
Pig	Transgenic expression of mutant *HTT* in mouse					N208-105Q (Yang *et al*., 2010)
Non-human primate	Transgenic expression of mutant *HTT* in monkey	Biologically, neurologically, physiologically and immunologically closer to human brain				rHD-2, rHD-3, rHD-4, rHD-5 (Yang *et al*., 2008)
Fragment rat	Transgenic expression of N-terminal fragment of mouse mutant *Htt* in rat	Relatively large body size and suitable for cognitive tests, lower living costs and higher reproductivity compared to large animal models		Lacks full-length human htt		tgHD-51Q (von Horsten *et al*., 2003)

2. Objectives of this study

The general goal of the present study was to generate and characterize a transgenic rat model of HD expressing full-length human mutant htt to fill the gap occurring in HD models for therapeutic studies and understanding of HD pathogenesis. Mouse models are limited by a small brain size and their limited ability to perform cognitive tasks, whereas large-animal models have a low reproductivity and long lifespan, which makes therapeutic studies less feasible and at a higher cost. So far, the only existing rat HD model carries an N-terminal fragment of htt and therefore lacks the entire context of a full-length htt protein in human patients.

The initial point of this work was to establish transgenic rat lines (BACHD rats), which have a stable germ-line transmission of the transgene with a high protein mhtt expression level. The subsequent object was to assess whether BACHD rats recapitulate clinical features and neuropathological changes at different ages as seen in human HD.

The specific goals of this study were as follows:

- To generate and select transgenic lines for further characterization based on confirmation of a single integration site, high expression levels of full-length htt mRNA and protein.
- To assess the degree, onset and progression of impairments and symptoms in rats. Accordingly, assess motor function, cognitive function and psychiatric changes using behavioral tests.
- To determine aggregation of mhtt and neurodegeneration by apoptosis assay, electron microscopy, caspase and calpain activity and analyze gliosis in transgenic rats.
- To analyze the transcriptome in brains of transgenic rats in comparison with human HD data, especially considering changes in mRNA level of BDNF.
- To determine synaptic plasticity using pre- and post-synaptic markers.
- To assess metabolic abnormalities including feeding, activity, and body weight as well as lipid and glucose metabolism in transgenic rats

3. Materials and methods

3.1 Materials

3.1.1 Oligonucleotides

All oligonucleotides (primers) used in this thesis were synthesized by Metabion (Germany) in a concentration of 100 mM. For usage, oligonucleotides were diluted into various concentrations, especially for real-time PCR. The amount of primers was optimized until efficiency of amplification was between 1.9 and 2.0. For mRNA quantification, the target genes and reference genes were amplified in the same plate, thus the annealing temperatures of reference genes were validated according to the target gene. For all DNA analyses including genotyping, transgene copy number estimation, fragment analysis, and sequencing, primers in Table 3.1 were used. For mRNA expression levels analysis including mRNA of mhtt expression level, alternative splicing variant of htt as well as mRNA transcription level of BDNF, primers in Table 3.2 were used.

Table 3.1: Oligonucleotides used for DNA analysis

Target	Code	Sequence of primers	AT (°C)	Concentration to use (µM)
Exon 1 of HTT and Htt	A898	ATGGCGACCCTGGAAAAGC	60	10.0
	A899	AGGTCGGTGCAGAGGCTCCTCTG		10.0
Exon 67 of HTT	C121	TGTGATTAATTTGGTTGTCAAGTTTT	58	10.0
	C122	AGCTGGAAACATCACCTACATAGACT		10.0
Intron 29 of HTT	A956	ACCGACCTTCTGAAGCCTACTTCT	60	2.0
	A957	TTCTCCTCCAAAGGATCACAACTC		2.0
	B005	5'FAM-CTAAGTGGCGCTGCGTAGTGCGAA-3'Bhq		2.0
Exon 2 of ß-Actin	A924	AGCCATGTACGTAGCCATCCA	60	4.0
	A925	TTCTCCTCCAAAGGATCACAACTC		4.0
	A926	5`FAM-CTAAGTGGCGCTGCGTAGTGCGAA-3`Bhq		4.0
Exon 1 of HTT	3787	5`Cy5'-GAT GAA GGC CTT CGA GTC CCT CAA GTC CTT CT	60	10.0
	3788	CGG CTG AGG CAG CAG CGG CTG T		10.0

Table 3.2: Oligonucleotides used for mRNA analysis

Target	Code	Sequence of primers	AT (°C)	Concentration to use (µM)
Exon 12 and13 of HTT and Htt	A779	ATCTTGAGCCACAGCTCCAGCCA	60	2.0
	A780	GGCCTCCGAGGCTTCATCAGG	60	2.0
	A781	TCTGAAAACGTCTGAGACTTCACCAG A	60	2.0
BDNF I	I629	CCAGGACAGCAAAGCCACAATGT	56	3.0
BNDF IIa	I631	GCAAGCTCCGGTTCCACCAGGT	56	2.0
BDNF V	I633	GGACCGGTCTTCCCCTAGAGCA	56	2.0
BDNF VI	I634	TGGACCCTGAGTTCCACCAGGT	56	3.0
BNDF total	H449	AGCGCGAATGTGTTAGTGGT	60	1.2
	H450	GCAATTGTTTGCCTCTTTTTCT		1.2
Exon 31, 32 of HTT-001 and HTT-011	J034	GCAGGAGAACGACACCTCGGG	60	2.0
	J035	TCGTGCTTCCACCAACGACAGC		2.0
	J036	GCACGGTTCTTTGTGACACTCGTG		2.0
ATP5B	H451	GGGTACAATGCAGGAAAGAATC	variable according to target gen	1
	J094	GGGTACAATGCAGGAAAGAATC		1
CanX3	H453	TGTCTGGCAGCGACCTATGATTGA		1.2
	H454	TCCTTGGTTTCCAGATTCCCTGGT		1.2
Eif4a2	H455	AAATGCATGCCAGGGACTTCACAG		1
	H456	TTGTTGCACATCAATCCCACGAGC		1

3.1.2 Enzymes and kits

Table 3.3: Enzymes and kits used

Enzymes/Kits	Manufacture
BioThermTM DNA Polymerase 1000 U 5 U/µl	GeneGraft
DNase	Sigma-Aldrich Chemie
Proteinase K	Roche Diagnostics GmbH
CEQ 2000 Dye Terminator Cycle Sequencing Kit	Beckman-Coulter
High Pure PCR Template Preparation Kit Roche	Roche Diagnostics GmbH
In Situ Cell Death Detection Kit, TMR red	Roche
LightCycler 480 Probes Master	Roche
Nuclear Extract Kit	Active Motif
QIAquick Gel Extraction Kit	Qiagen
QuantiTect ReverseTranscription Kit	Qiagen
QuantiTect SYBR Green PCR Kit	Qiagen
RNeasy Mini/Midi/Large Kit	Qiagen
Vectastain ABC Elite	Vector Laboratories

3.1.3 Gels and buffers ready to use

It is difficult to present the loading control α-tubulin and proteins of interest with large sizes (>200 kDa) in the same gel, especially for full-length htt, thus gradient gels were used, as well as appropriate running buffer.

NuPAGE® Novex 3-8% Tris-Acetate Gel	Invitrogen
NuPAGE® Tris-Acetate SDS Running Buffer (20X)	Invitrogen
Q-Solution	Qiagen
ECL / ECL-Plus Western Blotting Detection Reagents	GE Healthcare
Samples loading buffer for Sequencing	Beckman Coulter

3.1.4 DNA and protein markers

For the DNA and protein analyses the following markers were used.

100 bp DNA-Ladder	Invitrogen
HiMarker Pre-Stained Protein Standard	Invitrogen
Precision Plus Protein TM Dual Color Standard	Bio-Rad Laboratories GmbH

3.1.5 Membranes and papers

For Western blot Nitrocellulose membranes and Whatman-Paper were used as follows:

Nitrocellulose membrane (Optitran BA-S 83)	Schleicher & Schuell, Dassel, D
Whatman-Paper (GB002)	Schleicher & Schuell, Dassel, D

3.1.6 Antibodies

In Table 3.4, and Table 3.5 all primary antibodies and secondary antibodies used for Western blot, immunohistochemistry and immunofluorescence staining were summarized with working concentrations and manufacturer.

Table 3.4: Primary antibodies and secondary antibodies used for Western blot (WB), immunohistochemistry (IHC) and immunoflorescence (IF)

Antibody	Host	Concentration WB	Concentration IHC/	Concentration IF	obtained from
MAB 2166	mouse	1:2000			Millipore
MAB2168	mouse	1:2000			Millipore

2B7	mouse	1:2000			Novartis Pharma AG
EM48	mouse		1:200		Millipore
S830	sheep		1:15,000		Millipore
Anti Iba-1	rabbit	1:5,000	1:7,000		Wako
Anti-Ferritin light chain	rabbit	1:3,000	1:5,000		Abcam
GFAP	rabbit	1:10,000	1:4,000		Dako Cytomation
NeuN	mouse		1:600		Millipore
Monoclonal anti-DARPP32	rabbit	1:2000	1:100,000		Epitomics
Anti-Tyrosine Hydroxylase	rabbit		1:4000		Millipore
Anti-PARP	rabbit		1:3000		Promega
Anti-cleaved Caspase-3	rabbit	1:2000	1:5000		Cell signaling
Anti-Caspase-6(Mch2)	rabbit	1:2000			Biomol
Anti-Calpain 2	rabbit	1:1000		1:300	abcam
Anti-Calpain 10	rabbit	1:1000		1:300	abcam
Spectrin alpha chain (brain) SPTAN1 Antibody	mouse	1:3000			Acris antibodies
Anti-NMDA-receptor 2B Polyclonal antibody	rabbit	1:2000			Invitrogen
PSD-95, mAb (7E3-1B8)	mouse	1:2000			Enzo life science GmbH
Anti-Synapsin Ia/b	rabbit	1:1000			Santa Cruz
Anti-Synaspsin IIa	rabbit	1:1000			Santa Cruz

Table 3.5: Secondary Antibodies used for Western blot (WB), immunohistochemistry (IHC) and immunoflorescence (IF)

Antibody	Use	Concentration	Manufacturer
Sheep anti-mouse IgG-HRP	WB	1:4000	Amersham Biosciences
Donkey anti-mouse IgG-HRP	WB	1:5000	Amersham Biosciences
Donkey anti-goat IgG-HRP	WB	1:5000	Santa Cruz
Biotinylated donkey anti-mouse rat adsorbed	IHC	1:500	Vector Laboratories
Biotinylated goat anti-rabbit IgG	IHC	1:1000	Vector Laboratories
Biotinylated rabbit anti-sheep IgG	IHC	1:1000	Vector Laboratories
Donkey Anti-rabbit IgG (488)	IF	1:300	Dianova

3.1.7 Buffers and solutions

For Western blot the following buffer and solutions were used.

HEPES buffer (pH=7.0)	HEPES	50 mM
	NaCl	150 mM
	EDTA	10 mM
	NP-40	1 %
	Deoxycholate	0.5%
	SDS	0.1 %
	BSA	1 %
5x Laemmili buffer	Tris-HCl pH 6.8	62.5 mM
	ß-Mercaptoethanol	5%
	Glycerin	10%
	SDS	2%
PAGE	Glycin	192 mM
	Tris base	25 mM
	SDS	0.1%
TBST buffer	Tris base pH 7.5	10 mM
	NaCl	150 mM
	Tween 20	0.1%
Transfer buffer	Tris base pH 7.5	25 mM
	Glycine	192 mM
	Methanol	10-20%

For immunohistochemistry and immunofluorescence the following buffer and solutions were used.

PBS (pH 7.4)	Na2HPO4	10 mM
	KH2PO4	2 mM
	NaCl	137 mM
	KCl	2.7 Mm
TBST (pH 7.4)	Tris-HCl	25 mM
	NaCl	137 mM
	KCl	2.7 mM
	Triton-100X	0.4%
BT buffer (40 ml)	sulfosuccinimidyl-6-(biotinamide) hexanoate	100 mg
	tyramine	32 mg
	Sodium borate pH 8.0	50 mM
TI buffer (pH 7.2)	Tris	50 mM
	Imidazol	
Substrate Buffer (pH 7.4)	Tris	50 mM
	Imidazole	50 mM
	NiSO4.6HaO	0.6%
Thionin Acetate (pH 4.8)	Thionin acetate	0.003%
	Sodium acetate	100 mM
	Actetic acid	80 mM
Mounting Medium for DAB stained sections (pH 10.0)	NH4HCO3	80 mM
	Gelatin	0.02 %
Mounting Medium for	NH4OAC	80 mM

Nissel staining (pH 7)	EthOH Gelatin	20 % 10%

3.1.8 Regularly used equipment and chemical reagents

Table 3.6: Regularly used equipment

Equipments	Manufacturer
700 MHz NMR spectrometer	Brucker BioSpin
8-capilar-sequencer CEQ 800	Backman Coulter
Accelerated rotarod for rats 7750	Ugo Basile
AxioCaMHR-Camera	Carl Zeiss
Axioplan 2 imaging microscopy	Carl Zeiss
Bath Sonicator	Bandelin Sonorex Biotechnique
BioPhotometer	Eppendorf
Centrifuge 5415R (Rotor F45-24-11)	Eppendorf
Concentrator 5301	Eppendorf-Netheler-Hinz GmbH
Consort Electrophoresis Power Supply E385	Sigma Aldrich
Electrophoresis Chamber for agarose gel	PEQLAB Biotechnologie GmbH
Electrophoresis Chamber for SDA-PAGE	Invitrogen
Electrophoresis Chamber for SDA-PAGE	PEQLAB Biotechnologie GmbH
Embedding equipment TP1020	Leica
GenAmp PCR Systems 9600	Applied Biosystems GmbH
Horizontal 7 T magnet	Magnex Scientific Ltd.
Light Cycler 480 instrument	Roche
Linear RF volume-coil	Rapid Biomedical GmbH
Microtom RM 2155	Leica Instruments
Microwave	LG Electronics Deutschland GmbH
Milli-Q	Millipore GmbH
MJ Research PTC-200 Peltier Thermal Cycler	Biozym Diagnostics GmbH
Perfluoropolyether	FOMBLIN® LC08, Solvay Solexis
PET scanner	Siemens Preclinical Solutions
PhenoMaster system	TSE
pH-Meter MP 230	Mettler, Toledo
Skinner Boxes 259900-SK-RAT-LA/1	TSE
Thermomixer 5436	Eppendorf
Tissure homogeniser (model T25)	Janke und Kunkel GmbH, Ika-Labortechnik,Co. KG

Table 3.7: Regularly used chemical reagents

Chemical reagent	Manufacturer
29:1 Acrylamid; N,N`-Methylen-Bisacrylamid	Bio-Rad Laboratories GmbH
Agarose	Invitrogen GmbH
Ampuwa Water	Fresenius Kabi
BioThermTM 10x buffer	GeneCraft
Sulfosuccinimidyl-6-(biotinamide) hexanoate	Pierce
Boric acid	Carl Roth GmbH
Bromphenolblau	Sigma-Aldrich Chemie
BSA (100x BSA 10 mg/ml)	New England Biolabs GmbH
Cacodylate	Sigma-Aldrich Chemie
Chromium Potassium Sulfate	Sigma-Aldrich Chemie
Complete Protease Inhibitor Cocktail tables	Roche Diagnostics GmbH
CV-Mount	Leica
Dabco	Sigma-Aldrich Chemie
DAPI	Sigma-Aldrich Chemie
Deoxycholate	Sigma-Aldrich Chemie
Developer G135	Agfa-Gaevert NV
Diethyl pyrocarbonat (DEPC)	Sigma-Aldrich Chemie
DMSO	Sigma-Aldrich Chemie
dNTP Solution 25µmol	Invitrogen GmbH
Acetic acid	Merck KGaA
Ethanol	Merck KGaA
Ethidiumbromid 1%	Sigma-Aldrich Chemie
Ethylendiamin tetraacetic acid (EDTA)	Sigma-Aldrich Chemie
Fetal Calf Serum (FCS)	GIBCOTMInvitrogen GmbH
Rodent purified Diet (259901-PEL-45)	TSE
Gelatin	Sigma-Aldrich Chemie
Glycerin	Carl Roth GmbH
Glycine	Carl Roth GmbH
Glycogen	Invitrogen GmbH
HEPES	Sigma-Aldrich Chemie
Igepal CA-630(NP-40)	Sigma-Aldrich Chemie
Imidazol	Sigma-Aldrich Chemie
Ketamine	Bela-Pharm GmbH
KCl	Merck KGaA
Magermilchpulver Naturaflor	Töpfer GmbH
Methanol	Merck KGaA
Mowiol 4-88	Merck KGaA
NaCl	Merck KGaA

NaOAcetat	Merck KGaA
NaOH	Carl Roth GmbH
NH4HCO3	Sigma-Aldrich Chemie
NH4OAC	Merck KGaA
NiSO4.6HaO	Sigma-Aldrich Chemie
Normal donkey serum	Dianova GmbH
Paraformaldehyd	Merck KGaA
Protein Assay	Bio-Rad Laboratories GmbH
RNase free Water	Affymetrix, Inc.
SDS (Sodium Dodecyl Sulfat)	Carl Roth GmbH
Sodium acetate	Carl Roth GmbH
Sodium borohydride	Merck KGaA
Sulfosuccinimidyl-6-(biotinamide) hexanoate	Pierce
ß-Mercaptoethanol	Sigma-Aldrich Chemie
TEMED	Carl Roth GmbH
Thionin acetate	Sigma-Aldrich Chemie
TritonX-100	Carl Roth GmbH
Trizma®base	Sigma-Aldrich Chemie
Tween20	Merck KGaA
Tyramine hydrochloride	Sigma-Aldrich Chemie
Xylazin	Albrecht GmbH
Xylene	BDH prolabo international GmbH

3.2 Methods

3.2.1 Generation of transgenic rats

Bacterial artificial chromosomes (BACs) containing human genomic DNA spanning the full-length *HTT* gene with 97 CAG/CAA repeats and including all regulatory elements (Gray *et al.*, 2008), were microinjected into the pronucleus of oocytes of Sprague–Dawley rats.

3.2.1.1 Genotyping and determination of BAC transgene integrity

Genotyping and determination of BAC transgene integrity were performed via PCR analysis using genomic DNA extracted from ear biopsy tissue using High Pure PCR Template Preparation Kit. Two primer pairs were designed, one pair binding to exon 1 of both endogenous *Htt* and exogenous mutant *HTT* with different amplicons lengths of approximately 200 bp and 5000 bp (code: A898/A899, Table 3.1), while the second primer pair binds specifically to the last exon of the *HTT* transgene producing an approximately 200-bp amplicon (code: C121/C122, Table 3.1). PCR was carried out as described in Table 3.8.

Table 3.8: Standard PCR for genotyping

Reaction mix of PCR (total 25 µl)		**Thermo-cycler-program**		
Reagent	Volume (µl)	Target (°C)	Hold (hh:mm:ss)	Cycler
PCR-buffer (10x)	2.5	94	00:05:00	1
Q-solution (5x)	5.0	94	00:00:30	40
dNTPs (10 mM each)	0.8	60/58 (Exon1/Exon 67)	00:00:30	
Taq-polymerase	0.25	72	00:01:00	
primer mix	2.0	72	00:05:00	1
H_2O	12.45	10	Indefinitely	1

3.2.1.2 Transgene copy number and number of integration sites

To estimate relative transgene copy number of the BAC insertion and number of integration sites, probe-based real-time PCR (*TaqMan* PCR) was performed using genomic DNA. For the *TagMan* PCR, an oligonucleotide probe containing a reporter fluorescent dye on the 5' end and a quencher dye on the 3' end is designed to hybridize to the DNA sequence between the PCR primers. Amplification of target sequence results in cleavage of the probe by the 5' nuclease activity of the *Taq* DNA polymerase, thereby the reporter dye and quencher dye are separated leading to an increase of report signal. A two-step PCR was designed to achieve that annealing

and elongation were carried out at 60 °C for both primers, while the probe annealing temperature was 10 °C higher at 70 °C. Briefly, primers and probe were designed to bind specifically to intron 29 of the *HTT* transgene (code: A956/A957/B005, Table 3.1). The Ct values of all samples were normalized to β-actin serving as reference gene. The relative copy number of transgene for all F1 rats was compared within and between each line. Reaction mix and thermo cycler program are presented in Table 3.9 and 3.10.

Table 3.9: Reaction Mix for TagMan PCR with a total volume of 20 µl

Reagent	Concentration	Volume (µl)
Master Probe Mix	2 X	10.0
Primer Mix of target gene	2 µM each	1.0
Probe of target gene	1 mM	1.0
Primer Mix of reference gene	4 mM each	1.0
Probe of reference gene	2 mM	1.0
H_2O		4.0

Table 3.10: Thermo-cycler program for TagMan PCR

Step	**Target (°C)**	**Hold (hh:mm:ss)**	**Ramp rate (°C/s)**	**note**
Denaturation	95	00:15:00	4.6	
Amplification	94	00:00:15	2.5	45 repeats
	60	00:01:00	2.4	
Melting	95	00:00:15	4.6	
	65	00:00:20	2.4	
	95	-	0.04	Acquisitions: 15°C
Cooling	40	00:00:30	2.0	

3.2.1.3 Analysis of the CAG-CAA repeats length in BACHD rats

In order to verify the conservation of the polyQ repeat length, we analyzed the PCR fragment length of DNA samples extracted from 100 peripheral nerve tissues and different brain regions. DNA extractions were performed as described before and rat samples were collected considering different rat generations, gender and ages of the rats. PCRs were carried out employing a Cy5 labeled forward primer and a reverse primer (code: 3787/3788, Table 3.1) amplifying a fragment of *HTT* exon 1 including the CAG-CAA repeats. The fragment lengths of the amplicons were determined and analyzed using the fluorescence-based capillary electrophoresis sequencer

CEQ8800 and genetic analysis system software in a complete set from Beckman Coulter. CAG-CAA repeat numbers were calculated according to the individual fragment length and the human *HTT* sequence published on the NCBI database.

3.2.1.4 Sequencing of DNA sequence containing CAG-CAA repeats

Sequencing of the CAG-CAA repeats containing region in ex*on* 1 was performed amplifying DNA using the same primers as for the fragment analysis, which hybridize upstream and downstream of the CAA-CAG region, respectively (code: 3787/3788, Table 3.1). PCR reaction mix and thermo-cycler program was the same as the genotyping standard PCR for exon 1 (Table 3.7). PCR products were purified using QIAquick Gel Extraction Kit according to the manufacturer's instruction.

Sequencing reactions were performed on the 8-capilar-sequencer CEQ 800 using the MJ Research PTC-200 Peltier Thermal Cycler and Quick Start Kit. Two primers for the PCR reaction were employed for bidirectional reading of the CAG repeats region of mhtt (code: 3787/3788, Table 3.1), respectively. After the thermal cycling program was finished reaction (10 µl) was stopped with 5 µl Stop-Mix consisting of 2 parts 3M Sodium Acetate (pH 5.2), 2 parts 100 mM Na_2-EDTA (pH 8.0) and 1 part 20mg/ml glycogen; adding 60 µl ice cold 100% ethanol resulted in DNA precipitation. Following centrifugation (13.000 rpm at 4 °C) for 30 minutes pellets were rinsed twice with 70% ethanol and centrifuged at the same condition for 15 minutes. After each rinse the supernatant was removed. The remaining ethanol was removed on low heat for 30 minutes in Concentrator 5301, and then resuspended in 40µl sample loading buffer to sequence.

Table 3.11: Sequencing reaction

Sequencing reaction Mix		Thermal Cycler		
Reagent	Volume(µl)	Hold	Target (°C)	Cycler
H_2O	3	90 sec.	94	1
purified PCR product	3	20 sec.	96	31
Primer	1	20 Sec.	50	
DTCS (Quick Start Master Mix)	3	4 min.	60	
		Indefinitely	10	1

3.2.2 RNA analysis

3.2.2.1 mRNA isolation and cDNA synthesis

Total mRNA was extracted from whole brain (for htt mRNA expression) or brain regions (for BNDF expression and HTT alternative splicing) using the RNeasy Lipid Tissue Midi/middle/Large Kit and cDNA was synthesized using a QuantiTect Reverse Transcription Kit following manufacturers' instructions.

3.2.2.2 Quantification of cDNA

Real-time PCR using QuantiTect SYBR Green PCR Kits were performed for the analysis of htt mRNA expression levels from each line, alternative splicing variations of htt as well as BDNF mRNA expression. Absolute quantification of cDNA was performed using the Light Cycler 480 instrument with the aid of built-in Light Cycler software. A general reaction mix (Table 3.12) and Thermo-cycler-profiling (Table 3.13) were designed for all the real-time PCRs with variations of annealing temperature and concentration of primers (Table 3.2). The annealing temperature of the reference gene was adapted from the target gene, as both were amplified on the same plate. For the assessment of mutant htt expression level, endogenous htt and β-actin were used as reference gene, the other real-rime PCRs used ATP5B and Cnx3 in cortex, ATP5B and Eif4a in striatum, and CnX3 and Eif4a in cerebellum as reference genes.

Table 3.12: Reaction mix (total 10 µl each sample) for SYBR Green real-time PCR

Component	Volume (µl)
SYBR Green mastermix (2x)	5
Primermix (variable concentration)	1
cDNA Template	2
H_2O	1

Table 3.13: Thermo-cycler program for SYBR Green real-time PCR

Step	Target (°C)	Hold (hh:mm:ss)	Ramp rate (°C/s)	Note
Denaturation	95	00:15:00	4.6	
Amplification	94	00:00:15	2.5	45 repeats
	variable	00:00:40	2.4	
	72	00:00:20	4.6	
Melting	95	00:00:15	4.6	
	65	00:00:20	2.4	
	95	-	0.04	Acquisitions: 15°C
Cooling	40	00:00:30	2.0	

All primers of mRNA were designed spanning exon-exon junction. For the analysis of mRNA level of htt in different lines one common forward primer for human htt and endogenous rat htt were designed hybridizing to exon 12, and reverse primers with individual sequences binding to exon 13 of human and rat htt, respectively.

For the assessment of BDNF mRNA expression, one common reverse primer hybridizing to the protein encoding sequence in the last exon was used for the quantification of total BDNF and all isoforms. Forward primers in exon I, II, IV, VI for the specific isoforms and in exon IX for total BDNF were designed individually (Figure 3.1).

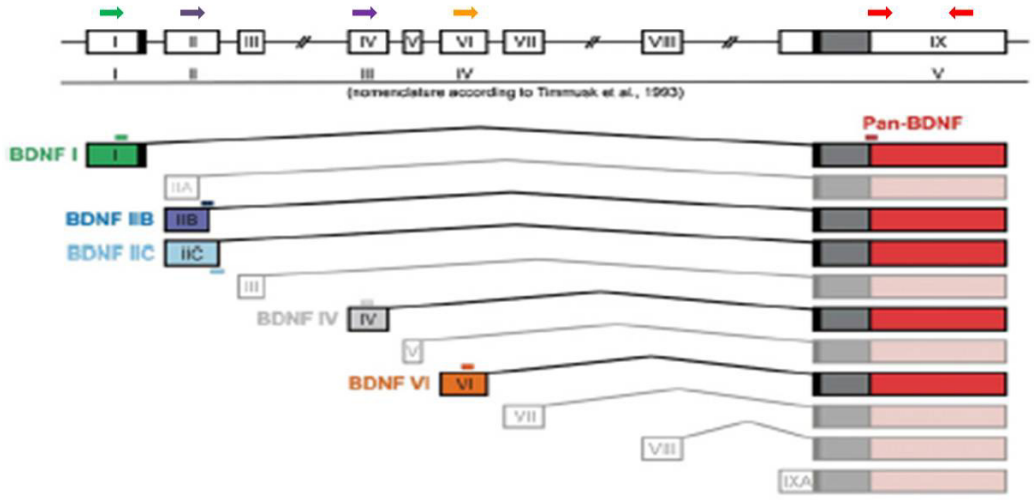

Figure 3.1: Primer design for the analysis of BDNF mRNA. Arrows on top represented with different colors indicate hybridizations position of primers for specific isoforms. (modified according to Chiaruttini et al., 2007)

Two protein encoding splicing variants of the htt mRNA have been identified and listed in the Ensemble Genome Browser so far (HTT-001, transcript ID: ENST00000355072 and HTT-011, transcript ID: ENST00000509618). The longer one (HTT-001) includes all 67 exons encoding for the full-length huntingtin, the smaller one (HTT-011) consists only of 3 exons, the last 31 bases of exon 29, exon 30 and 31 as well as the 96 bases of the following intron 31-32. A forward primer was designed to bind to both transcripts in exon 31 of HTT-001 and reverse primers were chosen to bind specifically to each variant (code: J034/J035/J036, Table 3.2). For HTT-001, the reverse primer binds to exon 32 whereas for HTT-011, the primer was directed against a region within the last 96 nucleotides. Brain samples from the striatum, the cortex and the cerebellum were taken for analysis.

3.2.3 Protein analysis

3.2.3.1 Preparation of protein lysates

Brain regions of rats were homogenised with a tissue homogeniser at a speed of 30,000 rpm for 30 seconds in 10 volumes (w/v) modified HEPES buffer with Complete Protease Inhibitor Cocktail tablets. After a further 5-minute sonication with a bath sonicator for shearing genomic DNA, the lysates were centrifuged at 4 °C for 15 min at 16,200xg, and the supernatant was removed and stored at -80°C for non-fractionated Western blot analysis. In order to detect full-length and fragment htt level in nuclear and cytoplasmic fractions at different ages, subcellular fractions were prepared using Nuclear Extract Kit following manufacturers' instructions.

3.2.3.2 Western blotting

For Western blot analysis, protein samples were prepared incubated in Laemmli sample loading buffer for 10 minutes at 70 °C (target protein > 200 kDa) or for 5 minutes at 96°C (target protein < 200 kDa) and subsequently subjected to electrophoresis in 3-8% Tris-Acetate NuPAGE gels or in SDS-containing polyacrylamide gels running in Tris-Acetate running buffer or PAGE buffer. Wet-transfer of protein onto nitrocellulose membrane was performed with transfer buffer containing Tris-glycine and methanol according to protein size (10% for protein > 200 kDa, 20% for protein < 200 kDa). Blots were blocked in TBST buffer containing 5% milk powder, then incubated in primary antibody and appropriate HRP-conjugated secondary antibody. Finally, blots were developed with ECL/ECL plus.

Table 3.14: Composition of separating and stacking gel

Composition of 5 ml separating gel (µl)		Composition of 2 ml 4%stacking gel (µl)	
ddH_2O	variable	ddH_2O	1130
29:1 Acrylamid/Bisacrylamid	variable	29:1 Acrylamid/Bisacrylamid	333
1.5 M Tris base (pH=8.8)	1300	0.5 M Tris base (pH=8.8)	500
10% SDS	50	10% SDS	20
10% APS	50	10% APS	15
TEMED	4	TEMED	5

3.2.4 Morphology-based analysis

3.2.4.1 Immunohistochemistry

Rats were deeply anesthetised with ketamine/xylazin (100/10 mg/kg i.p.) and transcardially perfused with 4 % paraformaldehyde in 0.1 M sodium cacodylate buffer (pH 7.4), followed by post-fixation of the brains in the same fixative over night.

For lightmicroscopical immunohistochemistry 16 rat brains were embedded in one gelatin block, 40 µm coronal sections were freeze-cut and collected into 24 series (Figure 3.2) (This work was done by NeuroScience Associates, USA). One or more series were taken for each staining and the entire series was stained together in one container so that all sections received the exact same staining conditions for all steps. Free-floating staining was performed as previously described (Osmand *et al.*, 2006). Sections were pretreated with 0.5% Sodium borohydride in PBS for 30 minutes. After permeabilization by 0.4% Triton X-100 in TBS buffer for 50 minutes the sections were incubated with primary antibody over night followed by the respective secondary antibodies for 2 hours. Then sections were treated with an avidin-biotin-peroxidase complex for 1 hour, and exposed to nickel-DAB-H_2O_2 dissolved in substrate buffer until a suitable staining intensity had developed. TI buffer containing imidazole was used to enhance staining quality. S830 staining was routinely amplified using a single round of biotinylated tyramine (BT buffer) amplification prior to the final ABC step. Sections were mounted in mounting medium for DAB stained sections. All steps were performed at room temperature. Thionin acetate was used for counterstaining, 2 series of sections at 12 months of age (#1 and #12) were evaluated by nissel staining using thionin acetate as well. Numerous protein markers were used once or at ages of the rats for immunohistological stainings depending on the time points when changes in the expression of those markers were expected . Table 3.15 summarizes which number of the series have been used for the staining of a certain protein marker at the indicated time points. (Table 3.15).

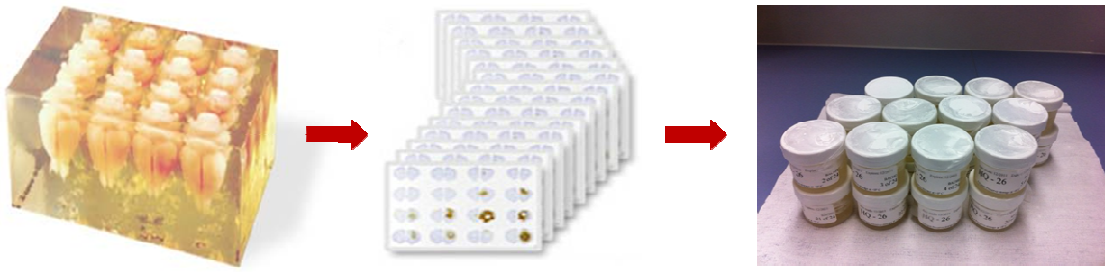

Sixteen rats brain embeted in one gelatin

40 µm coronal sections freeze-cuted

Sections collected into 24 serieses

Figue 3.2: Working flow of sectioning rats brain in the company NeuroScience Associates. (modified according to the home page of NeuroScience Associates).

Table 3.15: Several series of brain sections were used for immonohistological staining

Protein marker	Respect	3 m	6 m	9 m	12 m	15 m	18 m
Iba-1	Microglia				#21		#7
Ferritin	Microglia					#6,#14,#22	#6, #14
GFAP	Astrocyse				#15	#4,#16	#4
MBP	Myeling sheath	½#8	#10	#10		#10	½#8, #10
Human htt	Aggregates of mhtt	#2		#2,#8	#5, #17	#2,	
DARPP32	MSNs				#2, #6	#3,#11,#19	
NeuN	all Nuerons	½#8				#8	½#8
PARP	Apoptosis					#24	#2
Act caspase 3	Apoptosis				#20	#5	#19
TH	Tyrosine Hydoxylase containing Neurons				#18		
Enkephalin	Neurons expressing Enkephalin		#12	#12		#12	
DR2	Dopamine production	#15		#15			#11, #15,#24
Calbindin D-28K	Neurons expressing Calcium-binding protein	#24	#2		#11	#20	
ChAT	Choline acetyltransferase sythesing Neurons				#23		

3.2.4.2 Immunofluorescence staining

For immunofluorescence staining, either cryosections or paraffin sections were used. Cryosections were pre-mounted on superfrost plus slides, while paraffin sections were deparaffinized in xylene, and rehydrated in graded alcohol baths. In the following steps, the sections were permeabilized by 0.3% Triton X-100 in TBS for 10 minutes and blocked with 5% appropriate serum (depending on species of secondary antibody producer) for 30 minutes at room temperature. Incubation of both primary and secondary antibodies were performed at 4 °C overnight and 2 hours, respectively. Finally, 4' 6-diamidino-2-phenylindole (DAPI) at a concentration of 0.2 µg/ml was used for nuclear counterstaining.

3.2.4.3 Light microscopy analysis

Images were taken using an Axioplan 2 Microscope with a digital camera and imaging acquisition software (AxioVision-6, Zeiss). Quantification was performed using ImageJ (National Institutes of Health).

3.2.4.4 Quantitative assessment of morphological changes in the striosome compartment

Calbindin immunostaining of rats at 6 months of age was used (TG5:TG9:WT = 5:4:5) to perform a relative quantification of the striatal striosome compartment. Four striata of each rat were measured in coronal 40µm thick brain sections between Bregma 1.44 and -0.24 mm (Paxinos and Franklin, 2006). The striatum was outlined medially adjacent to the lateral ventricle, dorsolaterally below the corpus callosum and ventrally by a line through the ventral tip of the ventricle as the region of interest (ROI) using ImageJ. The striosomal area was determined within the ROI by outlining the faintly stained calbindin areas. The rater was blind to the rats´ genotype.

3.2.5 TUNEL staining

For the detection of apoptotic cells in BACHD rats' brain, terminal deoxynucleotidyl transferase-mediated dUTP nick end-labeling (TUNEL) staining was performed using a TMR red *in situ* cell death detection kit following manufacturer's instruction at 18 months of age (TG5:TG9:WT = 6:5:5). As a negative control one section underwent the same treatment using all the reagents except for terminal transferase. One P1-rat-brain section and one section pretreated with 1mg/ml DNase were used as positive controls. DAPI counterstaining was used to visualize nuclei of cells. Stained sections were analyzed using fluorescence microscopy with red fluorescence for

TUNEL staining, blue fluorescence for DAPI staining, thus the purple signal was taken as sign of apoptosis cells, when signals of nucleus and dUTP nick end-labeling were merged.

3.2.6 Behavioural assessment

Rats were group-housed with mixed genotypes in a constant temperature-humidity room (22±1°C, 55±10% RH) with a 12 hours light-dark cycle (lights on/off at 2:00 am/pm). Food and water were provided *ad libitum*. All behavioural tests were performed only with male rats during the dark phase, which is the physiological activity period of the rats. Controls were an equal mix of WT littermates from both lines and the experimenters were blind to the individual animals' genotype. All animal procedures were approved by the state government of Baden–Württemberg, Germany, and are in accordance with animal protection guidelines.

3.2.6.1 Modified SHIRPA

Basic primary health of rats was assessed using a modified protocol for mice (Vekovischeva et al., 2004) which was developed based on the primary description of SHIRPA (**S**mithKline Beecham Pharmaceuticals - **H**arwell, MRC Mouse Genome Centre and Mammalian Genetics Unit - **I**mperial College School of Medicine at St Mary's - **R**oyal London Hospital, St Bartholomew's and the Royal London School of Medicine - **P**henotype – **A**ssessment) (Rogers, 1997). Rats were screened at 1, 6, 12 and 18 months of age (n=12). Additionally, hematological screening was performed by measuring fresh blood samples collected in EDTA tubes at the same ages (n=6 each time point). The following parameter were analyzed: the number of red blood cells (RBCs), the number of white blood cells (WBCs), the total amount of hemoglobin in blood, the fraction of blood composed of red blood cells (hematocrit), the mean corpuscular volume (MCV) which is the size of the red blood cells, as well as the calculated mean corpuscular hemoglobin concentration (MCHC).

3.2.6.2 Rotarod test

Rotarod experiments were used to measure fore- and hind-limb motor coordination. BACHD transgenic rats and WT littermates were trained on 3 consecutive days with 4 trials per day. Directly after training they were tested on 2 consecutive days with 2 trials per day and an interval of 1 hour between individual trials. During the training period, the rats were placed on the rotating rod at a constant speed of 12 rpm for 2

minutes. Rats were returned to the rod after falling during the training period up to 10 falls per trial. Individual tests were assessed for a maximum of 5 minutes with accelerating speed from 4 to 40 rpm over a period of 4 minutes, and the latencies to fall were recorded. Rats from the same cohort (n=12) were tested every month from 1 to 15 months of age. Three rats were excluded from the analysis because already at younger ages they fell off the rotarod immediately when placed on it, despite extensive training.

3.2.6.3 Footprint test

A footprint test was used to analyze gait abnormalities in BACHD rats. BACHD transgenics and WT littermates were evaluated in this task at 14 months of age (n=11). The front and hind paws of the animals were painted with nontoxic paint of different colors. On the day before testing, the rats were trained in 3 sessions. The best performance out of 3 tests with each rat was selected for data analysis. The stride width of the hind paw, the step length (left paw to left paw) and the overlap (distance between front and hind paw) were measured in 3 consecutive steps, and the average was taken for further analysis.

3.2.6.4 Elevated plus maze

An Elevated plus maze was used to assess the anxiety of BACHD rats. To eliminate the possibility of habituation effects, different cohorts of rats were tested at 1(n=13 per genotype), 4 (n=13 per genotype), and 12 (TG5:WT=8:11) months of age as described previously (Nguyen *et al.*, 2006). Rats were placed at the center of an elevated plus maze (with two open and two closed arms), facing an open arm and were monitored for 5 minutes. The time spent in the open arms was recorded as a percentage of the total time for analysis.

3.2.6.5 Measurments of locomotor activity, food intake and metabolic factors

Rats were monitored using the PhenoMaster system, which represents a modular set-up that screens rats in a home-cage like environment for their ambulatory activity, rearing as well as feeding and drinking behaviour. The activity detection is achieved using infrared sensor pairs arranged in horizontal (x,y level for ambulatory activity) and vertical (z level for rearing) strips. Food and water consumption were recorded by two weighting sensors. The same cohort of animals (TG5:TG9:WT = 16:19:18) was individually screened for 22 hours every 3 months until the age of 18 months. Data were automatically collected with one-minute intervals and analyzed either

entirely or only for the dark (active) phase. Rats, which did not drink more than 3 ml water within 24 hours were excluded from the data analysis since this might have confounded feeding behaviour and activity.

3.2.6.6 Simple swimming test

Together with the master student Erik Jassion, we have designed a simple swimming test (two-choice test) and Skinner Boxes test (see below). Simple swimming test was used to assess procedural learning, which dependents on striatal function. For this test, an aquarium that measured 150 x 25 x 40 cm (L x W x H) and a glass platform of 19.5 x 15 x 16.5 cm (L x W x H) were used. Room temperatured water was filled to a depth of 18.5 cm and colored with black non-toxic paint to mask the platform under water. Rats were tested at 4 and 6 months of age (n=12 for each time point), with acquisition and reversal learning phases at each time point. In both learning phases, rats were trained with 3 sets of 3 consecutive trials spaced 2 hours apart for two days. During tests, rats were gently placed into the starting area of the tank (30 cm wide area in the middle of the aquarium) facing away from the platform. The time required for the rats to reach the platform and the initial swimming direction were recorded and analyzed using two-way ANOVA at each time point. Rats were given a score of 0 if their initial swimming direction was towards the platform, and given a score of 1 if they initially headed away from the platform. Cut off time for each single trial was set to 90 seconds. Rats were guided to the platform in case they did not find the platform within 90 seconds.

3.2.6.7 Skinner Boxes tests

Skinner Boxes tests was used for further cognitive assessment of BACHD rats. The Boxes were equipped with two levers on the left and right side of the wall with a cue light above each lever. During tests only one lever was active. A food-tray was positioned between both levers, and additionally a house light was installed at the ceiling (Figure 3.3 A).

In order to increase their motivation in acquiring and performing the task, the food of rats was restricted to approximately 60 % of libitum ration (12g) starting 3 days before the tests, The rats were weighted daily and feeding was adjusted to keep the body weight at 90% of their free feeding body weight.

The experiment was designed with a combination of discipline and reward; a correct response (pressing the active lever) following stimulation (presentation of the green

cue light) induced reward with a food pellet being delivered into food tray. The reward was followed by a time-out (no cue light being presented for a specific time) during which the rat was supposed to refrain from pushing any lever. Pressing the (inactive) lever during the time out without a stimulation cue light only restarted the time out (Figure 3.3 B).

Rats were tested at 3 months of age (TG5:TG9:WT = 13:12:11), with 30 minutes trials in their dark phase each day. After acquisition, 3 experiments were performed in the following order: 1. Aquisition learning with 5 seconds time-out, 2. Acquisition learning with 15 seconds time-out, and 3. Reversal leaning with 5 seconds time-out. During reversal learning the light signal was reversed so that the green light indicated the time out while no light signal indicated that the lever was active. Each experiment was terminated when all three groups of rats reached a performance plateau (difference of performance within 3 days < 5%). All responses of rats were monitored and recorded by a computer with TSE Operant Behaviour software v1.68. The ratio of correct lever press / total lever press was analyzed using two-way ANOVA among three groups (TG5, TG9 and WT), while the mean of plateau were compared using one-way ANOVA.

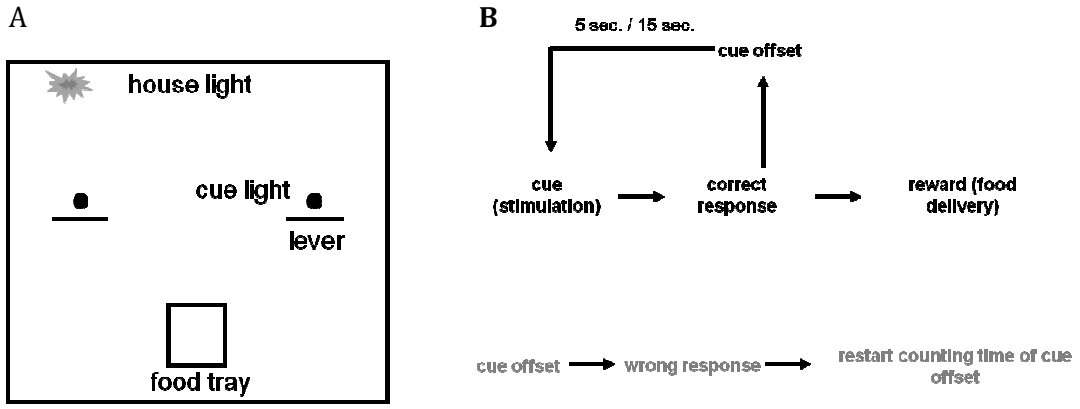

Figure 3.3: Skinner Box set up. (A) Equipment of Skinner Box. (B) Experimental design.

3.2.7 Statistical analysis

Standard two-way ANOVA (data not matched) and repeated-measures two-way ANOVA (repeated or matched data) were conducted to assess the effects of genotype and age and genotype x age interaction. Bonferroni *post hoc* tests were conducted to compare individual genotype effects at individual ages. For the analysis of the rotarod test results, only data until 10 months were taken into account because

most TG5 rats fell immediately from the rotarod during the final 5 months (from age 11 to 15 months) leading to a non-normal distribution of the data in the final 5 months. For data where only one time point was assessed (such as the footprint test and matrix/striosome analysis), one-way ANOVA was conducted to evaluate the effects of genotype, followed by Tukey post-hoc test for multiple comparisons. Data are presented as mean ± S.E.M. Differences were considered significant if $p<0.05$.

4. Results

4.1 Generation and establishment of BACHD rats

4.1.1 BACHD construct

The BACHD construct was a gift from Dr. William X. Yang, UCLA, Los Angeles, USA. This construct was generated using a human bacterial artificial chromosome (BAC) containing human genomic DNA spanning the full-length *HTT* gene and the flanking genomic sequences 20 kb upstream and 50 kb downstream, which included all regulatory elements (Yang *et al.*, 1997; Kazantsev *et al.*, 1999; Gray *et al.*, 2008). Wild type *HTT* exon 1 was replaced by mutant *HTT* exon 1 containing 97 CAA/CAG mix repeats flanked by two LoxP sites. Therefore the BAC construct allows for a conditional and inducible elimination of mutant *HTT* exon 1 by Cre recombinase activity (Figure 4.1).

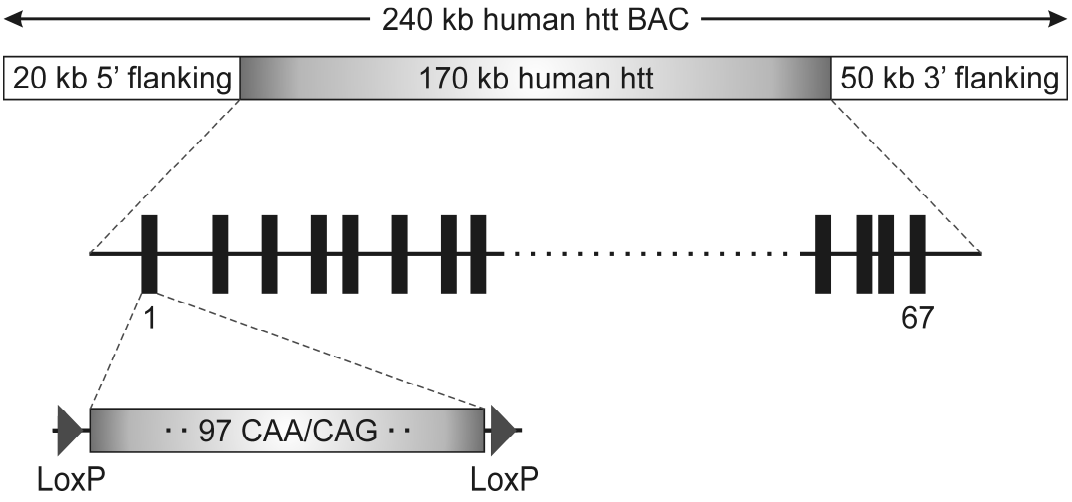

Figure 4.1: Schematic representation of the BACHD construct. The BACHD construct was designed using a bacterial artificial chromosome containing the entire 170 kb of the *HTT* genomic locus with approximate 20 kb upstream and 50 kb downstream flanking sequences. Mutant *HTT* exon 1 including 97 CAA-CAG trinucleotide repeats in place of endogenous *HTT* exon 1 is flanked by two loxP sites.

4.1.2 Genotyping of BACHD rats

Following microinjection, 21 out of 24 transgenic founder rats generated F1 progeny (Figure 4.2), which were used to evaluate the integrity of the transgene. Three different primer pairs were used in the PCR analysis elongating a fragment of the first and last exon, and intron 29 of the HTT gene. Of 21 founder rats, 18 possessed the full length HTT gene, three founders had to be withdrawn as they were lacking at minimum the last exon (Figure 4.3). Genomic transgene copy number was analyzed

using TaqMan real-time PCR. Three lines LY.014, LY.015 and LY.017 were found to have multiple insertion sites of the BAC constructs, with a standard deviation between littermates of 0,76, 1,60 and 2,93, respectively (Figure 3.4). They were therefore excluded from further experiments.

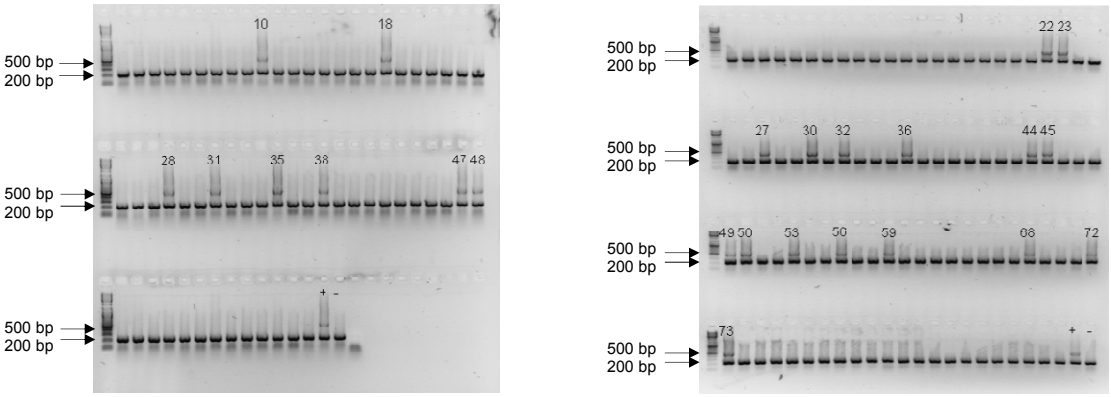

Figure 4.2: PCR results from a screen of 155 rat pups. After microinjections, 155 pups were genotyped using standard PCR. The primer pair was designed to bind to human and rat huntingtin, producing approximately 500 bp and 200 bp long fragments, respectively. Twenty-four potential founders were detected to show both human (500 bp) and rat (200 bp) huntingtin PCR products: lanes 10, 18, 28, 31,35,38, 47, 48 (left panel) and lanes 22, 23, 27, 30, 32, 36, 44, 45, 49, 50, 53, 56, 59, 68, 72, 73 (right panel). +, positive control; -, WT rat as negative control.

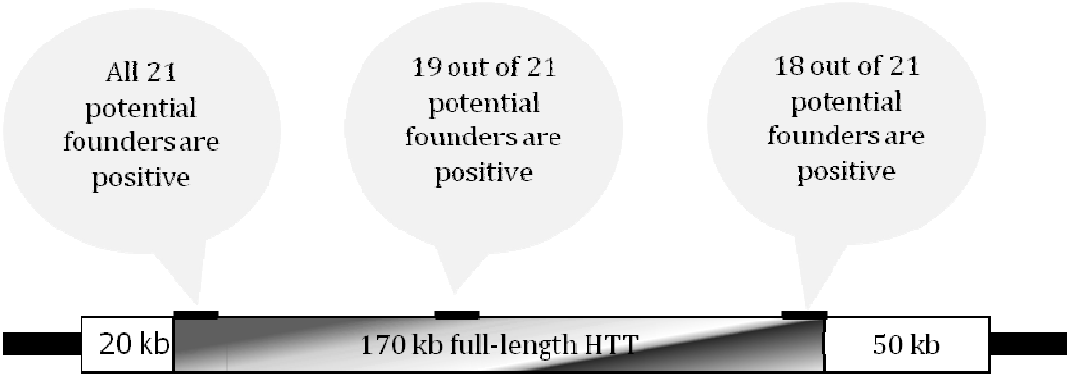

Figure 4.3: Three lines were found to have only a fragment of the mutant human huntingtin gene integrated into the genome. Three primer pairs were designed to amplify different parts of the huntingtin gene. Two lines were detected to have a fragment shorter than 29 exons, the other line lacked at least exon 67.

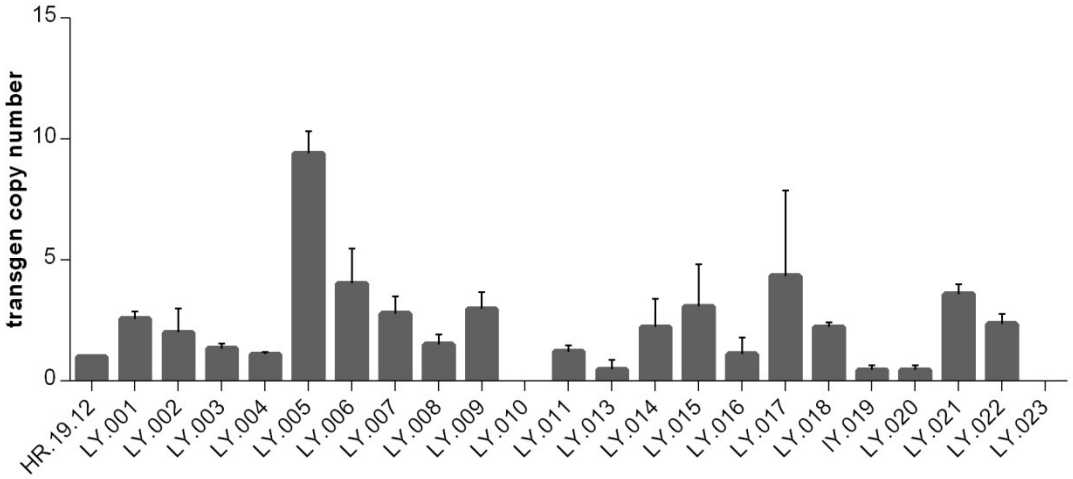

Figure 4.4: Relative quantification of transgenic copy number. The DNA samples of all F1 animals were performed by real time PCR in comparison to a previous established line (HR.19.12). With standard errors of 40 to 55 percent in different F1 transgenic rats from the same litter, line LY.002, LY.014, line LY.015, line LY.016 and line LY.017 were demonstrated to have more than 1 insertion site of the BAC construct. Line LY.010 was identified to exhibit only a fragment of htt, showing no PCR amplification of intron 29.

4.1.3 Analysis of mRNA and protein expression in BACHD rats

Expression levels of mRNA were quantified with Sybr Green quantitative PCR, indicating line LY.005 had the highest mRNA expression of mutant Huntingtin (data not shown). Huntingtin protein levels of 1-month-old transgenic rats were quantified by Western blot with the antibody MAB2166 (Figure 4.5), which recognizes both human and rat huntingtin. The highest protein expression was found in line LY.005, which was consistent with the mRNA results, whereas line LY.009 displayed a comparable level of mRNA and protein as the well characterized BACHD mice (Figure 4.6). Consequently, these two lines, which contain a single insertion site and express intact full-length huntingtin were selected for subsequent phenotypic characterization.

The relative transgene expression level compared to endogenous rat huntingtin mRNA was estimated by semi-quantitative analysis. The estimated expression level of mhtt is approximately 4.5 times higher than endogenous htt in the transgenic line LY.005, and 2.5 times higher than endogenous rat htt in line LY.009.

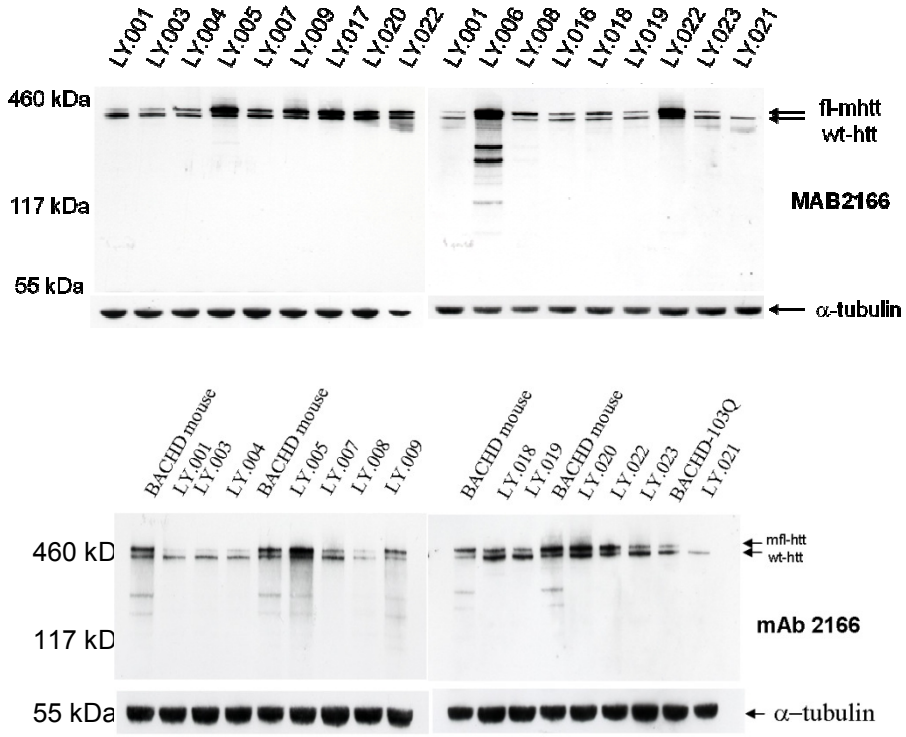

Figure 4.5: Western Blot analysis of mutant huntingtin (mhtt) expression in different transgenic lines and compared to a BACHD mouse. Whole brain lysates of animals from the F1 generation and from each line were used. Both mhtt and endogenous WT rat htt are recognized by MAB2166 showing bands of ~360 kDa and ~330 kDa, respectively. Line LY.005 shows the highest protein expression compared to all other transgenic lines, and line LY.009 exhibits a comparable expression level as a BACHD mouse. The same blots were re-probed with anti-α-tubulin antibody for the loading control.

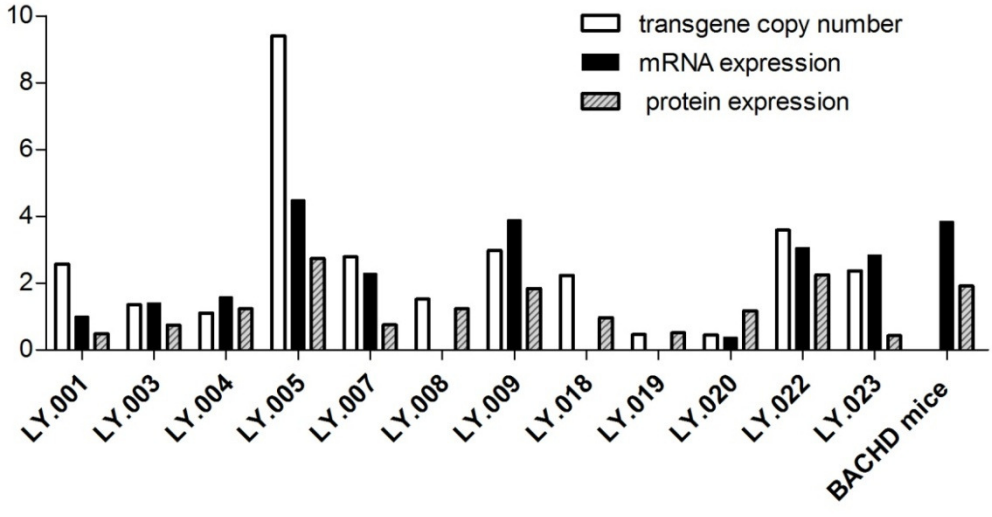

Figure 4.6: Comparison of copy number of BAC insertion. Eleven lines, which express full-length human huntingtin, and which only have one insertion site, were compared in terms of transgene copy number (gray column), mRNA (red bar) and protein (yellow bar) expression level. Additionally, a BACHD mouse was used for comparison. From lines LY.008, LY.018 and LY.019, no samples for mRNA were obtained, thus the data of mRNA expression level in these lines were missing. Line LY.005 shows the highest transgene copy number, RNA expression level as well as protein expression level, while line LY.009 presents a comparable mRNA and protein expression levels to the BACHD mouse.

To assess the expression pattern of mhtt in different brain regions of transgenic BACHD rats, protein extracts of 6 brain subregions (cerebellum, cortex, striatum, olfactory bulb, brain stem, and hypothalamus) from 1 month old TG5 and TG9 rats were analyzed utilizing Western blot analysis (Figure 4.7). The blots were stained with the antibody MAB2168 to visualize the signal of mhtt. The results revealed that mhtt is equally expressed in the cerebellum, striatum and cortex, whereas the hypothalamus, olfactory bulb and brain stem show less abundance of mhtt.

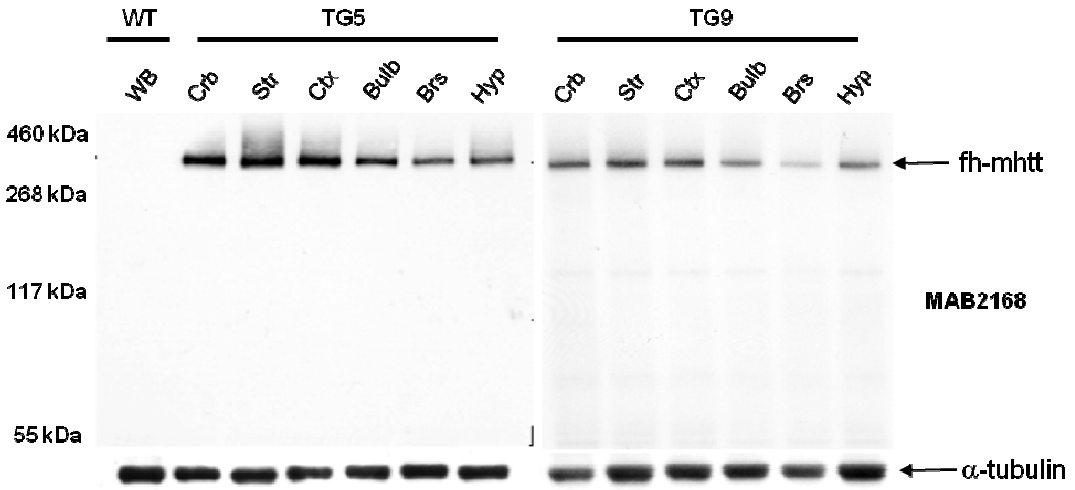

Figure 4.7: Western blot analysis of mhtt expression in various brain regions in transgenic line 5 (TG5) and transgenic line 9 (TG9) using MAB2168. In both lines, mhtt is abundantly present in cerebellum (Crb), striatum (Str) and cortex (Ctx), whereas the olfactory bulb (Bulb), brain stem (Brs) and hypothalamus (Hyp) show a relatively reduced expression of mhtt. A whole brain of WT rat (WB) was used as negative control and showed no immunoreactivity of MAB2168. The same blots were re-probed with anti-α-tubulin antibody for the loading control.

4.1.4 Stable CAG repeat number in BACHD rats

The stability of the CAG repeat expansions is critically important for therapeutic studies, since the age of onset of HD inversely correlates with the number of CAG repeats (Duyao *et al.*, 1993). The polyQ coding sequence of the BACHD construct was therefore generated using reiteration of CAA CAG CAG CAA CAG CAA. This sequence, as opposed to the reiteration of only CAG results in enhanced stability of the polyglutamine stretch (Kazantsev *et al.*, 1999; Dorsman *et al.*, 2002). Using four generations and both genders, 100 peripheral nerve samples and samples from different brain regions of transgenic rats of different ages up to 18 months were taken to verify the stability of the polyglutamine stretch in our transgenic rat model. The fragment length of PCR amplicons covering the CAG-CAA repeats were analyzed using a capillary sequencer. Several fragments of variable length would have been detected if the number of CAG-CAA repeats was not maintained. However, only one

single peak was detected in each sample with an identical size as the original BACHD construct (Figure 4.8). As already observed in BACHD mice (Gray *et al.*, 2008), our analysis revealed a stability of the polyQ encoding sequence in both germline and somatic brain regions at different ages, gender and rat generations.

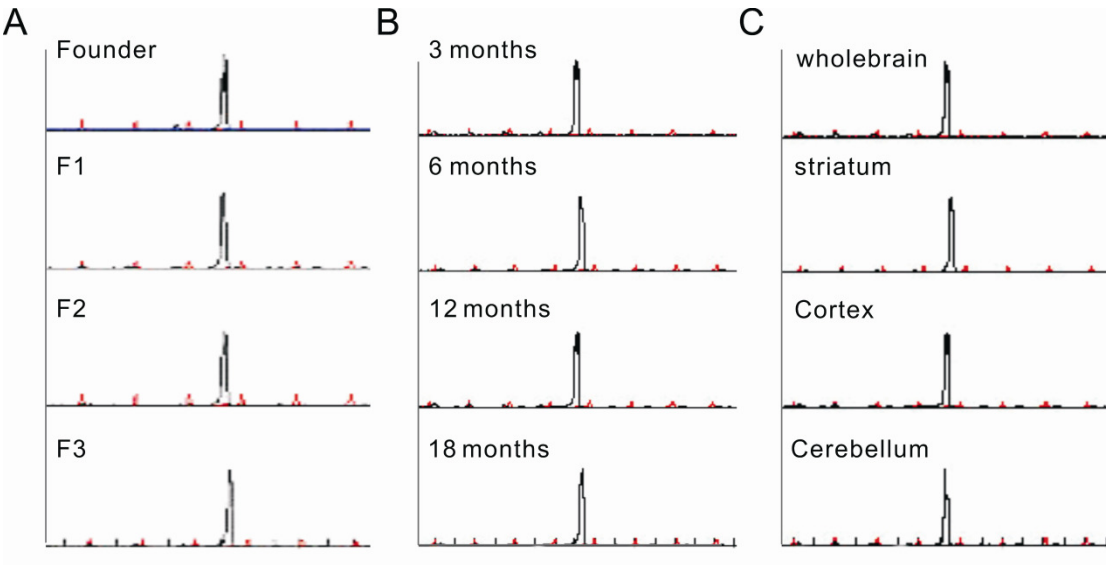

Figure 4.8: Stable polyglutamine repeat length in BACHD transgenic rats. One hundred samples of different brain regions or periphery tissue were analyzed for the fragment length after PCR amplification of the entire CAG repeat in transgenic *HTT* exon 1. Images of the scan generated show a single peak in all the samples of different generations (A), ages (B) and brain regions (C). The fragment length was found to be the expected size of a PCR product spanning 97 CAG/CAA repeats in all the samples.

4.1.5 Sequencing of the construct

The results of the fragment analysis revealed that the PCR products spanning the CAG repeats of all founders and the constructs themselves were approximately 18 nucleotides less than expected; therefore sequencing of the construct, which was used for microinjection, was performed. It was possible to screen the entire CAG repeat sequence as well as the polyproline coding sequence. Sixteen repeats of the nucleotide sequence CAA CAG CAG CAA CAG CAA along with an additional CAA were confirmed in the BACHD construct, which demonstrated that all the founders contain a CAA/CAG repeat of 97 residues and which is the same as in the BACHD mice (Gray *et al.*, 2006). Furthermore, 11 polyproline coding sequences downstream of the CAG repeats were confirmed as published for *Homo sapiens* in the NCBI data base.

4.1.6 Alternative splicing variants of mutant human huntingtin in BACHD rats

Real-time PCR was carried out to determine alternative splicing variants of mhtt mRNA. Samples of different brain regions of BACHD rats were analyzed for the presence of both protein-encoding transcript variants, which have been previously identified (transcript HTT-001 and HTT-011 were reported in Ensemble Genome Browser). Both the small (HTT-011) and the 67 exon spanning large transcript (HTT-001) were identified in all analyzed brain samples and the ratio of the transcript variants was quantified (Figure 4.9). The ratio of the transcript variants was similar in the different brain regions in TG5 with approximately 3.5 times more HTT-001 than HTT-011. In TG9 rats the HTT-001:HTT-011 ratio was highest in the cerebellum (4.32), moderate in the striatum (2.76) and lowest in the cortex (1.04).

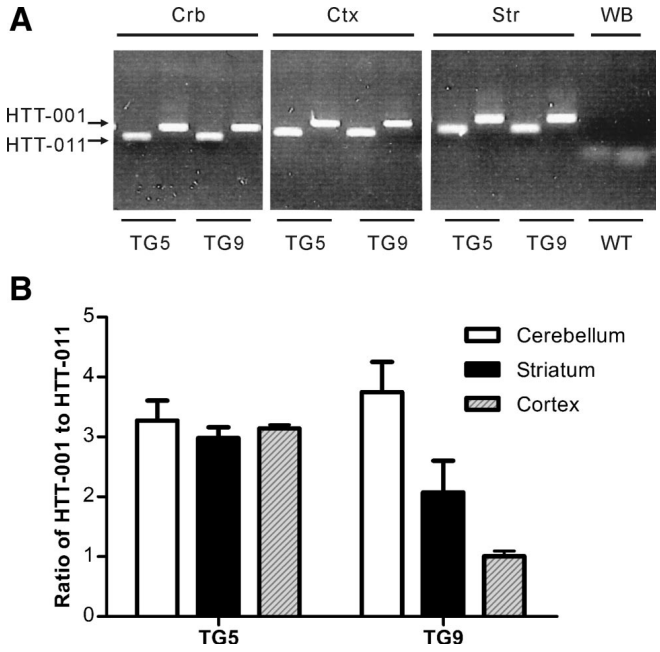

Figure 4.9: Both protein-encoding variants were determined in BACHD transgenic rats. Real-time PCR was performed using one common forward primer binding to both variants of *HTT-001* and *HTT-011*, while the reverse primers were chosen specifically to bind to each variant. (A) Image of gel electrophoresis. The BACHD rats of line TG5 and line TG9 exhibit both transcript variants (*HTT-001* and *HTT-011)* in cerebellum (Crb), cortex (Ctx) and striatum (Str). (B) Quantification of the ratio of *HTT-001/HTT-011* in different brain regions of both transgenic lines. The ratios vary between 2.49 and 4.40 in all brain regions investigated in both TG5 and TG9, except in the cortex of TG9 rats, where an equal expression of *HTT-001* and *HTT-011* is present.

As impaired general health could be a confounding factor in behavioral experiments, this information is crucial for proper interpretation of behavioral results. A modified SHIRPA protocol was therefore performed to assess basic health at 1, 6, 12 and 18 months of age. Transgenic rats from both lines, TG5 and TG9 did not differ significantly from WT rats on all parameters examined including a hematological screen over 18 months (Table 3.1).

Table 3.1: Primary basic healthy screen in BACHD rats

Hematological screen	No significant difference
Behaviour recorded in the viewing jar	No significant difference
Behaviour recorded in the arena	No significant difference
Behaviour recorded above the arena	No significant difference
Lacrimation and defection	No significant difference
Physiological reflexes	No significant difference

4.3 behaviour study

4.3.1 Early-onset progressive motor deficits in BACHD rats

Motor deficits are an important clinical feature of Huntington disease patients including involuntary movements, motor dyscoordination and gait disturbances. In order to assess motor function in our transgenic animals, we performed the rotarod test, footprint analysis and the clasping test.

Four trials on an accelerated rotarod were conducted with 1-month-old rats and repeated every month until the age of 15 months. The average latency until the animal fell off the rotating rod was measured and analysed. Repeated-measures ANOVA revealed a highly significant main effect of genotype ($F_{2,270}$=22.86, p<0.0001) and a statistically significant genotype X age interaction ($F_{18,270}$=1.67, p=0.0448), reflecting a significant difference between the performance of BACHD rats and WT rats with increasing age. Subsequent post-hoc analysis with Bonferroni tests demonstrated a progressive decline in rotarod performance in the TG5 group relative to both WT and TG9 animals (Figure 4.10). Significant differences were already evident at 1 month of age (p<0.01). Here, TG5 rats exhibited significant difficulties in maintaining balance on the rod at higher rotation speeds and were unable to remain on the rod longer than 97.31 ± 19.45 s. In comparison, WT rats showed an average latency to fall of 156.88 ± 8.48 s. At 4 months of age, the performance of TG5 rats dropped drastically, but it was maintained over the next 4 months. A similar drastic reduction in performance was observed again between 9 and 11 months of age, when most of the TG5 rats were unable to walk on the rod even at the lowest velocity (4 rpm) (Figure 4.10).

Video recordings provided additional insight into the rats' performance on the rotarod. At young ages (< 3 months), both transgenic and WT rats displayed similar walking behaviour on the rotarod. Starting with 3 and 5 months of age respectively, TG5 and

TG9 transgenic rats adopted an abnormal walking strategy. After being placed on the rod, the transgenic animals turned 180° and instead of performing a coordinated walk, they started to jump backwards (movie 1 and 2). The number of transgenic rats adapting this unusual strategy increased with age, which partly compensated for the decline in rotarod performance. None of the WT littermates displayed this abnormal movement strategy. Taken together, the results of the rotarod test demonstrated an early-onset and progressive motor function deficit in BACHD transgenic rats of line TG5.

Another rat cohort was used to study the motor skill learning ability at 2 months of age employing the rotarod test. The rats were trained in twelve training sessions and the number of falls in the last eight sessions were analyzed. The results indicate that only TG9 rats can improve their performances due to learning (one-way ANOVA, $p<0.05$), while TG5 were unable to improve their performances in the analyzed training sessions (Figure 4.11).

In order to investigate the gait of BACHD transgenic rats, footprints from all genotypes (n=11 each) were analyzed at 14 months of age. The stride width of the hind limbs as well as the step length and the overlap of hind and fore limbs of each individual rat were measured. One-way ANOVA revealed that 14-month-old transgenic TG5 rats made significantly shorter steps with fore and hind limbs ($p<0.0001$) than TG9 and WT. Furthermore, TG5 rats showed an increased stride width ($p<0.01$) and a reduced overlap between fore and hind limb placement ($p<0.0001$) (Figure 4.12) in comparison to the other groups, indicating that BACHD transgenic rats TG5 have gait abnormalities at older ages compared to WT rats.

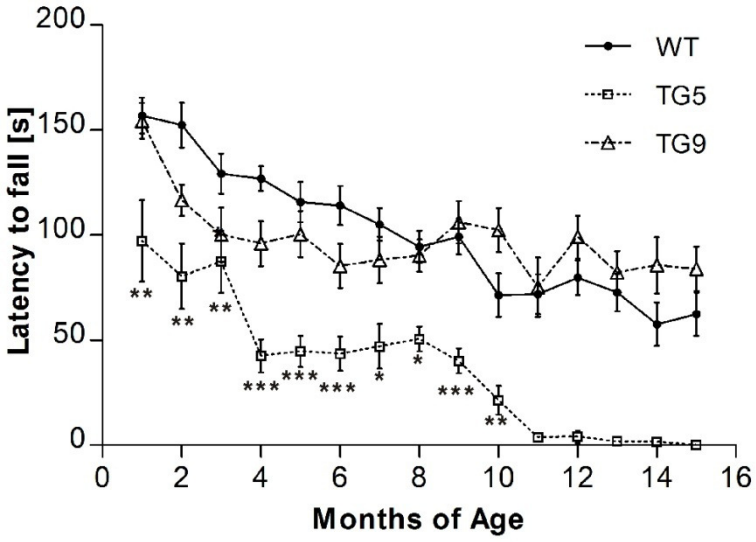

Figure 4.10: Motor function analysis of BACHD rat lines TG5 and TG9 using rotarod test. (A) Rats underwent four test sessions each month on an accelerating rod (4-40 rpm in 4 min). Mean latencies to fall (± SEM) were compared among different genotypes over 15 months (n=12 per genotype). TG5 rats displayed a progressive decrease in performance from 1 month of age, whereas TG9 showed an impaired performance at three and four months. Starting with the fifth test month, TG9 rats adapted an alternative strategy to remain on the rotating rod which yielded comparable performances compared to WT rats. Data are expressed as means ± SEM, **p*<0.05; ***p* <0.01; ****p* <0.001.

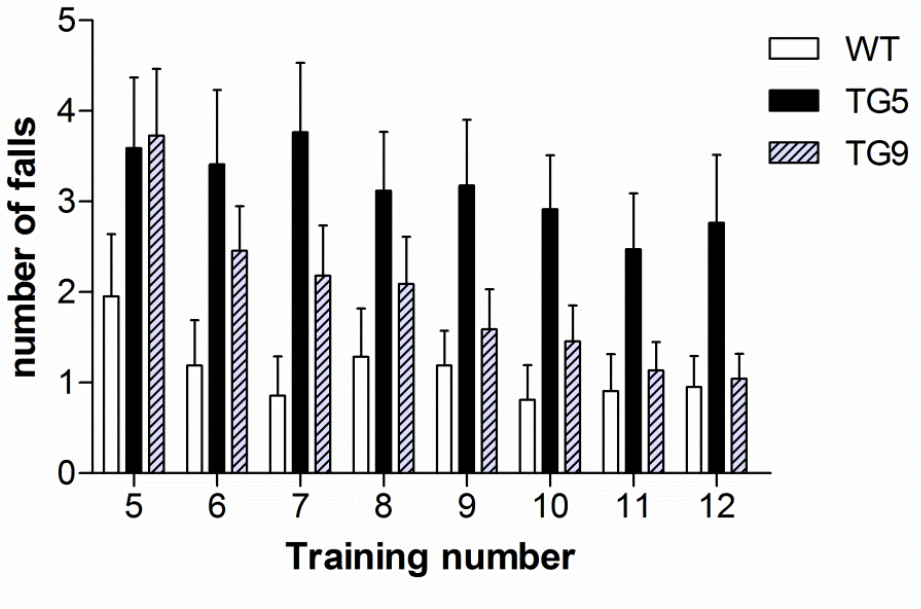

Figure 4.11: Impaired acquisition of new motor skill in BACHD rats. Rats were trained for 12 sessions under a constant speed (12 rpm, 2 min. each session) before the rotarod test was carried out. A reduction in the number of falls in the sessions of the first training presumably reflects motor skill learning ability. TG5 and TG9 rats had difficulties in improving their motor skill learning ability. TG5 rats did not improve at all over the period of 12 training sessions, while the WT rats performed well at the 5th trial; TG9 rats showed a significantly reduced number of falls in the 12th training session compared to the 5th.

In order to analyze the gait change in BACHD transgenic rats, footprints were taken at 2, 6, 10 and 14 months of age (n=11 per time point). The stride width of the hind limbs, the step length and the overlap of hind and fore limb of each individual rat were analyzed. Younger BACHD rats did not display any differences compared to wild type littermates (data not shown), whereas 14-month-old transgenic TG5 rats took significantly shorter steps with their fore and hind limbs. Furthermore, TG5 rats showed an increased stride width and reduced overlap between fore and hind limb placements (Figure 4.12), indicating an affected limb coordination. This data suggests that BACHD transgenic rats have gait difficulties at older ages compared to wild type rats.

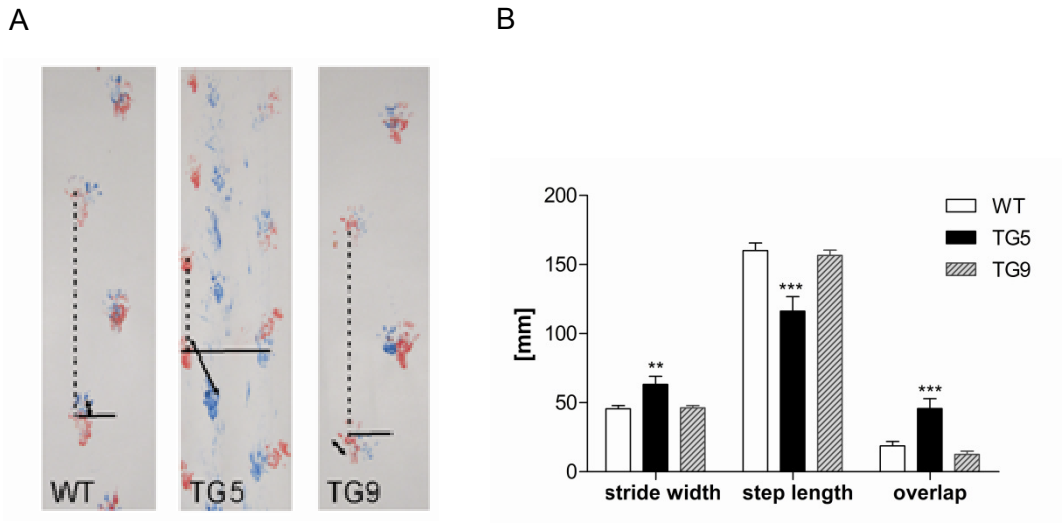

Figure 4.12: Footprint analysis. (A) Footprints at 14 months of age. Stride width: continuous line; step length: dotted line; and overlap between front and hind limbs: two directional arrows. (B) Statistical analysis of footprints examined at 14 months of age. TG5 exhibited a significantly abnormal gait with increased stride width, decreased overlap as indicated by a greater distance between hind and front paw placement and decreased step length. Data are expressed as means ± SEM, $^{**}p$ <0.01; $^{***}p$ <0.001.

Additionally, characteristic hindlimb clasping behaviour was observed during tail suspension in both transgenic lines at 3 weeks of age (Figure 4.13).

All together these results indicate that both BACHD transgenic rat lines show early and progressive motor function deficits and impaired motor skill learning.

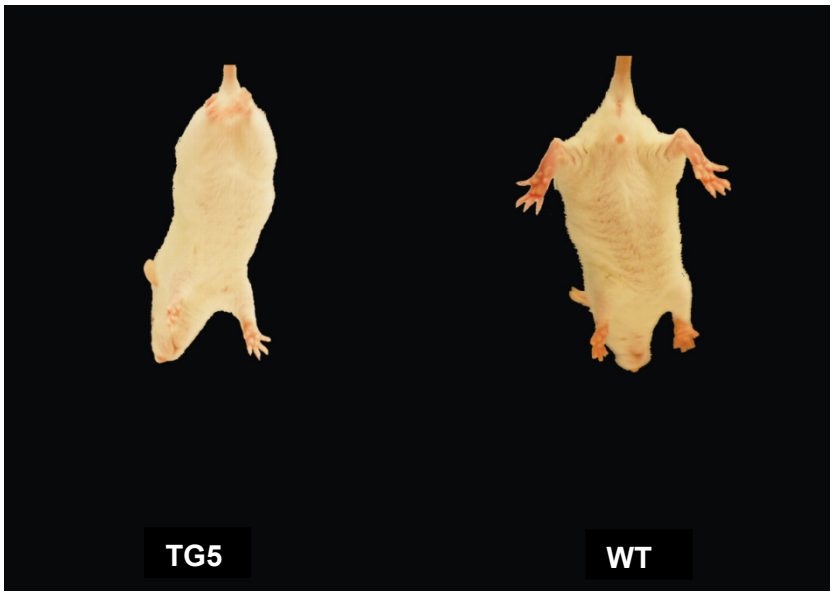

Figure 4.13: Hind limb clasping in BACHD transgenic rats at 3 weeks of age.

4.3.2 Emotional changes in BACHD rats

Additional clinical features of HD patients involve multiple psychiatric symptoms. In order to score the anxiety level of the BACHD transgenic rats, we utilised the elevated plus maze test. Independent cohorts of TG5 rats and WT littermates were used at 1, 4 and 12 months of age. One month old and 4 months old BACHD TG5 rats spent significantly more time on the open arms compared to WT (10.30% and 9.55% at 1 and 4 months of age respectively, $p<0.05$ at each time point), (Figure 4.14 B). At 12 months of age, the difference between TG5 and WT rats further increased with a mean difference of 13.43% ($p<0.01$). The significance of these observations was confirmed by two-way ANOVA, which indicated a highly significant main effect of genotype ($F_{1,65}=25.56$, $p<0.0001$) as well as a main effect of age ($F_{2,65}=37.7$, $p<0.0001$). However, there was no significant interaction between genotype and age ($F_{2,65}=0.26$, $p=0.7753$) because the percentage of time spent on the open arms of the maze decreased in both genotypes with increasing age.

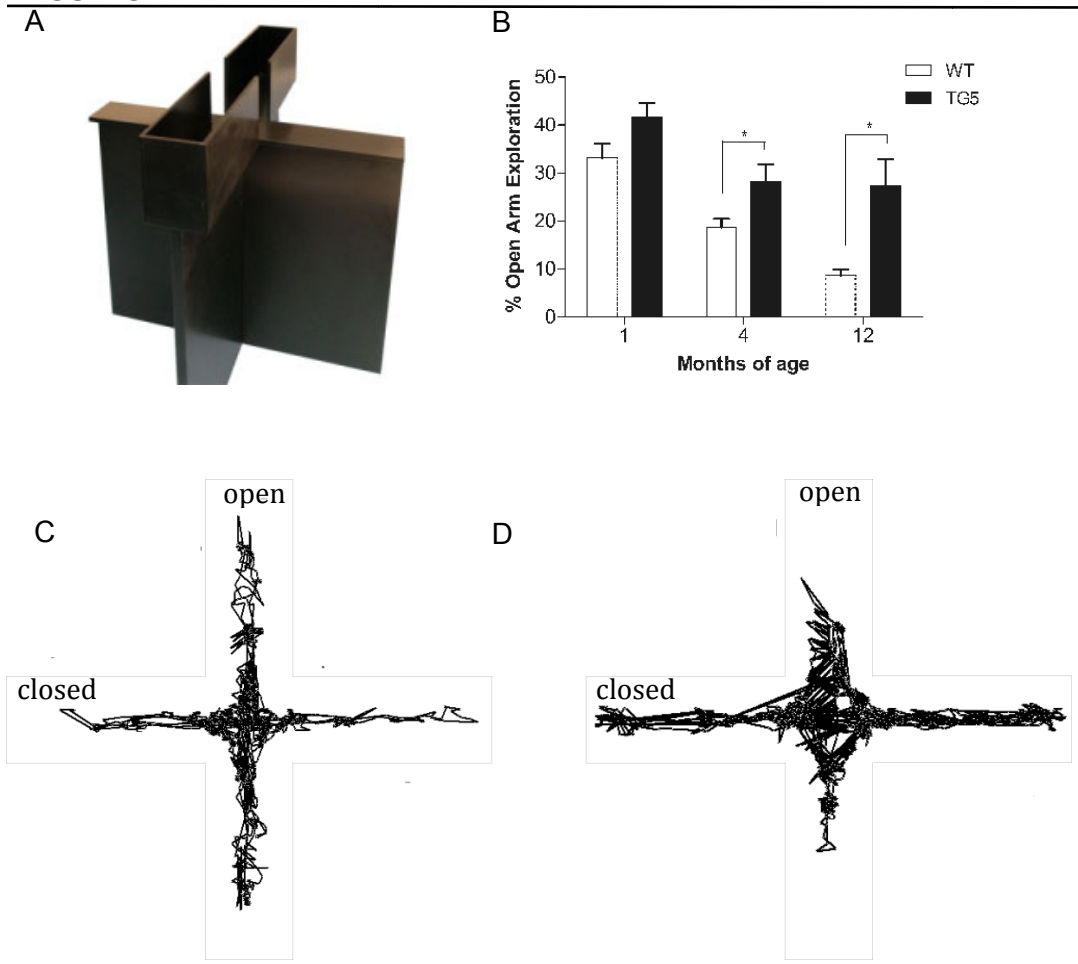

Figure 4.14: **Emotional changes in BACHD rats.** (A) Picture of elevated plus maze used (from www.eb-instruments.com) (B) Independent cohorts of TG5 and WT control rats were tested in the elevated plus maze at 1, 4 and 12 months of age. Data are reported as mean ± SEM for the percentage of time spent in the open arms. TG5 rats exhibited significantly increased open arm exploration compared to WT controls at all three ages, the time spent in the open arms increased from the 4th month to the 12th month. (C) Representative running pattern of a TG5 rat (left) and a WT littermate (right). Data are expressed as means ± SEM, *p <0.05.

Rats were subjected to a social interaction test every other month until 18 months of age (WT:TG5:TG9, N=16:14:20). Social interaction behavior including sniffing, following and touching was analyzed utilizing one-way ANOVA at each time point, as well as grooming (Figure 4.15). There was no difference in social interaction behavior observed between neither any genotype nor any age within the same genotype. In contrast, grooming time in wild type controls increased as they aged, while rats of both transgenic lines show a constant length of time for grooming until 18 months of age. Therefore in later stages, BACHD transgenic rats displayed reduced time for grooming compared to wildtype littermates when exposed to an unfamiliar rat.

However, this reached statistical significance only in 12-month-old and 16-month-old TG9 rats.

A

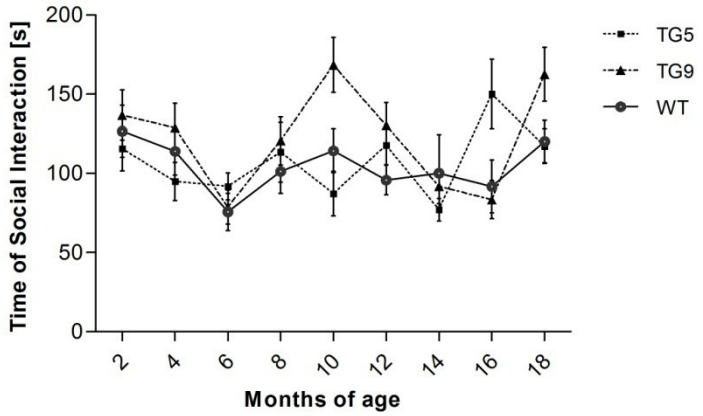

B

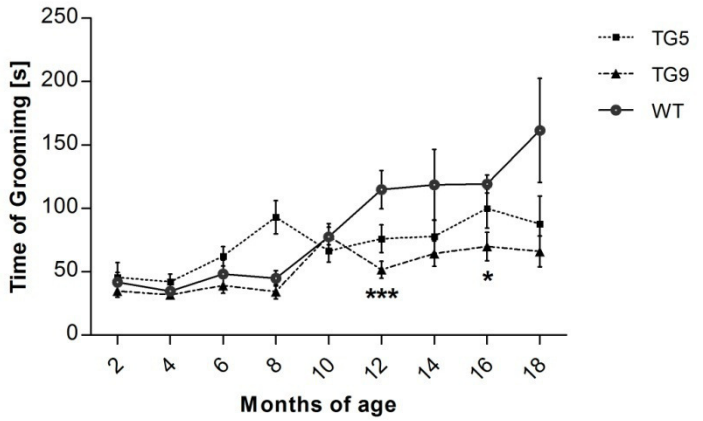

Figure 4.15: Social interaction screening. Rats of the same cohort were tested for social interaction with two months intervals until 18 months of age. Each time rats were paired with a foreign rat of the same genotype which they had never met before. There was no difference in social interaction time observed over 18 months (A), while the grooming time of both transgenic lines seems to be decreased compared with WT littermates at later stage (B), but this difference reached significance only for TG9 rats at 12 and16 months of age. Data are expressed as means ± SEM, *p<0.05, ***p<0.0001.

4.3.3 BACHD rats show a cognitive deficit in a simple swimming test

A simple swimming test was designed to assess the ability of BACHD rats in learning to find and remember the position of the escape platform. The experiment was designed with two stages: acquisition and reverse learning. The same cohorts of rats were tested at 4 and 6 months of age. Both BACHD transgenic rats and WT controls very quickly learned to escape by reaching the platform even in the first test at 4 months of age.

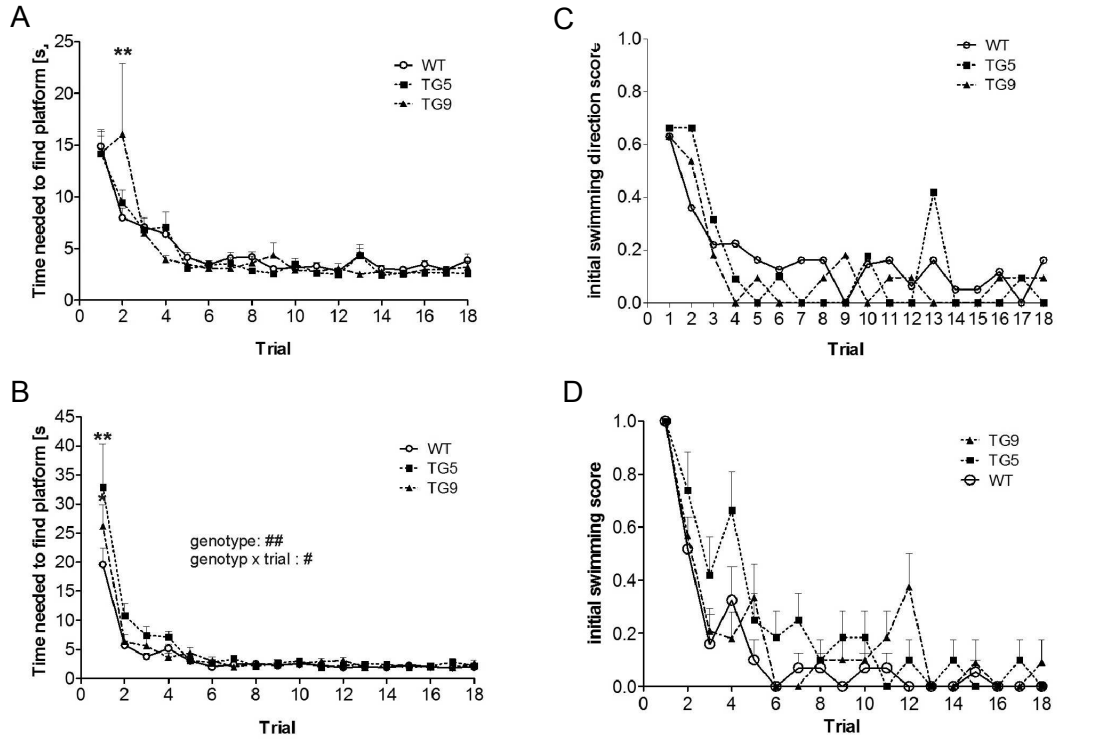

Figure 4.16: Initial simple swimming test at 4 months of age. The experiments were designed with acquisition (A) and reversal learning (B) stages with 6 tests each day. Time needed to find the platform and initial swimming direction score were analyzed using two-way ANOVA. In both stages, rats from all genotypes learnt how to find the platform within 4 trials. In the acquisition stage, TG9 occasionally needed longer time to find the platform in the second test; this difference was caused by a single rat, which could have been influenced by motivation. In the reversal learning stage both TG5 and TG9 rats displayed a significantly increased latency to find the platform at the first trial, a significant interaction of genotype X trials was detected as well. There was no significant difference of initial swimming direction score in both acquisition and reversal learning stage. Data are expressed as means ± SEM, #p<0.05; ##p<0.01.

At 4 months of age, there was no difference between genotypes during acquisition training (Figure 4.16 A). During reversal training, two-way ANOVA analysis revealed an interaction between genotype and number of trials ($p = 0.0162$) and a separate genotype effect ($p = 0.0068$) on the time needed to reach the platform. In addition, on the first trial of reversal, both TG5 and TG9 rats needed significantly longer time than WT to find the platform ($p<0.001$ and $p<0.05$ respectively). No significant results were seen in the learning curve for the swimming pattern score (Figure3.17 B). Apart from the significant effect of the number of trials noted above, no significant results were found in any of the learning curves for acquisition and reversal with six months old rats (Figure 4.17).

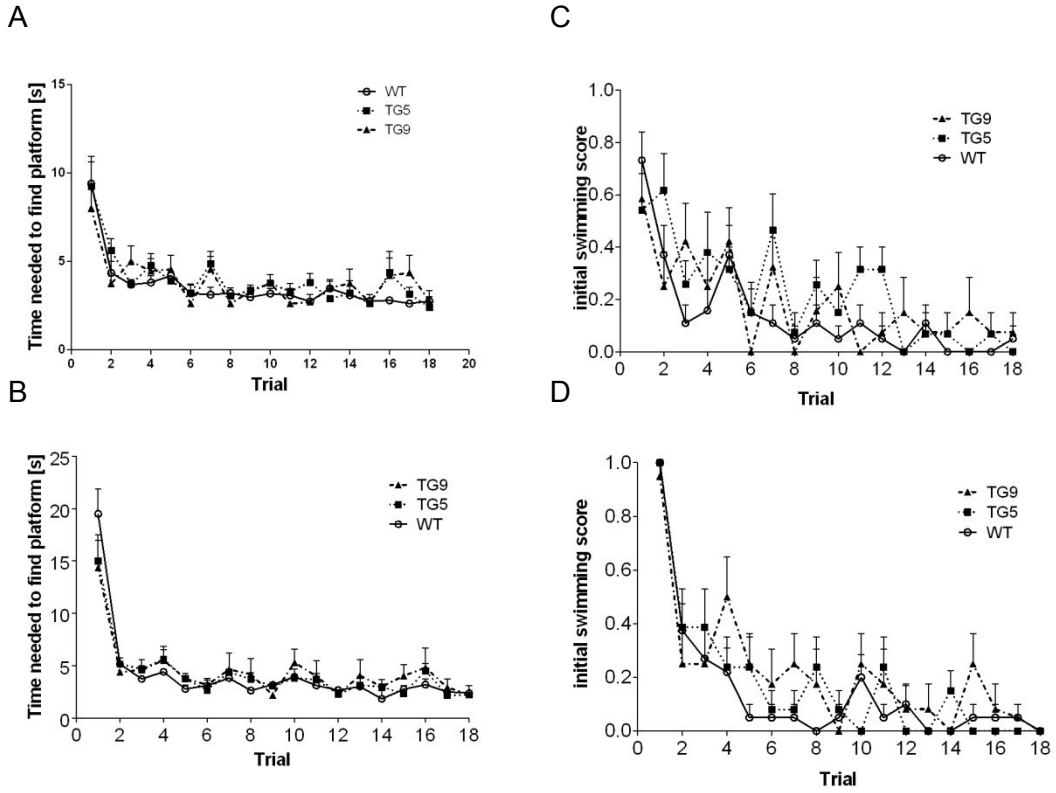

Figure 4.17: Repeated simple swimming test at 6 months of age. All rats learned more quickly than at 4 months of age. With regards to the time needed to find the platform, in both learning stages, by the second trial all rats had reached a plateau level. No difference was determined between transgenic rats and WT controls.

4.3.4 Early cognitive decline in the Skinner Box tests

To demonstrate cognitive changes in BACHD rats, Skinner box testing was performed with BACHD rats from both lines and WT controls at 10 weeks of age. The entire experiment continued for 6 consecutive weeks. During the experiment, the body weight of all rats was reduced by approximately 10-20% in comparison to their initial body weight. While TG5 showed the largest reduction of body weight over 6 weeks, WT rats lost the least amount (Figure 4.18 A). All rats were motivated to push the lever in order to retrieve food pellets, which lead to a habituation phase until reversal learning. The learning curves for all genotypes showed a significant effect on performance with the number of trials (p<0.0001).

No significant differences between or effects of the genotypes were found when analyzing performance during the initial lever training. Although TG5 rats showed a slight trend towards requiring more training before starting to retrieve 100 pellets within the time limit, no significant differences were found (Figure 4.18 B).

RESULTS

The learning curve from the 5-second time out phase showed that all the rats from all three genotypes reached a performance plateau as of the 5th training day (plateau was defined as no more than 5% variation in performance within 3 days). Two-way ANOVA revealed a significant interaction (genotype x training sessions) ($F_{12,198}$=5.45, p<0.0001 and a significant effect of genotype ($F_{2,198}$=4.83, p<0.05) (Figure 4.19 A). One-way ANOVA and post-hoc analysis with Bonferroni test detected a significant worse performance in both TG5 and TG9 during the plateau stage (p<0.001) (Figure 4.19. C). In contrast, in the 15-second time out phase only a significant lower percentage of correct response was detected in TG5 during the plateau stage (p<0.01) (Figure 4.19 D), neither significant interaction nor effect of genotype was observed ($F_{16,264}$=0.55, p=0.9179, $F_{2,264}$=1.37, p=0.2690, respectively) (Figure 4.19.B).

In the light reversal phase, there was a significant interaction between genotype and number of trials ($F_{12,198}$=3.89, p<0.0001) (Figure3.20 A). However this statistical difference may not be truly representable. Both transgenic strains initially showed a better performance than WT rats in the initial trial, but progressed only slightly towards a lower performance plateau than the WT rats with a lower percentage of correct responses. Due to the initial performance difference, the learning curve in the transgenics was less pronounced than WT rats. The 'better' initial performance of the transgenics could be contributed to their inability to reach the WT performance level in the acquisition stage. In addition, Both TG5 and TG9 rats showed a significant worse performance during plateau stage (one-way ANOVA, p<0.05) (Figure 4.20 B).

The number of lever pushes reflects the motivation of the rats which could influence their performance. The numbers of lever-press were analyzed during the 5-second and 15-second time out phases as well as the reversal phase. In all learning phases, the number of trials had a significant effect on the total number of lever presses (p<0.0001 in 5- and 15-second time out phases, p<0.018 in reversal learning phase) as seen through a reduction in the number of lever pushes as the test progressed (Figure 4.21). This result indicates that rats reduced ineffective attempts as they learned the cue of response. We normalized the data of 5-second, 15-second time out phase and the reversal training phase to the lever pushes. The statistical significances remain similar to the non-normalized results (data not shown).

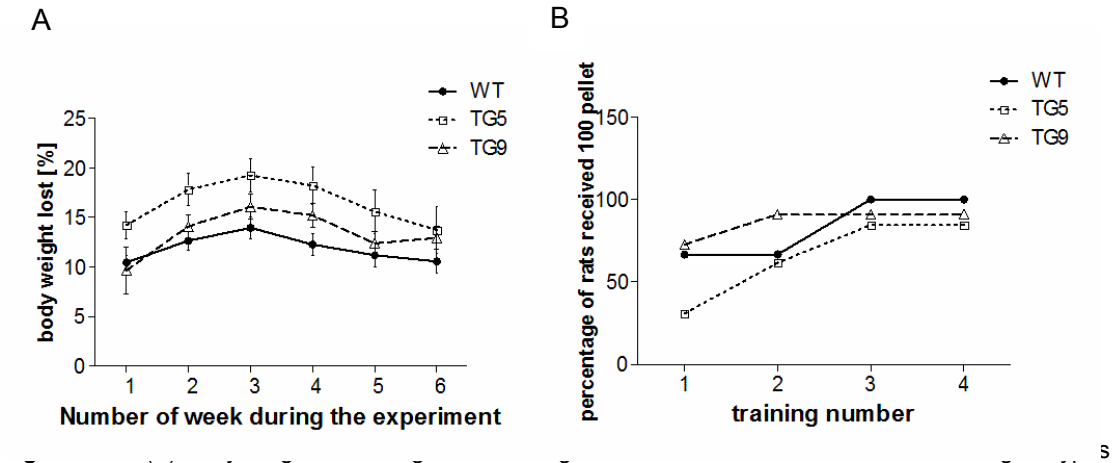

showed 10-20% body weight reduction during the entire experiment. There was a tendency that TG5 rats lost in average more body weight compared to WT littermates, however it was not significant. (B) Percentage of rats receiving 100 pellets in the acquisition stage. After 3 trials, most rats received100 pellets within 30 min.

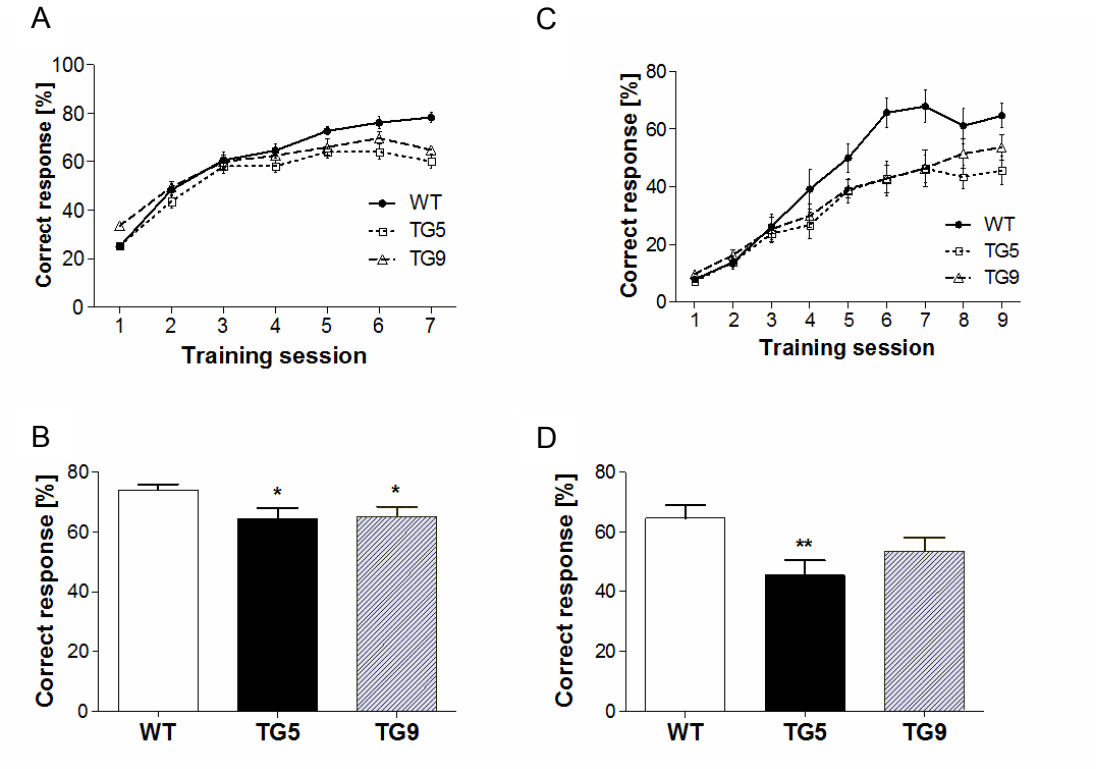

Figure 4.19: Correct responses of rats during acquisition stage. (A) Correct responses during 5-second time out stage; (B) Correct responses during 15-sencond-time out stage; (C) Correct responses in the plateau phase of 5-second time out; (D) Correct responses in the plateau phase of 15-second time out. Rats of TG5, TG9 and WT littermates received 1 training session of 30 minutes each day, the average of correct responses were recorded and analyzed. Data are presented as mean ± SEM of each trial. **p*<0.05, ***p*<0.01.

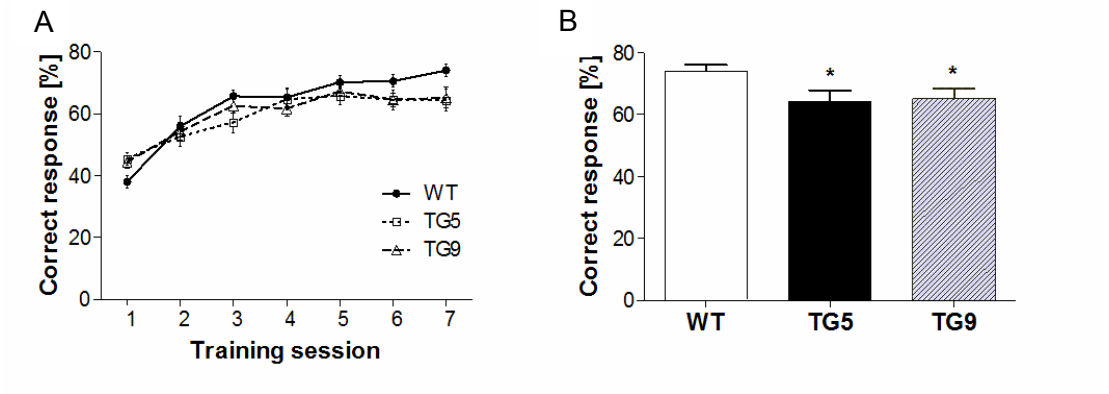

Figure 4.20: Correct responses of rats during reversal stage. (A) Data from the entire experiment; (B) Data from the plateau phase only. *p<0.05.

The number of lever pushes reflects the motivation of the rats which could influence their performance. The numbers of lever pushes were analyzed during the 5-second and 15-second time out phases as well as the reversal phase. In all learning phases, the number of trials had a significant effect on the total number of lever presses ($p<0.0001$ in 5- and 15-second time out phases, $p<0.018$ in reversal learning phase) as seen through a reduction in the number of lever pushes as the test progressed (Figure 4.21). This result indicates that rats reduced ineffective attempts as they learned the cue of response. We normalized the data of 5-second, 15-second time out phase and the reversal training phase to the lever pushes. The significances remain similar to the non-normalized results (data not shown).

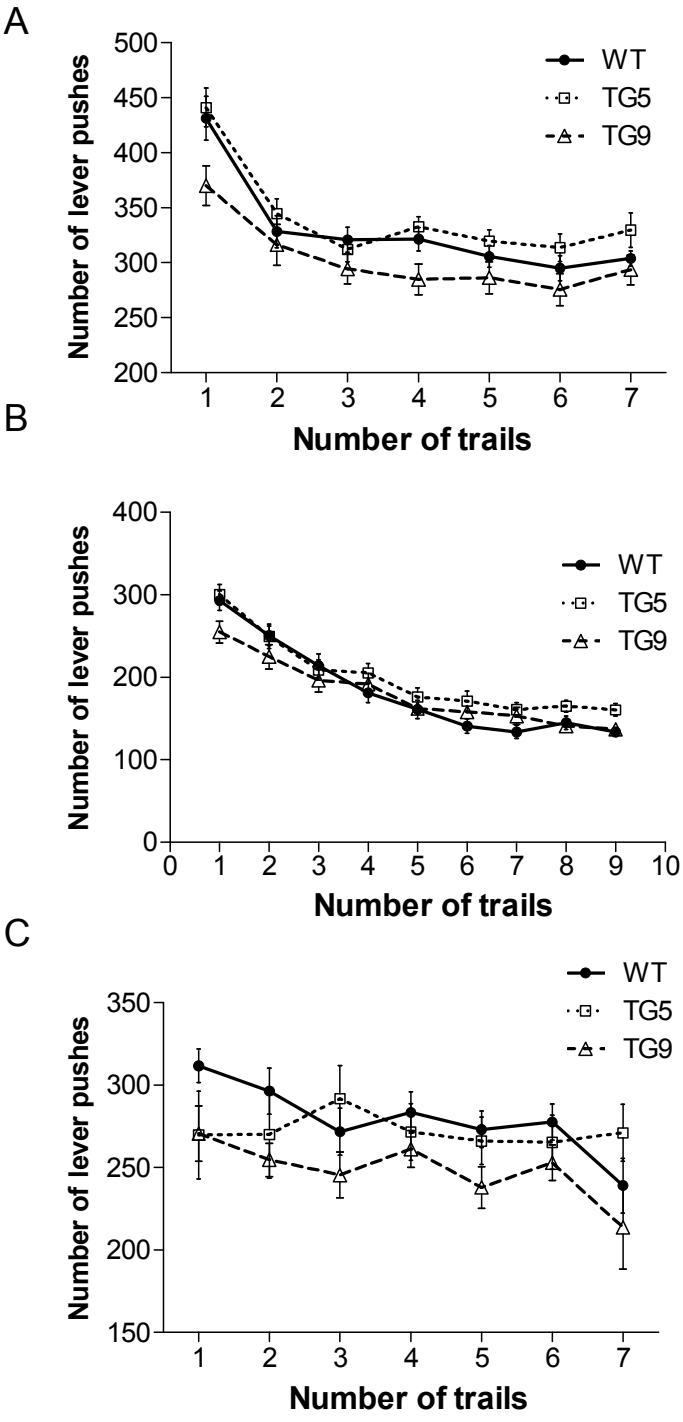

Figure 4.21: Number of lever pushes in different learning stages. In each leaning stage, rats obtained one 30-min training session per day. The number of total lever pushes were recorded and analyzed. During the 5-second time out (A) and 15-second time out (B) stages, there was no effect of genotype observed. In contrast, the number of training sessions showed a strong effect (p<0.0001) on the total lever pushes. This effect remained strongly significant till the reversal learning stage (C), where it was reduced (p<0.01) due to a prolonged learning phase.

Taken together, both BACHD TG5 and TG9 rats showed impairments in learning ability during the acquisition stage, TG5 rats still performed worse than the WT controls even after 4 training weeks. With this data, it is not possible to screen the cognition of BACHD and WT rats in the reversal learning stage as most of the TG5 rats were unable to reach the performance level of the controls. This data is consistent with the simple swimming test results, demonstrating a decline in cognitive function in BACHD rats in early stages.

4.4 Metabolic disturbances in BACHD transgenic rats over-expressing full-length mutant huntingtin

4.4.1 Body weights and body composition in BACHD rats

Studies of HD have been focused on the disturbance of the basal ganglia, but now it is well recognized that a widespread pathology including metabolic changes are involved in HD. Therefore, some aspects of metabolism were assessed in BACHD transgenic rats.

Since it has been shown that an increased expression of full-length mhtt in mice is associated with a dose-dependent increase in body weight (Van Raamsdonk *et al.*, 2006), we have monitored body weight in both lines of BACHD rats and their WT littermates weekly (Figure 4.22). All rats gained body weight during entire study period (72 weeks of age) with neither significant interaction between genotype and age, nor main effect of genotype (repeated-measures ANOVA, $p>0.05$).

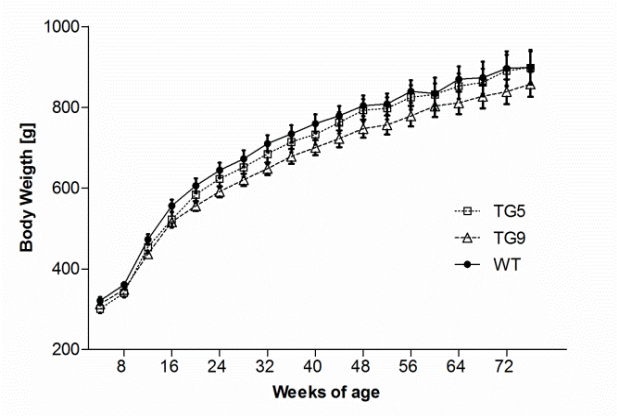

Figure 4.22: Comparison of body weights of BACHD rats and WT littermates. The body weight was measured once a week and showed a continuous increase over 75 weeks but was not significantly different among the three genotypes. WT:TG5:TG9, N = 20:16:22.

The question still remained if body composition differed between genotypes. Together with colleague Laura Clements, we measured the weight of epididymal fat and the perirenal fat tissues relative to body weight and compared data between

BACHD transgenic rats TG5 and WT littermates at 13 months of age (n=12), as well as the weight of the gastrocnemius muscle. A strong significant increase in both epididymal fat and perirenal fat tissues was measured in BACHD rats of line TG5 compared to WT littermates (*student t-test*, $p<0.0001$). In contrast, the weight of the gastrocnemius muscle showed a highly significant decrease in TG5 rats (*student t-test*, $p<0.0001$) (Figure 4.23).

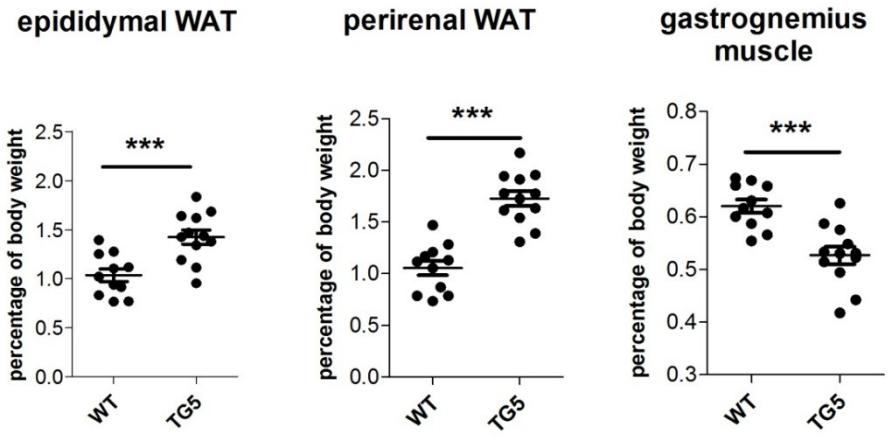

Figure 4.23: Body composition. Epididymal WAT (white adipose tissue), perirenal WAT and gastrognemius muscle were compared between BACHD transgenic rat TG5 and WT littermates at 13 months of age (n=12, student t-test). Both the relative amount of epididymal WAT and perirenal WAT strongly increased in TG5 rats as compared to WT littermates while the weight of the gastrognemius muscle strongly decreased in TG5. ***: $p<0.0001$.

4.4.2 Changes in metabolism related factors detected by PhenoMaster system

Locomotor activity and food consumption of BACHD rats were registered in an automated, home-cage-like environment (PhenoMaster, TSE Systems, Bad Homburg), as well as other metabolism related factors including oxygen consumption, CO_2 production and respiratory exchange ratio (RER). Measurements were taken from one cohort of each rat line (n= 16, 19, 18 for TG5, TG9 and wild type, respectively) every 3 months over a period of 18 months. Oxygen consumption, CO_2 production and RER were measured starting at 9 months of age as a required accessory piece of the PhenoMaster system was unavailable prior to this time point. At each time point, locomotor activities over 22 hours as well as ambulatory and rearing activities during the dark phase were analyzed. Both transgenic and wild type rats showed a pronounced dark-light cycle in all activities with their main activity during the dark phases. The daily behaviour pattern did not differ between different genotypes (Figure 4.24).

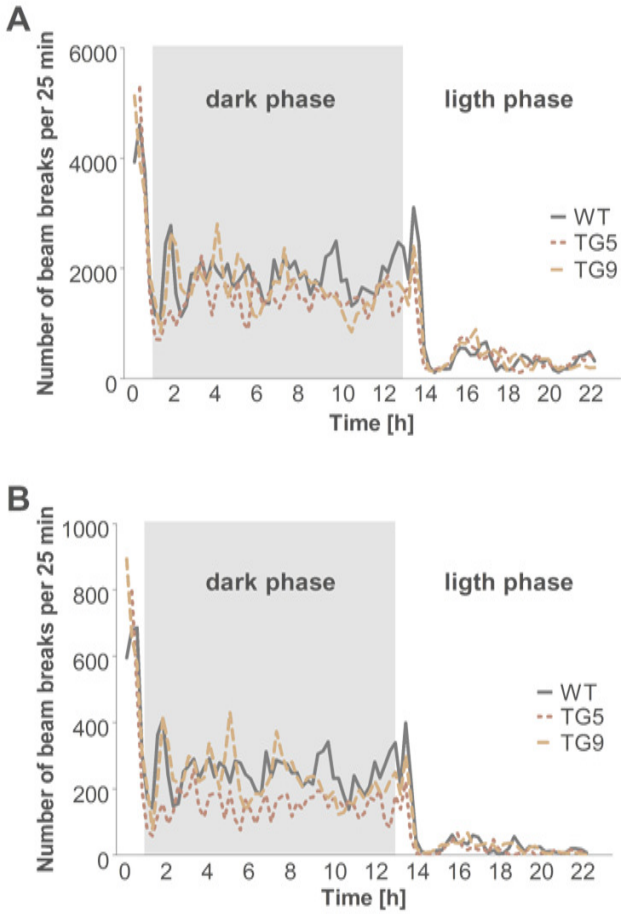

Figure 4.24: Similar circadian pattern of ambulatory and rearing activity in BACHD and wild type rats. Representative plotted ambulatory activity (A) and rearing activity (B) of BACHD TG5, TG9 and wild type littermates during a light-dark cycle. Both transgenic and wild type rats show a light-dark cycle rhythm in all activity measures with their main activity during the whole dark phase of 12 hours.

The total food consumption during the dark phase was compared between the three genotypes over 15 months. Analysis with two-way ANOVA revealed a highly significant main effect of genotype in both water intake ($F_{2,259}$=32.52, p<0.0001) and food intake ($F_{2,259}$=67.80, p<0.0001) (Figure 4.25 A and B). BACHD rats of both lines showed a reduced food intake throughout the study, which was due to a reduced food intake in both transgenic rat lines compared to WT littermates with a mean value of 8.79 g in TG5 and 4.90 g in TG9 in food intake compared to 20.71g in WT. However, water intake reduction was only observed in TG5 with a mean value of 13.91 g compared to 28.54 g in WT. There was no significant interaction between genotype and age in both water ($F_{10,259}$=0.88, p=0.5520) and food consumption ($F_{10,259}$=1.06, p=0.3965).

Highly significant differences in ambulatory activity were found at early time points in both transgenic rat lines compared to WT (both TG5 and TG9 p<0.001 at 3 and 6 months of age) (Figure 4.25 C and D). The reduction in rearing activity was only observed in TG5 compared to WT control rats at early time points (p<0.05 at 3 months of age, p<0.0001 at 6 months of age). The significance of these observations was confirmed by two-way ANOVA, which indicated a highly significant interaction effect (genotype X age: $F_{10,259}$=4.22, p<0.0001) in ambulatory activity, a main effect of genotype in both ambulatory activity ($F_{2,259}$=22.32, p<0.0001) and rearing activity ($F_{2,248}$=15.11, p<0.0001) as well as a main effect of age ($F_{5,259}$=217.89, p<0.0001 in ambulatory activity; $F_{5,248}$=23.23, p<0.0001 in rearing activity).

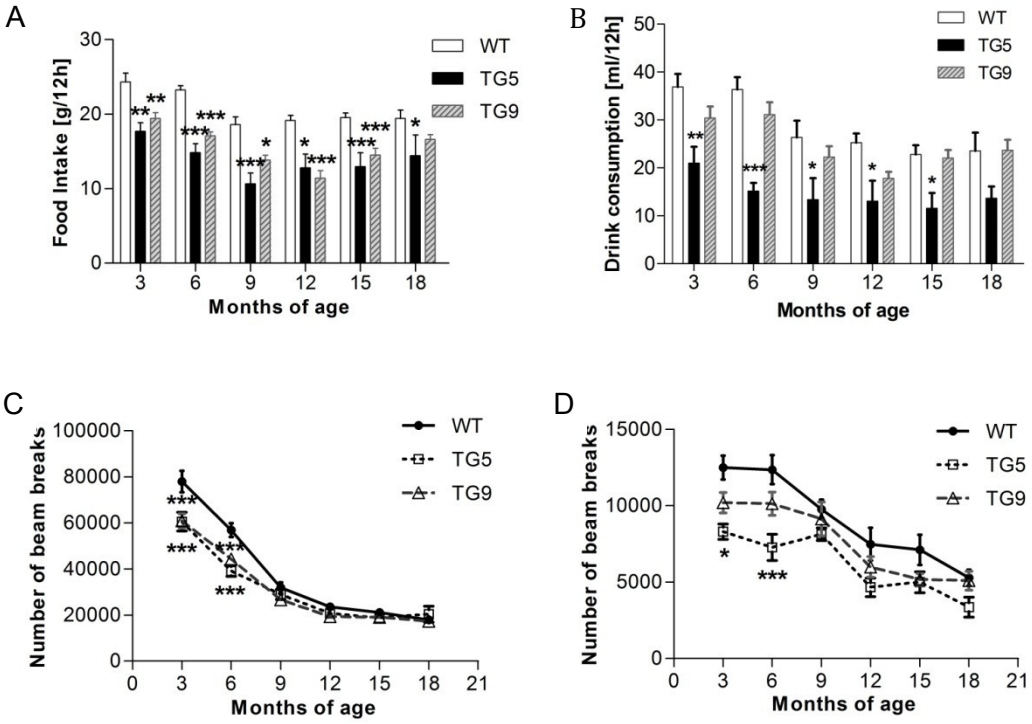

Figure 4.25: Reduced food consumption and locomotor activity in BACHD rats. Over an 18 month period with 3-month intervals, a cohort of TG5 (n=16), TG9 (n=20) and WT rats (n=22), was measured for food (A) and water (B) intake, as well as ambulatory activity (C) and rearing (D) during the 12 hours of a dark phase. We found a significantly decreased food consumption in both transgenic lines over 18 months (asterisks), while the water intake reduction was only observed in line TG5. Both ambulatory activity and rearing decreased in all three genotypes over time, whereas significantly lower activity and rearing in both TG5 and TG9 compared to the WT rats were only observed up to 6 months of age. Data are expressed as means ± SEM, *p <0.05; **p<0.01; ***p<0.001.

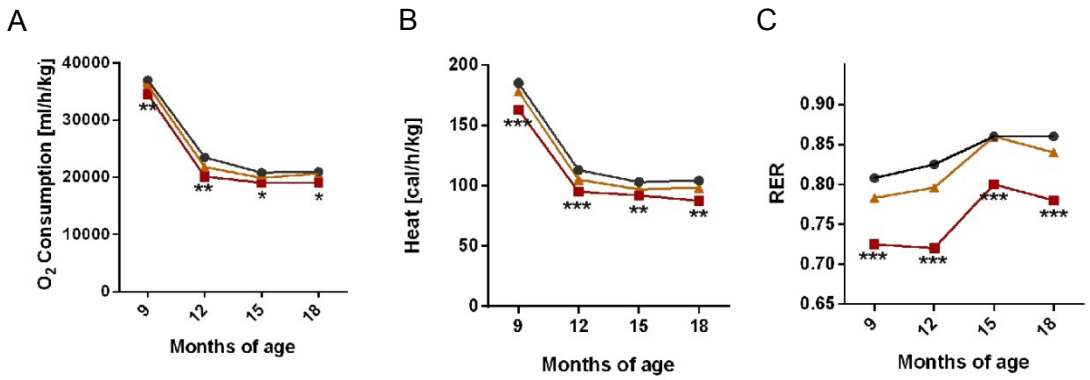

Figure 4.26: Reduced oxygen consumption, heat and RER in TG5 rats at all time points investigated. The same cohort of rats was measured for oxygen consumption (A), heat (B) and RER (C) starting at 9 months of age until 18 months of age. Both oxygen consumption and heat obviously dropped in the first 3 months, and remained relatively stable in the last 6 months. One-way ANOVA analysis at each time point revealed a highly significant decrease of oxygen consumption and heat in TG5 rats compared with WT littermates at 9 and 12 months of age. However this difference was less striking in the last 6 months of measurements. RER showed a slight increase over time, and a highly statistical significance was determined between TG5 and Wt. Data are presented as mean ± SEM, **p* <0.05; ***p*<0.01; ****p*<0.001.

Oxygen consumption, heat and RER were compared between BACHD transgenic rats with WT controls in the dark phase as well. The analysis was performed using the average measurement from the three days at each time point, employing one-way ANOVA. Heat and oxygen consumption of rats from all genotypes clearly dropped from 9 months to 12 months of age and then remained relatively constant until the last time point investigated, the RER however showed a tendency to increase over time (Figure 4.26 A, B and C). The results revealed a highly significant decrease of all of these three factors in BACHD transgenic TG5 rats compared to WT animals at all time points. In contrast only a slight reduction was detected in TG9 showing no significant difference. Food consumption analysis revealed a decreased food intake in the transgenic rats, which could have resulted in a reduction of RER due to hunger. To test this hypothesis the time course of these parameters during all three days was analyzed for the transgenic animals at 18 months. However, no significant difference for all parameters was found between the first and last day of testing (Figure 4.27), and therefore a hunger effect is unlikely to affect the RER in the transgenics.

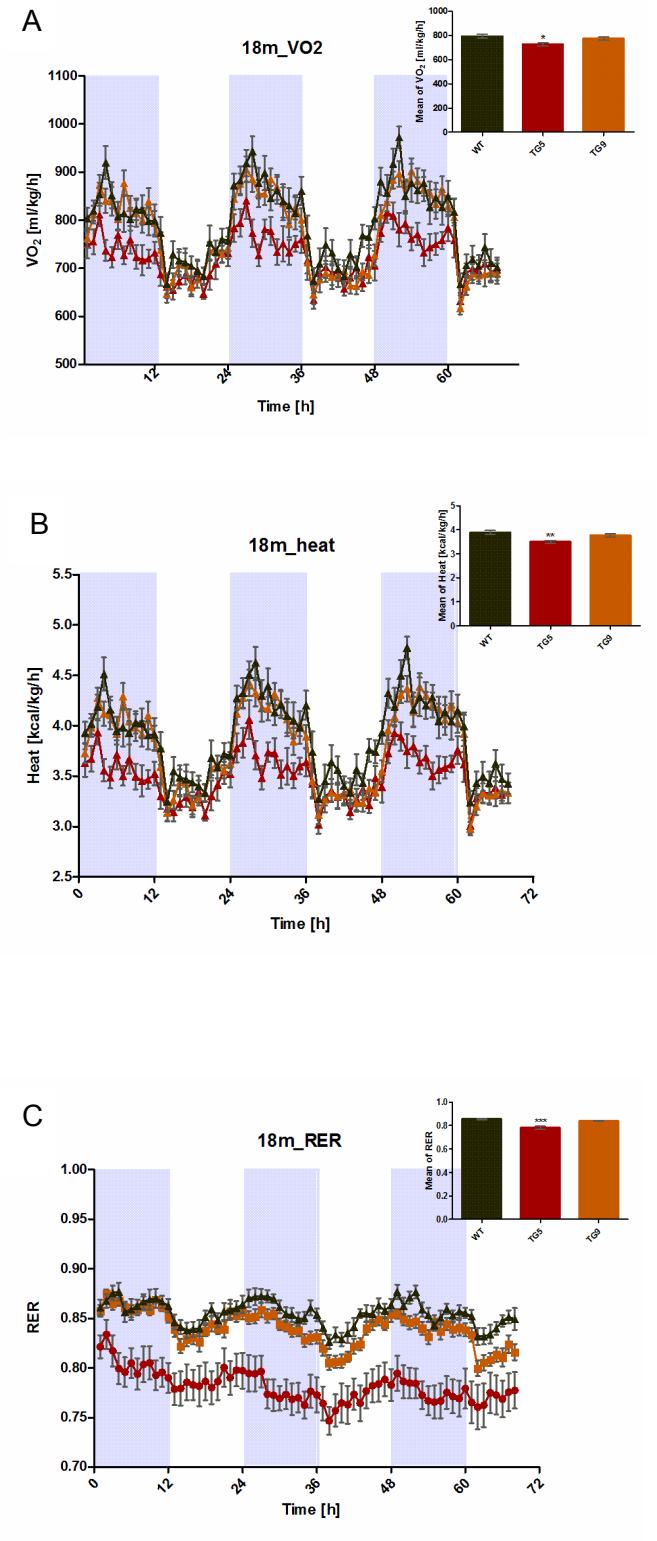

Figure 4.27: Time course of oxygen consumption, heat and RER measurements over a period of 3 days at 18 months of age. Data were reported as mean of oxygen consumption (A), heat (B) per kilo each hour and average of RER in each hour (C). All the genotypes showed a similar circadian pattern. Data summaries indicated a significantly decrease in oxygen consumption, heat as well as RER in TG5. Data were expressed as mean ± SEM, **p*<0.05; ***p*<0.01; ****p*<0.0001.

In summary, the data from the PhenoMaster demonstrates a reduced food and water intake in BACHD TG5 rats. Although the decrease in ambulatory and rearing activity was only detected in the early stages up to 6 months of age, TG5 rats still show a reduced oxygen consumption and CO_2 production as well as RER over the time

points investigated. In the younger ages, a decreased food consumption and ambulatory activity were found in TG9 rats as well, although this was not as striking as in TG5 rats.

4.5 Huntingtin aggregates increase over time and are widely distributed in BACHD rats

In order to investigate the regional distribution pattern of mhtt-positive aggregates in BACHD transgenic rats, we used the polyclonal sheep antibody S830 in serial brain sections at 12 months of age (Figure 4.28). In TG5 and TG9, the aggregates are abundantly distributed in the neocortex (layer I-V), comparably very few aggregates can be detected in the caudate putamen (CPu) as well as its projection regions such as the lateral globus pallidus and the substantia nigra (data not shown). The cerebellar cortex showed a few small aggregates throughout the three layers (molecular, granule and the purkinje cell layers) (data not shown). Furthermore, the aggregates are widely distributed in all limbic structures with an abundant expression in nucleus accumbens, hippocampus (specifically in the CA3 region), bed nuclei of the stria terminals (BNST), the amygdala, the lateral septum and hypothalamus (Figure 4.29). A slightly reduced expression was observed in most thalamic nuclei (data not shown). Finally, the distribution of mhtt aggregates were summarized in a graph in detail (Figure 4.30). Chain-like structures were observed throughout the brain areas with abundant mhtt indicating that mhtt aggregates are primarily located in the neuropil.

Both the size and number of aggregates increased with age, showing the largest and most abundant aggregates in amygdala, in the CA3 region of the hippocampus, and in the cerebral cortex, indicating that aggregate formation continued to progress in these regions (Figure 4.31).

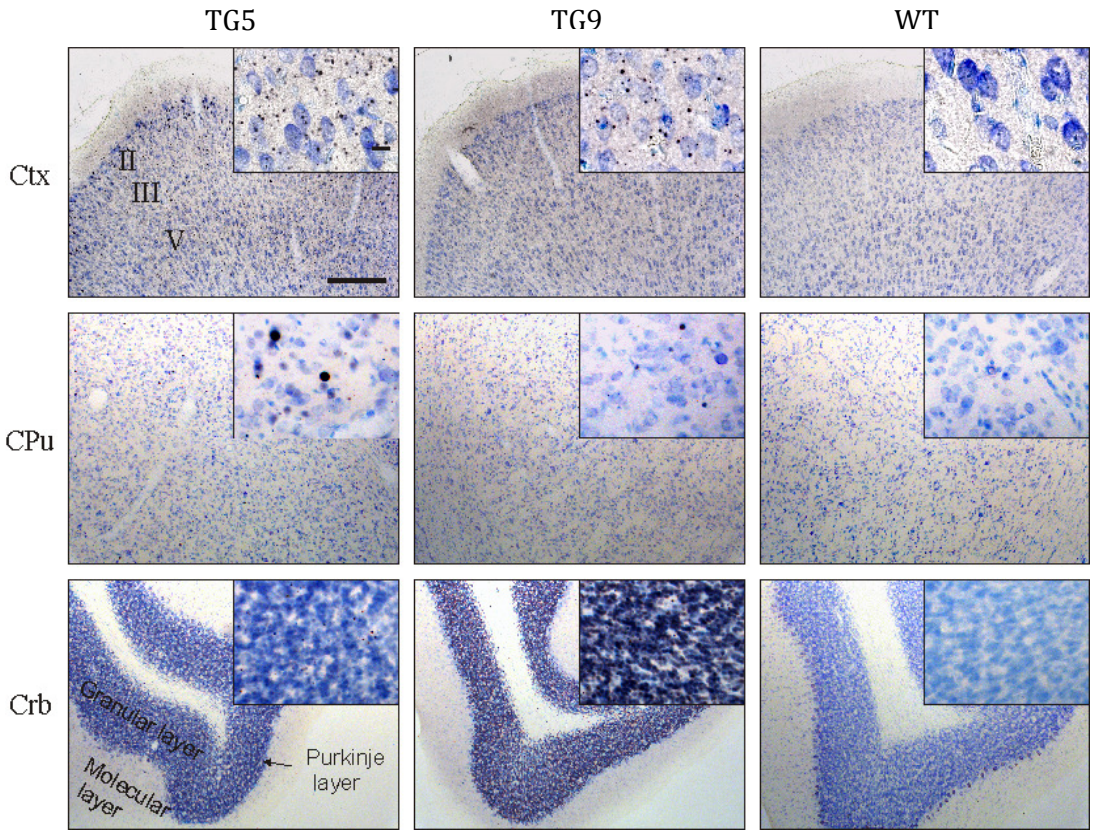

Figure 4.28: Mutant htt S830 immunoreactivity is widely distributed in different layers of cerebral cortex, but few in CPu. Coronal brain sections of rats at age of 12 months of age were stained by polyclonal antibody S830, nickel-DAB (black) visualizes immunoreactivity of mhtt, the counterstaining with thionin (blue) marks nuclei. In both TG5 and TG9 rats, aggregates varying in size and formation were abundant in the cortex (Ctx) with highest expression in layer I, II/III and V. In contrast, only few aggregates were found in the caudate putamen (CPu). Very little aggregates were observed in the cerebellum (Crb) throughout all three layers (granular layer, molecular layer and purkinje layer). The abundance of aggregates in both lines TG5 and TG9 correlates with the protein expression level as the aggregates were larger and more abundantly distributed in TG5 compared to TG9. Scale bars: inlay showing high magnification images, 20 µm; in low magnification images, 200 µm.

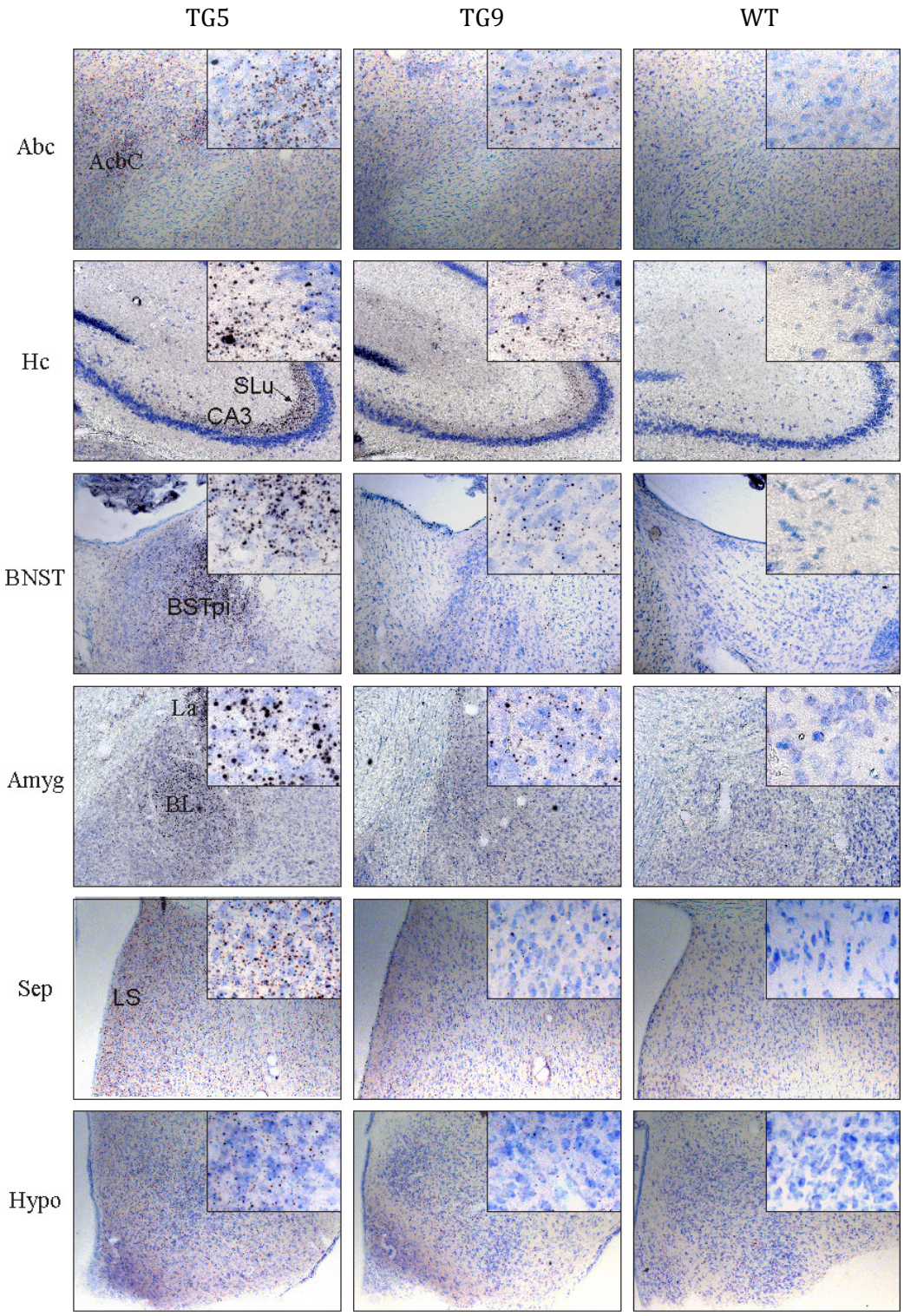

Figure 4.29: Mutant htt immunoreactivity is widely distributed in limbic structures in BACHD rats. Coronal brain sections of rats at age of 12 months of age were stained by polyclonal antibody S830, nickel-DAB (black) visualizes immunoreactivity of mhtt, the counterstaining with thionin (blue) marks nuclei. In BACHD transgenic rats of lines TG5 and TG9, aggregates were abundantly distributed in all the limbic structures. Most aggregates with a large size were found in the hippocampus (Hc), especially in the stratum lucidum (SLu) of CA3 area (arrow), as well as in posterointermediate bed nucleus of stria terminals (BSTpi) and all the nuclei of amygdala (Amyg). Relatively smaller aggregates were found in nucleus accumbens core (AcbC), lateral septum (LS) and most nuclei of the hypothalamus. There was no immunoreactivity found in WT rats. Scale bars: inlay showing high magnification images, 20 µm; in low magnification images, 200 µm.

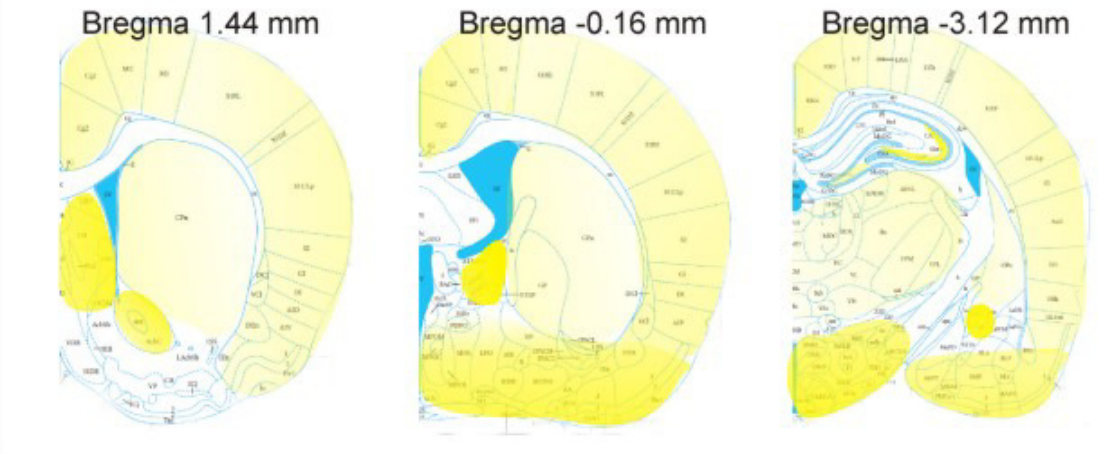

Figure 4.30: Summary of aggregates distribution in BACHD rats brain at 12 months of age. The density of aggregates is represented by a color gradient (darker yellow: more abundant, lighter yellow: less abundant).

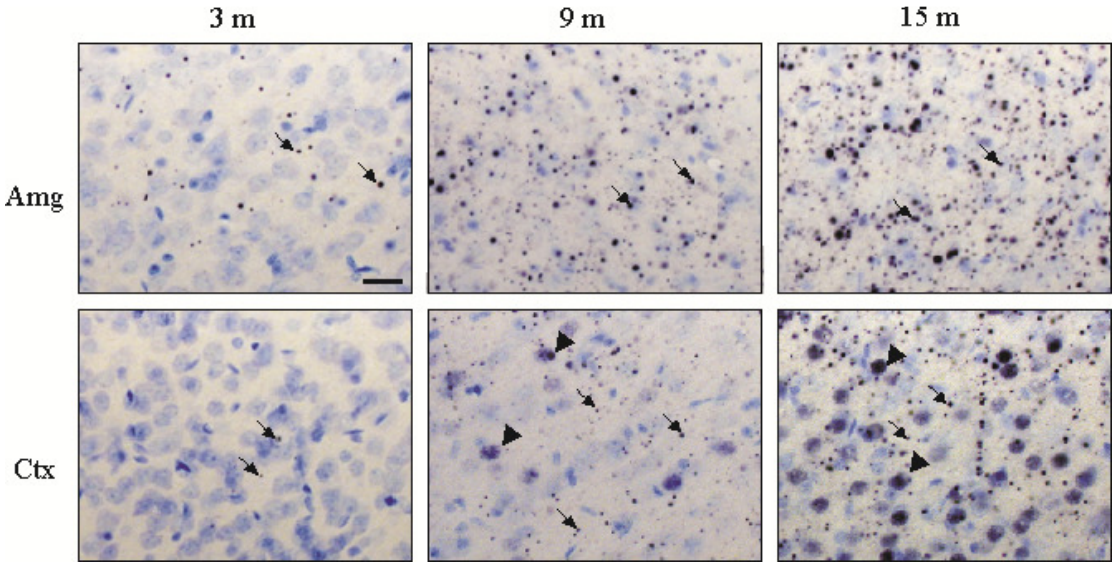

Figure 4.31: Spatio-temporal accumulation of mhtt in amygdala (Amg) and cortex (Ctx) of TG5 rat brains. An increase in both number and size of neuropil aggregates (arrows) was observed in both regions during aging; nuclear accumulation of mhtt (arrow heads) appeared only in cortex at 9 months of age becoming more abundant at 15 months of age. Scale bar, 20 µm.

Only in older rats, nuclear accumulation of N-terminal huntingtin was found in the cerebral cortex, striatum and the granule cells of the dentate gyrus. Nuclear accumulation was observed after the age of 9 months and increased over time. Large magnification imaging showed an uneven distribution of htt accumulation in the nuclei (Figure 4.32). No immunoreactivity of the antibody S830 was observed in wild type rats in all the investigated time points.

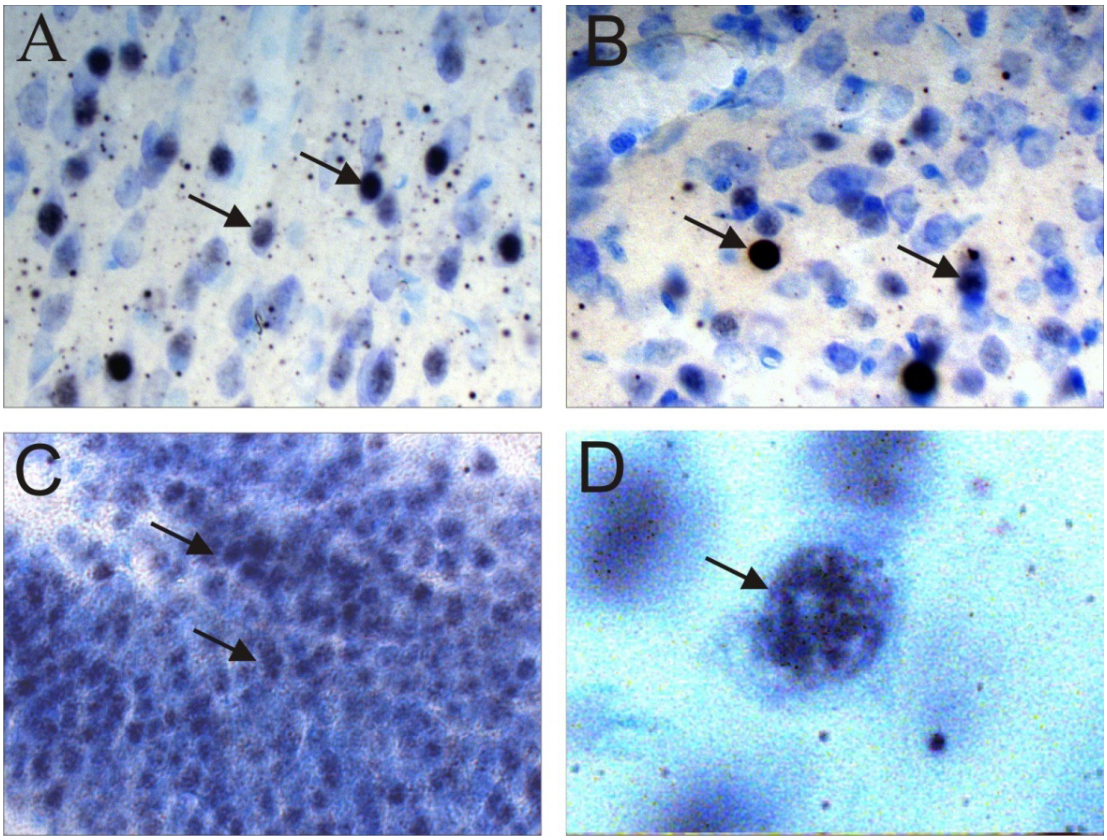

Figure 4.32: Nuclear accumulation of N-terminal mhtt in BACHD transgenic rats at 12 months of age. Immunoreactivity of S830 of different density merged with thionin staining was observed in cerebral cortex layer II/III (A), striatum (B), the granule cells in hippocampus (not shown), cerebellum (not shown) and olfactory bulb (C). (D) A large magnification image of a nucleus with mhtt accumulation, some granule structure was observed showing uneven distribution of mhtt accumulation.

4.6 Imbalance of striosome and matrix compartments in early disease stages in BACHD rats

Calbindin immunostaining was performed to determine changes in the striosome and matrix compartments, as calbindin is strongly expressed in the matrix surrounding the Calbindin-poor striosomes (Figure 4.33 A). The intensity of the calbindin staining either in the matrix or in the irregular shaped striosomes was not altered in BACHD rats compared to WT littermates (Figure 4.33 A), nor was the total matrix area or the number of the striosomes (Figure 4.33 B). However, the total striosome area (Figure 4.33 C) and the mean area of the striosomes (Figure 4.33 D) were significantly reduced in TG5 transgenic rats compared to WT littermates (29%, p<0,001 and 34%, p=0,044). TG9 rats did not show this significant reduction in striosomal area. This imbalance in the striosome-matrix compartments in TG5 rats may affect the equilibrium of inhibitory and excitatory output from the striatum to downstream neurons.

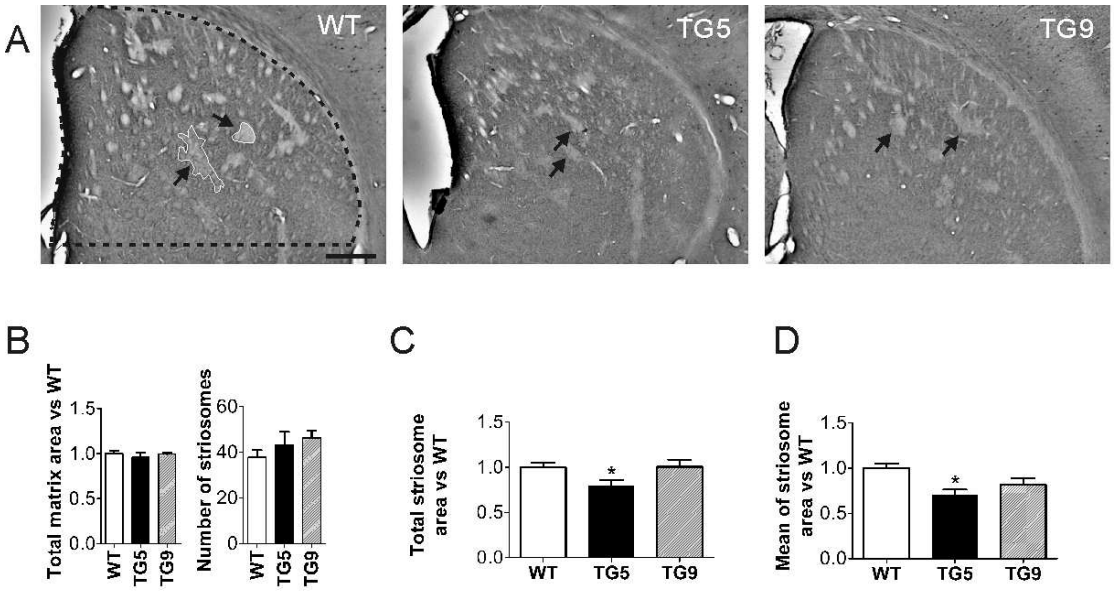

Figure 4.33: Striosome abnormalities in the striatum of BACHD rats. The region of interest is outlined in in dotted black line. (A) Calbindin immunostained sections of WT, TG5, and TG9 rats at 6 months of age show striosomes visible by faint calbindin staining ((arrows and outlined in continuous white line), while the intense staining visualizes the matrix surrounding the striosomes. Scale bar, 0.5 mm. (B) The total matrix area and number of striosomes (B) was similar in WT, TG5 and TG9 rats. A significant decrease in both total (C) and mean striosome areas (D) was only observed in TG5 rats compared to WT littermates. Data is expressed as means ± SEM, **p*<0.05.

4.7 Analysis of apoptosis in BACHD rats

BACHD rats show a reduced brain volume compared to WT littermates in advanced stages of the disease suggesting neuronal cell death in aged animals. Since the basis of neuron death still remains elusive, BACHD rats were analyzed for molecular markers involved in cell death.

4.7.1 TUNEL assay and anti-PARP staining

TUNEL assay (Terminal deoxynucleotidyl transferase dUTP nick end labeling) is a method for detecting apoptosis via labeling the terminal end of nucleic acids identifying DNA fragmentation. Coronal cryosections of the BACHD rats lines TG5 and TG9 as well as WT controls were used for TUNEL staining. Sections of all brain regions of transgenic and WT rats were included into the analysis. An unspecific TUNEL labeling caused by labeling of synthesized RNA is indicated by a red staining in close proximity to the DAPI labeled nuclei (Figure 4.34). A co-localization of TUNEL-labeling and the DAPI staining was not detected indicating no DNA fragmentation in both BACHD transgenic rats and WT controls.

In order to confirm the results of the TUNEL assay, anti-poly (ADP-ribose) polymerase (PARP) staining was performed. PARP is cleaved by members of the caspase family during early apoptosis. Coronal cryosections from TG5, TG9 and WT rats were used for the immunohistological staining with anti-PARP. A strong black staining in neurons were found in the positive control (brain sections of postnatal day one rat, data not shown), however there was no positive staining in brain sections of both transgenic and WT rat at the age of 15 and 18 months.

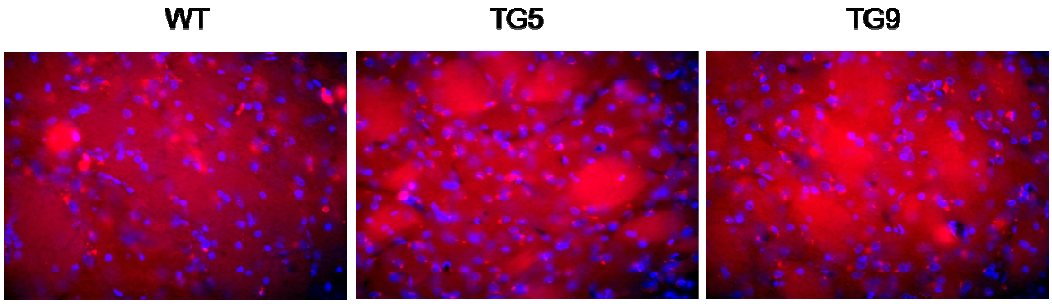

Figure 4.34: TUNEL assay in BACHD rats at 18 months of age. TMR red fluorescence detects dUTP nick end labeling, blue fluorescence indicates nuclei. There is no obvious overlap of red and blue fluorescence indicating no apparent DNA fragmentation and therefore apoptosis in both BACHD transgenic rats and WT controls.

4.7.2 Analysis of caspase activity in BACHD rats

Caspase-3 and caspase-6 are two important effector caspases which are activated by initial cleaving of the inactive pro-forms. It was reported for HD that as the disease progresses, caspase 3 is transcriptionally up-regulated and its protein is activated (Chen M, 2006). Increased caspase-mediated cleavage of huntingtin increases the generation of huntingtin fragments and depletes WT huntingtin (Ona VO, 1999). It was also reported that the N-terminal proteolytic processing of mutant huntingtin can be modulated with an effect on aggregation and cell death rate (Katrin Juenemann, 2011). The active (cleaved) caspase-3 was detected by immunohistological staining and Western Blot analysis at 15 months of age. Immunohistological staining against active caspase-3 show some positive cells with staining in both cell body and their processes in the positive control sections (brain section of P1 rat), but not in the sections of both BACHD transgenic rats and WT littermates at 18 months of age (Figure 4.35). Western blotting was performed using striatal lysates of rats at 18 months of age. In the positive control (pretreated cell lysate), the active form of the caspase-3 was detected with a size of 17 kDa. In contrast, only two weak unspecific bands with an approximate size of 23 kDa and 24 kDa were present in BACHD rats and WT littermates showing no difference between BACHD rats and the WT control

(Figure 4.36). Taken together, no elevated apoptosis markers were detected in the BACHD transgenics up to 18 month of age as indicated by the results of TUNEL-labelling, silver staining (data not shown) and cleavage of PARP and caspase-3.

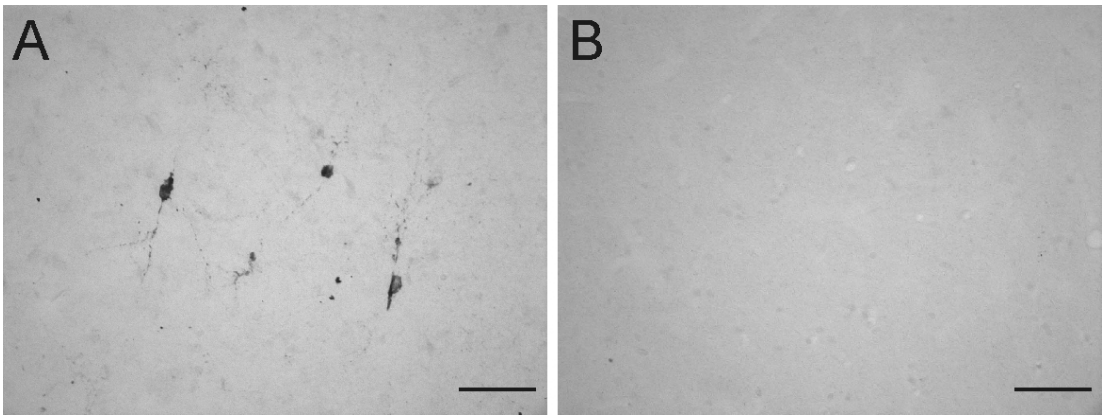

Figure 4.35: Caspase-3 immunohistological staining. Brain sections of BACHD rats and WT controls at 15 months of age were stained with an antibody recognizing the active form of caspase-3 (TG5:TG9:WT= 6:5:5). Brain sections of P1 rat was taken as positive control showing several active caspase-3 positive cells with darkly stained cell body and neuronal processes (A), the sections of BACHD rats and WT controls present similar immunoreactivity, although positively stained cells could not be detected in all of three genotypes. Scalebar 50 µm.

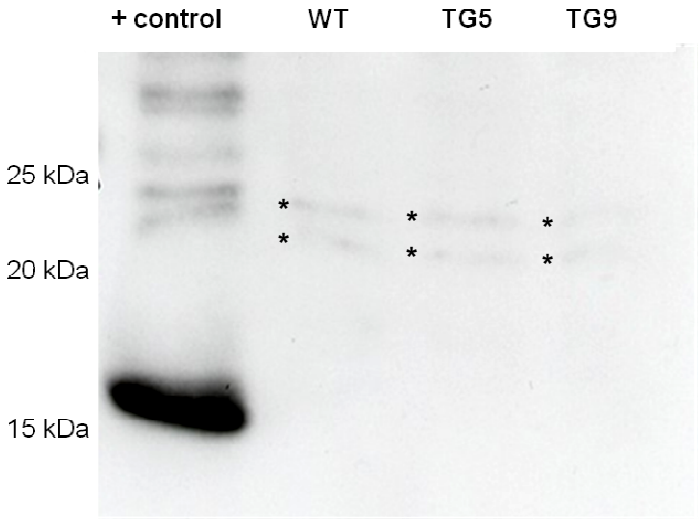

Figure 4.36: Activated caspase-3 detected via western blotting. 50 µg of striatal lysates from BACHD rats and WT littermates at 18 months of age were taken for SDS-PAGE. Cell extract treated in vitro with cytochrome c was used as positive control. After long exposure, only two unspecific bands (stars) were detected in the BACHD and WT rat samples, while a strong 17 kDa band was detected in the positive control sample.

It was described, that cell dysfunction and degeneration requires cleavage of caspase-6 in a HD transgenic mouse model and preventing proteolysis at the capase-6 consensus sequence at amino acid 586 of mutant huntingtin prevents the development of behavioral, motor and neuropathological features (Graham *et al.*, 2006). It was also reported that caspase-6 is active in the YAC mouse MSNs and increased caspase-6 expression results in cell death (Warby *et al.*, 2008). In order to

assess the caspase-6 activity in BACHD transgenic rats, we stained coronal brain sections of 15-month-old rats (TG5:TG9:WT=6:5:5) and performed Western blot using striatal lysates of rat brains of the same age. Comparable with the results for caspase-3, no immunreactivity was found in immunohistological stainings and no active form of caspase-6 was detected in Western blot analyses (data not shown).

4.7.3 Analysis of calpain activation and spectrin cleavage

Cell death in neurodegenerative diseases involves multiple mechanisms, and different death pathways interact with each other. In both programmed apoptosis and non programmed necrotic cell death, calpains are activated by the increase of intracellular calcium, when cells are exposed to extreme stress conditions.

In addition to an altered subcellular localization it was reported that the calpain expression level is increased in HD patients in the medium spiny cells and in the cells close to the lateral ventricle. Immunofluorescence staining of calpain-2 and calpain-10 was performed using paraffin sections of rat brains at 9 and 15 months of age. Calpain-1, which is the predominantly activated member of the calpains, was left out due to difficulties in detection. The immunoreactivity of calpain-2 and calpain-10 was detected in the region of interest (ROI) including striatum, cortex and thalamus showing a cytoplasmic distribution in some large neurons (Figure 4.37). A slightly reduced immunofluorescence signal was found in striatum, cerebral cortex and cerebellum for both anti-calpain-2 and -10 in BACHD TG5 rats. There was no difference in the subcellular localization between transgenic rats and the WT littermates. In order to detect the activated forms of calpain, Western blots were performed using striatal lysates of rats at 18 month of age (n=3) (Figure 4.38). The blot probed with anti-calpain-2 showed only one band at about 72 kDa, whereas the blot probed with anti-calpain-10 showed a band with a size of approximately 75 kDa, and more bands around 65 kDa, which represent the cleaved and uncleaved form of calpain-10, respectively. Band intensities did not display any difference between the genotypes, which indicated that calpain-10 activation was not altered in BACHD rats. Since we failed to detect calpain activation, we wondered whether calpains are truly not activated in BACHD transgenic rats, or whether the changes were too subtle to be detected.

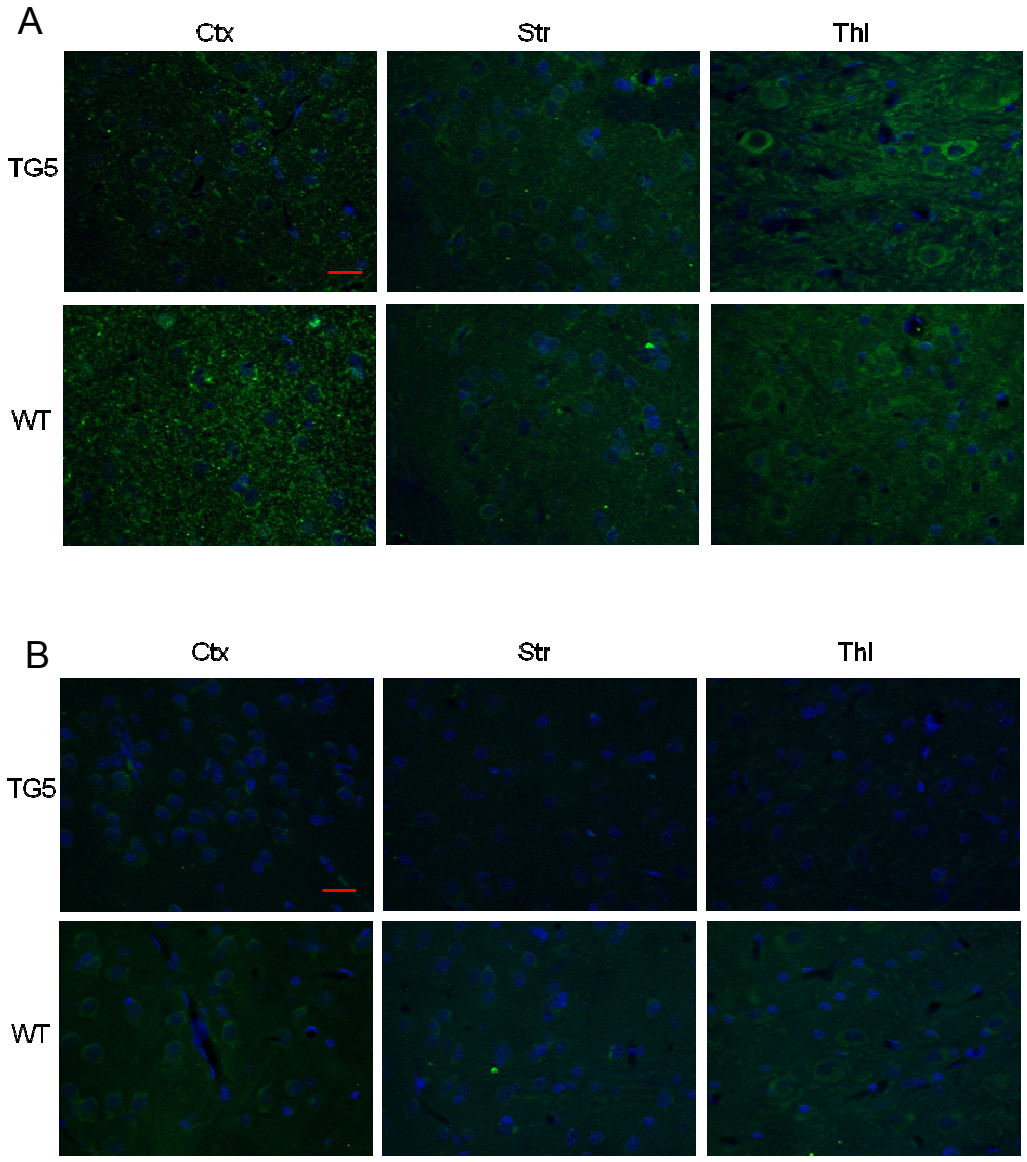

Figure 4.37: Immunofluorescence staining of calpain-2 (A) and calpain-10 (B) at 15 months of age. Paraffin sections of BACHD TG5 rats and WT controls at 15 months of age were stained with anti-calpain-2 and anti-calpain-10 (n=2) separately. Immunoreactivity of both calpain-2 and calpain-10 were mainly detected in the cytoplasm showing similar staining intensity of calpain-2 in each brain region of both genotypes (A). A fainter staining of calpain-10 was detected in the striatum of WT compared to cortex and thalamus, while in BACHD TG5 rats the immunoreactivity of calpain-10 was slightly less than in the WT controls in all brain regions investigated (B). Scalebar 50 µm.

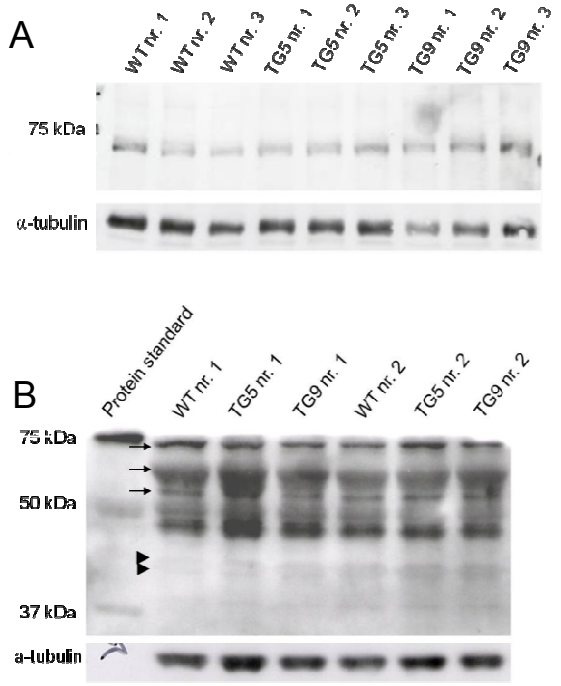

Figure 4.38: Western blot analysis of calpain-2 and calpain-10 in striatum. Western blots were performed using striatal lysates of 18-month-old BACHD transgenic rats and WT littermates. (A) In the blot probed with anti-calpain-2, a single band of approximately 70 kDa was detected in all genotypes, whereas the density of bands was equally present in all samples. (B) In the blot probed with anti-calpain-10, 3 bands between 60 and 75 kDa (arrows) were present in all the genotypes with similar density, as well as two bands of approximately 45 kDa (arrowheads) most likely representing unspecific binding of the antibody.

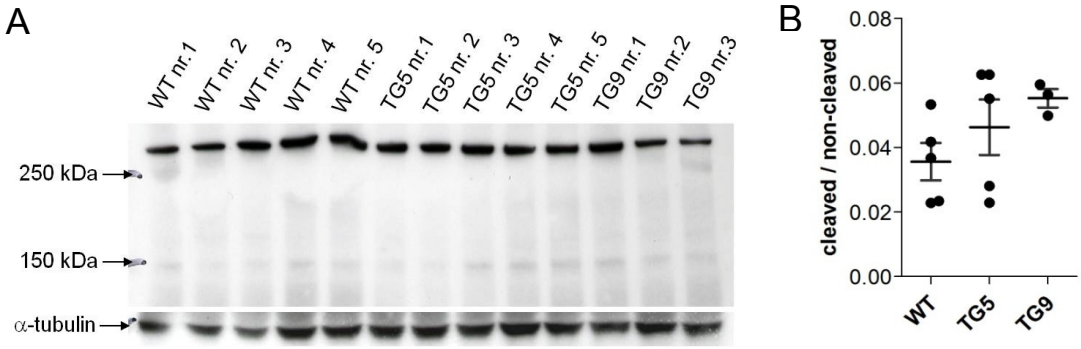

Figure 4.39: Western Blot analysis of spectrin cleavage. Western blots were performed utilizing striatal lysates of 12-month-old BACHD transgenics and WT littermates and probed with anti-spectrin. (A) A strong non-cleaved band of 280 kDa and a faint 150 kDa band were detected in the blot. (B) The quantification of the ratio between cleaved and non-cleaved bands using one-way ANOVA did not reveal any statistical significance between the genotypes.

Spectrin is one of the most important substrates of the calpains. Their abundance and high stability has been observed in experimentally induced cell pathology as well as in clinical studies. A link beween calpain activation and the earliest stages of neuronal cell degeneration is also well described (Vanderklish and Bahr, 2000). Cleavage of spectrin was therefore analyzed utilizing Western blot in striatal lysates of BACHD rats and WT controls at 15 months of age (n=5). Western blot analyses showed a very strong band of approximately 280kDa (full-length spectrin) and a weak band of about 150 kDa (cleaved fragment, Figure 4.39). Quantification using

ImageJ did not yield any differences in the intensity of both 280 kDa and 150 kDa bands between transgenics and WT rats.

4.7.4 Assessment of neuronal architecture (number, morphology and organization of neurons) in BACHD rat brains

In order to assess neuronal degeneration, the numbers and the distribution of cells were evaluated by Nissl and NeuN staining using rat brain sections of BACHD rats and WT littermates at 3 and 12 months of age. Nissl staining of both younger and older rats show a normal distribution and number of densely packed neurons with smaller neighboring glia cells in BACHD transgenic rats compared with WT controls. Morphology and size of neurons appeared normal in both groups (data only shown for 12-month-old animals). The staining also showed a normal cellular organization and orientation in different brain structures (Figure 4.40). There was no obvious cell loss throughout the whole brain. Very few condensed dark neurons were found in cortex and striatum in all the genotypes showing no difference in severity.

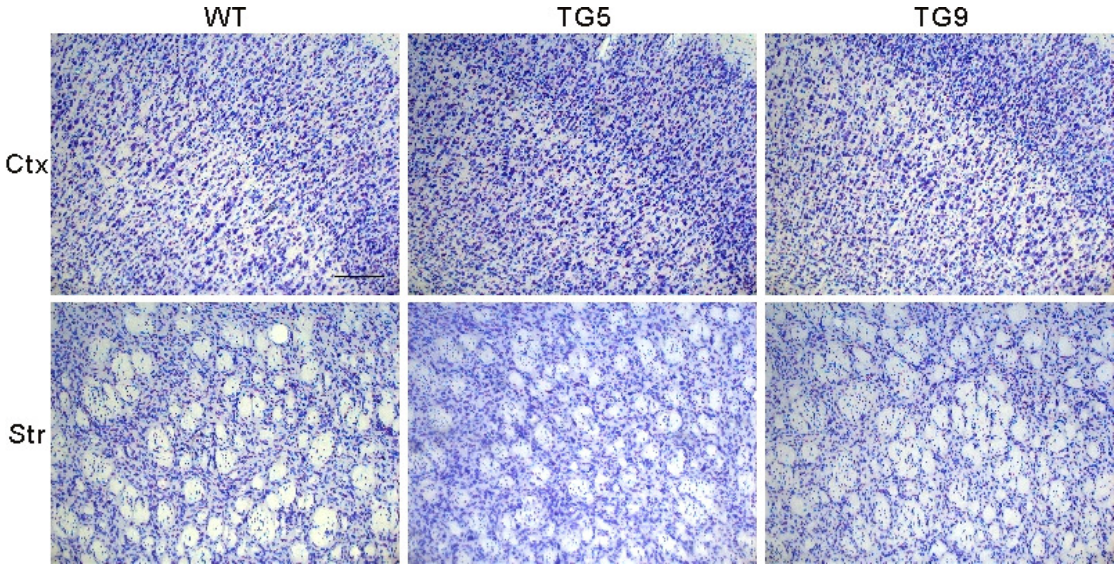

Figure 4.40: Staining of brain sections with thionine reveals a normal brain architecture in BACHD transgenic rats at 12 months of age. The Nissl substance (rough endoplasmic reticulum) is darkly-stained by thionine. The cell bodies of neurons, which contain a lot of rough endoplasmic reticulum, appear as dark granules at low magnification. The cortex plate of BACHD transgenic TG5 and TG9 seem slightly thinner compared to the WT littermates showing normal cell organization and cell orientation in different cortical layers. There is no obvious cell loss in both cortex and striatum. Scale bar: 200µm.

Comparable with Nissl staining, the anti-NeuN staining detected a normal size, morphology as well as distribution and orientation of neurons with a homogenous

immunoreactivity in the nuclei of neurons in BACHD transgenics (Figure 4.41). Especially the cortical columns were visible with NeuN staining and the cerebral cortex shows an organization with indistinct layers indicating a normal cellular architecture in BACHD rats. There was no obvious sign of neuron loss in different brain regions.

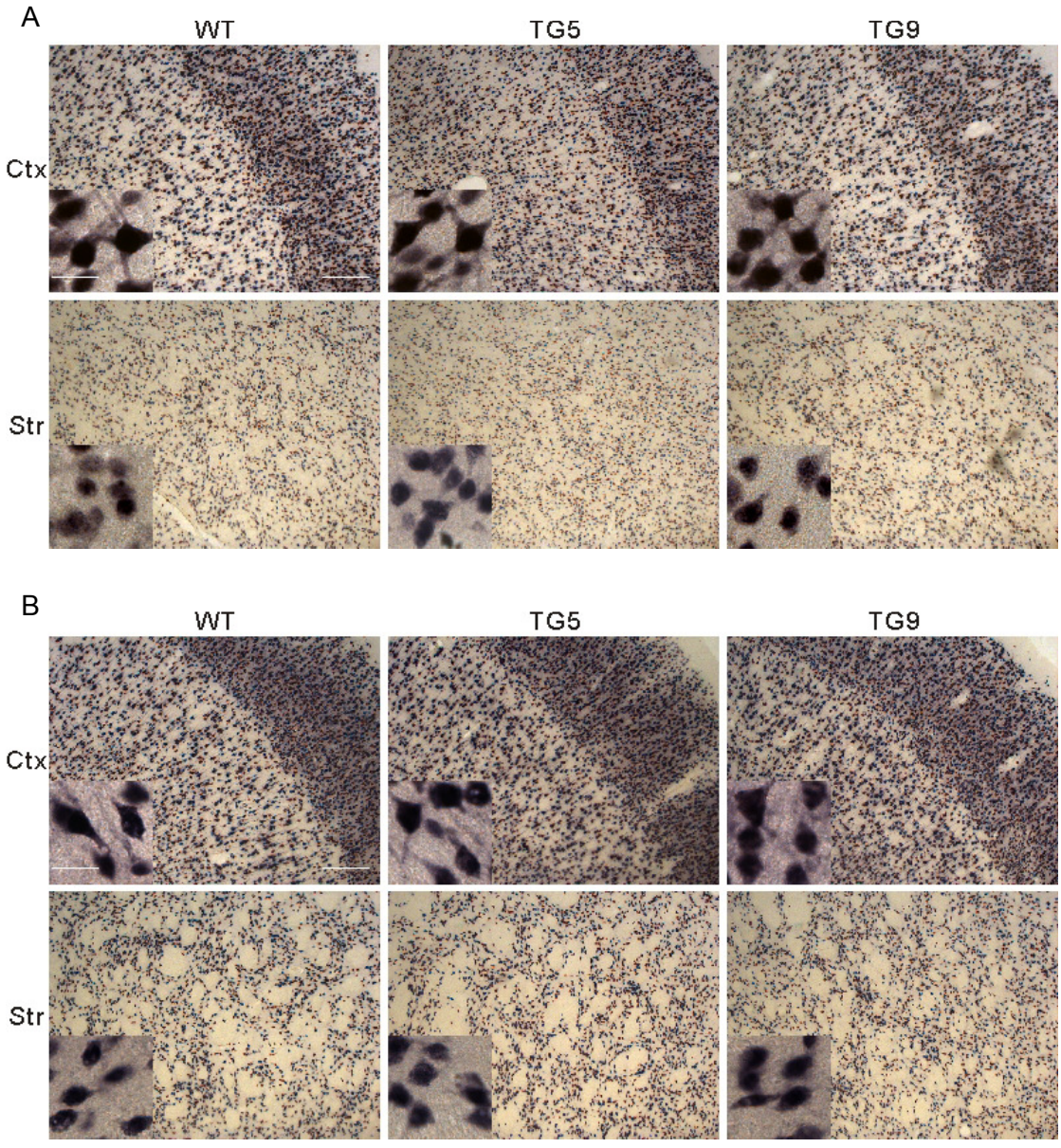

Figure 4.41: Staining of brain sections with anti-NeuN reveals a normal brain architecture and neuron density in BACHD transgenics. Anti-NeuN staining was used to recognize the neuron-specific DNA-binding protein in cortex and striatum at 3 (A) and (B) 18 months of age. Neurons in BACHD transgenics show the same morphology, size and density compared to WT controls indicating no obvious changes in brain structure and neuron loss until 18 months of age. Scale bar in lower magnification images: 200µm; Scale bar in inlay: 20 µm.

4.7.5 Reduction in cross-sectional thickness of axon bundles in the striatum

As described above, no distinct changes in cell number and morphology were observed in BACHD rats untill 18 months of age, although a robust progressive behavioural phenotype is present starting at 1 month of age. In order to further investigate the underlying pathological changes in BACHD rats, the thickness of axon bundles in the striatum were assessed by immunohistological staining with anti-Myelin Basic Protein (MBP), which is a major constituent of the myelin sheath of oligodendrocytes in the CNS. In TG5 rats at both young (6 months of age) and old (15 months of age) ages a peculiar reduction in cross-sectional area of the single axon bundle in the striatum was demonstrated (Figure 4.42). The reduction in size of axon bundles was found throughout the whole striatum, while no obvious decrease in the number of axon bundles was observed. There was no aggravating severity of this alteration found in TG5 across age. In comparison, no distinct abnormalities in axon bundles were detected in TG9.

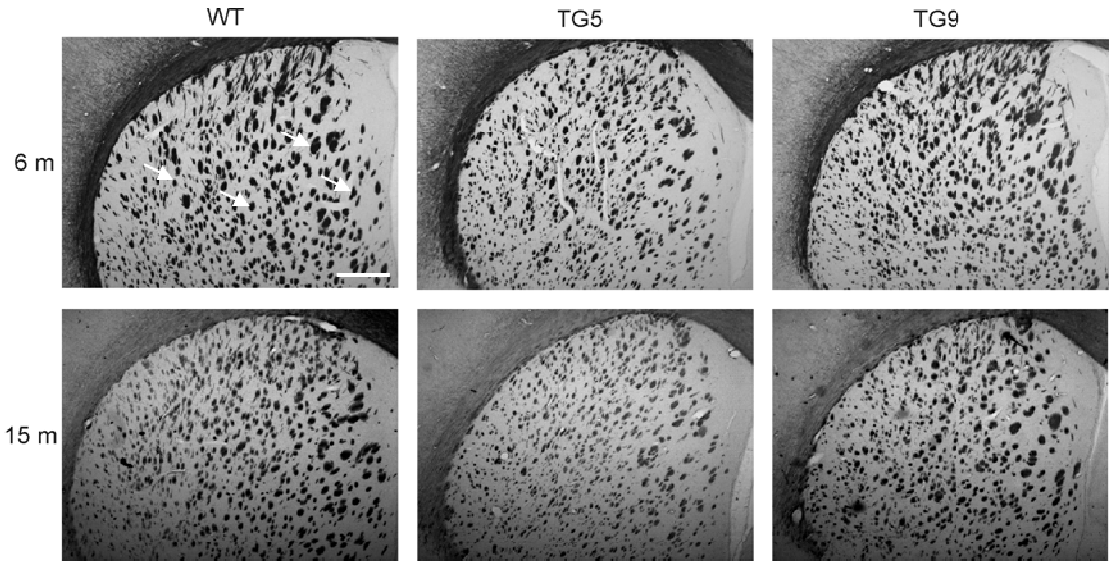

Figure 4.42: Axonal change in BACHD rats at young and old ages. Coronal brain sections of rats at 6 and 15 months of age were immuhistologically stained with antibody against MBP. Microscopy images at low magnification visualized a reduced area of axon bundle (arrows) in TG5 rats at both 6 and 15 months of age. Scalebar: 0.5 mm.

4.8 Analysis of gliosis in BACHD rats

4.8.1 Analysis of microgliosis

Activated microglia cells are known to cluster around the extracellular amyloidal plaque in Alzheimer disease patients (Meda *et al.*, 1995; Sasaki *et al.*, 1997). Activated microglia is also associated with damaged neurons in patients with Parkinson disease (McGeer and McGeer, 1998). Several studies have shown that microglia are activated in premanifest HD patients (Tai *et al.*, 2007) and symptomatic HD patients (Sapp *et al.*, 2001) and that microglia activation correlates with disease severity (Pavese *et al.*, 2006). Microgliosis was therefore determined in the BACHD rat in younger and aged rats by using both immunohistological stainings and Western blotting methods.

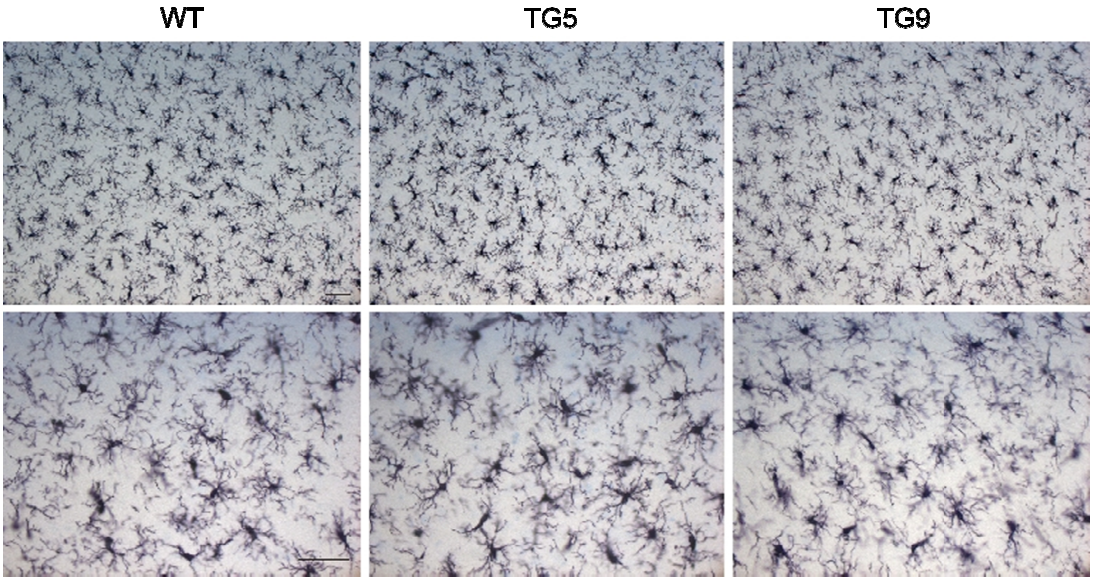

Figure 4.43: Immunochemistry staining using anti-Iba1 shows specific immunoreactivity in microglia cells (representative images of rats at 12 months of age). Lower magnification (upper row) revealed a homogenous distribution of microglia cells throughout the brain, there was no difference of density of microglia cells observed till 18 months of age. Higher magnification images (below) demonstrated non-activated, non-dystrophic morphologies of microglia cells. No glia scar formation was observed in any genotype at any age. Scale bars: 200 µm.

Because we had observed neurodegeneration and reduced brain volume starting at 12 months of age in BACHD rats, coronal brain sections of 15-month and 18-month-old rats (TG5:TG9:WT=6:5:5, at each time point) were used for analysis of microgliosis in both BACHD transgenics and WT controls. Anti-Iba1 (ionizing calcium-binding adaptor molecule 1) staining shows a regular distribution of microglia cells throughout the brain in both BACHD and WT rats (Figure 4.43). The morphology of microglia cells with a small cell body and a ramified form did not differ

in different brain regions or between different genotypes. There was also no amoeba-like microglia and no microglia scar was observed in rats of all three genotypes. No difference in immunoreactivity of anti-Iba1 was detected between BACHD transgenics and WT controls at both ages. In order to more precisely quantify Iba1 expression level in BACHD transgenics and WT controls, Western blotting was performed by using rat brain lysates of striatum and cortex samples of animals at 3, 6, 9, 12 and 15 months of age. The blots of the striatum and cortex samples show a band of 21 kDa in BACHD transgenic and WT rats. The intensity of this band did not show an obvious variation between all the animals (only the results of 12months are shown in Figure 4.46). The blots of brain lysates at 3 and 12 months of age were quantified using ImageJ. Data analysis (two-way ANOVA) did not detect any difference between BACHD rats and WT littermates in both cortex and striatum.

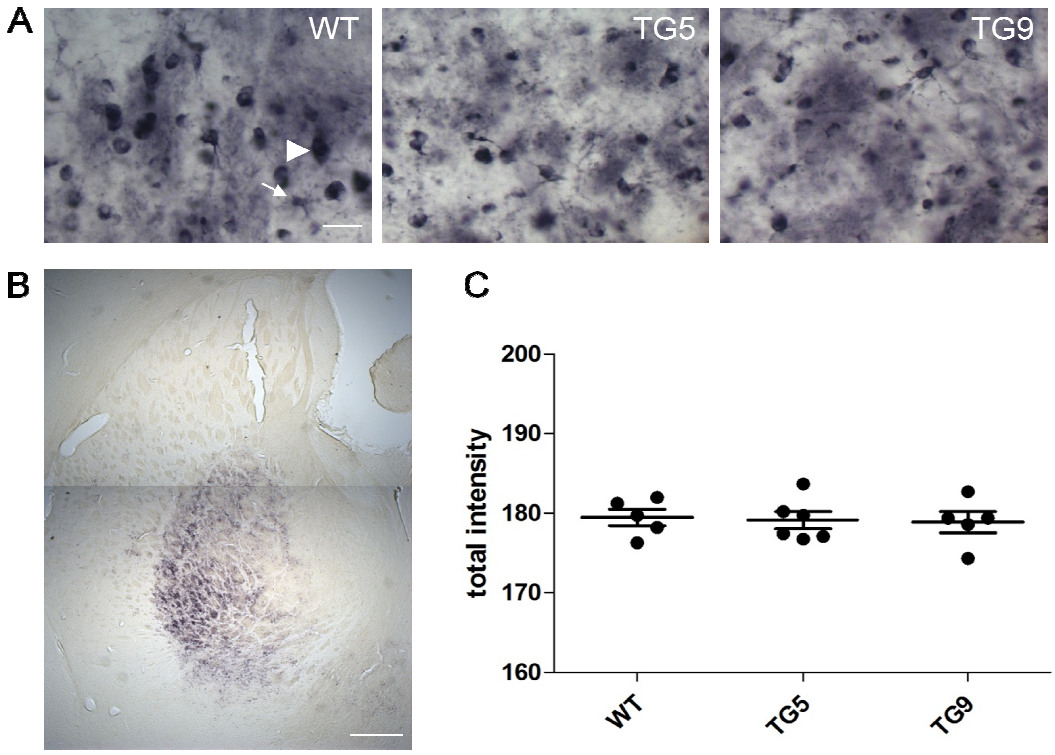

Figure 4.44: Immunohistochemistry using anti-ferritin displayed a specific staining in the globus pallidus (B). Immunoreactivity was observed in some neurons (arrow head) and glia cells (arrow), as well as in the extracellular matrix (A). There was no dystrophic morphology of neurons and glia cells observed in both BACHD transgenics and WT controls. Each of the eight brain section were taken for statistical analysis. Total intensity of anti-ferritin staining did not differ between transgenic and WT littermates (C, one-way ANOVA). Scale bar in A: 20 µm, scale bar in B: 0,5 mm.

Another marker for microglia cells is ferritin, which is increased after activation. Ferritin expression level was therefore examined using immunohistological stainings

at 15 months of age and Western blotting at 3, 6, 9, 12 and 15 months of age (Figure 4.44). Anti-ferritin staining presents an abundant immunoreactivity in the globus pallidus (GP). Positive cells in GP could be separated in cells with large and with small size having different shapes indicating immunoreactivity in both neurons and microglia cells (Figure 4.45). Only a small number of positive microglia cells were observed in the striatum and very few positive microglia cells were present in the cerebral cortex. In both neurons and microglia cells, immunoreactivity of anti-ferritin was identified in cell bodies and the processes of cells or only in cell somata. The intensities of the anti-ferritin immunreactivity was then analyzed in GP (TG5:TG9:WT = 6:5:5) utilizing ImageJ. Statistical analysis using one-way ANOVA did not yield any difference between BACHD transgenics and WT littermates. Western blotting at each age showed a constant expression in all rat striatum and cortex samples. The quantification using ImageJ at both 3 and 12 months of age did not reveal a significant difference in the expression level of ferritin in striatum and cortex throughout the measured time interval (Figure 4.45) (one- way ANOVA and two-way ANOVA).

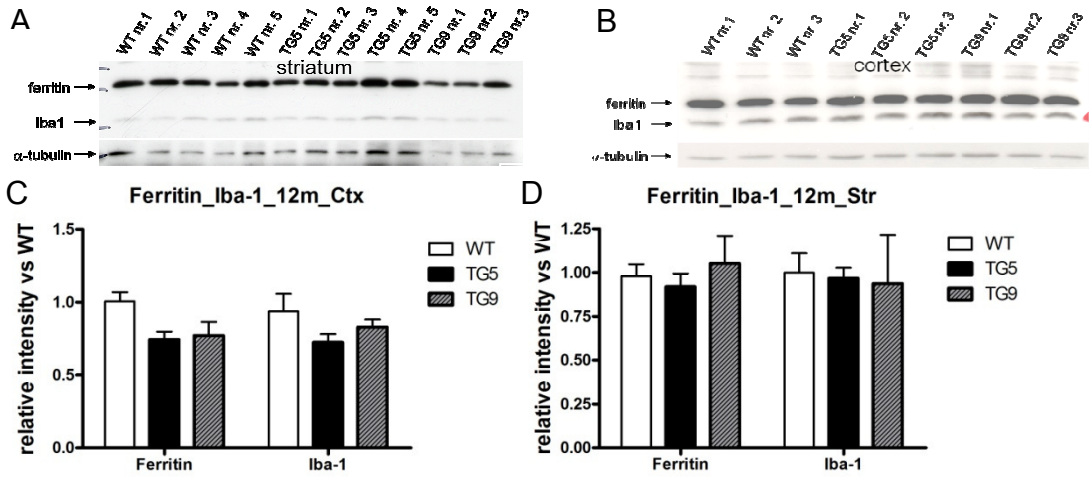

Figure 4.45: Microglia marker Iba-1 and ferritin show equally abundant expression in cortex and striatum of BACHD rats and WT controls. (A) Representative Western blots of brain extracts from rats at 12 months of age. Western blots were performed using cortical and striatal lysates of BACHD rats and WT littermates (n=3 for cortex; TG5:TG9:WT= 5:3:5 for striatum). α-tubulin was used as loading control, ferritin and Iba-1 show a specific band at 21 kDa and 17 kDa, respectively, displaying bands with comparable intensities between all genotypes. (B) The quantification of band intensities shows a similar protein expression level of both ferritin and Iba-1 in cortex (C) and striatum (D).

4.8.2 Analysis of astrocyte regulation

It is well known that astrocytes play an important role in stabilization of cell-cell communication and maintenance of extracellular environment including iron storage. Recently, several other functions of astrocytes were revealed, which implicated a role in neurodegenerative diseases such as an impact on neurotransmitter synthesis, neuronal metabolism and synaptic plasticity (Tsacopoulos and Magistretti, 1996; Haberg *et al.*, 2001; Rouach *et al.*, 2008). Selective expression of mutant huntingtin in astrocytes in a mouse model also revealed the contribution of astrocytes to HD pathogenesis (Bradford *et al.*, 2010). The astrocyte marker GFAP (Glial Fibrillary Acidic Protein) was therefore examined in BACHD rats using immunohistological staining and Western blotting. At 15 and 18 months of age, immunostainings of astrocytes displayed a predominant distribution in the corpus callosum the neighboring dorsolateral striatum and the cortical outer layer (Figure 4.46 A). The astrocytes formed local cell groups (clusters) of 10-20 cells (Figure 4.46 B). No obvious changes in morphology and distribution of astrocyte clusters were observed (Figure 4.46 C). The immunoreactivity and density of astrocytes showed a high variation throughout the brain and within the genotypes.

A trend of a reduction of GFAP immunoreacitivity was seen in 3 out of 6 TG5 rats throughout the whole brain (Figure 4.47). Each 12^{th} striatum section was taken for the analysis with ImageJ. The intensities of the images of the different genotypes were evaluated by using one-way ANOVA. However, statistical analysis did not show a significant difference in the intensities of the immunohistological stainings at 15 and 18 months of age, most probably due to the high variation between rats of the same genotype. There was no difference between BACHD transgenics and WT rats in the density and number of astrocytes in each cluster. Western blotting was performed for better quantification using brain lysates of rats at 3, 6, 9, 12 and 15 months of age (only data at 12 months of age is shown, Figure 4.48). The results were consistent with the immunohistological staining. A single 50-kDa band was present in all animals investigated with a big variation of the band intensity observed at each analyzed time point. Thus, no significant difference was found at each time point.

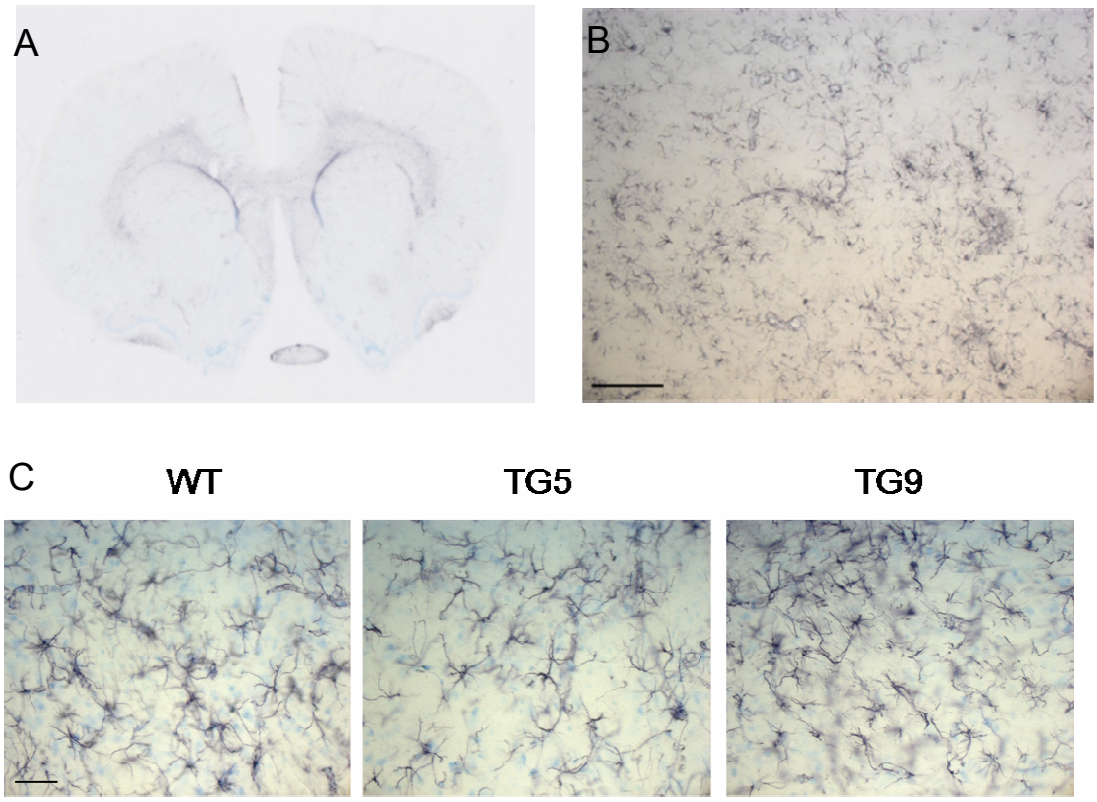

Figure 4.46: Immunohistochemical analysis of astrocytes using anti-GFAP. (A) Image of whole brain sections show a predominant distribution of astrocytes in the corpus callosum followed by the dorsolateral striatum and the outer layer of the cortex. (B) Astrocytes form bundles containing 10-15 cells in the striatum, which do not differ between BACHD transgenic and WT littermate. (C) There is no dystrophic morphology of astrocytes observed in any genotype throughout the brain. No changes either in number or in the length of the asctrocyte processes could be determined. Scale bar in B 200 µm, scale in C 50 µm.

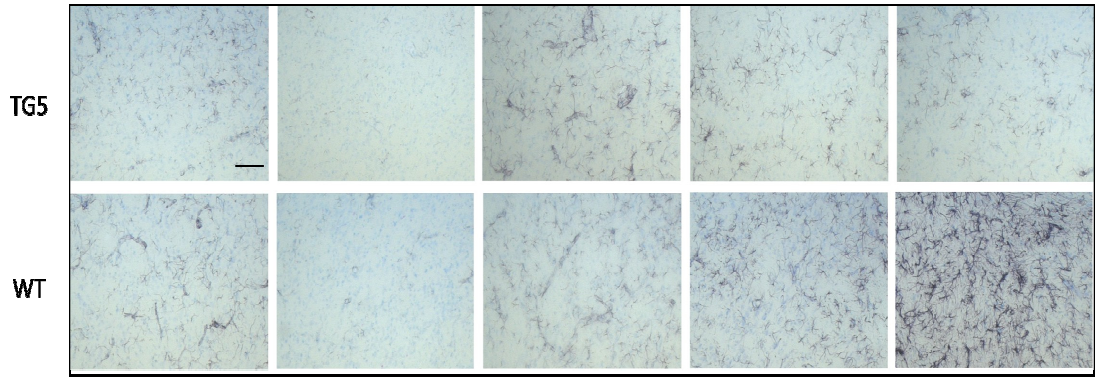

Figure 4.47: Large variability of GFAP expression levels in rats of the same genotype. Coronal brain sections of rats at 18 months of age were stained with anti-GFAP. Images with lower magnification displayed a very large variability within BACHD trasgenics and WT control. Scale bar: 200µm.

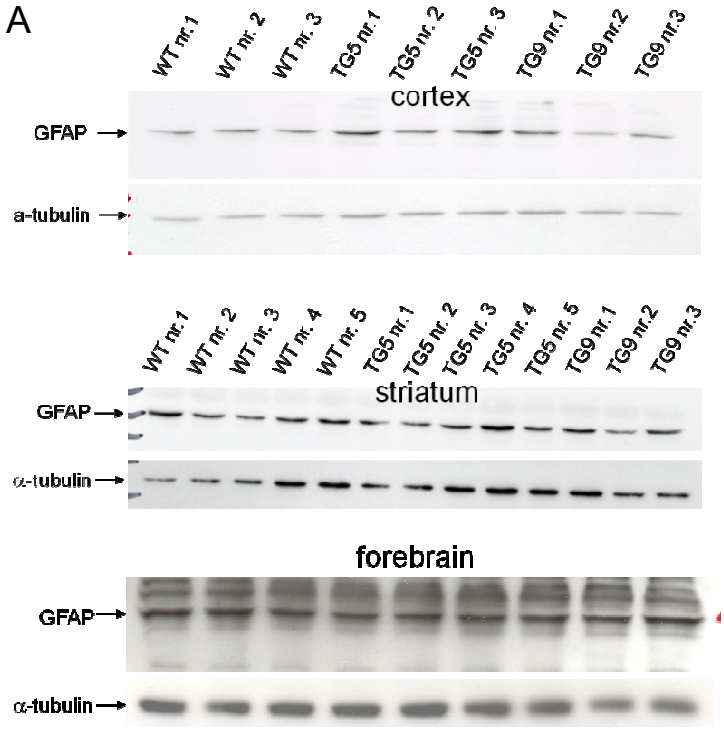

Figure 4.48: Western blot quantification of GFAP expression level. (A) Western blots probed with anti-GFAP show a specific band at 50 kDa. High variation in the intensity of the band is seen among the animals of the same genotype. (B) Statistical analysis didn't reveal any difference between genotypes in any brain region.

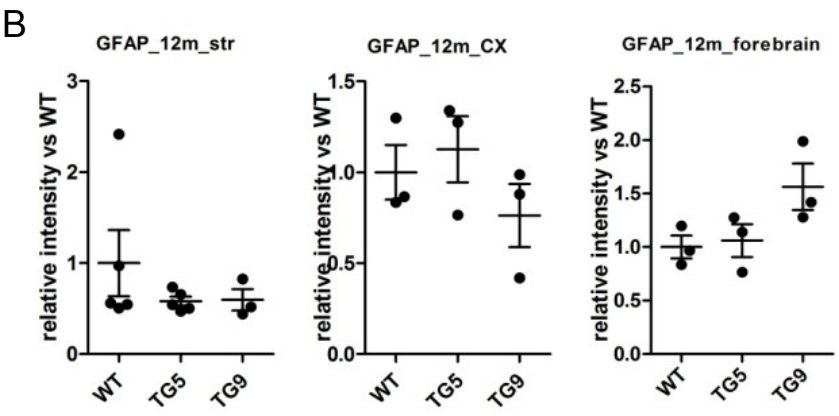

4.9 Analysis of protein changes in a consequence of htt aggregation

4.9.1 Soluble mutant huntingtin and endogenous rat huntingtin

It is still not clear whether soluble or aggregated mutant huntingtin is the toxic component leading to cell death. Recently, it was reported that soluble htt is inversely correlated to aggregated huntingtin *in vivo* and *in vitro* (Baldo *et al.*, 2012). To assess the amount of soluble mutant htt and endogenous rat huntingtin, Western blots were performed using brain lysates of rats at different ages till 18 months. Antibody 2B7 recognizing both mutant and endogenous huntingtin detected the full-length and N-terminal fragment of htt. Both full-length mhtt and N-terminal fragments are present at

comparable levels in younger and advanced aged animals of the same genotype. Similarly, the expression level of endogenous htt was not altered in all three genotypes (Figure 4.49 A and B). Soluble htt was further investigated in cytosolic and nuclear fractions (Figure 4.49 C and D). Comparable to the results of whole brain homogenates, no changes in the level of soluble mutant and endogenous htt were observed either in cytosolic or in nuclear fractions between younger and advanced ages. The blot performed using cytoplasmic lysates presented weaker bands between 80 and 200 kDa, while the smaller bands between 50 and 70 kDa seen in the nuclear fractions could not be detected. These results suggested that htt fragments are mainly localized in the nucleus. Taken together, no reduction of either full-length htt or htt fragment was observed in any subcellular fraction in BACHD rats with advanced age.

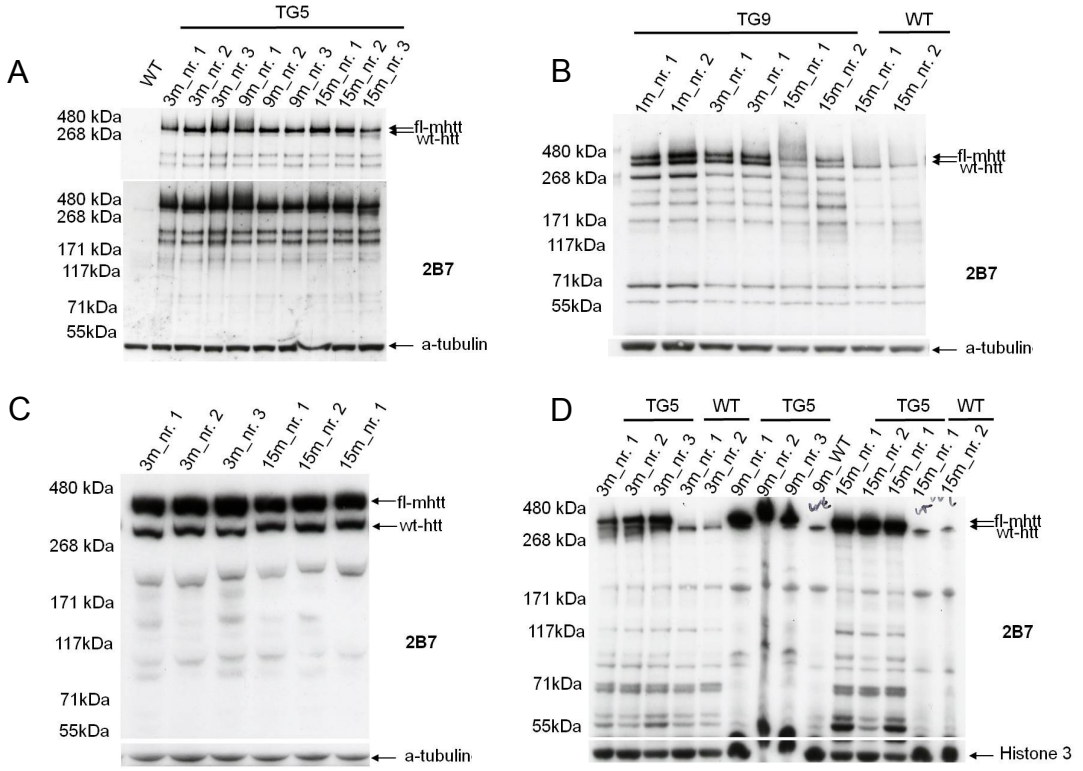

Figure 4.49: Western blot detection of soluble mhtt and wt-htt in cortical brain lysates of BACHD rats at different ages. (A) TG5 transgenic rat brain lysates probed with antibody 2B7 at shorter exposure time show a clear image of both full-mhtt and endogenous rat htt (top). With longer exposure times, the blot presents different fragments of htt. There was no obvious change in the level of full-length mhtt and rat htt observed, as well as of all the N-terminal fragment forms of both htt. A reduction of full length mhtt and rat htt was observed in cortical lysates of TG9 rats at 15 months of age, as well as rat htt in WT littermates at the same age, which suggested protein degradation during the lysate storage. (C) Blot of cytosolic fractions of TG5 show a reduced number of fragments compared to the tissue homogenate. Both mhtt and rat htt bands were present with comparable intensities. (D) Nuclear fractions of TG9 showed an abnormal band pattern due to influences of the sample preparation of TG9 rats. Therefore, only TG5 rat brain lysates at 3 months and 15 months of age can be compared with each other. Both full-length htt and Nterminal htt fragments showed bands with comparable intensity.

4.9.2 Huntingtin-associated protein 1

Huntingtin-associated protein 1 (HAP1) was found to bind to htt in a polyQ dependent manner, i.e. HAP1 is bound tighter to mhtt than wt-htt. Since aggregates of htt were found starting at 3 months of age, it could be hypothesized that HAP1 is possibly recruited into the aggregates, subsequently reducing the amount of soluble HAP1. Soluble HAP1 was therefore analyzed using Western blot. Rat brain lysates of the cortex, where most of the aggregates were observed, of WT and transgenic rats at 15 and 18 month of age were prepared. The blots probed with anti-HAP1 show a specific band at 66.8 kDa with comparable intensity in each sample (Figure 4.50). Levels of HAP1 did not differ between genotypes until 18 months, at which aggregates were found abundantly throughout the brain.

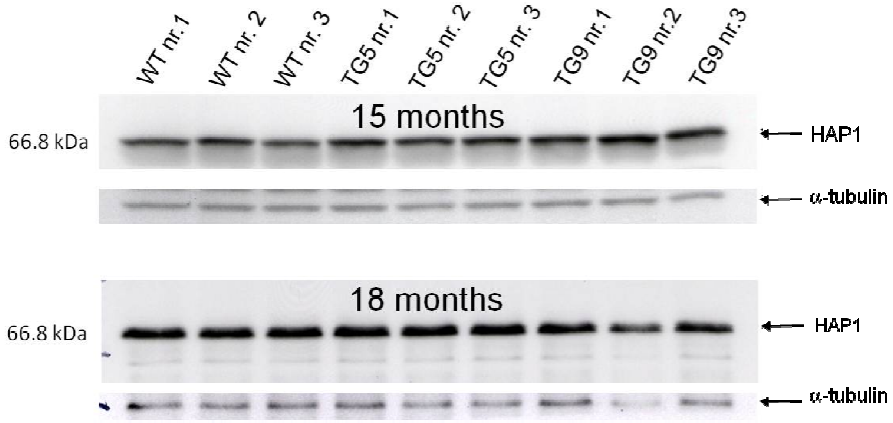

Figure 4.50: Western blot detection of HAP1 in the cortex. Representative blots of both 15 and 18 months do not present obvious changes in protein levels of soluble HAP1.

4.9.3 Brain-derived neurotrophic factors

Brain-derived neurotrophic factors (BDNF) have been reported to be down-regulated in HD patients and transgenic animals (Zuccato *et al.*, 2001) due to the presence of mutant huntingtin, which may disrupt binding of transcription factors to DNA. Since BACHD transgenic rats TG5 and TG9 also presented progressive nuclear accumulation of N-terminal htt, BDNF mRNA expression in the cortex of rats at 12 months of age was quantified by real-time PCR. Four different isoforms I, IIB, IV and VI, which have been well documented in the literature (Chiaruttini, et al., 2008), as well as total BDNF were quantified in cortical brain tissues of BACHD rats and WT littermates. The results revealed a strong decrease in total BNDF mRNA level (62%, one-way ANOVA, Tukey's post test, $p<0.001$), specifically in exon IV (52%, one-way

ANOVA, Tukey's post test, $p<0.001$) in BACHD transgenic rats TG5 at 12 months of age (Figure 4.51 A). Additionally we compared the relative amounts of each isoform at the mRNA level and confirmed that exon IV has the highest relative expression compared to the other isoforms (Figure 4.51 B). These findings are consistent with earlier findings described in literature. In order to confirm the results seen at 12 month of age, the mRNA expression level of BDNF IV was subsequently quantified in the cortex of BACHD rats at 15 months of age. The data also revealed a significant decrease of mRNA level in BACHD TG5 rats at 15 months of age (Figure 4.51 C) (one-way ANOV Tukey's post test), however with lower significance ($p<0.05$) and reduced difference (32%).

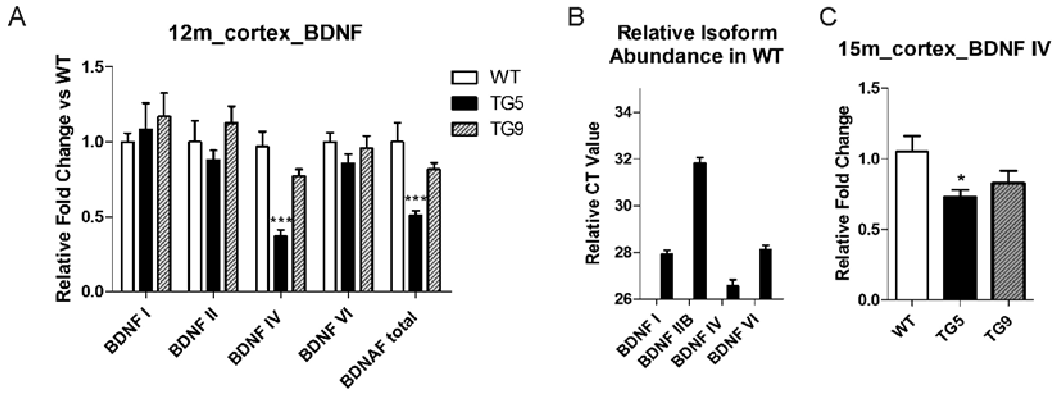

Figure 4.51: Quantification of BDNF using real-time PCR. (A) Relative fold changes of different BDNF isoformes and total BDNF in cortex of BACHD rats at 12 months of age. BNDF IV is decreased by appropriately 62% in TG5 compared to WT littermates, while the total BDNF is reduced by about 32% in TG5. No significant changes of BDNF levels were observed in TG9. (B) Relative abundance of the BDNF isoforms in WT rats. The CT values were compared between all isoforms investigated, showing a much lower CT value in isoform IV. This indicates a higher expression level of BDNF IV. (C) Relative fold change of BDNF IV in cortex of BACHD rats at 15 months of age. In TG5, 32% reduction of BDNF IV was detected. Data are presented as mean ± SEM; ***: $p<0.001$, *: $p< 0.05$.

4.10 Changes of synaptic proteins

Neurite and synaptic degeneration were already detected via electron microscopy as described above, but the question remains whether the synaptic proteins can be taken as marker for neurite and synaptic degeneration in BACHD transgenic rats. The presynaptic marker synapsin II and the postsynaptic marker PSD-95 were assessed by Western blotting in forebrain samples of BACHD rats at 12 months of age, a time point at which synaptic degeneration was detected via EM (Yu-Taeger *et al.*, 2012, performed by our collaboration partner Elisabeth Petrasch-Parwez). Synapsin II showed a slight reduction in the expression levels in both BACHD transgenic rat lines, whereas increased PSD-95 was detected in BACHD rats,

especially obvious in TG5 (Figure 4.52). Due to a small sample number (n=3), statistical analysis did not reach significance.

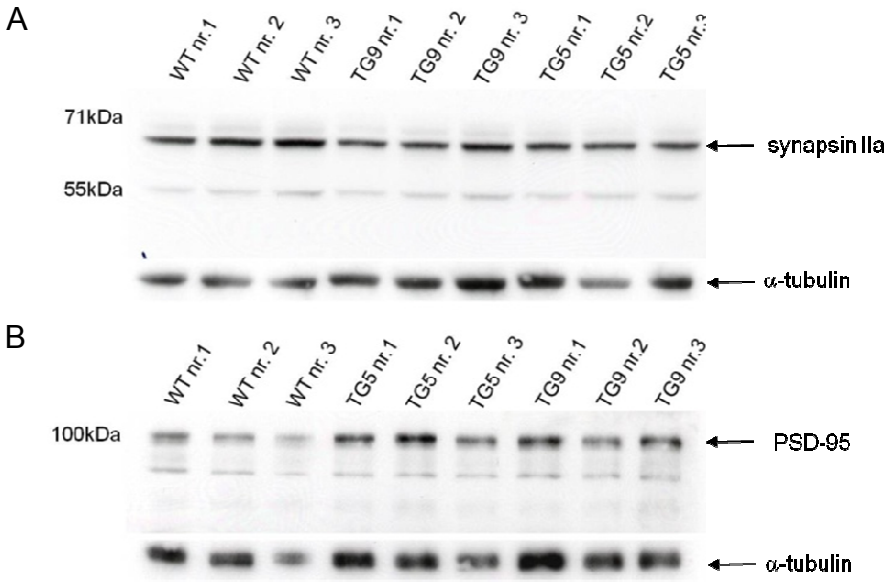

Figure 4.52: Synapse protein markers were assessed in BACHD transgenic rats. (A) The blot was probed with anti-synapsin IIa showing a strong band at approximately 65 kDa and a weaker band at approximately 55 kDa. This did not resemble the expected band size of 74 kDa. Both bands present a reduced intensity in both BACHD transgenic lines compared to WT controls. (B) The blot probed with anti-PSD-95 shows a strong band at 95 kDa with higher intensities in BACHD transgenics, especially inTG5.

Excitotoxicity in neurons resulting in cell death was proposed as one hypothesis in HD. Excitotoxicity is considered to be mediated by over stimulation with glutamate (Sattler and Tymianski, 2001; Mattson, 2003), since glutamate is the major excitatory neurotransmitter. Most intensive studies of glutamate receptor evoked excitotoxicity were done with NMDA2B receptor (NMDAR2B), which exhibits several features related to neuronal death. NMDAR2B was examined in BACHD transgenics in both cortex and striatum at advanced disease stages with 12, 15 and 18 months of age (n=3 at each time point). Starting at 15 months of age, Western blot showed a decrease of NMDAR2B in striatum in some transgenic rats of TG5 and TG9 (Figure 4.53), while no difference was revealed in cortex until 18 months. However with the high variation within genotype and the low number of samples in each group, the difference between genotypes did not reach statistical significance.

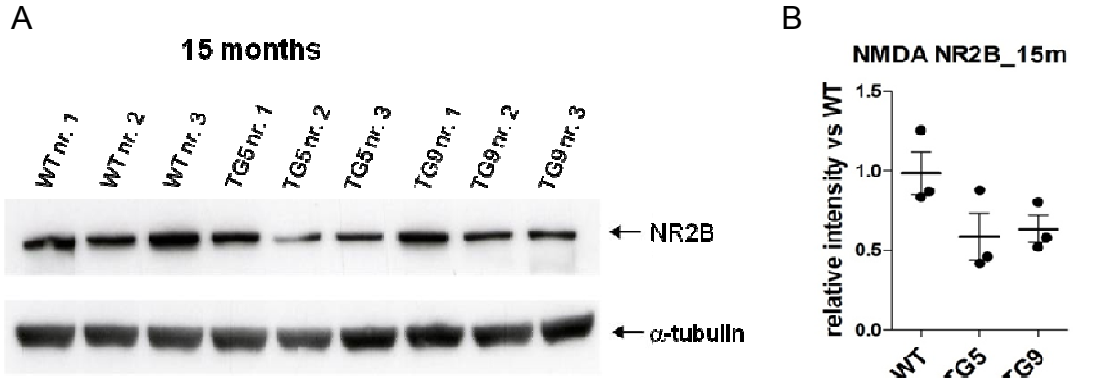

Figure 4.53: NMDAR2B is decreased in BACHD transgenics in the striatum. (A) Representative Western blot image shows a band at 166 kDa. In TG5 and TG9, a mild reduction in the band intensites was found in two out of three samples. (B) Due to the high variation of band intensities within each group, no significant difference was determined between genotypes (one-way ANOVA, $p<0.05$).

5. Discussion

5.1 Advantages of BACHD rats

5.1.1 Generation of BACHD transgenic rats

For the generation of an animal model, several factors should be considered for the design of the construct and for ensuring the stability of protein expression throughout the following generations. Firstly, great consideration should be taken by choosing the promoter, which influences protein expression in a tissue-specific and development-stage-specific manner. For modeling the disease, the promoter should allow an expression pattern similar to that of the endogenously expressed protein. Secondly, transgene silencing may occur when the transgene is inserted in a transcriptionally inactive region, or the promoter of the transgene may influence gene expression of genes located further downstream. Since the animal model should show only symptoms relevant for the disease, any changes in gene expression of other genes should be avoided. Additionally, the integration of multiple copies of the transgene in a concatemeric array should be avoided, since this may lead to protein expression variation between littermates. Furthermore, when working with proteins containing polyQ stretches, the stability of the CAG repeat expansions should be ensured since the age of onset of HD inversely correlates with the number of CAG repeats (Duyao *et al.*, 1993; Stine *et al.*, 1993).

In this project, BACHD rats were generated using BACs containing the full-length human mutant *HTT* genomic sequence and all regulatory elements to obtain a protein expression pattern similar to that observed in HD patients. This was verified by transgene expression profiling in all brain regions revealing a ubiquitous and abundant mhtt expression in all relevant brain regions as seen in human HD (Li *et al.*, 1993). By introducing additional 20 kb upstream and 50 kb downstream flanking sequences the position effect of the transgene should be reduced. Both BACHD transgenic lines TG5 and TG9 exhibit HD-like symptoms and a neuronal pathology depending on the mhtt expression level of each line. To our knowledge no apparent phenotype not being related to HD was observed in both transgenic lines indicating that a position effect did not occur in BACHD rats. In the BACHD construct, the endogenous CAG repeats in exon 1 were replaced by 97 mixed CAA/CAG repeats leading to a stable CAG/CAA repeat number in both germline and brain tissues of aged animals as indicated by fragment analysis of exon 1 (Gray *et al*., 2008). A

comparable transgene copy number among the entire F1 offspring of both lines suggests a single integration site in TG5 and TG9, which was confirmed by a stable and equally severe phenotype in all offspring of each line throughout all analyzed generations. Remarkably, two LoxP sites flanking exon1 were also included in the construct, which enable the conditional silencing of transgene expression in a tissue-specific manner. Therefore, BACHD transgenic rats are a useful tool for studying HD pathogenesis.

5.1.2 BACHD rats express splicing variants of *HTT* as observed in humans

Transgenic *HTT* in BACHD rats undergoes natural splicing as confirmed by the presence of the two naturally occuring mRNA isoforms. Even though the small splicing variant does not contain a polyQ stretch, it may fulfill additional functions relevant for the disease process. Since both of these isoforms were found in humans (www.ensembl.org/Homo_sapiens/Gene/Summary?g=ENSG00000197386;r=4:3076408-3245676), the BACHD rat model closely resembles the HD patient condition in this respect.

5.1.3 Comparable body weight in BACHD rats and WT controls excludes body weight as a confounding factor in behavioural tests

BACHD transgenic rats expressing fl-mhtt exhibit several robust HD-like behavioural phenotypes as well as changes at the molecular and cellular levels. Importantly, there was no significant difference in body weight between BACHD rats of both lines and WT littermates (Figure 4.22). This is in contrast to what has been reported in BACHD mice and YAC128 mice (Menalled *et al.*, 2009), where overexpression of fl-mhtt is associated with a significantly increased body weight. It has been postulated that body weight is modulated by levels of fl-htt with increased levels of fl-wthtt or fl-mhtt leading to an increased body and organ weight in mice, while a decrease of fl-htt is associated with body weight loss (Van Raamsdonk *et al.*, 2006). The increase of body weight in mice resulted from an increase of both total fat mass and fat-free mass and was associated with increased levels of plasma IGF-1 (Pouladi *et al.*, 2010). Interestingly, we also observed an increase in body fat mass in BACHD rats. But in contrast to the published mouse data a decrease in organ weight in BACHD rats of line TG5 was found resulting in a comparable body weight between BACHD rats and WT rats (preliminary results, data not shown). This discrepancy is especially intriguing since the same construct was used to generate BACHD mice and rats. It

might be attributed to species-specific differences and is less likely caused by integration site effects as we did not observe an increased body weight in any of the 18 full-length BACHD rat lines. Furthermore, there is a proportional correlation between the severity of the HD phenotype and the protein expression level in the two BACHD lines arguing against an integration site effect. As progressive rotarod deficits are readily apparent in BACHD rats of line TG5 these are very likely motor defects rather than a consequence of increased body weight. Also, we can exclude that differences in body weight confound other behavioral tests in BACHD rats rendering this model valuable for further phenotype studies.

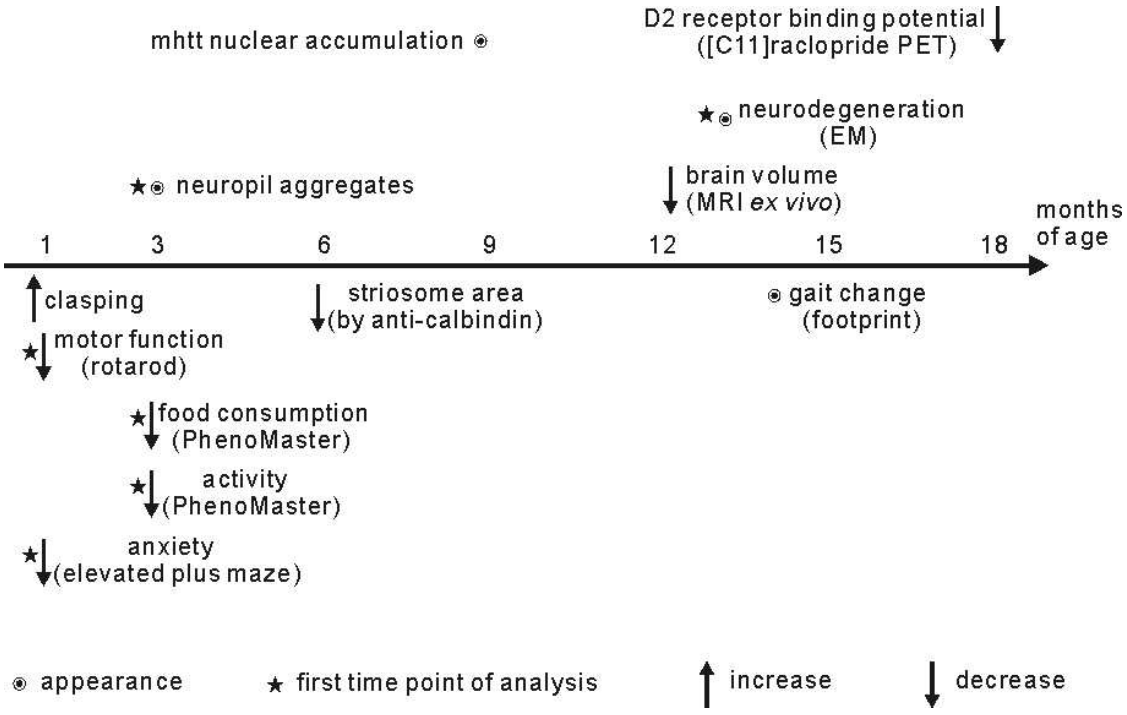

Figure 5.1: Progression of various phenotypes in BACHD TG5 rats. The findings of this study are summarized according to the earliest onset or appearance of each phenotype.

5.1.4 Strong and robust phenotype in BACHD rats make them valuable for preclinical therapeutic studies

Another advantage of the BACHD rat is its strong and robust phenotype (Figure 5.1). In comparison to the already existing fragment tgHD rats BACHD rats show an earlier onset and a faster progression of motor deficits without the need to breed for homozygosity as heterozygous tgHD rats show only subtle deficits (von Horsten *et al.*, 2003; Nguyen *et al.*, 2006; Brooks *et al.*, 2009). Recently, a milder phenotype in

tgHD rats as originally described has been reported (Casteels *et al.*, 2011; Blockx *et al.*, 2012); (Casteels *et al.*, 2011; Antonsen *et al.*, 2012). Also, while striatal atrophy was found in some groups of old tgHD rats (von Horsten *et al.*, 2003; Kantor *et al.*, 2006; Nguyen *et al.*, 2006), other studies revealed little or no evidence for atrophy (Winkler *et al.*, 2006; Bode *et al.*, 2008; Blockx *et al.*, 2011). Most importantly, the behavioural phenotype of BACHD rats has now been confirmed by 2 independent CROs (Evotec, Germany: Abada et al., submitted; and Porsolt, France) indicating a robust phenotype as seen in several labs.

5.2 Deliberation on experimental designs

5.2.1 Rotarod tests

Although motor dysfunction is involved in various neurodegenerative diseases including Parkinson disease (PD), spinocerebellar ataxia (SCA) and HD, each disease is characterized by neurodegeneration in a specific brain region (at least in initial stages) resulting in characteristic motor symptoms. This raises the question which behavioral test is suitable for which disease model. Rotarod is the most commonly used test to assess motor dysfunction in HD rodent models as shown in numerous studies (Carter *et al.*, 1999). In this study, both rotarod and the beam walking test were performed to assess motor function in BACHD rats. TG5 rats show a progressive worsening in the performance on the rotating rod starting at 1 month of age, while the beam walking test did not reveal any significant differences between transgenic and WT rats until 12 months of age (the latest observation time point in this study) (Data not shown). This finding may be due to a higher sensitivity of the rotarod test compared to the beam walking test as this has been shown by Hamm and colleagues (Hamm *et al.*, 1994). In an attempt to evaluate the effectiveness of rotarod and beam walking test, rats with mild and moderate basal ganglia injury were evaluated. The results demonstrated that rats of both groups possessed an impaired rotarod performance, however beam walking only revealed a statistical significant difference in rats with moderate injury suggesting that the rotarod test is more sensitive in detecting motor impairments.

Since HD is a progressive neurodegenerative disease, we also expected to observe a progression of deficits in BACHD transgenic rats. Indeed, we detected a worsening of motor performance in the rotarod test with age as confirmed by 2-way ANOVA with significant interaction of the factors age and genotype. Moreover, a highly significant

effect of age was detected, as the performance of wild type rats also deteriorated with age with an approximately 50% reduction within 10 months (Figure 5.2 A). In contrast, the wild type littermates of the tgHD rats carrying a fragment of *HTT* maintain a similar latency to fall off the rotating rod until 9 months of age, which was demonstrated previously in our laboratory (Figure 5.2 B) (Nguyen *et al*., 2006). Both transgenic strains were derived from a Sprague-Dawley (SPRD) background, but present a huge discrepancy in their body weight (Figure 5.2 C and D). This might be attributed to the fact that tgHD rats were inbred for more than 26 generations by mating of heterozygous tgHD rats with each other (Antonsen et al., Brain Structure and Function 2012), whereas the BACHD rats were strictly kept on an outbred SPRD background through mating with SPRD rats bought from Charles River, Germany.

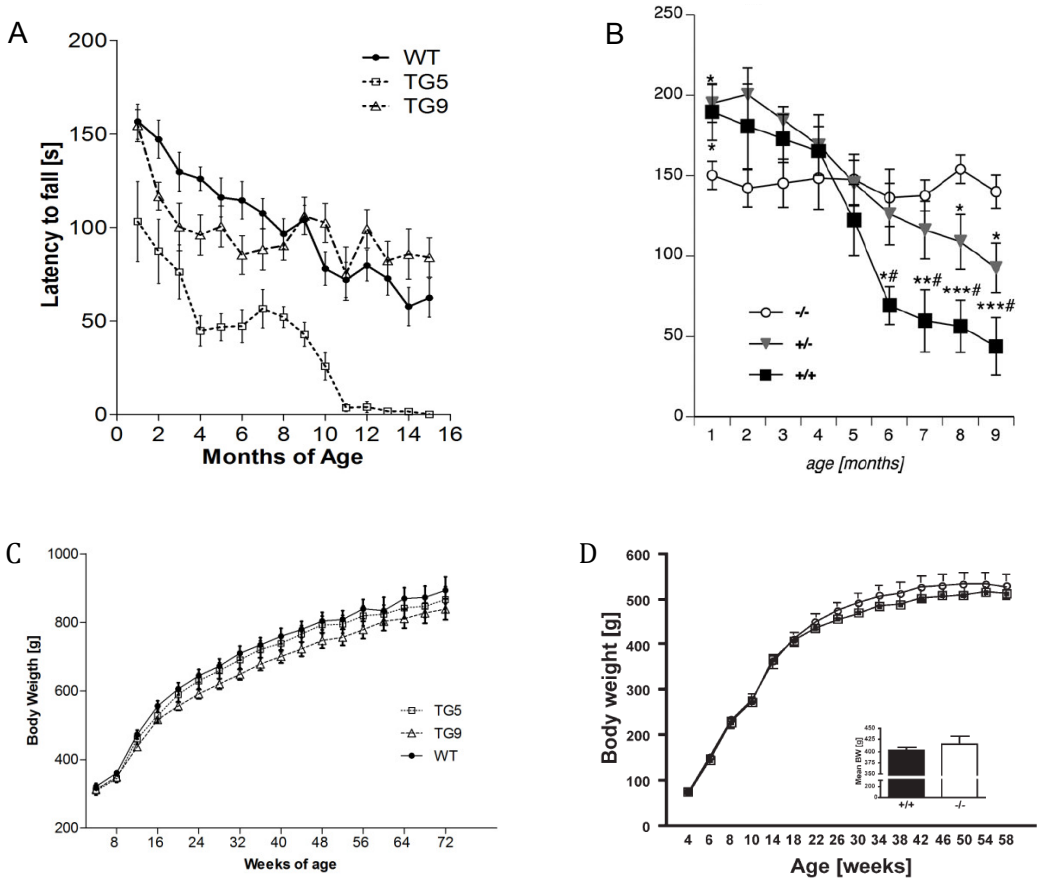

Figure 5.2: Comparison of performance on rotarod and body weight between BACHD and tgHD rats. (A) Rotarod test in BACHD rats. (B) rotarod test in tgHD rats. (C) Body weight of BACHD rats. (D) Body weight of tgHD rats. A and C were from Nguyen et al., 2006.

The average body weight of WT controls of the tgHD line reaches a plateau with 500 g at 8 months of age (Bode *et al.*, 2008), while WT littermates of BACHD rats display a mean body weight of 473.1 g already at 3 months of age, which keeps increasing to 900 g at 18 months of age. The increased body weight results in a larger body size

of the BACHD line, thus increasing the difficulty to stay on the rod. This larger body size also reduces the difficulty to get off the rod because the relative distance to the ground is lower, since the rotarod setup was identical for the BACHD and the tgHD rats (accelerating speed from 4 to 40 rpm over a period of 4 minutes by using an accelerod from TSE-System, Nguyen *et al.*, 2006). Thus, WT littermates of BACHD rats might have lost motivation to continue walking on the rod at an earlier time point than the smaller WT controls of tgHD rats. Taken together, the diameter of the rod and the distance to the ground under the rod should be considered when analyzing motor function of BACHD rats to account for the larger body size of these animals.

It is remarkable that the TG9 rats were able to maintain their performance on the rotarod from 6 months of age up to the end of the measurements at 15 months of age. At older ages their performance was even better than that of wild type littermates. TG5 also displayed a slight increase in the rotarod performance during 4 to 7 months of age. This seems to be mainly due to the adapted jumping strategy as described in the results section. Only BACHD transgenic rats show this peculiar 'jumping backwards' behavior, while some other rats turn around briefly and then turn again to the original direction. This behavior seems to be related with the protein expression level, because TG5 rats started this behavior with 3 months of age while TG9 rats began to show this behavior at 5 months of age. The number of rats per genotype using this adapted strategy was increasing with the age of the rats (Table 5.1). Once the animals started to jump backwards, they did not return to walking forward (even when we tried to make them). The animals were not enjoying the process of turning around, this jumping behavior helped them to stay on the rotating rod. This is because firstly, moving both front limbs and hind limbs at same time needs less reaction time (Kelso *et al.*, 1979). It was also discussed that by increasing the frequency of anti-phase movements, the tendency toward symmetry becomes stronger and, finally, results in an unavoidable transition from anti-phase to in-phase (Haken *et al.*, 1985; Verbessem *et al.*, 2002); Secondly, by turning around and moving backwards on the rod, the rats movement has changed from an uphill to downhill direction which is supported by the gravity. According to our observation this behavior relates to the bimanual voluntary movement (bimanual coordination). Considering that this turning around behaviour occurred at the beginning of the rotarod tests when the rotarod was not moving fast, we have strong indications that this is not because of rats being 'bored'.

Overall, this jumping backwards behavior in transgenic rats indicates an impairment of motor function in transgenic rats although it enables TG9 rats to stay even longer on the rod than their wild type littermates. In future experiments, the adaptation of other walking strategies should be accounted for – either only by measuring forward movements on the rod or by forcing all rats to move forward only - to improve the accuracy of the data.

Table 5.1: The number of rats using backwards jumping strategy

Moths of Age	3	4	5	6	7	8	9	10	11	12	13	14	15
TG5	3 (12)	6 (11)	9 (11)	9 (11)	8 (10)	10 (12)	10 (12)	8 (10)	1 (2)	1 (2)	0 (0)	0 (0)	0 (0)
TG9	0 (12)	0 (12)	3 (12)	4 (12)	6 (12)	6 (12)	5 (12)	5 (12)	6 (12)	9 (12)	9 (12)	9 (12)	9 (12)
WT	0 (12)	0 (12)	0 (12)	0 (12)	0 (12)	0 (12)	0 (12)	0 (12)	0 (12)	0 (12)	0 (12)	0 (12)	0 (12)

(): the total number of rats that were subjected to the rotarod test.

5.2.2 Skinner box tests

Skinner boxes tests demonstrated impaired cognition in BACHD rats at early ages. However the experimental design that was used in our study needs to be improved. First of all, cognitive deficits in HD are based on neuropathological changes in the prefrontal cortex and striatum. In presymptomatic HD mutation carriers the impairment in an attentional set shifting task was found to be most predominant (Jason *et al.*, 1988; Verbessem *et al.*, 2002). In order to assess cognitive performance in set shifting tasks, probands of all experimental groups need to reach a similar success level in a specific task before moving on to another task that requires strategy shifting. However, in our skinner boxes tests rats were only trained to reach a performance plateau in the acquisition task. As demonstrated, transgenic rats and WT littermates had a significantly different plateau level at the end of acquisition training (Figure 4.19 C and D), which may have affected reversal learning in the next task and subsequently confounded the quality of the results. Secondly, several lesion studies have implied that intradimensional shift and extradimensional shift tasks as well as reversal learning are associated with the cingulate cortex, the medial prefrontal cortex, and the orbitofrontal cortex, respectively (McAlonan and Brown, 2003; Ng *et al.*, 2007; Bissonette *et al.*, 2008). In the present study, only simple discrimination (rats needed to learn to respond with a lever press to appearance of the stimulus 'green cue light') and reversal discrimination (rats needed

to learn to respond with a lever press to the absence of the 'green cue light') were investigated, but the extradimensional shift using other stimuli such as audio or odor stimuli to assess medial prefrontal cortex function in BACHD rats was not tested. Thirdly, besides investigating the cognitive function, Skinner boxes can be used for the analysis of sensorimotor function by measuring the speed of initiation (reaction time) and execution (movement time). However, with limitations in the equipment, such a design could not be realized with the Skinner boxes used in this study.

5.2.3 Simple swimming tests

The simple swimming test is used to assess simple procedural learning and reversal as measure of cognitive function. This test has demonstrated cognitive decline in YAC128 mice at 8 months of age with transgenic mice requiring a significantly longer time to find the platform and showing an increased frequency of false initial swimming direction (Van Raamsdonk *et al*., 2005). Although BACHD rats initially had difficulties in finding the platfrom in the reversal learning phase at each time point significant differences in the latency to find the platform were observed only at 4 months of age, but not at 6 months of age. There were no significant differences in the score for the initial swimming direction.

One reason why we didn't detect differences in the initial swimming direction may be attributed to the simple and unspecific scoring system. The scores (only being either '0' or '1') do not account for the fact that some rats had an initially false swimming direction before they turned around and headed to the correct direction where the platform was located, or conversely, they first swam into the correct direction but then turned to the direction opposite to the platform. Thus, a more elaborate scoring system especially in combination with video analysis should be introduced to give a better chance of revealing differences. A further possibility is that the simplicity of this test, while being a strength for therapeutic studies, may not be appropriate to differentiate between BACHD rats and WT littermates. In fact, rats of all three genotypes successfully learned the task within 4 trials as both the latency to find the platform and the initial swimming direction reached a plateau after that.

We expected to observe a progressive cognitive decline with increasing age, however the data at 6 months of age could not even recapitulate the differences present at 4 months of age. This can be attributed to the fact that the same group of rats was used at both time points. The performance on the second occasion may

have been confounded by the previous training and could potentially mask the negative effect of cognitive decline. Indeed, all three genotypes showed clear differences in their performance when comparing the two testing time points. While WT rats seemed to improve only on the acquisition phase both transgenic strains improved on both reversal and acquisition from testing at 4 months until 6 months of age. Hence it should be considered to use different rat cohorts for the simple swimming test at different ages.

5.2.4 PhenoMaster

Locomotor activity and food consumption of BACHD rats as well as other calorimetric measures including oxygen consumption, CO_2 production and respiratory exchange ratio (RER) were screened in an automated, home cage-like environment (PhenoMaster system). Several rats consumed less than 3 ml water per day, especially rats of the TG5 line (more than 50 % of the total group). This could be the result of stress due to the new environment. However, it may also be influenced by motor dysfunction or cognitive impairment since food and water were provided in different food cribs and water bottles and which were more difficult to access than in the home-cage. Rats, which did not drink more than 3 ml water within 24 hours were excluded from data analysis since a reduced water uptake may influence the activity and feeding behaviour of the rats. However, this strongly reduced the sample size for statistical analysis. For future experiments, it will be necessary to separate the investigation of food and/or fluid consumption from the locomotor activity and calorimetric tests or food and water should be provided in the same manner as in the home cages.

5.3 Early onset of motor dysfunction and hypokinesia in BACHD rats

Motor function was assessed utilizing rotarod tests (see above), footprint analysis and clasping test. The length of the expanded CAG repeat correlates with the severity of HD and inversely with age at onset. In humans, CAG expansions with more than 60 repeats cause a severe phenotype leading to juvenile HD (JHD) (Bruyn, 1968). CAG expansions of more than 80 repeats may cause infantile HD (IHD) with an age at onset earlier than 10 years of age and a dramatic progression rate (Squitieri *et al.*, 2002). Furthermore, TG5 rats express 4.5 fold more mhtt compared to the endogenous rat htt. In both HD patients and HD animals model, a higher expression level of mhtt aggravates the phenotype, with homozygous HD

patients and homozygous transgenic animals showing more severe and an earlier onset of symptoms. Thus, it is likely that the early onset of deficits in BACHD rats results from a longer CAG repeat and a higher mhtt expression level.

Footprint analysis of BACHD transgenic rats at advanced ages showed an abnormal gait in TG5 including step length, step width as well as overlap of front- and hind-limps. In addition, reduced activity was observed in both TG5 and TG9 at young ages until 6 months of age. Taken together, we observed a progressive impairment of voluntary movements and hypokinesia manifested at a young age. Most of the JHD and IHD cases, which carry a large expansion of the CAG repeat, exhibit predominantly dystonia and bradykinesia instead of chorea (Squitieri *et al.*, 2000). Besides that, rigidity frequently occurs in JHD and IHD associated with widespread brain atrophy (Squitieri *et al.*, 2000). It was hypothesized by Squitieri that adult and JHD have different mechanisms contributing to severity and age at onset of disease (Squitieri *et al.*, 2006). BACHD rats recapitulate clinical features of JHD and IHD and may be useful for the study of pathogenesis initiating in JHD.

Table 5.2: The age of onset in motor functions alterations in different HD animals models

	Performance on rotarod	Gait change	Clasping	Hyperkinesia	Hypokinesia
R6/2 mice	4 months (1)	6 weeks (1)	6 weeks (3)	not assessed	6 weeks (3)
YAC mice	through 100 weeks without progression (1)	16 weeks (1)	not assessed	3 months (4,5)	6 months (4,5)
BACHD mice	4 weeks (1)	36 weeks (1)	not assessed	not assessed	4 weeks (1)
BACHD rats	**1 month**	**14 months**	**3 weeks**	**1 month**	**3 moths**
tgHD rats	6 months (2)	3-4 months (6)	not assessed	1-2 months (2)	not assessed

(1) (Menalled *et al.*, 2009); (2) (Nguyen *et al*, 2006); (3) (Stack *et al.*, 2005); 4 (Slow *et al*., 2003); 5 (Van raamsdonk *et al*, 2005); (6) (Vandeputte *et al.*, 2010)

In comparison, HD mice models R6/2, BACHD and YAC as well as tgHD rats carrying a fragment of mhtt exhibit a deficit in motor function and an alteration in activity with various severity and age of onset, which are related to the expression level of mhtt and the CAG repeats length. Data was summarized in Table 5.2.

The performance on the rotarod may be related to the coordination of complex inter-limb tasks, which relies on temporal coordination. It was found that in bimanual tasks

the functional segments of the two hands are tightly synchronized. Coordination for bimanual tasks is orchestrated by several brain regions in the cortex and in subcortical regions, which form interconnected networks (Figure 5.3). These brain regions include the premotor cortex (PMC), the parietal cortex, the medial motor cortices, more specifically the supplementary motor area (SMA), the cingulate motor cortex (CMC), the primary motor cortex (M1), and the cerebellum (Debaere *et al.*, 2001; Jantzen *et al.*, 2005; Romanelli *et al.*, 2005). Therefore, the impaired rotarod performance in BACHD rats might result from a pathological change in the involved cortical regions and/or the cerebellum.

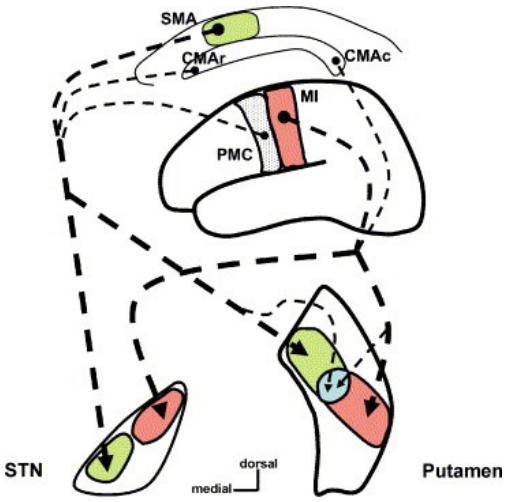

Figure 5.3: The network of all the brain regions involved in motor coordination. The figure shows how primary motorcortex (MI) and caudal cingulated motor area (CMAc) projections are directed to the laterodorsal subthalamic nucleus (STN) and lateral postcommissural putamen while the supplementary motor area (SMA), premotor cortex (PMC), and rostral cingulated motor area (CMAr) are directed to the medial STN and medial putamen. A central region within the putamen is characterized by an overlap of MI and SMA projections. Pantaleo Romanell *et al*..Brain research review. 2005 Feb;48(1):112-28.

BACHD rats and other HD transgenic mice particularly display hypoactivity in various stages of the disease raising the possibility of a lower neuronal activity in the substantia nigra. The dopaminergic neurons in the substantia nigra provide input for dopaminergic neurons in the striatum thus influencing their activity (Costall *et al.*, 1976). Previous studies have shown that the depletion of D1 or D2 receptor in mice induce a decreased locomotor activity depending on the D1 and D2 receptor dosage (Kelly *et al.*, 1998; Tran *et al.*, 2005). Therefore, these findings provide a link to Parkinson disease, which results from a loss of dopamine-producing neurons in the substantia nigra and is clinically characterized by rigidity and a slowness of movements. However no direct evidence was reported to date for HD, which might be due to a lack of biomarkers for HD at early stages of the disease. So far, bust firing and functional imaging of dopamine-producing neurons in the substantia nigra gave some promising data but these methods need to be established before further insights into HD pathology can be obtained.

Overall, BACHD rats show robust motor symptoms with a wide spectrum of motor deficits in comparison to other rodent HD models. Additionally, BACHD transgenic rats exhibit hypokinesia at early disease stages similar to what is observed in IHD patients. Compared to the HD fragment rat model with 51 CAG repeats, which genetically mirrors more faithfully the typical adult onset of the disease, this rat model expressing mhtt with a larger polyQ expansion might follow a different mechanism for initiating pathogenesis.

5.4 Reduced anxiety-like behavior in BACHD rats

The results of the elevated plus maze experiments revealed a significant reduction of time spent on the open arms for TG5 rats compared to WT controls. This indicates a decreased anxiety-like behavior in BACHD rats, which shows a tendency toward to progress with age (Figure 3.15 B). In contrast, most HD mouse models display increased anxiety with HdhQ111 mice showing only an increased anxiety-like behavior in males (Orvoen *et al.*, 2012). Conflicting results were reported for YAC128 mice, which show no changes in anxiety in stress-induced hyperthermia tests (Pouladi *et al.*, 2009), but a high level of anxiety in the open field (Southwell *et al.*, 2009). BACHD mice also display an increase in anxiety-like behavior (Southwell *et al.*, 2009; Menalled *et al.*, 2009), and only for R6/2 mice a reduced anxiety-like behaviour was reported (File *et al.*, 1998). Interestingly, overexpression of BDNF in astrocytes delays the decrease in anxiety (Giralt *et al.*, 2011). Both heterozygous and homozygous tgHD rats spent significantly more time on the open arms of the elevated maze, which correlated with the level of mhtt expression (Nguyen *et al.*, 2006).

It is well known that the amygdala in particular controls fear-like behaviors. (File *et al.*, 1998). Many efforts to manipulate amygdala function resulted in changes of fear-driven behavior (Fanselow and LeDoux, 1999). The majority of excitatory transmissions in the amygdala are mediated by glutamate receptors. The amygdala also receives input of dopaminergic fibers, since both D1 and D2 receptor are expressed in this region (Asan, 1998; Ito *et al.*, 2008). Dopamine (especially D1) agonists and antagonists potentiate and reduce fear in animals, respectively, indicating an essential function of dopamine in modulation of anxiety-related behaviors (for review, see (Pezze and Feldon, 2004)). Dopaminergic neurons are predominantly localized in the substantia nigra in rodents and primates (Dahlstroem and Fuxe, 1964; Felten and Sladek, 1983; Paxinos and Franklin, 2001). These cells

also exist in some nuclei of the hypothalamus, the striatum and the olfactory bulb, which provide output to the neighboring areas of the amygdale (Weihe *et al.*, 2006). Thus the reduced anxiety levels in BACHD rats might be the result from the inactivation of dopamine-secreting neurons in some brain regions e.g. hypothalamus. However, there are still some other types of neurotransmitter promoting cells in the amygdala, such as 5-hydroxytriptamine (5-HT) (Levinson, 2006). It cannot be ruled out, that other neurotransmitter signaling pathways contribute to the reduction of anxiety in BACHD rats.

Interestingly, most rodent HD models exhibit an increased or decreased anxiety-like behavior compared to WT littermates. However, with respect to the lower anxiety level in both full-length and fragment rat models and R6/2 mouse model, these anxiety variations are unlikely to be affected either by different experiment setups in different laboratories or by the unequal anatomy of rats and mice. The variation is also not depending on the CAG repeat length, since both BACHD mice and rats possess the same CAG repeat length but display a discrepancy in anxiety-like behavior.

In the tgHD and the BACHD transgenic rat models, aggregates are abundantly expressed in the amygdala (Petrasch-Parwez *et al.*, 2007). In contrast, only few aggregates were observed in the amygdala of BACHD mice (unpublished data from our collaborator Alex Osmand), which show an increased anxiety-like behaviour in the elevated plus maze. Unfortunately, no comparable data on aggregate load in the amygdala of R6/2 mice are available to us.

Subcellular localization of aggregates was investigated in collaboration with Elisabeth Petrasch-Parwez at the University of Bochum. By electron microscopy we demonstrated that neuropil aggregates are localized in axons and synaptic terminals (Yu-Taeger *et al.*, 2012) where they may affect axonal transport and synaptic transmission. Since a reduced firing rate of cells in the amygdala correlates with an increase in anxiety, this decrease in the excitability of the amygdala might be caused by an altered synaptic transmission of dopaminergic neurons, possibly triggered by the numerous and fairly large aggregates in the amygdala. Furthermore, all brain regions involved in the signaling pathways projecting to the amygdala (Figure 5.4) including hippocampus, BSTA, hypothalamus, and the olfactory bulb presented highly abundant aggregates. This might influence the balance of the excitatory and

inhibitory signaling leading to an altered anxiety-like behavior in HD transgenic models.

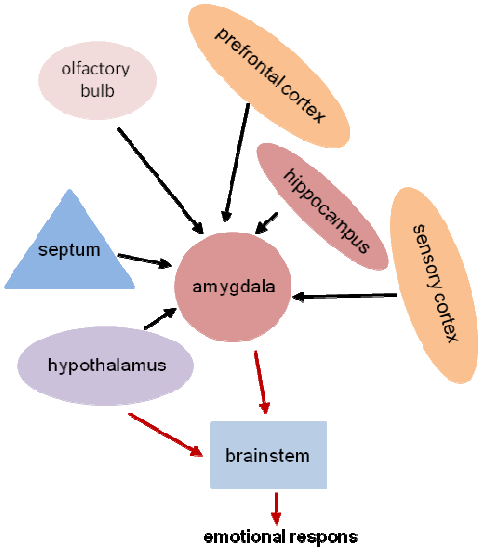

Figue 5.4: The afferent projections of the amygdala. The amygdala has a wide range of connections with other brain regions. Part of the input is received from the hippocampus. Visceral inputs come from the hypothalamus, septum, orbital cortex (prefrontal cortex). Additional olfactory sensory information is transferred from the olfactory bulb to the amygdala. Auditory, visual and somatosensory information comes from the temporal and anterior singulate cortices (sensory cortex).

5.5 Aggregation and intranuclear accumulation of mhtt in BACHD rats

5.5.1 Regional and subcellular distribution of mhtt aggregates in BACHD rat brains

While rats of both BACHD transgenic lines display wide-spread deposits of aggregates throughout the entire brain, the distribution is not homogenous and found in distinct patterns. Compared to TG5, TG9 rats have a strikingly reduced number and size of aggregates. These results demonstrate that aggregate formation correlates with the level of mhtt expression. The expression of mhtt was found to be relatively similar across all brain regions in which wild type huntingtin was also expressed. Interestingly, although overall equal amounts of mhtt were found, the density of aggregates varied from region to region. Large differences of mhtt aggregation between the striatum and cerebral cortex were observed, even though these regions expressed comparable mhtt levels at different ages (data not shown). This data suggests that mhtt preferentially aggregates in certain neuron populations. This preferential aggregation could depend on several factors, such as length of neurites, the capacity of each neuronal type to clear misfolded proteins, oxidative stress or differences in neuronal firing rate.

Remarkably, the BACHD rat model reflects many aspects of the aggregation pattern of mhtt found in HD patients. The aggregates occur more frequently in the cortex than in the striatum and neuropil aggregates appear earlier than mhtt accumulation in

the nucleus (DiFiglia *et al.*, 1997; Gutekunst *et al.*, 1999). In contrast, R6/2 mice display mainly diffuse mhtt throughout the nucleus with intensively stained nuclear aggregates (Kosinski *et al.*, 1999; Wang *et al.*, 2008). In the fragment rat model for HD, cortical aggregates are far less expressed than in the limbic striatum (von Horsten *et al.*, 2003; Nguyen *et al.*, 2006). BACHD mice display a similar mhtt aggregate distribution pattern as our BACHD rats with prevalence of neuropil aggregates and paucity of intranuclear inclusions, but both are less abundant than in BACHD rats and appear at a later time point; the diffuse nuclear mhtt accumulation was not detected until 18 months of age (Gray *et al.*, 2008). In comparison, YAC128 mice display both neuropil aggregates and intranuclear inclusions, which were present at 15 months of age, particularly in ventral striatum, amygdala and cortex (Bayram-Weston *et al.*, 2011). Interestingly, neuropil aggregates are much more common in HD patients with an adult onset than in juvenile onset patients, and the number of neuropil aggregates correlates with the extent of disease. While intranuclear aggregates were not detected in the presymptomatic patient, neuropil aggregates were observed in the cortex of the same presymptomatic patient (DiFiglia *et al.*, 1997; Gourfinkel-An *et al.*, 1998; Gutekunst *et al.*, 1999). This difference in the aggregation pattern might be explained by sequence differences in the human mutant *HTT* transgenes harboured by the BACHD models and the YAC128 mice, including single nucleotide polymorphisms as well as differences in the nature of CAA interruptions of the CAG tract (Pouladi *et al.*, 2012).

5.5.2 Association of mhtt aggregates with neurodegeneration

Progressive and wide distributed mhtt aggregates and nuclear accumulation of mhtt were found in BACHD rats starting at 3 months of age. However, whether the extent of aggregation or numbers of aggregates predicts neuronal death remains controversial. Several studies have reported that aggregated mhtt in the nucleus and cytoplasm recruits and tightly binds several interacting proteins with subsequent loss of their essential functions. These proteins include TBP, HIPP1, and CBP (Harjes and Wanker, 2003; Li and Li, 2004), and can cause apoptosis either through directly modulating transcription or indirectly due to abnormal histone acetylation (Steffan *et al.*, 2000; Jiang *et al.*, 2003; Klevytska *et al.*, 2010; Datta and Bhattacharyya, 2011). Similarly, mhtt tightly interacts with HAP1, which is involved in axonal transport and thereby impairs anterograde and retrograde intracellular trafficking (Rong *et al.*, 2006; Twelvetrees *et al.*, 2010; Yang *et al.*, 2011). The formation of neuropil

aggregates can induce axonal degeneration (Li *et al.*, 2001). Additionally, they can affect mitochondrial transport along both axons and dendrites, thereby impairing energy supply within neuronal processes (Chang *et al.*, 2006). Importantly, BACHD rats show mhtt deposits prominently expressed in axons and synaptic terminals (Yu-Taeger, 2012). In contrast, other studies have suggested that aggregation may exert beneficial effects by protecting against polyglutamine toxicity, since the aggregation of N-terminal htt reduces the amount of monomeric and oligomeric N-terminal htt, which possesses a higher toxicity (Arrasate *et al.*, 2004; Lajoie and Snapp, 2010; Miller *et al.*, 2010).

Electron microscopy (by Elisabeth Petrasch-Parwez) revealed numerous dark degenerating neurons and axons in BACHD rats in brain regions where prominent numbers of aggregates were present (Figure 5.5) (Yu-Taeger *et al.*, 2012). Furthermore, dark neurons and axons containing aggregates were frequently observed suggesting a connection between aggregate formation and neurodegeneration. Additionally, we demonstrated in collaboration with Cerebricon, Finland, a wide-spread brain volume reduction in BACHD rats by *ex vivo* T2 magnetic resonance imaging (MRI). A significant brain volume reduction was seen starting at 12 months of age, especially in the striatum (Figure 5.6). These results support our electron microscopic findings on neurodegeneration. Interestingly, brain volume reduction took place predominantly in the striatum, even though abundant nuclear accumulation and neuropil aggregates occurred in the cortex and elsewhere, and although only minimal nuclear accumulations and few neuropil aggregates were observed in the dorsolateral striatum. Furthermore, neurodegeneration occurred much later than the formation of the aggregates. While these results indicate that aggregation may contribute to neurodegeneration, after a lengthy process, neuronal loss in the striatum might only be fully accounted for by additional mechanisms.

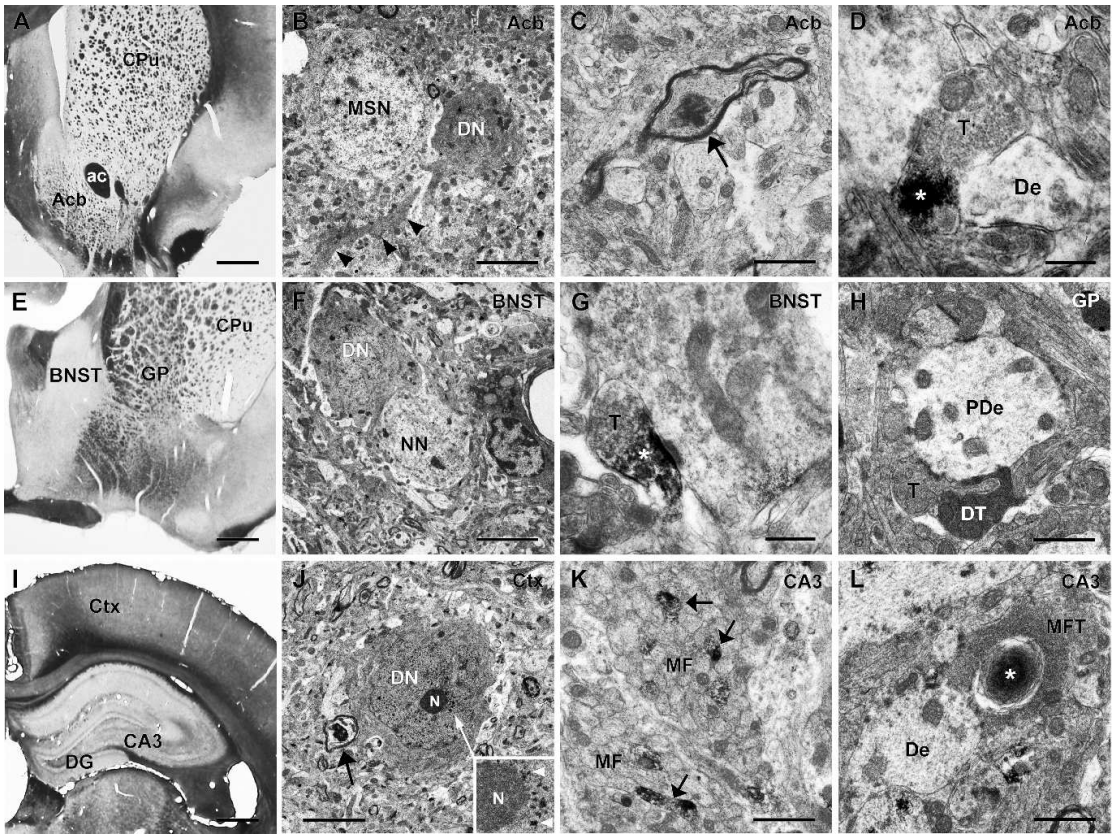

Figure 5.5: Neurodegeneration and subcellular localization of mhtt aggregates in TG5 brains (A, E, I). Vibratome sections (50µm) show the areas investigated by EM48 immune-electron microscopy. (B, F, J) Dark degenerated neurons (DN) and dendrites (arrowheads in B) were detected in the nucleus accumbens (Acb), bed nucleus of the stria terminalis (BNST) and cortex (Ctx), the latter with punctate nuclear htt reactivity as seen adjacent to the nucleolus (N) at higher enlargement (N, inlay in J). DN were seen localized near normal neurons, medium sized spiny neurons (MSN in B) or myelinated nerve fibers showing evidence of degeneration (arrow in J). Htt aggregates (*) were observed in axons (ax in C) and synaptic terminals (T in D, G) often contacting dendrites (De). Dark terminals (DT in H) were seen in the globus pallidus (GP) apposing pallidal dendrites (PDe). In the hippocampal CA3 region of hippocampus mossy fiber bundles (MF) emerging from the dentate gyrus (DG) exhibited immunoreactive unmyelinated fibers (arrows in K); htt reactivity engulfed by lamellated structures was also observed in mossy fiber terminals (MFT in L), adjacent to neuronal dendrites (De). Caudate putamen (CPu); anterior commissure (ac). Scale bars: in A, E, I = 0.5 mm; in B, F, J = 5 µm; in C, H, K, L = 1 µm; in D, G = 0.5 µm. (from Yu-Taeger et al., 2012). Data were provided by Elisabeth Petrasch-Parwez at university of Bochum.

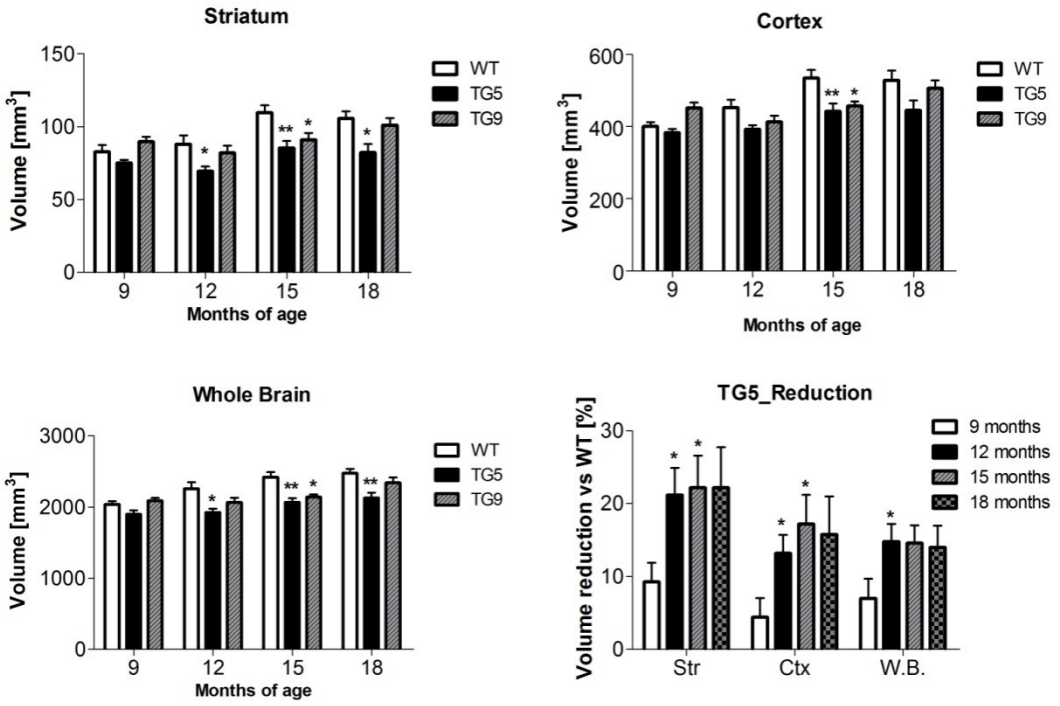

Figure 5.6: Progressive brain volume reduction is seen in aged BACHD rats using *ex vivo* MRI. TG5 exhibited striatal (A) and total brain volume (C) reduction compared to WT starting at 12 months, whereas TG9 showed a significant reduction in these volumes only at 15 months of age. TG5 exhibited more severe brain volume reduction in the striatum than in the cortex (B). (D) Percentage of brain volume reduction in different brain regions of TG5 rats compared to WT. The reduction of brain volume was quantified in striatum, cortex and whole brain across time, stars indicate the progressive volume reduction in rats at 12 and 15 months of age compared to rats at 9 months of age in all the investigated areas. Data are expressed as means ± SEM, *p<0.05; **p<0.01.

5.5.3 Intranuclear accumulation of N-terminal mhtt

Intranuclear accumulation of N-terminal huntingtin was found diffused throughout the outer layers of the cortex, as well as in all the granule cells of the hippocampus, while only a few cells punctually distributed in the striatum showed nuclear accumulations. This might be caused by the capacity of specific neuron types to cleave huntingtin, e.g. proteolysis of htt by caspase-6, thus triggering the translocation of N-terminal huntingtin into the nucleus.

High resolution microscopy detected a non-homogeneous distribution of accumulated mhtt in the nucleus, showing a similar structure as chromatin. It is likely, that mhtt is associated with the chromatin, since htt was found to interact with transcription regulatory factors and co-activators as well as chromatin regulation proteins (Faber *et al.*, 1998; Huang *et al.*, 1998; Boutell *et al.*, 1999; Goehler *et al.*, 2004). In line with this, several studies have shown that gene expression is altered in the brains of transgenic HD animals and HD patients. Therefore, the transcriptome of BACHD rats

in comparison to wildtype littermates was analyzed by microarrays in our microarray facility (data not shown). The results show transcriptional dysregulation of several genes at 12 months of age. In particular the level of BDNF mRNA was reduced, but no differences were found at 3 months of age, when no nuclear accumulation was observed. These results support the hypothesis that htt plays an essential role in neuronal gene transcription.

5.5.4 Soluble mhtt in BACHD rats

It has been demonstrated that htt contains a nuclear export signal (NES) at the carboxy-terminus (Xia, 2003, human m. Genetics). Therefore, cleavage of htt results in a nuclear localization of the N-terminal fragment due to a release of the NES. Landles and colleagues showed a reduction of small N-terminal fragments in the nucleus with increasing formation of NII indicating a depletion of N-terminal mhtt fragments, which were recruited into NII (Landles *et al.*, 2010). In the present study, soluble fl-htt and various fragments were compared cross age in striatal lysates and different subcellular fractions. Consistent to previous studies, small N-terminal fragments of both mhtt and endogenouss htt were found in striatal lysates. In contrast, these fragments were not detected in the cytoplasmic fraction. Interestingly, the abundance of N-terminal fragments did not differ between young and old BACHD rats (Figure 3.50). Immunohistological staining showed an increased diffuse nuclear staining with the S830 antibody implying an accumulation of N-terminal mhtt fragments. Taken together, these results suggest an aggregation of N-terminal mhtt fragments without depletion of soluble N-terminal fragments, which might be balanced by new synthesized mhtt in the ribosome.

5.6 Cell death in BACHD Rats

The primary neuropathological hallmark of HD is atrophy and neuronal loss in the striatum, but neurodegeneration is also seen in other parts of the basal ganglia, as well as in the cerebral cortex, thalamus, subthalamic nucleus, hypothalamus, hippocampus, and cerebellum (Macdonald and Halliday, 2002; Gardian and Vecsei, 2004). Apoptosis and necrosis are two distinct processes leading to cell death. Apoptosis is a programmed cell death with chromatin condensation and fragmentation, membrane blebbing and formation of an apoptosis body. Necrosis is the consequence of physico-chemical stress, characterized by cell swelling and lysis often associated with an inflammatory response. The typical morphology of both cell

death pathways as well as caspase activation was only sparsely identified in HD patients' brains. Increased DNA fragmentation in neurons of HD patients has been identified as a sign of apoptosis (Dragunow *et al.*, 1997; Butterworth *et al.*, 1998), while inflammation as an indicator for necrosis was readily detected in HD patients' brains. The first observation was an activated complement system in human HD (Singhrao *et al.*, 1999), the following detailed studies showed morphologically active microglia and accumulations of microglia in HD patients' brains (Sapp *et al.*, 2001). However, while dark neurons, dark degenerated axons and synaptic terminals were detected via electron microscopy, no indicators of apoptosis nor necrosis were identified in BACHD rats, although they show a robust HD-like phenotype and a reduced brain volume.

Huntingtin interacts with several nuclear proteins such as p53, GAPDH, and Sp1 as well as proteins implicated in the programmed cell death machinery of HD neurons (Hickey and Chesselet, 2003). As a transcription factor, activation of p53 can induce cell differentiation, senescence, and DNA repair processes, but best understood is the ability of p53 to induce cell cycle arrest and apoptotic cell death. One study has reported the significant lower cancer incidence in HD patients in comparison to healthy controls (Sorensen *et al.*, 1999). The same result was observed in BACHD rats. Without performing any statistical tests, it was noticed that both transgenic BACHD lines had a lower chance to develop cancer compared to WT littermates. In addition, transgenic rats displayed a shorter body length, as well as a reduced weight of several organs such as liver, spleen or kidney and brain (data not shown). But it is not clear whether the lower brain weight and reduced brain volume is caused by neurodegeneration or a deceleration in growth. Still, these events imply an active function of p53 in growth arrest and induction of apoptosis, which cannot solely be explained by an interaction of mhtt with p53 and a subsequent integration into the aggregates leading to a loss of function of p53. Steffan and colleagues have demonstrated that both mutant htt and WT htt interact with the p53 coactivator CBP and the corepressor mSir3a (2000). In HD patients and HD animals' models, the transcription of numerous genes was found to be down-regulated. Since p53 acts also as a transcription factor after activation, the sequestration of its coactivator CBP caused by an interaction and aggregation with mhtt could explain the down-regulation of these genes. Especially in the absence of p53, mhtt binds also to the p53 corepressor mSir3a triggering the same signaling cascade as p53 associated

with mSir3a, which alters transcriptional events leading to apoptotic cell death and deceleration of growth.

During apoptosis, cells shrink first followed by chromatin condensation and their disintegration into enclosed apoptotic bodies. Important to know is that the plasma membrane remains intact throughout the whole process thus ensuring that no proapoptotic factors are released to the surrounding cells (Majno and Joris, 1995). Activated proteinases cleave cellular skeletal structures as well as chromatin into nucleosomal fragments. However, these key features of apoptosis including morphology changes, proteinase activation and DNA fragmentation could not be detected in BACHD rats. Furthermore, there seems to be no progressive cell loss in the brains of BACHD rats as a reduced brain volume was already observed at 9 months (the first time point of investigation). But also in other HD rodent models, apoptotic cell death was not detected. On the other hand, Yang and colleagues have confirmed apoptosis in HD transgenic pig with postnatal death within 53 hours (Yang *et al*., 2010).

Apoptosis occurs frequently in the development of neuronal systems to remove excess neurons (Hutchins and Barger, 1998; Gilbert, 2006), thus apoptosis in this pig HD model is unlikely to be caused by mhtt. Many studies have demonstrated an association of apoptosis and ageing factors under physiological condition (Muskhelishvili *et al.*, 1995; Higami and Shimokawa, 2000; Lin and Beal, 2006). Ageing is a stochastic process combining predictable and random effects that lead to the accumulation of unrepaired cellular damage, weakening cellular repair and compensatory mechanisms (Kirkwood *et al.*, 2003). Ageing is associated with mitochondrial dysfunction, increased free radical production with shortening of telomeres associated with reduced survival and with oxidative stress, which may lead to genomic instability and DNA mutations, (Migliore and Coppede, 2009). In neurodegenerative disorders, neuronal cells are more vulnerable to ageing factors resulting in an increased apoptotic cell death. The results of this study show a constant growth in both CNS and body weight of BACHD rats and WT controls until the last investigated time point at 18 months of age. These results raise the question whether BACHD rats and other rodent models do not have a sufficiently long life-span to be affected by ageing to a degree that causes measurable DNA damage, oxidative stress or accumulation of damaged molecules.

Necrosis is another cell death pathway, distinct from apoptosis, and is accompanied by a plasma membrane disruption that leads to the release of intracellular components into the surrounding environment, which evokes inflammation (Scaffidi *et al.*, 2002; Han *et al.*, 2008). For a long time, necrosis has been thought to occur accidentally and uncontrolled as a result of environmental perturbations. Recently, programmed necrosis depending on caspases has been described in the literature (Thornberry *et al.*, 1992; Yamashita *et al.*, 1999; Proskuryakov *et al.*, 2002). Necrosis is required for cell demise (cell elimination) in a biological consequence; in neurodegenerative diseases necrotic cell death is often caused by excitotoxins. In terms of HD, necrosis is caused by an elevated excitation of glutamate receptors including NMDA, AMPA. Western blotting shows an increased NMDA2B receptor level in the striatum of BACHD rats evident at 12 months of age implying an elevated signalling of NMDA in BACHD rats at advanced stages of the disease. It is well studied that antagonists of these glutamate receptors are able to trigger necrosis (Allen *et al.*, 2002).

A further initiator of necrosis in HD is oxidative stress. Neurons are considerably susceptible to ROS, because of the lower levels of antioxidants compared to other mammalian cell types (Cooper and Kristal, 1997). In addition to ROS, both nitric oxide (NO) and peroxynitrite (ONO_2^-) are known as reactive oxygen (nitrogen species) resulting in oxidative stress (Finkel and Holbrook, 2000).

An impaired respiratory chain function in mitochondria has been identified in aged BACHD rats (Eckmann and Clemens *et al.*, submitted). This impairment of the respiratory chain disrupts the electron transfer and therefore generates oxide radicals leading to oxidative stress and cell death. Increased oxidative stress may induce apoptosis or necrosis, however maintaining a certain level of ATP is crucial for the execution of the energy-dependent apoptotic process (Eguchi *et al.*, 1997; Leist *et al.*, 1999). In the absence or a decreased level of ATP, apoptosis will be switched to the energy-independent necrosis or the lack of ATP directly induces necrosis. In PC12 neuroblastoma cells, inhibition of complex I of the respiratory chain stimulated necrotic cell death (Hartley *et al.*, 1994). This may explain, why no sign of apoptosis was found in BACHD rats throughout the 18 months of age. The presence of dark neurons detected using electron microscopy suggests that necrosis accounts for the majority of neuronal death in this HD animal model. Additionally, abundant mhtt aggregates were detected throughout the entire brain in BACHD rats, which are mostly localized in neuropil. Neuropile aggregates might influence the axonal

transport of mitochondria since numerous proteins involved in axonal transport are recruited into the aggregates. Impaired axonal transport of the mitochondria may cause a local lack of ATP supply leading to axonal necrosis, which was observed in BACHD rats. In agreement with this hypothesis, we have observed impaired axonal transport of mitochondria in primary striatal and cortical neurons obtained from BACHD rats (Clemens *et al*., unpublished data).

5.7 Imbalance of striosome and matrix compartments

The striatum is composed of two interdependent compartments: the striosome (patch) and the matrix, which can be distinguished by the differential expression of neurotransmitter-related molecules (Goldman-Rakic, 1982; Graybiel *et al.*, 1990; Holt *et al.*, 1997). Discriminative input and output connections suggest that the striosome and matrix compartments participate in limbic-based and sensorimotor/associative forebrain circuits, respectively (Donoghue and Herkenham, 1986; Gerfen, 1992). In HD patients, an imbalanced loss of neurons in the striosome and matrix compartments has been described leading to a reduced total matrix area whereas the volume of the striosome is not affected (Ferrante *et al.*, 1987; Seto-Ohshima *et al.*, 1988; Hersch and Ferrante, 1997). Conversely, it has also been reported that this imbalance in neuron loss is initially found in the striosomes but affects both compartments equally in later stages of the disease (Reiner *et al.*, 1988; Hedreen and Folstein, 1995; Lawhorn *et al.*, 2008). Striosomes exchange information with the surrounding matrix, the integrated signal will be subsequently sent through D1 (excitatory) and D2 (inhibitory) medium spiny neurons (MSNs) via direct and indirect pathways to the thalamo-cortical circuits (Figure 5.7). However, the striosome and matrix compartments contain disproportionate amounts of D1 and D2 neurons and the imbalance of those two compartments influence the proportion of excitatory and inhibitory signaling in limbic-based and sensorimotor/associative forebrain circuits. Thus, a change in the established equilibrium, as is the case in HD, causes a disorder of the basal ganglia. In BACHD rats, we observed early changes in the pattern of striosome and matrix compartments, as well as a decrease in the total and mean striosome area. This could cause alterations in the basal ganglia and lead to neuronal dysfunction and clinical signs of HD. However, the exact mechanism behind this is unknown and how this is linked to the neuropil aggregates within the sensorimotor circuit and the limbic-based circuits still needs to be answered.

In BACHD rats, the reduced area of striosomes was determined at early stages with 6 months of age, however not at advanced stages with 15 months of age. Several studies demonstrated that striosomes contain the only striatal neurons that project to the substantia nigra pars compacta (SNc), which contain dopamine-producing neurons that project back to the striatum (Gerfen, 1984; Tokuno *et al.*, 2002; Fujiyama *et al.*, 2011). Therefore, the reduction of striosomes might modulate the firing of dopamine neurons in the substantia nigra, consequently influencing the neuronal activity in its projection region in the dorsal striatum. Whether the decreased striosome area indicates a reduction of output signaling of the striosome needs to be proofed by further experiments. Nevertheless, hypokinesia in BACHD rats at younger ages might be related to the reduction of striosome area (ratio of striosome/matrix). Interestingly, the significant reduction in the ratio of striosome/matrix area disappeared at the age when hypoactivity vanished in BACHD rats. This event supports the possibility that hypokinesia in BACHD rats at early stages of the disease result from a reduced striosome modulated activity of dopamine neurons.

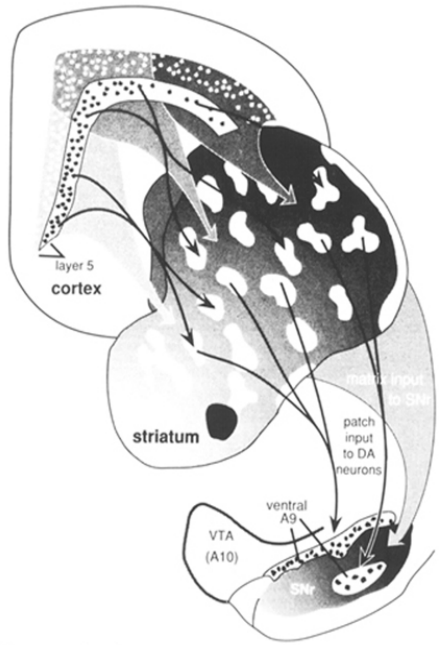

Figure 5.7: Organization of patch-matrix compartments in corticostriatal and striatonigral pathways. Corticostriatal neurons in the deep parts of layer 5 provide inputs to the striatal patch compartment, whereas superficial layer 5 neurons provide inputs to the striatal matrix. Patch neurons provide inputs to the location of dopaminergic neurons in the ventral tier of the substantia nigra pars compacta and islands of dopamine neurons in the pars reticulata. Striatal matrix neurons provide inputs to the location of GABAergic neurons in the substantia nigra pars reticulata (SNr). Charles R. Gerfen Annual Review of Neuroscience 15:285–320 (1992)

5.8 Metabolic changes in BACHD rats

HD clinical symptoms are accompanied by metabolic disturbances including modulated body weight (Van Raamsdonk *et al.*, 2006, Gray *et al.*, 2008), insulin resistance (Lalic *et al.*, 2008)(Lalic, 2008), and lipid metabolism disorder in both HD patients and animals models (Valenza *et al.*, 2007a; Valenza *et al.*, 2007b; del Toro *et al.*, 2010; Leoni *et al.*, 2011). In this study, body weight was screened weekly till 72

weeks of age showing a comparable body weight in BACHD rats and WT littermates across age. However, the proportion of muscle as percentage of body weight was significantly reduced compared to WT controls at 12 months of age, whereas the percentage of white adipose tissue was increased. Additionally, longitudinal measurement of serum glucose and lipid were performed by our collaborator Kim Verwaest at the University of Antwerp, and IGF-1 and leptin levels in plasma were measured by Mahmoud A. Pouladi working at Centre for Molecular Medicine and Therapeutics, UBC, Canada. The results revealed increases in blood glucose and leptin accompanied by reduced IGF-1 and lipid in BACHD rats TG5, and a tendency in TG9 (unpublished data, Table 5.3 and Figure 5.8).

Table 5.3: Changes in glucose and lipids in serum

		3 months		12 months		18 month	
		male	female	Male	female	male	female
Glucose	TG5	↓ p<0.05	↑ p<0.05	Ns	↑ p<0.05	↑ p<0.05	not available
	TG9	ns	ns	↑ p<0.05	↑ p<0.05	↑ p<0.05	not available
Lipids	TG5	↑ p<0.05	↓ p<0.05	↓ p<0.05	↓ p<0.05	↓ p<0.05	not available
	TG9	ns	ns	↓ p<0.05	↓ p<0.05	↓ p<0.05	not available

Data were provided by Kim Verwaest at the University of Antwerp.

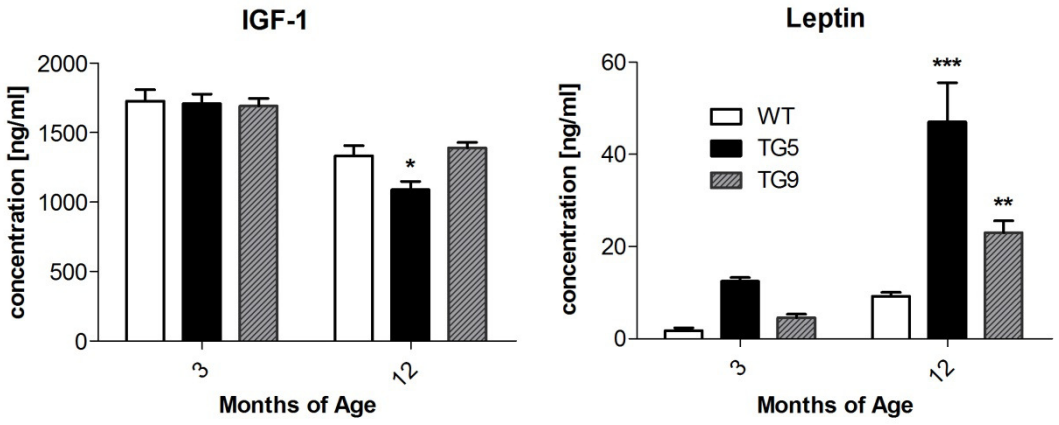

Figure 5.8: Plasma IGF-1 and leptin. IGF only shows a statistically significant decrease in TG5 at 12 months of age (bonferroni post test). Plasma leptin displayed a strong significant interaction of genotype X age, as well as a highly significant difference in main effect of genotype (two-way ANOVA). Post test indicate highly significant differences in TG5 and TG9 in comparison to WT littermates. Data were presented in mean ± SEM. *: p<0.05; **: P<0.01; ***: p<0.0001. Data were provided by Mahmoud A. Pouladi at Centre for Molecular Medicine and Therapeutics, UBC, Canada.

In comparison, increased body weight was seen in YAC and BAC mice expressing fl-htt (Van Raamdonk *et al*., 2006; Gray *et al*., 2008), R6/2 show a reduced body weight with increased white and brown adipose tissue modulated by reduced lipolysis and reduced muscle mass (Fain *et al.*, 2001; Phan *et al.*, 2009). TgHD rats displayed a sex-specific abnormal body weight, with male rats having a reduced body weight, whereas female tgHD rats showing an increased body weight (Bode *et al.*, 2008). Interestingly, fat tissue accumulation in BACHD mice is likely also sex-dependent: female BACHD mice displayed significantly increased body fat across age, in comparison male mice only presented a significant higher body fat at 4 months of age (Hult *et al.*, 2011). Interestingly, R6/2, YAC and BACHD mice exhibited reduced lipid and increased glucose levels as seen in BACHD rats. IGF-1 was found decreased in all these models except for BACHD mice, while leptin was increased in three models except for R6/2 mice (Table 5.4).

Table 5.4: Disturbed metabolism homeostasis in BACHD rats in comparison to other HD rodent models

Molecule	HD rodent model	Change	Reference
cholesterol	R6/2 mice	reduced	Valenza *et al*., 2007b
	YAC mice	reduced	Valenza *et al*., 2007a
	BACHD rat (lipid)	reduced	unpublished
glucose	R6/2 mice	increased	(Luesse *et al*., 2001)
	BAC mice	increased	Hult *et al*., 2011
	BAC rats	increased	unpublished
IGF-1	R6/2 mice	decreased	Pouladi *et al*., 2010
	YAC mice	decreased	Pouladi *et al*., 2010
	BACHD mice	increased	Hult *et al*., 2011
	BACHD rats	decreased	unpublished
Leptin	R6/2 mice	decreased	Phan *et al*., 2009
	YAC mice	increased	Pauladi *et al.*, 2010
	BACHD mice	increased	Hult *et al*., 2011
	BACHD rats	increased	unpublished

Altered cholesterol homeostasis is caused by two pathways. One pathway is the dysregulated expression of lipid biosynthesis genes leading to a decreased lipid synthesis and secretion. Reduced sterol biosynthesis has been found in HD patients compared to healthy individuals (del Toro *et al*., 2010) as well as in some HD cell lines (Sipione *et al.*, 2002; Valenza *et al.*, 2005). The second pathway is associated with increased conversion of cholesterol into 24-OHC leading to a reduction of itself. Cholesterol is a major component of the myelin sheath (70%). The lower level of cholesterol might influence formation of the myelin sheath, which plays an essential role in the signal transduction along neurites. Furthermore, the resistance of the myelin sheath depends on the myelin thickness, which can influence signal transduction in neurons. Cholesterol is also an important component of the cell membrane and the mitochondrial membrane as the cholesterol content affects membrane fluidity. Indeed a decreased cholesterol level was found in the mitochondrial membrane of BACHD rats resulting in an increased fluidity (Eckmann and Clemens et al., submitted). Different types of lipid possess various functions, only total lipid in serum was analyzed so far, it still needs to be investigated which specific lipid was altered and how it lead to metabolic disturbances. In addition, lipid cannot pass the brain-blood barrier (BBB), the level in serum might not reflect the changes in the brain. Thus, it is considered to measure lipid levels in brain or cerebrospinal fluid (CSF) in future studies.

Increased glucose levels might be modulated by reduced insulin or insulin resistance in HD patients and animal models. It was also hypothesized that increased glucose levels result from an abnormal glycolysis process, which was supported by increased lactate levels in HD patients (Garseth *et al.*, 2000)(Gårseth M, 2000).

Leptin is mainly produced in white adipose tissue and signals to hypothalamus. It plays an essential role in inhibiting appetit and the regulation of metabolism. As expected, the increased leptin level in BACHD rats was accompanied with reduced food consumption, while R6/2 mice show a reduced leptin level with increased food consumption. Elevated leptin levels and an increase in body weight (indicating an increase of adipose tissue mass) were found in YAC and BACHD mice. It was expected that the increased leptin level inhibits appetite therefore induce a decrease of food consumption. However, the food intake is increased in both mouse models suggesting a resistance to leptin in the hypothalamus (Van Raamsdonk *et al*., 2006, Hult *et al*., 2011).

DISCUSSION

Numerous studies have been carried out to investigate the cause of metabolic disturbances in HD patients and animals. These studies mainly focused on two mechanisms: first to study dysregulation of genes, which are involved in the metabolism process (Sipione *et al.*, 2002), second to investigate how neurodegeneration in the hypothalamus and disruption of hypothalamic neurocircuitries lead to altered metabolism (Kremer *et al.*, 1990). In future studies, gene regulation involved in metabolism especially in the lipid metabolism pathway should be analyzed as well as the function of hypothalamic circuitries at the cellular and molecular level.

6. Conclusion and outlook

In summary, the present study shows the development of a novel transgenic rat model for Huntington disease, which expresses fl-mhtt with 97 polyQ repeats under the control of the human htt promoter and regulatory elements. These BACHD rats display a robust, early-onset and progressive HD-like phenotype combined with characteristic neuropathological features of Huntington disease making them a valuable model for preclinical pharmacological studies. Furthermore, the slow progressive character of the disease is a valuable tool for analyzing age-related neuropathological changes in detail. Besides using these BACHD rat models for preclinical pharmacological studies, further experiments, can be carried out, which may complete the characterization of these models and bring light into the understanding of the disease mechanisms.

a. Additional behavioural characterization. In this thesis, motor deficits, intradimensional shift cognitive decline, hypokinesia and a reduced anxiety-like behavior in BACHD rats was demonstrated. In HD Patients, extradimensional shift discrimination is commonly altered before (Lawrence *et al.*, 1996). Furthermore, depression is a major psychiatric symptom besides anxiety in HD patients. Therefore, it will be important to assess extradimensional shift discrimination and depression in BACHD rats with validated behavioral tests. Based on these studies, new biomarkers may be found which are changed in early stages of the disease and therefore may be important for therapeutic studies.
b. Behavioral and pathological characterization of female BACHD rats. In this thesis, all experiments were carried out by using male rats. However, in several studies a sex-dependent social behaviour and anxiety-like behaviour as well as sex-specific metabolic changes were observed in HD transgenic mice and rats (Bode *et al*., 2008). Pharmacological investigations cannot ignore female patients. As for the male BACHD rats, also for female BACHD rats a protocol for therapeutic trials has to be developed. Gender-separated data will provide a reliable foundation for preclinical pharmacological studies considering HD patients with different gender. Additionally, if any sex-specific phenotype occurs in BACHD rats, these rats can further contribute to the investigation of the underlying mechanisms.
c. Brain structural and functional imaging *in vivo*. In this thesis, we measured the brain volume *ex vivo* in collaboration with Cerebricon, Finland, indicating a

global brain volume reduction predominantly in the striatum. It will be beneficial to be able to monitor brain volume in life rats by using MRI in future preclinical therapy studies. This would help us to longitudinally assess the effect of pharmacological substance using the same cohort of rats. It would not be necessary to sacrifice experimental animals at different ages to determine the delay of neuropathological changes, which hopefully result from pharmacological substance. In addition, cellular dysfunction is rather the key cause for HD symptoms than cell death (Menalled and Chesselet, 2002), therefore functional imaging would provide earlier indicators for the treatment than the reduction of brain volume induced by neurodegeneration.

d. Quantification of pre- and post-synaptic markers using purified enriched fractions of synaptic proteins. In the present study, we observed a change in the expression level of several synaptic markers in BACHD rats, however in most of cases these changes did not reach statistical significant levels. Numerous synaptic proteins are synthesized in neuronal somata and transported afterwards to the synaptic endings implying that most synaptic proteins are not exclusively localized in the synapse. Also the localization of some neurotransmitter receptors such as the NMDA receptor can be subdivided into an intrasynaptic and an extrasynaptic group. Therefore quantification using brain lysates is not suitable to analyze synaptic dysfunctions and degeneration. By using a purified, enriched fraction of synaptic proteins, we can quantify the pre- and post-synaptic proteins and draw reliable conclusions on synaptic degeneration in different brain regions as well as changes in the surface expression of various neurotransmitter receptors in BACHD rats.

e. Analysis of huntingtin aggregates in different cell populations and its effects on degeneration of neurites. In this thesis, we demonstrated that BACHD rats present abundant neuropil aggregates of mhtt starting at 3 months of age. Until 12 months of age, brain volume reductions in BACHD rats were detected via MRI *ex vivo* throughout the brain. However, only a few degenerated neurons were found, which stands in contrast to the numerous degenerated neuronal fibers revealed in brain regions comprising most aggregates(Yu-Taeger *et al.*, 2012). This raises the question whether axonal degeneration contributes mainly to the brain volume reduction, and whether this axonal reduction is associated with neuropil aggregates of mhtt. Moreover, it is still not clarified which cell populations are affected by mhtt

aggregation and thus potentially undergo degeneration. The mammalian brain consists of various cell populations possessing distinct chemical compositions and communicative connections and therefore being involved in specific physiological functions. Differences in cellular gene expression and organization, which in the end determines the physiological role of the cell, may render different cells more or less susceptible to excitotoxicity triggered by mhtt aggregation. The illustration of cell populations, in which aggregates are predominantly formed and/or axonal degeneration occurs, will provide answers to fundamental questions in HD research (e.g. what is the origin of the aberrant neuronal signaling) and help us to understand the abnormal neuronal network in HD. Additionally, the results of this study will provide a reliable foundation for therapy studies selective to certain cell populations, such as htt lowering by siRNA.

f. Mechanisms of metabolic disturbances and their influence on neurodegeneration in HD. In this study, we revealed with our collaboration partners an altered lipid and glucose metabolisms in BACHD rats. However the mechanisms behind these changes still remain unclear. In future studies, the mechanisms underlying can be particular determined by analyzing the dysregulation of genes, which are involved in the metabolic processes, as well as by investigation of neurodegeneration in the hypothalamus and the disruption of hypothalamic neurocircuitries. So far, a decreased cholesterol level was revealed in the mitochondrial membrane of BACHD rats resulting in an increased fluidity (by our collaborator Janett Eckmann at Goethe-University). It would be interesting to further determine the fluidity of the cell membrane and thickness of the myelin sheath, in which cholesterol is the major component, therefore their physical and/or physiological properties can be modulated by reduced cholesterol levels. Resulting data will help to better understand the neuropathogenesis in HD and may lead to a new therapeutic approach.

7. References

Al-Jader LN, Harper PS, Krawczak M, Palmer SR (2001) The frequency of inherited disorders database: prevalence of Huntington disease. Community Genet 4:148-57.

Al-Jader LN, Meredith AL, Ryley HC, Cheadle JP, Maguire S, Owen G, Goodchild MC, Harper PS (1992) Severity of chest disease in cystic fibrosis patients in relation to their genotypes. J Med Genet 29:883-7.

Allen JW, Shanker G, Tan KH, Aschner M (2002) The consequences of methylmercury exposure on interactive functions between astrocytes and neurons. Neurotoxicology 23:755-9.

Andrew SE, Goldberg YP, Kremer B, Telenius H, Theilmann J, Adam S, Starr E, Squitieri F, Lin B, Kalchman MA, Et Al. (1993) The relationship between trinucleotide (CAG) repeat length and clinical features of Huntington's disease. Nat Genet 4:398-403.

Antonsen BT, Jiang Y, Veraart J, Qu H, Nguyen HP, Sijbers J, Von Horsten S, Johnson GA, Leergaard TB (2012) Altered diffusion tensor imaging measurements in aged transgenic Huntington disease rats. Brain Struct Funct.

Aronin N, Chase K, Young C, Sapp E, Schwarz C, Matta N, Kornreich R, Landwehrmeyer B, Bird E, Beal MF, Et Al. (1995) CAG expansion affects the expression of mutant Huntingtin in the Huntington's disease brain. Neuron 15:1193-201.

Arrasate M, Mitra S, Schweitzer ES, Segal MR, Finkbeiner S (2004) Inclusion body formation reduces levels of mutant huntingtin and the risk of neuronal death. Nature 431:805-10.

Asan E (1998) The catecholaminergic innervation of the rat amygdala. Adv Anat Embryol Cell Biol 142:1-118.

Baldo B, Paganetti P, Grueninger S, Marcellin D, Kaltenbach LS, Lo DC, Semmelroth M, Zivanovic A, Abramowski D, Smith D, Lotz GP, Bates GP, Weiss A (2012) TR-FRET-based duplex immunoassay reveals an inverse correlation of soluble and aggregated mutant huntingtin in huntington's disease. Chem Biol 19:264-75.

Bates G (2003) Huntingtin aggregation and toxicity in Huntington's disease. Lancet 361:1642-4.

Bayram-Weston Z, Jones L, Dunnett SB, Brooks SP (2011) Light and electron microscopic characterization of the evolution of cellular pathology in YAC128 Huntington's disease transgenic mice. Brain Res Bull.

Beal MF, Henshaw DR, Jenkins BG, Rosen BR, Schulz JB (1994) Coenzyme Q10 and nicotinamide block striatal lesions produced by the mitochondrial toxin malonate. Ann Neurol 36:882-8.

Becher MW, Kotzuk JA, Sharp AH, Davies SW, Bates GP, Price DL, Ross CA (1998) Intranuclear neuronal inclusions in Huntington's disease and dentatorubral and pallidoluysian atrophy: correlation between the density of inclusions and IT15 CAG triplet repeat length. Neurobiol Dis 4:387-97.

Bence NF, Sampat RM, Kopito RR (2001) Impairment of the ubiquitin-proteasome system by protein aggregation. Science 292:1552-5.

Bissonette GB, Martins GJ, Franz TM, Harper ES, Schoenbaum G, Powell EM (2008) Double dissociation of the effects of medial and orbital prefrontal cortical lesions on attentional and affective shifts in mice. J Neurosci 28:11124-30.

Bjorkqvist M, Wild EJ, Thiele J, Silvestroni A, Andre R, Lahiri N, et al. (2008) A novel pathogenic pathway of immune activation detectable before clinical onset in Huntington's disease. J Exp Med 205:1869-77.

Blockx I, Van Camp N, Verhoye M, Boisgard R, Dubois A, Jego B, Jonckers E, Raber K, Siquier K, Kuhnast B, Dolle F, Nguyen HP, Von Horsten S, Tavitian B, Van Der Linden A (2011) Genotype specific age related changes in a transgenic rat model of Huntington's disease. Neuroimage 58:1006-16.

Blockx I, De Groof G, Verhoye M, Van Audekerke J, Raber K, Poot D, Sijbers J, Osmand AP, Von Horsten S, Van Der Linden A (2012) Microstructural changes observed with DKI in a transgenic Huntington rat model: evidence for abnormal neurodevelopment. Neuroimage 59:957-67.

Boado RJ, Kazantsev A, Apostol BL, Thompson LM, Pardridge WM (2000) Antisense-mediated down-regulation of the human huntingtin gene. J Pharmacol Exp Ther 295:239-43.

Bode FJ, Stephan M, Suhling H, Pabst R, Straub RH, Raber KA, Bonin M, Nguyen HP, Riess O, Bauer A, Sjoberg C, Petersen A, Von Horsten S (2008) Sex differences in a transgenic rat model of Huntington's disease: decreased 17beta-estradiol levels correlate with reduced numbers of DARPP32+ neurons in males. Hum Mol Genet 17:2595-609.

Borrell-Pages M, Zala D, Humbert S, Saudou F (2006) Huntington's disease: from huntingtin function and dysfunction to therapeutic strategies. Cell Mol Life Sci 63:2642-60.

Bossy-Wetzel E, Petrilli A, Knott AB (2008) Mutant huntingtin and mitochondrial dysfunction. Trends Neurosci 31:609-16.

Bots GT, Bruyn GW (1981) Neuropathological changes of the nucleus accumbens in Huntington's chorea. Acta Neuropathol 55:21-2.

Boutell JM, Thomas P, Neal JW, Weston VJ, Duce J, Harper PS, Jones AL (1999) Aberrant interactions of transcriptional repressor proteins with the Huntington's disease gene product, huntingtin. Hum Mol Genet 8:1647-55.

Bradford J, Shin JY, Roberts M, Wang CE, Li XJ, Li S (2009) Expression of mutant huntingtin in mouse brain astrocytes causes age-dependent neurological symptoms. Proc Natl Acad Sci U S A 106:22480-5.

Bradford J, Shin JY, Roberts M, Wang CE, Sheng G, Li S, Li XJ (2010) Mutant huntingtin in glial cells exacerbates neurological symptoms of Huntington disease mice. J Biol Chem 285:10653-61.

Brooks S, Fielding S, Dobrossy M, Von Horsten S, Dunnett S (2009) Subtle but progressive cognitive deficits in the female tgHD hemizygote rat as demonstrated by operant SILT performance. Brain Res Bull 79:310-5.

Browne SE, Bowling AC, Macgarvey U, Baik MJ, Berger SC, Muqit MM, Bird ED, Beal MF (1997) Oxidative damage and metabolic dysfunction in Huntington's disease: selective vulnerability of the basal ganglia. Ann Neurol 41:646-53.

Bruyn GW (1979) [Huntington's chorea]. Tijdschr Ziekenverpl 32:101-5.

Butters N, Sax D, Montgomery K, Tarlow S (1978) Comparison of the neuropsychological deficits associated with early and advanced Huntington's disease. Arch Neurol 35:585-9.

Butters N, Wolfe J, Martone M, Granholm E, Cermak LS (1985) Memory disorders associated with Huntington's disease: verbal recall, verbal recognition and procedural memory. Neuropsychologia 23:729-43.

Butterworth NJ, Williams L, Bullock JY, Love DR, Faull RL, Dragunow M (1998) Trinucleotide (CAG) repeat length is positively correlated with the degree of DNA fragmentation in Huntington's disease striatum. Neuroscience 87:49-53.

Caine ED, Ebert MH, Weingartner H (1977) An outline for the analysis of dementia. The memory disorder of Huntingtons disease. Neurology 27:1087-92.

REFERENCES

Cannella M, Gellera C, Maglione V, Giallonardo P, Cislaghi G, Muglia M, Quattrone A, Pierelli F, Di Donato S, Squitieri F (2004) The gender effect in juvenile Huntington disease patients of Italian origin. Am J Med Genet B Neuropsychiatr Genet 125B:92-8.

Carmichael J, Chatellier J, Woolfson A, Milstein C, Fersht AR, Rubinsztein DC (2000) Bacterial and yeast chaperones reduce both aggregate formation and cell death in mammalian cell models of Huntington's disease. Proc Natl Acad Sci U S A 97:9701-5.

Carter RJ, Lione LA, Humby T, Mangiarini L, Mahal A, Bates GP, Dunnett SB, Morton AJ (1999) Characterization of progressive motor deficits in mice transgenic for the human Huntington's disease mutation. J Neurosci 19:3248-57.

Casteels C, Vandeputte C, Rangarajan JR, Dresselaers T, Riess O, Bormans G, Maes F, Himmelreich U, Nguyen H, Van Laere K (2011) Metabolic and type 1 cannabinoid receptor imaging of a transgenic rat model in the early phase of Huntington disease. Exp Neurol 229:440-9.

Cha JH, Frey AS, Alsdorf SA, Kerner JA, Kosinski CM, Mangiarini L, Penney JB, Jr., Davies SW, Bates GP, Young AB (1999) Altered neurotransmitter receptor expression in transgenic mouse models of Huntington's disease. Philos Trans R Soc Lond B Biol Sci 354:981-9.

Chang CM, Yu YL, Fong KY, Wong MT, Chan YW, Ng TH, Leung CM, Chan V (1994) Huntington's disease in Hong Kong Chinese: epidemiology and clinical picture. Clin Exp Neurol 31:43-51.

Chang DT, Rintoul GL, Pandipati S, Reynolds IJ (2006) Mutant huntingtin aggregates impair mitochondrial movement and trafficking in cortical neurons. Neurobiol Dis 22:388-400.

Chattopadhyay B, Baksi K, Mukhopadhyay S, Bhattacharyya NP (2005) Modulation of age at onset of Huntington disease patients by variations in TP53 and human caspase activated DNase (hCAD) genes. Neurosci Lett 374:81-6.

Che HV, Metzger S, Portal E, Deyle C, Riess O, Nguyen HP (2011) Localization of sequence variations in PGC-1alpha influence their modifying effect in Huntington disease. Mol Neurodegener 6:1.

Chen MK (1977) Hypothesis on nurse role strain: are knowledgeable patients necessarily pests in hospitals? Med Care 15:350-3.

Conneally PM (1984) Huntington disease: genetics and epidemiology. Am J Hum Genet 36:506-26.

Cooper AJ, Kristal BS (1997) Multiple roles of glutathione in the central nervous system. Biol Chem 378:793-802.

Costall B, Marsden CD, Naylor RJ, Pycock CJ (1976) The relationship between striatal and mesolimbic dopamine dysfunction and the nature of circling responses following 6-hydroxydopamine and electrolytic lesions of the ascending dopamine systems of rat brain. Brain Res 118:87-113.

Coyle JT, Schwarcz R (1976) Lesion of striatal neurones with kainic acid provides a model for Huntington's chorea. Nature 263:244-6.

Crook ZR, Housman D (2011) Huntington's disease: can mice lead the way to treatment? Neuron 69:423-35.

Cui L, Jeong H, Borovecki F, Parkhurst CN, Tanese N, Krainc D (2006) Transcriptional repression of PGC-1alpha by mutant huntingtin leads to mitochondrial dysfunction and neurodegeneration. Cell 127:59-69.

Cyr M, Sotnikova TD, Gainetdinov RR, Caron MG (2006) Dopamine enhances motor and neuropathological consequences of polyglutamine expanded huntingtin. FASEB J 20:2541-3.

Dahlstroem A, Fuxe K (1964) Evidence for the Existence of Monoamine-Containing Neurons in the Central Nervous System. I. Demonstration of Monoamines in

the Cell Bodies of Brain Stem Neurons. Acta Physiol Scand Suppl:SUPPL 232:1-55.

Datta M, Bhattacharyya NP (2011) Regulation of RE1 protein silencing transcription factor (REST) expression by HIP1 protein interactor (HIPPI). J Biol Chem 286:33759-69.

Davies SW, Turmaine M, Cozens BA, Difiglia M, Sharp AH, Ross CA, Scherzinger E, Wanker EE, Mangiarini L, Bates GP (1997) Formation of neuronal intranuclear inclusions underlies the neurological dysfunction in mice transgenic for the HD mutation. Cell 90:537-48.

Debaere F, Swinnen SP, Beatse E, Sunaert S, Van Hecke P, Duysens J (2001) Brain areas involved in interlimb coordination: a distributed network. Neuroimage 14:947-58.

Del Toro D, Xifro X, Pol A, Humbert S, Saudou F, Canals JM, Alberch J (2010) Altered cholesterol homeostasis contributes to enhanced excitotoxicity in Huntington's disease. J Neurochem 115:153-67.

Diaz-Hernandez M, Valera AG, Moran MA, Gomez-Ramos P, Alvarez-Castelao B, Castano JG, Hernandez F, Lucas JJ (2006) Inhibition of 26S proteasome activity by huntingtin filaments but not inclusion bodies isolated from mouse and human brain. J Neurochem 98:1585-96.

Difiglia M, Sapp E, Chase KO, Davies SW, Bates GP, Vonsattel JP, Aronin N (1997) Aggregation of huntingtin in neuronal intranuclear inclusions and dystrophic neurites in brain. Science 277:1990-3.

Difiglia M, Sapp E, Chase K, Schwarz C, Meloni A, Young C, Martin E, Vonsattel JP, Carraway R, Reeves SA, Et Al. (1995) Huntingtin is a cytoplasmic protein associated with vesicles in human and rat brain neurons. Neuron 14:1075-81.

Difiglia M, Sena-Esteves M, Chase K, Sapp E, Pfister E, Sass M, Yoder J, Reeves P, Pandey RK, Rajeev KG, Manoharan M, Sah DW, Zamore PD, Aronin N (2007) Therapeutic silencing of mutant huntingtin with siRNA attenuates striatal and cortical neuropathology and behavioral deficits. Proc Natl Acad Sci U S A 104:17204-9.

Donoghue JP, Herkenham M (1986) Neostriatal projections from individual cortical fields conform to histochemically distinct striatal compartments in the rat. Brain Res 365:397-403.

Dorsman JC, Bremmer-Bout M, Pepers B, Van Ommen GJ, Den Dunnen JT (2002) Interruption of perfect CAG repeats by CAA triplets improves the stability of glutamine-encoding repeat sequences. Biotechniques 33:976-8.

Dragatsis I, Efstratiadis A, Zeitlin S (1998) Mouse mutant embryos lacking huntingtin are rescued from lethality by wild-type extraembryonic tissues. Development 125:1529-39.

Dragunow M, Macgibbon GA, Lawlor P, Butterworth N, Connor B, Henderson C, Walton M, Woodgate A, Hughes P, Faull RL (1997) Apoptosis, neurotrophic factors and neurodegeneration. Rev Neurosci 8:223-65.

Durr A, Hahn-Barma V, Brice A, Pecheux C, Dode C, Feingold J (1999) Homozygosity in Huntington's disease. J Med Genet 36:172-3.

Duyao MP, Auerbach AB, Ryan A, Persichetti F, Barnes GT, Mcneil SM, Ge P, Vonsattel JP, Gusella JF, Joyner AL, Et Al. (1995) Inactivation of the mouse Huntington's disease gene homolog Hdh. Science 269:407-10.

Eguchi Y, Shimizu S, Tsujimoto Y (1997) Intracellular ATP levels determine cell death fate by apoptosis or necrosis. Cancer Res 57:1835-40.

Ehrnhoefer DE, Butland SL, Pouladi MA, Hayden MR (2009) Mouse models of Huntington disease: variations on a theme. Dis Model Mech 2:123-9.

Engqvist-Goldstein AE, Kessels MM, Chopra VS, Hayden MR, Drubin DG (1999) An actin-binding protein of the Sla2/Huntingtin interacting protein 1 family is a novel component of clathrin-coated pits and vesicles. J Cell Biol 147:1503-18.

REFERENCES

Faber PW, Barnes GT, Srinidhi J, Chen J, Gusella JF, Macdonald ME (1998) Huntingtin interacts with a family of WW domain proteins. Hum Mol Genet 7:1463-74.

Fain JN, Del Mar NA, Meade CA, Reiner A, Goldowitz D (2001) Abnormalities in the functioning of adipocytes from R6/2 mice that are transgenic for the Huntington's disease mutation. Hum Mol Genet 10:145-52.

Fan J, Cowan CM, Zhang LY, Hayden MR, Raymond LA (2009) Interaction of postsynaptic density protein-95 with NMDA receptors influences excitotoxicity in the yeast artificial chromosome mouse model of Huntington's disease. J Neurosci 29:10928-38.

Fan MM, Fernandes HB, Zhang LY, Hayden MR, Raymond LA (2007) Altered NMDA receptor trafficking in a yeast artificial chromosome transgenic mouse model of Huntington's disease. J Neurosci 27:3768-79.

Fanselow MS, Ledoux JE (1999) Why we think plasticity underlying Pavlovian fear conditioning occurs in the basolateral amygdala. Neuron 23:229-32.

Felten DL, Sladek JR, Jr. (1983) Monoamine distribution in primate brain V. Monoaminergic nuclei: anatomy, pathways and local organization. Brain Res Bull 10:171-284.

Fernandes HB, Baimbridge KG, Church J, Hayden MR, Raymond LA (2007) Mitochondrial sensitivity and altered calcium handling underlie enhanced NMDA-induced apoptosis in YAC128 model of Huntington's disease. J Neurosci 27:13614-23.

Ferrante RJ, Kowall NW, Beal MF, Martin JB, Bird ED, Richardson EP, Jr. (1987) Morphologic and histochemical characteristics of a spared subset of striatal neurons in Huntington's disease. J Neuropathol Exp Neurol 46:12-27.

Ferrante RJ, Kowall NW, Richardson EP, Jr. (1991) Proliferative and degenerative changes in striatal spiny neurons in Huntington's disease: a combined study using the section-Golgi method and calbindin D28k immunocytochemistry. J Neurosci 11:3877-87.

File SE, Mahal A, Mangiarini L, Bates GP (1998) Striking changes in anxiety in Huntington's disease transgenic mice. Brain Res 805:234-40.

Finkel T, Holbrook NJ (2000) Oxidants, oxidative stress and the biology of ageing. Nature 408:239-47.

Fletcher JM, Hughes RA (2009) Modified low molecular weight cyclic peptides as mimetics of BDNF with improved potency, proteolytic stability and transmembrane passage in vitro. Bioorg Med Chem 17:2695-702.

Foroud T, Siemers E, Kleindorfer D, Bill DJ, Hodes ME, Norton JA, Conneally PM, Christian JC (1995) Cognitive scores in carriers of Huntington's disease gene compared to noncarriers. Ann Neurol 37:657-64.

Fujiyama F, Sohn J, Nakano T, Furuta T, Nakamura KC, Matsuda W, Kaneko T (2011) Exclusive and common targets of neostriatofugal projections of rat striosome neurons: a single neuron-tracing study using a viral vector. Eur J Neurosci 33:668-77.

Gabery S, Murphy K, Schultz K, Loy CT, Mccusker E, Kirik D, Halliday G, Petersen A (2010) Changes in key hypothalamic neuropeptide populations in Huntington disease revealed by neuropathological analyses. Acta Neuropathol 120:777-88.

Gafni J, Hermel E, Young JE, Wellington CL, Hayden MR, Ellerby LM (2004) Inhibition of calpain cleavage of huntingtin reduces toxicity: accumulation of calpain/caspase fragments in the nucleus. J Biol Chem 279:20211-20.

Garcia EP, Mehta S, Blair LA, Wells DG, Shang J, Fukushima T, Fallon JR, Garner CC, Marshall J (1998) SAP90 binds and clusters kainate receptors causing incomplete desensitization. Neuron 21:727-39.

Gardian G, Vecsei L (2004) Huntington's disease: pathomechanism and therapeutic perspectives. J Neural Transm 111:1485-94.

Garseth M, Sonnewald U, White LR, Rod M, Zwart JA, Nygaard O, Aasly J (2000) Proton magnetic resonance spectroscopy of cerebrospinal fluid in neurodegenerative disease: indication of glial energy impairment in Huntington chorea, but not Parkinson disease. J Neurosci Res 60:779-82.

Gauthier LR, Charrin BC, Borrell-Pages M, Dompierre JP, Rangone H, Cordelieres FP, De Mey J, Macdonald ME, Lessmann V, Humbert S, Saudou F (2004) Huntingtin controls neurotrophic support and survival of neurons by enhancing BDNF vesicular transport along microtubules. Cell 118:127-38.

Gerfen CR (1984) The neostriatal mosaic: compartmentalization of corticostriatal input and striatonigral output systems. Nature 311:461-4.

Gerfen CR (1992) The neostriatal mosaic: multiple levels of compartmental organization. Trends Neurosci 15:133-9.

Gilbert SF. Developmental Biology (8th.). Sunderland: Sinauer; 2006.

Giralt A, Carreton O, Lao-Peregrin C, Martin ED, Alberch J (2011) Conditional BDNF release under pathological conditions improves Huntington's disease pathology by delaying neuronal dysfunction. Mol Neurodegener 6:71.

Gizatullina ZZ, Lindenberg KS, Harjes P, Chen Y, Kosinski CM, Landwehrmeyer BG, Ludolph AC, Striggow F, Zierz S, Gellerich FN (2006) Low stability of Huntington muscle mitochondria against Ca2+ in R6/2 mice. Ann Neurol 59:407-11.

Goehler H, Lalowski M, Stelzl U, Waelter S, Stroedicke M, Worm U, et al. (2004) A protein interaction network links GIT1, an enhancer of huntingtin aggregation, to Huntington's disease. Mol Cell 15:853-65.

Goety CG, Tanner CM, Cohen JA, Thelen JA, Carroll VS, Klawans HL, Fariello RG (1990) L-acetyl-carnitine in Huntington's disease: double-blind placebo controlled crossover study of drug effects on movement disorder and dementia. Mov Disord 5:263-5.

Goldberg YP, Kremer B, Andrew SE, Theilmann J, Graham RK, Squitieri F, Telenius H, Adam S, Sajoo A, Starr E, Et Al. (1993) Molecular analysis of new mutations for Huntington's disease: intermediate alleles and sex of origin effects. Nat Genet 5:174-9.

Goldman-Rakic PS (1982) Cytoarchitectonic heterogeneity of the primate neostriatum: subdivision into Island and Matrix cellular compartments. J Comp Neurol 205:398-413.

Goto S, Hirano A (1990) Synaptophysin expression in the striatum in Huntington's disease. Acta Neuropathol 80:88-91.

Gourfinkel-An I, Cancel G, Duyckaerts C, Faucheux B, Hauw JJ, Trottier Y, Brice A, Agid Y, Hirsch EC (1998) Neuronal distribution of intranuclear inclusions in Huntington's disease with adult onset. Neuroreport 9:1823-6.

Graham RK, Deng Y, Carroll J, Vaid K, Cowan C, Pouladi MA, Metzler M, Bissada N, Wang L, Faull RL, Gray M, Yang XW, Raymond LA, Hayden MR (2010) Cleavage at the 586 amino acid caspase-6 site in mutant huntingtin influences caspase-6 activation in vivo. J Neurosci 30:15019-29.

Graham RK, Deng Y, Slow EJ, Haigh B, Bissada N, Lu G, Pearson J, Shehadeh J, Bertram L, Murphy Z, Warby SC, Doty CN, Roy S, Wellington CL, Leavitt BR, Raymond LA, Nicholson DW, Hayden MR (2006) Cleavage at the caspase-6 site is required for neuronal dysfunction and degeneration due to mutant huntingtin. Cell 125:1179-91.

Gray M, Shirasaki DI, Cepeda C, Andre VM, Wilburn B, Lu XH, Tao J, Yamazaki I, Li SH, Sun YE, Li XJ, Levine MS, Yang XW (2008) Full-length human mutant huntingtin with a stable polyglutamine repeat can elicit progressive and selective neuropathogenesis in BACHD mice. J Neurosci 28:6182-95.

REFERENCES

Graybiel AM, Ohta K, Roffler-Tarlov S (1990) Patterns of cell and fiber vulnerability in the mesostriatal system of the mutant mouse weaver. I. Gradients and compartments. J Neurosci 10:720-33.

Greene JG, Porter RH, Eller RV, Greenamyre JT (1993) Inhibition of succinate dehydrogenase by malonic acid produces an "excitotoxic" lesion in rat striatum. J Neurochem 61:1151-4.

Gutekunst CA. The neuropathology of Huntington's disease. In: Gillian Bates PH, Lesley Jones, editor. Huntinton's disease. New York: Oxford University Press Inc.; 2002.

Gutekunst CA, Li SH, Yi H, Mulroy JS, Kuemmerle S, Jones R, Rye D, Ferrante RJ, Hersch SM, Li XJ (1999) Nuclear and neuropil aggregates in Huntington's disease: relationship to neuropathology. J Neurosci 19:2522-34.

Gw B. Huntington's chorea: historical, clinical and laboratory synopsis. In: Vinken PJ BG, editor. Handbook of clinical neurology. Amsterdam: North Press Publishing; 1968. p. 298-378.

Haberg A, Qu H, Saether O, Unsgard G, Haraldseth O, Sonnewald U (2001) Differences in neurotransmitter synthesis and intermediary metabolism between glutamatergic and GABAergic neurons during 4 hours of middle cerebral artery occlusion in the rat: the role of astrocytes in neuronal survival. J Cereb Blood Flow Metab 21:1451-63.

Hackam AS, Yassa AS, Singaraja R, Metzler M, Gutekunst CA, Gan L, Warby S, Wellington CL, Vaillancourt J, Chen N, Gervais FG, Raymond L, Nicholson DW, Hayden MR (2000) Huntingtin interacting protein 1 induces apoptosis via a novel caspase-dependent death effector domain. J Biol Chem 275:41299-308.

Haken H, Kelso JA, Bunz H (1985) A theoretical model of phase transitions in human hand movements. Biol Cybern 51:347-56.

Hamm RJ, Pike BR, O'dell DM, Lyeth BG, Jenkins LW (1994) The rotarod test: an evaluation of its effectiveness in assessing motor deficits following traumatic brain injury. J Neurotrauma 11:187-96.

Hammer RE, Maika SD, Richardson JA, Tang JP, Taurog JD (1990) Spontaneous inflammatory disease in transgenic rats expressing HLA-B27 and human beta 2m: an animal model of HLA-B27-associated human disorders. Cell 63:1099-112.

Han SI, Kim YS, Kim TH (2008) Role of apoptotic and necrotic cell death under physiologic conditions. BMB Rep 41:1-10.

Harjes P, Wanker EE (2003) The hunt for huntingtin function: interaction partners tell many different stories. Trends Biochem Sci 28:425-33.

Harms L, Meierkord H, Timm G, Pfeiffer L, Ludolph AC (1997) Decreased N-acetyl-aspartate/choline ratio and increased lactate in the frontal lobe of patients with Huntington's disease: a proton magnetic resonance spectroscopy study. J Neurol Neurosurg Psychiatry 62:27-30.

Harper JD, Lansbury PT, Jr. (1997) Models of amyloid seeding in Alzheimer's disease and scrapie: mechanistic truths and physiological consequences of the time-dependent solubility of amyloid proteins. Annu Rev Biochem 66:385-407.

Harper P (1991) Huntington's Disease. WB Saunders, London.

Hartley A, Stone JM, Heron C, Cooper JM, Schapira AH (1994) Complex I inhibitors induce dose-dependent apoptosis in PC12 cells: relevance to Parkinson's disease. J Neurochem 63:1987-90.

Hedreen JC, Folstein SE (1995) Early loss of neostriatal striosome neurons in Huntington's disease. J Neuropathol Exp Neurol 54:105-20.

Heinsen H, Strik M, Bauer M, Luther K, Ulmar G, Gangnus D, Jungkunz G, Eisenmenger W, Gotz M (1994) Cortical and striatal neurone number in Huntington's disease. Acta Neuropathol 88:320-33.

Heinsen H, Rub U, Gangnus D, Jungkunz G, Bauer M, Ulmar G, Bethke B, Schuler M, Bocker F, Eisenmenger W, Gotz M, Strik M (1996) Nerve cell loss in the thalamic centromedian-parafascicular complex in patients with Huntington's disease. Acta Neuropathol 91:161-8.

Heng MY, Detloff PJ, Wang PL, Tsien JZ, Albin RL (2009) In vivo evidence for NMDA receptor-mediated excitotoxicity in a murine genetic model of Huntington disease. J Neurosci 29:3200-5.

Hersch S, Ferrante R. Neuropathology and Pathophysiology of Huntington's Disease. Watts R, Koller W, editors. New York: McGraw-Hill; 1997.

Hickey MA, Chesselet MF (2003) Apoptosis in Huntington's disease. Prog Neuropsychopharmacol Biol Psychiatry 27:255-65.

Higami Y, Shimokawa I (2000) Apoptosis in the aging process. Cell Tissue Res 301:125-32.

Hilditch-Maguire P, Trettel F, Passani LA, Auerbach A, Persichetti F, Macdonald ME (2000) Huntingtin: an iron-regulated protein essential for normal nuclear and perinuclear organelles. Hum Mol Genet 9:2789-97.

Ho LW, Brown R, Maxwell M, Wyttenbach A, Rubinsztein DC (2001) Wild type Huntingtin reduces the cellular toxicity of mutant Huntingtin in mammalian cell models of Huntington's disease. J Med Genet 38:450-2.

Hodges A, Strand AD, Aragaki AK, Kuhn A, Sengstag T, Hughes G, et al. (2006) Regional and cellular gene expression changes in human Huntington's disease brain. Hum Mol Genet 15:965-77.

Hodgson JG, Agopyan N, Gutekunst CA, Leavitt BR, Lepiane F, Singaraja R, Smith DJ, Bissada N, Mccutcheon K, Nasir J, Jamot L, Li XJ, Stevens ME, Rosemond E, Roder JC, Phillips AG, Rubin EM, Hersch SM, Hayden MR (1999) A YAC mouse model for Huntington's disease with full-length mutant huntingtin, cytoplasmic toxicity, and selective striatal neurodegeneration. Neuron 23:181-92.

Holbert S, Denghien I, Kiechle T, Rosenblatt A, Wellington C, Hayden MR, Margolis RL, Ross CA, Dausset J, Ferrante RJ, Neri C (2001) The Gln-Ala repeat transcriptional activator CA150 interacts with huntingtin: neuropathologic and genetic evidence for a role in Huntington's disease pathogenesis. Proc Natl Acad Sci U S A 98:1811-6.

Holmberg CI, Staniszewski KE, Mensah KN, Matouschek A, Morimoto RI (2004) Inefficient degradation of truncated polyglutamine proteins by the proteasome. EMBO J 23:4307-18.

Holt DJ, Graybiel AM, Saper CB (1997) Neurochemical architecture of the human striatum. J Comp Neurol 384:1-25.

Hu J, Matsui M, Corey DR (2009) Allele-selective inhibition of mutant huntingtin by peptide nucleic acid-peptide conjugates, locked nucleic acid, and small interfering RNA. Ann N Y Acad Sci 1175:24-31.

Huang CC, Faber PW, Persichetti F, Mittal V, Vonsattel JP, Macdonald ME, Gusella JF (1998) Amyloid formation by mutant huntingtin: threshold, progressivity and recruitment of normal polyglutamine proteins. Somat Cell Mol Genet 24:217-33.

Hult S, Soylu R, Bjorklund T, Belgardt BF, Mauer J, Bruning JC, Kirik D, Petersen A (2011) Mutant huntingtin causes metabolic imbalance by disruption of hypothalamic neurocircuits. Cell Metab 13:428-39.

Humbert S, Bryson EA, Cordelieres FP, Connors NC, Datta SR, Finkbeiner S, Greenberg ME, Saudou F (2002) The IGF-1/Akt pathway is neuroprotective

in Huntington's disease and involves Huntingtin phosphorylation by Akt. Dev Cell 2:831-7.

Hutchins JB, Barger SW (1998) Why neurons die: cell death in the nervous system. Anat Rec 253:79-90.

Ito H, Takahashi H, Arakawa R, Takano H, Suhara T (2008) Normal database of dopaminergic neurotransmission system in human brain measured by positron emission tomography. Neuroimage 39:555-65.

Jacobsen JC, Bawden CS, Rudiger SR, Mclaughlan CJ, Reid SJ, Waldvogel HJ, Macdonald ME, Gusella JF, Walker SK, Kelly JM, Webb GC, Faull RL, Rees MI, Snell RG (2010) An ovine transgenic Huntington's disease model. Hum Mol Genet 19:1873-82.

Jantzen KJ, Steinberg FL, Kelso JA (2005) Functional MRI reveals the existence of modality and coordination-dependent timing networks. Neuroimage 25:1031-42.

Jason GW, Pajurkova EM, Suchowersky O, Hewitt J, Hilbert C, Reed J, Hayden MR (1988) Presymptomatic neuropsychological impairment in Huntington's disease. Arch Neurol 45:769-73.

Jenkins BG, Rosas HD, Chen YC, Makabe T, Myers R, Macdonald M, Rosen BR, Beal MF, Koroshetz WJ (1998) 1H NMR spectroscopy studies of Huntington's disease: correlations with CAG repeat numbers. Neurology 50:1357-65.

Jeste DV, Barban L, Parisi J (1984) Reduced Purkinje cell density in Huntington's disease. Exp Neurol 85:78-86.

Jiang H, Nucifora FC, Jr., Ross CA, Defranco DB (2003) Cell death triggered by polyglutamine-expanded huntingtin in a neuronal cell line is associated with degradation of CREB-binding protein. Hum Mol Genet 12:1-12.

Josiassen RC, Curry LM, Mancall EL (1983) Development of neuropsychological deficits in Huntington's disease. Arch Neurol 40:791-6.

Kantor O, Temel Y, Holzmann C, Raber K, Nguyen HP, Cao C, Turkoglu HO, Rutten BP, Visser-Vandewalle V, Steinbusch HW, Blokland A, Korr H, Riess O, Von Horsten S, Schmitz C (2006) Selective striatal neuron loss and alterations in behavior correlate with impaired striatal function in Huntington's disease transgenic rats. Neurobiol Dis 22:538-47.

Kazantsev A, Preisinger E, Dranovsky A, Goldgaber D, Housman D (1999) Insoluble detergent-resistant aggregates form between pathological and nonpathological lengths of polyglutamine in mammalian cells. Proc Natl Acad Sci U S A 96:11404-9.

Kelly MA, Rubinstein M, Phillips TJ, Lessov CN, Burkhart-Kasch S, Zhang G, Bunzow JR, Fang Y, Gerhardt GA, Grandy DK, Low MJ (1998) Locomotor activity in D2 dopamine receptor-deficient mice is determined by gene dosage, genetic background, and developmental adaptations. J Neurosci 18:3470-9.

Kelso JA, Southard DL, Goodman D (1979) On the nature of human interlimb coordination. Science 203:1029-31.

Kennedy L, Shelbourne PF (2000) Dramatic mutation instability in HD mouse striatum: does polyglutamine load contribute to cell-specific vulnerability in Huntington's disease? Hum Mol Genet 9:2539-44.

Kim YJ, Yi Y, Sapp E, Wang Y, Cuiffo B, Kegel KB, Qin ZH, Aronin N, Difiglia M (2001) Caspase 3-cleaved N-terminal fragments of wild-type and mutant huntingtin are present in normal and Huntington's disease brains, associate with membranes, and undergo calpain-dependent proteolysis. Proc Natl Acad Sci U S A 98:12784-9.

Kirkwood TB, Boys RJ, Gillespie CS, Proctor CJ, Shanley DP, Wilkinson DJ (2003) Towards an e-biology of ageing: integrating theory and data. Nat Rev Mol Cell Biol 4:243-9.

Klevytska AM, Tebbenkamp AT, Savonenko AV, Borchelt DR (2010) Partial depletion of CREB-binding protein reduces life expectancy in a mouse model of Huntington disease. J Neuropathol Exp Neurol 69:396-404.

Kosinski CM, Cha JH, Young AB, Mangiarini L, Bates G, Schiefer J, Schwarz M (1999) Intranuclear inclusions in subtypes of striatal neurons in Huntington's disease transgenic mice. Neuroreport 10:3891-6.

Kremer B, Almqvist E, Theilmann J, Spence N, Telenius H, Goldberg YP, Hayden MR (1995) Sex-dependent mechanisms for expansions and contractions of the CAG repeat on affected Huntington disease chromosomes. Am J Hum Genet 57:343-50.

Kremer HP, Roos RA, Dingjan G, Marani E, Bots GT (1990) Atrophy of the hypothalamic lateral tuberal nucleus in Huntington's disease. J Neuropathol Exp Neurol 49:371-82.

Kremer HP (1992) The hypothalamic lateral tuberal nucleus: normal anatomy and changes in neurological diseases. Prog Brain Res 93:249-61.

Kuemmerle S, Gutekunst CA, Klein AM, Li XJ, Li SH, Beal MF, Hersch SM, Ferrante RJ (1999) Huntington aggregates may not predict neuronal death in Huntington's disease. Ann Neurol 46:842-9.

Kuhl DE, Phelps ME, Markham CH, Metter EJ, Riege WH, Winter J (1982) Cerebral metabolism and atrophy in Huntington's disease determined by 18FDG and computed tomographic scan. Ann Neurol 12:425-34.

Kuhn A, Goldstein DR, Hodges A, Strand AD, Sengstag T, Kooperberg C, et al. (2007) Mutant huntingtin's effects on striatal gene expression in mice recapitulate changes observed in human Huntington's disease brain and do not differ with mutant huntingtin length or wild-type huntingtin dosage. Hum Mol Genet 16:1845-61.

Kuwert T, Lange HW, Langen KJ, Herzog H, Aulich A, Feinendegen LE (1990) Cortical and subcortical glucose consumption measured by PET in patients with Huntington's disease. Brain 113 (Pt 5):1405-23.

Laforet GA, Sapp E, Chase K, Mcintyre C, Boyce FM, Campbell M, Cadigan BA, Warzecki L, Tagle DA, Reddy PH, Cepeda C, Calvert CR, Jokel ES, Klapstein GJ, Ariano MA, Levine MS, Difiglia M, Aronin N (2001) Changes in cortical and striatal neurons predict behavioral and electrophysiological abnormalities in a transgenic murine model of Huntington's disease. J Neurosci 21:9112-23.

Lajoie P, Snapp EL (2010) Formation and toxicity of soluble polyglutamine oligomers in living cells. PLoS One 5:e15245.

Lalic NM, Maric J, Svetel M, Jotic A, Stefanova E, Lalic K, Dragasevic N, Milicic T, Lukic L, Kostic VS (2008) Glucose homeostasis in Huntington disease: abnormalities in insulin sensitivity and early-phase insulin secretion. Arch Neurol 65:476-80.

Landles C, Sathasivam K, Weiss A, Woodman B, Moffitt H, Finkbeiner S, Sun B, Gafni J, Ellerby LM, Trottier Y, Richards WG, Osmand A, Paganetti P, Bates GP (2010) Proteolysis of mutant huntingtin produces an exon 1 fragment that accumulates as an aggregated protein in neuronal nuclei in Huntington disease. J Biol Chem 285:8808-23.

Lange H, Thorner G, Hopf A, Schroder KF (1976) Morphometric studies of the neuropathological changes in choreatic diseases. J Neurol Sci 28:401-25.

Lawhorn C, Smith DM, Brown LL (2008) Striosome-matrix pathology and motor deficits in the YAC128 mouse model of Huntington's disease. Neurobiol Dis 32:471-8.

Lawrence AD, Sahakian BJ, Rogers RD, Hodge JR, Robbins TW (1999) Discrimination, reversal, and shift learning in Huntington's disease: mechanisms of impaired response selection. Neuropsychologia 37:1359-74.

Lawrence AD, Sahakian BJ, Hodges JR, Rosser AE, Lange KW, Robbins TW (1996) Executive and mnemonic functions in early Huntington's disease. Brain 119 (Pt 5):1633-45.

Leavitt BR, Van Raamsdonk JM, Shehadeh J, Fernandes H, Murphy Z, Graham RK, Wellington CL, Raymond LA, Hayden MR (2006) Wild-type huntingtin protects neurons from excitotoxicity. J Neurochem 96:1121-9.

Lecerf JM, Shirley TL, Zhu Q, Kazantsev A, Amersdorfer P, Housman DE, Messer A, Huston JS (2001) Human single-chain Fv intrabodies counteract in situ huntingtin aggregation in cellular models of Huntington's disease. Proc Natl Acad Sci U S A 98:4764-9.

Leist M, Single B, Naumann H, Fava E, Simon B, Kuhnle S, Nicotera P (1999) Inhibition of mitochondrial ATP generation by nitric oxide switches apoptosis to necrosis. Exp Cell Res 249:396-403.

Leoni V, Mariotti C, Nanetti L, Salvatore E, Squitieri F, Bentivoglio AR, Bandettini Di Poggio M, Piacentini S, Monza D, Valenza M, Cattaneo E, Di Donato S (2011) Whole body cholesterol metabolism is impaired in Huntington's disease. Neurosci Lett 494:245-9.

Leung CM, Chan YW, Chang CM, Yu YL, Chen CN (1992) Huntington's disease in Chinese: a hypothesis of its origin. J Neurol Neurosurg Psychiatry 55:681-4.

Levine MS, Klapstein GJ, Koppel A, Gruen E, Cepeda C, Vargas ME, Jokel ES, Carpenter EM, Zanjani H, Hurst RS, Efstratiadis A, Zeitlin S, Chesselet MF (1999) Enhanced sensitivity to N-methyl-D-aspartate receptor activation in transgenic and knockin mouse models of Huntington's disease. J Neurosci Res 58:515-32.

Levinson DF (2006) The genetics of depression: a review. Biol Psychiatry 60:84-92.

Li H, Wyman T, Yu ZX, Li SH, Li XJ (2003) Abnormal association of mutant huntingtin with synaptic vesicles inhibits glutamate release. Hum Mol Genet 12:2021-30.

Li H, Li SH, Yu ZX, Shelbourne P, Li XJ (2001) Huntingtin aggregate-associated axonal degeneration is an early pathological event in Huntington's disease mice. J Neurosci 21:8473-81.

Li SH, Li XJ (2004) Huntingtin and its role in neuronal degeneration. Neuroscientist 10:467-75.

Li SH, Schilling G, Young WS, 3rd, Li XJ, Margolis RL, Stine OC, Wagster MV, Abbott MH, Franz ML, Ranen NG, Et Al. (1993) Huntington's disease gene (IT15) is widely expressed in human and rat tissues. Neuron 11:985-93.

Li SH, Gutekunst CA, Hersch SM, Li XJ (1998) Interaction of huntingtin-associated protein with dynactin P150Glued. J Neurosci 18:1261-9.

Li XJ, Li SH, Sharp AH, Nucifora FC, Jr., Schilling G, Lanahan A, Worley P, Snyder SH, Ross CA (1995) A huntingtin-associated protein enriched in brain with implications for pathology. Nature 378:398-402.

Lim D, Fedrizzi L, Tartari M, Zuccato C, Cattaneo E, Brini M, Carafoli E (2008) Calcium homeostasis and mitochondrial dysfunction in striatal neurons of Huntington disease. J Biol Chem 283:5780-9.

Lin CH, Tallaksen-Greene S, Chien WM, Cearley JA, Jackson WS, Crouse AB, Ren S, Li XJ, Albin RL, Detloff PJ (2001) Neurological abnormalities in a knock-in mouse model of Huntington's disease. Hum Mol Genet 10:137-44.

Lin MT, Beal MF (2006) Mitochondrial dysfunction and oxidative stress in neurodegenerative diseases. Nature 443:787-95.

Liu L, Orozco IJ, Planel E, Wen Y, Bretteville A, Krishnamurthy P, Wang L, Herman M, Figueroa H, Yu WH, Arancio O, Duff K (2008) A transgenic rat that

develops Alzheimer's disease-like amyloid pathology, deficits in synaptic plasticity and cognitive impairment. Neurobiol Dis 31:46-57.

Lodi R, Schapira AH, Manners D, Styles P, Wood NW, Taylor DJ, Warner TT (2000) Abnormal in vivo skeletal muscle energy metabolism in Huntington's disease and dentatorubropallidoluysian atrophy. Ann Neurol 48:72-6.

Luesse HG, Schiefer J, Spruenken A, Puls C, Block F, Kosinski CM (2001) Evaluation of R6/2 HD transgenic mice for therapeutic studies in Huntington's disease: behavioral testing and impact of diabetes mellitus. Behav Brain Res 126:185-95.

Luthi-Carter R, Taylor DM, Pallos J, Lambert E, Amore A, Parker A, Moffitt H, Smith DL, Runne H, Gokce O, Kuhn A, Xiang Z, Maxwell MM, Reeves SA, Bates GP, Neri C, Thompson LM, Marsh JL, Kazantsev AG (2010) SIRT2 inhibition achieves neuroprotection by decreasing sterol biosynthesis. Proc Natl Acad Sci U S A 107:7927-32.

Macdonald ME, Vonsattel JP, Shrinidhi J, Couropmitree NN, Cupples LA, Bird ED, Gusella JF, Myers RH (1999) Evidence for the GluR6 gene associated with younger onset age of Huntington's disease. Neurology 53:1330-2.

Macdonald V, Halliday G (2002) Pyramidal cell loss in motor cortices in Huntington's disease. Neurobiol Dis 10:378-86.

Macdonald V, Halliday GM, Trent RJ, Mccusker EA (1997) Significant loss of pyramidal neurons in the angular gyrus of patients with Huntington's disease. Neuropathol Appl Neurobiol 23:492-5.

Maglione V, Marchi P, Di Pardo A, Lingrell S, Horkey M, Tidmarsh E, Sipione S (2010) Impaired ganglioside metabolism in Huntington's disease and neuroprotective role of GM1. J Neurosci 30:4072-80.

Majno G, Joris I (1995) Apoptosis, oncosis, and necrosis. An overview of cell death. Am J Pathol 146:3-15.

Mangiarini L, Sathasivam K, Seller M, Cozens B, Harper A, Hetherington C, Lawton M, Trottier Y, Lehrach H, Davies SW, Bates GP (1996) Exon 1 of the HD gene with an expanded CAG repeat is sufficient to cause a progressive neurological phenotype in transgenic mice. Cell 87:493-506.

Manley K, Shirley TL, Flaherty L, Messer A (1999) Msh2 deficiency prevents in vivo somatic instability of the CAG repeat in Huntington disease transgenic mice. Nat Genet 23:471-3.

Mann VM, Cooper JM, Javoy-Agid F, Agid Y, Jenner P, Schapira AH (1990) Mitochondrial function and parental sex effect in Huntington's disease. Lancet 336:749.

Martin WR, Clark C, Ammann W, Stoessl AJ, Shtybel W, Hayden MR (1992) Cortical glucose metabolism in Huntington's disease. Neurology 42:223-9.

Mattson MP (2003) Excitotoxic and excitoprotective mechanisms: abundant targets for the prevention and treatment of neurodegenerative disorders. Neuromolecular Med 3:65-94.

Mcalonan K, Brown VJ (2003) Orbital prefrontal cortex mediates reversal learning and not attentional set shifting in the rat. Behav Brain Res 146:97-103.

Mcgeer PL, Mcgeer EG (1998) Glial cell reactions in neurodegenerative diseases: pathophysiology and therapeutic interventions. Alzheimer Dis Assoc Disord 12 Suppl 2:S1-6.

Mcneil SM, Novelletto A, Srinidhi J, Barnes G, Kornbluth I, Altherr MR, Wasmuth JJ, Gusella JF, Macdonald ME, Myers RH (1997) Reduced penetrance of the Huntington's disease mutation. Hum Mol Genet 6:775-9.

Meda L, Cassatella MA, Szendrei GI, Otvos L, Jr., Baron P, Villalba M, Ferrari D, Rossi F (1995) Activation of microglial cells by beta-amyloid protein and interferon-gamma. Nature 374:647-50.

REFERENCES

Menalled L, El-Khodor BF, Patry M, Suarez-Farinas M, Orenstein SJ, Zahasky B, Leahy C, Wheeler V, Yang XW, Macdonald M, Morton AJ, Bates G, Leeds J, Park L, Howland D, Signer E, Tobin A, Brunner D (2009) Systematic behavioral evaluation of Huntington's disease transgenic and knock-in mouse models. Neurobiol Dis 35:319-36.

Menalled LB, Chesselet MF (2002) Mouse models of Huntington's disease. Trends Pharmacol Sci 23:32-9.

Menalled LB, Sison JD, Dragatsis I, Zeitlin S, Chesselet MF (2003) Time course of early motor and neuropathological anomalies in a knock-in mouse model of Huntington's disease with 140 CAG repeats. J Comp Neurol 465:11-26.

Metzger S, Saukko M, Van Che H, Tong L, Puder Y, Riess O, Nguyen HP (2010) Age at onset in Huntington's disease is modified by the autophagy pathway: implication of the V471A polymorphism in Atg7. Hum Genet 128:453-9.

Migliore L, Coppede F (2009) Environmental-induced oxidative stress in neurodegenerative disorders and aging. Mutat Res 674:73-84.

Mihm MJ, Amann DM, Schanbacher BL, Altschuld RA, Bauer JA, Hoyt KR (2007) Cardiac dysfunction in the R6/2 mouse model of Huntington's disease. Neurobiol Dis 25:297-308.

Miller J, Arrasate M, Shaby BA, Mitra S, Masliah E, Finkbeiner S (2010) Quantitative relationships between huntingtin levels, polyglutamine length, inclusion body formation, and neuronal death provide novel insight into huntington's disease molecular pathogenesis. J Neurosci 30:10541-50.

Mirkin SM (2006) DNA structures, repeat expansions and human hereditary disorders. Curr Opin Struct Biol 16:351-8.

Mirkin SM (2007) Expandable DNA repeats and human disease. Nature 447:932-40.

Mishra SK, Agostinelli NR, Brett TJ, Mizukami I, Ross TS, Traub LM (2001) Clathrin- and AP-2-binding sites in HIP1 uncover a general assembly role for endocytic accessory proteins. J Biol Chem 276:46230-6.

Morton AJ, Wood NI, Hastings MH, Hurelbrink C, Barker RA, Maywood ES (2005) Disintegration of the sleep-wake cycle and circadian timing in Huntington's disease. J Neurosci 25:157-63.

Moses JA, Jr., Golden CJ, Berger PA, Wisniewski AM (1981) Neuropsychological deficits in early, middle, and late stage Huntington's disease as measured by the Luria-Nebraska Neuropsychological Battery. Int J Neurosci 14:95-100.

Munoz-Sanjuan I, Bates GP (2011) The importance of integrating basic and clinical research toward the development of new therapies for Huntington disease. J Clin Invest 121:476-83.

Muskhelishvili L, Hart RW, Turturro A, James SJ (1995) Age-related changes in the intrinsic rate of apoptosis in livers of diet-restricted and ad libitum-fed B6C3F1 mice. Am J Pathol 147:20-4.

Myers RH, Macdonald ME, Koroshetz WJ, Duyao MP, Ambrose CM, Taylor SA, Barnes G, Srinidhi J, Lin CS, Whaley WL, Et Al. (1993) De novo expansion of a (CAG)n repeat in sporadic Huntington's disease. Nat Genet 5:168-73.

Nasir J, Floresco SB, O'kusky JR, Diewert VM, Richman JM, Zeisler J, Borowski A, Marth JD, Phillips AG, Hayden MR (1995) Targeted disruption of the Huntington's disease gene results in embryonic lethality and behavioral and morphological changes in heterozygotes. Cell 81:811-23.

Naze P, Vuillaume I, Destee A, Pasquier F, Sablonniere B (2002) Mutation analysis and association studies of the ubiquitin carboxy-terminal hydrolase L1 gene in Huntington's disease. Neurosci Lett 328:1-4.

Nellemann C, Abell K, Norremolle A, Lokkegaard T, Naver B, Ropke C, Rygaard J, Sorensen SA, Hasholt L (2000) Inhibition of Huntington synthesis by antisense oligodeoxynucleotides. Mol Cell Neurosci 16:313-23.

Ng CW, Noblejas MI, Rodefer JS, Smith CB, Poremba A (2007) Double dissociation of attentional resources: prefrontal versus cingulate cortices. J Neurosci 27:12123-31.

Nguyen HP, Metzger S, Holzmann C, Koczan D, Thiesen HJ, Von Horsten S, Riess O, Bonin M (2008) Age-dependent gene expression profile and protein expression in a transgenic rat model of Huntington's disease. Proteomics Clin Appl 2:1638-50.

Nguyen HP, Kobbe P, Rahne H, Worpel T, Jager B, Stephan M, Pabst R, Holzmann C, Riess O, Korr H, Kantor O, Petrasch-Parwez E, Wetzel R, Osmand A, Von Horsten S (2006) Behavioral abnormalities precede neuropathological markers in rats transgenic for Huntington's disease. Hum Mol Genet 15:3177-94.

Norremolle A, Riess O, Epplen JT, Fenger K, Hasholt L, Sorensen SA (1993) Trinucleotide repeat elongation in the Huntingtin gene in Huntington disease patients from 71 Danish families. Hum Mol Genet 2:1475-6.

Norton JC (1975) Patterns of neuropsychological test performance in Huntington's disease. J Nerv Ment Dis 161:276-9.

O'kusky JR, Nasir J, Cicchetti F, Parent A, Hayden MR (1999) Neuronal degeneration in the basal ganglia and loss of pallido-subthalamic synapses in mice with targeted disruption of the Huntington's disease gene. Brain Res 818:468-79.

Oliveira JM, Jekabsons MB, Chen S, Lin A, Rego AC, Goncalves J, Ellerby LM, Nicholls DG (2007) Mitochondrial dysfunction in Huntington's disease: the bioenergetics of isolated and in situ mitochondria from transgenic mice. J Neurochem 101:241-9.

Orvoen S, Pla P, Gardier AM, Saudou F, David DJ (2012) Huntington's disease knock-in male mice show specific anxiety-like behaviour and altered neuronal maturation. Neurosci Lett 507:127-32.

Osmand AP, Berthelier V, Wetzel R (2006) Imaging polyglutamine deposits in brain tissue. Methods Enzymol 412:106-22.

Oyanagi K, Takeda S, Takahashi H, Ohama E, Ikuta F (1989) A quantitative investigation of the substantia nigra in Huntington's disease. Ann Neurol 26:13-9.

Panov A, Obertone T, Bennett-Desmelik J, Greenamyre JT (1999) Ca(2+)-dependent permeability transition and complex I activity in lymphoblast mitochondria from normal individuals and patients with Huntington's or Alzheimer's disease. Ann N Y Acad Sci 893:365-8.

Pavese N, Gerhard A, Tai YF, Ho AK, Turkheimer F, Barker RA, Brooks DJ, Piccini P (2006) Microglial activation correlates with severity in Huntington disease: a clinical and PET study. Neurology 66:1638-43.

Paxinos G, Franklin K. The Mouse Brain in Stereotaxic Coordinates (2nd ed.). San Diego: Academic Press; 2001.

Paxinos G, Franklin K. The Rat Brain in stereotaxic coordinate. 6th ed. San Diego: Academic Press; 2006.

Pelton TA, Sharma S, Schulz TC, Rathjen J, Rathjen PD (2002) Transient pluripotent cell populations during primitive ectoderm formation: correlation of in vivo and in vitro pluripotent cell development. J Cell Sci 115:329-39.

Penney JB, Jr., Vonsattel JP, Macdonald ME, Gusella JF, Myers RH (1997) CAG repeat number governs the development rate of pathology in Huntington's disease. Ann Neurol 41:689-92.

Petrasch-Parwez E, Nguyen HP, Lobbecke-Schumacher M, Habbes HW, Wieczorek S, Riess O, Andres KH, Dermietzel R, Von Horsten S (2007) Cellular and subcellular localization of Huntingtin [corrected] aggregates in the brain of a rat transgenic for Huntington disease. J Comp Neurol 501:716-30.

REFERENCES

Peyser CE, Folstein M, Chase GA, Starkstein S, Brandt J, Cockrell JR, Bylsma F, Coyle JT, Mchugh PR, Folstein SE (1995) Trial of d-alpha-tocopherol in Huntington's disease. Am J Psychiatry 152:1771-5.

Pezze MA, Feldon J (2004) Mesolimbic dopaminergic pathways in fear conditioning. Prog Neurobiol 74:301-20.

Pfrieger FW (2003) Role of cholesterol in synapse formation and function. Biochim Biophys Acta 1610:271-80.

Phan J, Hickey MA, Zhang P, Chesselet MF, Reue K (2009) Adipose tissue dysfunction tracks disease progression in two Huntington's disease mouse models. Hum Mol Genet 18:1006-16.

Pouladi MA, Xie Y, Skotte NH, Ehrnhoefer DE, Graham RK, Kim JE, Bissada N, Yang XW, Paganetti P, Friedlander RM, Leavitt BR, Hayden MR (2010) Full-length huntingtin levels modulate body weight by influencing insulin-like growth factor 1 expression. Hum Mol Genet 19:1528-38.

Pouladi MA, Stanek LM, Xie Y, Franciosi S, Southwell AL, Deng Y, Butland S, Zhang W, Cheng SH, Shihabuddin LS, Hayden MR (2012) Marked differences in neurochemistry and aggregates despite similar behavioural and neuropathological features of Huntington disease in the full-length BACHD and YAC128 mice. Hum Mol Genet.

Pouladi MA, Graham RK, Karasinska JM, Xie Y, Santos RD, Petersen A, Hayden MR (2009) Prevention of depressive behaviour in the YAC128 mouse model of Huntington disease by mutation at residue 586 of huntingtin. Brain 132:919-32.

Proskuryakov SY, Gabai VL, Konoplyannikov AG (2002) Necrosis is an active and controlled form of programmed cell death. Biochemistry (Mosc) 67:387-408.

Puddifoot C, Martel MA, Soriano FX, Camacho A, Vidal-Puig A, Wyllie DJ, Hardingham GE (2012) PGC-1alpha negatively regulates extrasynaptic NMDAR activity and excitotoxicity. J Neurosci 32:6995-7000.

Qin ZH, Wang Y, Kegel KB, Kazantsev A, Apostol BL, Thompson LM, Yoder J, Aronin N, Difiglia M (2003) Autophagy regulates the processing of amino terminal huntingtin fragments. Hum Mol Genet 12:3231-44.

Rangone H, Humbert S, Saudou F (2004) Huntington's disease: how does huntingtin, an anti-apoptotic protein, become toxic? Pathol Biol (Paris) 52:338-42.

Reiner A, Albin RL, Anderson KD, D'amato CJ, Penney JB, Young AB (1988) Differential loss of striatal projection neurons in Huntington disease. Proc Natl Acad Sci U S A 85:5733-7.

Rigamonti D, Sipione S, Goffredo D, Zuccato C, Fossale E, Cattaneo E (2001) Huntingtin's neuroprotective activity occurs via inhibition of procaspase-9 processing. J Biol Chem 276:14545-8.

Rigamonti D, Bauer JH, De-Fraja C, Conti L, Sipione S, Sciorati C, Clementi E, Hackam A, Hayden MR, Li Y, Cooper JK, Ross CA, Govoni S, Vincenz C, Cattaneo E (2000) Wild-type huntingtin protects from apoptosis upstream of caspase-3. J Neurosci 20:3705-13.

Rising AC, Xu J, Carlson A, Napoli VV, Denovan-Wright EM, Mandel RJ (2011) Longitudinal behavioral, cross-sectional transcriptional and histopathological characterization of a knock-in mouse model of Huntington's disease with 140 CAG repeats. Exp Neurol 228:173-82.

Romanelli P, Esposito V, Schaal DW, Heit G (2005) Somatotopy in the basal ganglia: experimental and clinical evidence for segregated sensorimotor channels. Brain Res Brain Res Rev 48:112-28.

Rong J, Mcguire JR, Fang ZH, Sheng G, Shin JY, Li SH, Li XJ (2006) Regulation of intracellular trafficking of huntingtin-associated protein-1 is critical for TrkA protein levels and neurite outgrowth. J Neurosci 26:6019-30.

Roos RA, Pruyt JF, De Vries J, Bots GT (1985) Neuronal distribution in the putamen in Huntington's disease. J Neurol Neurosurg Psychiatry 48:422-5.

Roos RA, Bots GT, Hermans J (1986) Quantitative analysis of morphological features in Huntington's disease. Acta Neurol Scand 73:131-5.

Rouach N, Koulakoff A, Abudara V, Willecke K, Giaume C (2008) Astroglial metabolic networks sustain hippocampal synaptic transmission. Science 322:1551-5.

Sapp E, Kegel KB, Aronin N, Hashikawa T, Uchiyama Y, Tohyama K, Bhide PG, Vonsattel JP, Difiglia M (2001) Early and progressive accumulation of reactive microglia in the Huntington disease brain. J Neuropathol Exp Neurol 60:161-72.

Sasaki A, Yamaguchi H, Ogawa A, Sugihara S, Nakazato Y (1997) Microglial activation in early stages of amyloid beta protein deposition. Acta Neuropathol 94:316-22.

Sattler R, Tymianski M (2001) Molecular mechanisms of glutamate receptor-mediated excitotoxic neuronal cell death. Mol Neurobiol 24:107-29.

Sawa A, Wiegand GW, Cooper J, Margolis RL, Sharp AH, Lawler JF, Jr., Greenamyre JT, Snyder SH, Ross CA (1999) Increased apoptosis of Huntington disease lymphoblasts associated with repeat length-dependent mitochondrial depolarization. Nat Med 5:1194-8.

Scaffidi P, Misteli T, Bianchi ME (2002) Release of chromatin protein HMGB1 by necrotic cells triggers inflammation. Nature 418:191-5.

Scherzinger E, Sittler A, Schweiger K, Heiser V, Lurz R, Hasenbank R, Bates GP, Lehrach H, Wanker EE (1999) Self-assembly of polyglutamine-containing huntingtin fragments into amyloid-like fibrils: implications for Huntington's disease pathology. Proc Natl Acad Sci U S A 96:4604-9.

Schilling G, Becher MW, Sharp AH, Jinnah HA, Duan K, Kotzuk JA, Slunt HH, Ratovitski T, Cooper JK, Jenkins NA, Copeland NG, Price DL, Ross CA, Borchelt DR (1999) Intranuclear inclusions and neuritic aggregates in transgenic mice expressing a mutant N-terminal fragment of huntingtin. Hum Mol Genet 8:397-407.

Schilling G, Savonenko AV, Klevytska A, Morton JL, Tucker SM, Poirier M, Gale A, Chan N, Gonzales V, Slunt HH, Coonfield ML, Jenkins NA, Copeland NG, Ross CA, Borchelt DR (2004) Nuclear-targeting of mutant huntingtin fragments produces Huntington's disease-like phenotypes in transgenic mice. Hum Mol Genet 13:1599-610.

Seto-Ohshima A, Emson PC, Lawson E, Mountjoy CQ, Carrasco LH (1988) Loss of matrix calcium-binding protein-containing neurons in Huntington's disease. Lancet 1:1252-5.

Sharp AH, Loev SJ, Schilling G, Li SH, Li XJ, Bao J, Wagster MV, Kotzuk JA, Steiner JP, Lo A, Et Al. (1995) Widespread expression of Huntington's disease gene (IT15) protein product. Neuron 14:1065-74.

Shelbourne PF, Killeen N, Hevner RF, Johnston HM, Tecott L, Lewandoski M, Ennis M, Ramirez L, Li Z, Iannicola C, Littman DR, Myers RM (1999) A Huntington's disease CAG expansion at the murine Hdh locus is unstable and associated with behavioural abnormalities in mice. Hum Mol Genet 8:763-74.

Shirendeb UP, Calkins MJ, Manczak M, Anekonda V, Dufour B, Mcbride JL, Mao P, Reddy PH (2012) Mutant huntingtin's interaction with mitochondrial protein Drp1 impairs mitochondrial biogenesis and causes defective axonal transport and synaptic degeneration in Huntington's disease. Hum Mol Genet 21:406-20.

Siemers E, Foroud T, Bill DJ, Sorbel J, Norton JA, Jr., Hodes ME, Niebler G, Conneally PM, Christian JC (1996) Motor changes in presymptomatic Huntington disease gene carriers. Arch Neurol 53:487-92.

REFERENCES

Singhrao SK, Neal JW, Morgan BP, Gasque P (1999) Increased complement biosynthesis by microglia and complement activation on neurons in Huntington's disease. Exp Neurol 159:362-76.

Sipione S, Rigamonti D, Valenza M, Zuccato C, Conti L, Pritchard J, Kooperberg C, Olson JM, Cattaneo E (2002) Early transcriptional profiles in huntingtin-inducible striatal cells by microarray analyses. Hum Mol Genet 11:1953-65.

Sipione S, Cattaneo E (2001) Modeling Huntington's disease in cells, flies, and mice. Mol Neurobiol 23:21-51.

Sittler A, Walter S, Wedemeyer N, Hasenbank R, Scherzinger E, Eickhoff H, Bates GP, Lehrach H, Wanker EE (1998) SH3GL3 associates with the Huntingtin exon 1 protein and promotes the formation of polygln-containing protein aggregates. Mol Cell 2:427-36.

Slow EJ, Van Raamsdonk J, Rogers D, Coleman SH, Graham RK, Deng Y, Oh R, Bissada N, Hossain SM, Yang YZ, Li XJ, Simpson EM, Gutekunst CA, Leavitt BR, Hayden MR (2003) Selective striatal neuronal loss in a YAC128 mouse model of Huntington disease. Hum Mol Genet 12:1555-67.

Snell RG, Macmillan JC, Cheadle JP, Fenton I, Lazarou LP, Davies P, Macdonald ME, Gusella JF, Harper PS, Shaw DJ (1993) Relationship between trinucleotide repeat expansion and phenotypic variation in Huntington's disease. Nat Genet 4:393-7.

Song W, Chen J, Petrilli A, Liot G, Klinglmayr E, Zhou Y, Poquiz P, Tjong J, Pouladi MA, Hayden MR, Masliah E, Ellisman M, Rouiller I, Schwarzenbacher R, Bossy B, Perkins G, Bossy-Wetzel E (2011) Mutant huntingtin binds the mitochondrial fission GTPase dynamin-related protein-1 and increases its enzymatic activity. Nat Med 17:377-82.

Sorensen SA, Fenger K, Olsen JH (1999) Significantly lower incidence of cancer among patients with Huntington disease: An apoptotic effect of an expanded polyglutamine tract? Cancer 86:1342-6.

Southwell AL, Ko J, Patterson PH (2009) Intrabody gene therapy ameliorates motor, cognitive, and neuropathological symptoms in multiple mouse models of Huntington's disease. J Neurosci 29:13589-602.

Spampanato J, Gu X, Yang XW, Mody I (2008) Progressive synaptic pathology of motor cortical neurons in a BAC transgenic mouse model of Huntington's disease. Neuroscience 157:606-20.

Spargo E, Everall IP, Lantos PL (1993) Neuronal loss in the hippocampus in Huntington's disease: a comparison with HIV infection. J Neurol Neurosurg Psychiatry 56:487-91.

Squitieri F, Cannella M, Simonelli M (2002) CAG mutation effect on rate of progression in Huntington's disease. Neurol Sci 23 Suppl 2:S107-8.

Squitieri F, Sabbadini G, Mandich P, Gellera C, Di Maria E, Bellone E, Castellotti B, Nargi E, De Grazia U, Frontali M, Novelletto A (2000) Family and molecular data for a fine analysis of age at onset in Huntington disease. Am J Med Genet 95:366-73.

Squitieri F, Frati L, Ciarmiello A, Lastoria S, Quarrell O (2006) Juvenile Huntington's disease: does a dosage-effect pathogenic mechanism differ from the classical adult disease? Mech Ageing Dev 127:208-12.

Stack EC, Kubilus JK, Smith K, Cormier K, Del Signore SJ, Guelin E, Ryu H, Hersch SM, Ferrante RJ (2005) Chronology of behavioral symptoms and neuropathological sequela in R6/2 Huntington's disease transgenic mice. J Comp Neurol 490:354-70.

Steffan JS, Kazantsev A, Spasic-Boskovic O, Greenwald M, Zhu YZ, Gohler H, Wanker EE, Bates GP, Housman DE, Thompson LM (2000) The Huntington's disease protein interacts with p53 and CREB-binding protein and represses transcription. Proc Natl Acad Sci U S A 97:6763-8.

Sun Y, Savanenin A, Reddy PH, Liu YF (2001) Polyglutamine-expanded huntingtin promotes sensitization of N-methyl-D-aspartate receptors via post-synaptic density 95. J Biol Chem 276:24713-8.

Tabrizi SJ, Cleeter MW, Xuereb J, Taanman JW, Cooper JM, Schapira AH (1999) Biochemical abnormalities and excitotoxicity in Huntington's disease brain. Ann Neurol 45:25-32.

Tabrizi SJ, Blamire AM, Manners DN, Rajagopalan B, Styles P, Schapira AH, Warner TT (2005) High-dose creatine therapy for Huntington disease: a 2-year clinical and MRS study. Neurology 64:1655-6.

Tabrizi SJ, Workman J, Hart PE, Mangiarini L, Mahal A, Bates G, Cooper JM, Schapira AH (2000) Mitochondrial dysfunction and free radical damage in the Huntington R6/2 transgenic mouse. Ann Neurol 47:80-6.

Taherzadeh-Fard E, Saft C, Wieczorek S, Epplen JT, Arning L (2010) Age at onset in Huntington's disease: replication study on the associations of ADORA2A, HAP1 and OGG1. Neurogenetics 11:435-9.

Tai YF, Pavese N, Gerhard A, Tabrizi SJ, Barker RA, Brooks DJ, Piccini P (2007) Microglial activation in presymptomatic Huntington's disease gene carriers. Brain 130:1759-66.

Tanaka M, Machida Y, Niu S, Ikeda T, Jana NR, Doi H, Kurosawa M, Nekooki M, Nukina N (2004) Trehalose alleviates polyglutamine-mediated pathology in a mouse model of Huntington disease. Nat Med 10:148-54.

Tang TS, Tu H, Chan EY, Maximov A, Wang Z, Wellington CL, Hayden MR, Bezprozvanny I (2003) Huntingtin and huntingtin-associated protein 1 influence neuronal calcium signaling mediated by inositol-(1,4,5) triphosphate receptor type 1. Neuron 39:227-39.

Telenius H, Kremer HP, Theilmann J, Andrew SE, Almqvist E, Anvret M, Greenberg C, Greenberg J, Lucotte G, Squitieri F, Et Al. (1993) Molecular analysis of juvenile Huntington disease: the major influence on (CAG)n repeat length is the sex of the affected parent. Hum Mol Genet 2:1535-40.

Thakur AK, Jayaraman M, Mishra R, Thakur M, Chellgren VM, Byeon IJ, Anjum DH, Kodali R, Creamer TP, Conway JF, Gronenborn AM, Wetzel R (2009) Polyglutamine disruption of the huntingtin exon 1 N terminus triggers a complex aggregation mechanism. Nat Struct Mol Biol 16:380-9.

Thornberry NA, Bull HG, Calaycay JR, Chapman KT, Howard AD, Kostura MJ, Miller DK, Molineaux SM, Weidner JR, Aunins J, Et Al. (1992) A novel heterodimeric cysteine protease is required for interleukin-1 beta processing in monocytes. Nature 356:768-74.

Thu DC, Oorschot DE, Tippett LJ, Nana AL, Hogg VM, Synek BJ, Luthi-Carter R, Waldvogel HJ, Faull RL (2010) Cell loss in the motor and cingulate cortex correlates with symptomatology in Huntington's disease. Brain 133:1094-110.

Tokuno H, Chiken S, Kametani K, Moriizumi T (2002) Efferent projections from the striatal patch compartment: anterograde degeneration after selective ablation of neurons expressing mu-opioid receptor in rats. Neurosci Lett 332:5-8.

Tong Y, Ha TJ, Liu L, Nishimoto A, Reiner A, Goldowitz D (2011) Spatial and temporal requirements for huntingtin (Htt) in neuronal migration and survival during brain development. J Neurosci 31:14794-9.

Tran AH, Tamura R, Uwano T, Kobayashi T, Katsuki M, Ono T (2005) Dopamine D1 receptors involved in locomotor activity and accumbens neural responses to prediction of reward associated with place. Proc Natl Acad Sci U S A 102:2117-22.

Trottier Y, Devys D, Imbert G, Saudou F, An I, Lutz Y, Weber C, Agid Y, Hirsch EC, Mandel JL (1995) Cellular localization of the Huntington's disease protein and discrimination of the normal and mutated form. Nat Genet 10:104-10.

Trushina E, Dyer RB, Badger JD, 2nd, Ure D, Eide L, Tran DD, et al. (2004) Mutant huntingtin impairs axonal trafficking in mammalian neurons in vivo and in vitro. Mol Cell Biol 24:8195-209.

Trushina E, Singh RD, Dyer RB, Cao S, Shah VH, Parton RG, Pagano RE, Mcmurray CT (2006) Mutant huntingtin inhibits clathrin-independent endocytosis and causes accumulation of cholesterol in vitro and in vivo. Hum Mol Genet 15:3578-91.

Tsacopoulos M, Magistretti PJ (1996) Metabolic coupling between glia and neurons. J Neurosci 16:877-85.

Twelvetrees AE, Yuen EY, Arancibia-Carcamo IL, Macaskill AF, Rostaing P, Lumb MJ, Humbert S, Triller A, Saudou F, Yan Z, Kittler JT (2010) Delivery of GABAARs to synapses is mediated by HAP1-KIF5 and disrupted by mutant huntingtin. Neuron 65:53-65.

Valenza M, Carroll JB, Leoni V, Bertram LN, Bjorkhem I, Singaraja RR, Di Donato S, Lutjohann D, Hayden MR, Cattaneo E (2007a) Cholesterol biosynthesis pathway is disturbed in YAC128 mice and is modulated by huntingtin mutation. Hum Mol Genet 16:2187-98.

Valenza M, Leoni V, Karasinska JM, Petricca L, Fan J, Carroll J, Pouladi MA, Fossale E, Nguyen HP, Riess O, Macdonald M, Wellington C, Didonato S, Hayden M, Cattaneo E (2010) Cholesterol defect is marked across multiple rodent models of Huntington's disease and is manifest in astrocytes. J Neurosci 30:10844-50.

Valenza M, Rigamonti D, Goffredo D, Zuccato C, Fenu S, Jamot L, Strand A, Tarditi A, Woodman B, Racchi M, Mariotti C, Di Donato S, Corsini A, Bates G, Pruss R, Olson JM, Sipione S, Tartari M, Cattaneo E (2005) Dysfunction of the cholesterol biosynthetic pathway in Huntington's disease. J Neurosci 25:9932-9.

Valenza M, Leoni V, Tarditi A, Mariotti C, Bjorkhem I, Di Donato S, Cattaneo E (2007b) Progressive dysfunction of the cholesterol biosynthesis pathway in the R6/2 mouse model of Huntington's disease. Neurobiol Dis 28:133-42.

Van Der Burg JM, Bacos K, Wood NI, Lindqvist A, Wierup N, Woodman B, Wamsteeker JI, Smith R, Deierborg T, Kuhar MJ, Bates GP, Mulder H, Erlanson-Albertsson C, Morton AJ, Brundin P, Petersen A, Bjorkqvist M (2008) Increased metabolism in the R6/2 mouse model of Huntington's disease. Neurobiol Dis 29:41-51.

Van Raamsdonk JM, Gibson WT, Pearson J, Murphy Z, Lu G, Leavitt BR, Hayden MR (2006) Body weight is modulated by levels of full-length huntingtin. Hum Mol Genet 15:1513-23.

Van Raamsdonk JM, Pearson J, Rogers DA, Bissada N, Vogl AW, Hayden MR, Leavitt BR (2005) Loss of wild-type huntingtin influences motor dysfunction and survival in the YAC128 mouse model of Huntington disease. Hum Mol Genet 14:1379-92.

Vandeputte C, Taymans JM, Casteels C, Coun F, Ni Y, Van Laere K, Baekelandt V (2010) Automated quantitative gait analysis in animal models of movement disorders. BMC Neurosci 11:92.

Vanderklish PW, Bahr BA (2000) The pathogenic activation of calpain: a marker and mediator of cellular toxicity and disease states. Int J Exp Pathol 81:323-39.

Verbessem P, Op't Eijnde B, Swinnen SP, Vangheluwe S, Hespel P, Dom R (2002) Unimanual and bimanual voluntary movement in Huntington's disease. Exp Brain Res 147:529-37.

Von Horsten S, Schmitt I, Nguyen HP, Holzmann C, Schmidt T, Walther T, et al. (2003) Transgenic rat model of Huntington's disease. Hum Mol Genet 12:617-24.

Vonsattel JP, Difiglia M (1998) Huntington disease. J Neuropathol Exp Neurol 57:369-84.

Vonsattel JP, Myers RH, Stevens TJ, Ferrante RJ, Bird ED, Richardson EP, Jr. (1985) Neuropathological classification of Huntington's disease. J Neuropathol Exp Neurol 44:559-77.

Waelter S, Boeddrich A, Lurz R, Scherzinger E, Lueder G, Lehrach H, Wanker EE (2001a) Accumulation of mutant huntingtin fragments in aggresome-like inclusion bodies as a result of insufficient protein degradation. Mol Biol Cell 12:1393-407.

Waelter S, Scherzinger E, Hasenbank R, Nordhoff E, Lurz R, Goehler H, Gauss C, Sathasivam K, Bates GP, Lehrach H, Wanker EE (2001b) The huntingtin interacting protein HIP1 is a clathrin and alpha-adaptin-binding protein involved in receptor-mediated endocytosis. Hum Mol Genet 10:1807-17.

Wang CE, Tydlacka S, Orr AL, Yang SH, Graham RK, Hayden MR, Li S, Chan AW, Li XJ (2008) Accumulation of N-terminal mutant huntingtin in mouse and monkey models implicated as a pathogenic mechanism in Huntington's disease. Hum Mol Genet 17:2738-51.

Wang L, Lin F, Wang J, Wu J, Han R, Zhu L, Zhang G, Difiglia M, Qin Z (2012) Truncated N-terminal huntingtin fragment with expanded-polyglutamine (htt552-100Q) suppresses brain-derived neurotrophic factor transcription in astrocytes. Acta Biochim Biophys Sin (Shanghai) 44:249-58.

Warby SC, Doty CN, Graham RK, Carroll JB, Yang YZ, Singaraja RR, Overall CM, Hayden MR (2008) Activated caspase-6 and caspase-6-cleaved fragments of huntingtin specifically colocalize in the nucleus. Hum Mol Genet 17:2390-404.

Wareski P, Vaarmann A, Choubey V, Safiulina D, Liiv J, Kuum M, Kaasik A (2009) PGC-1{alpha} and PGC-1{beta} regulate mitochondrial density in neurons. J Biol Chem 284:21379-85.

Weihe E, Depboylu C, Schutz B, Schafer MK, Eiden LE (2006) Three types of tyrosine hydroxylase-positive CNS neurons distinguished by dopa decarboxylase and VMAT2 co-expression. Cell Mol Neurobiol 26:659-78.

Welch WJ, Gambetti P (1998) Chaperoning brain diseases. Nature 392:23-4.

Wellington CL, Ellerby LM, Gutekunst CA, Rogers D, Warby S, Graham RK, Loubser O, Van Raamsdonk J, Singaraja R, Yang YZ, Gafni J, Bredesen D, Hersch SM, Leavitt BR, Roy S, Nicholson DW, Hayden MR (2002) Caspase cleavage of mutant huntingtin precedes neurodegeneration in Huntington's disease. J Neurosci 22:7862-72.

Wexler NS, Young AB, Tanzi RE, Travers H, Starosta-Rubinstein S, Penney JB, Snodgrass SR, Shoulson I, Gomez F, Ramos Arroyo MA, Et Al. (1987) Homozygotes for Huntington's disease. Nature 326:194-7.

Wheeler VC, White JK, Gutekunst CA, Vrbanac V, Weaver M, Li XJ, Li SH, Yi H, Vonsattel JP, Gusella JF, Hersch S, Auerbach W, Joyner AL, Macdonald ME (2000) Long glutamine tracts cause nuclear localization of a novel form of huntingtin in medium spiny striatal neurons in HdhQ92 and HdhQ111 knock-in mice. Hum Mol Genet 9:503-13.

White JK, Auerbach W, Duyao MP, Vonsattel JP, Gusella JF, Joyner AL, Macdonald ME (1997) Huntingtin is required for neurogenesis and is not impaired by the Huntington's disease CAG expansion. Nat Genet 17:404-10.

Winkler C, Gil JM, Araujo IM, Riess O, Skripuletz T, Von Horsten S, Petersen A (2006) Normal sensitivity to excitotoxicity in a transgenic Huntington's disease rat. Brain Res Bull 69:306-10.

Wood SJ, Wypych J, Steavenson S, Louis JC, Citron M, Biere AL (1999) alpha-synuclein fibrillogenesis is nucleation-dependent. Implications for the pathogenesis of Parkinson's disease. J Biol Chem 274:19509-12.

REFERENCES

Xia J, Lee DH, Taylor J, Vandelft M, Truant R (2003) Huntingtin contains a highly conserved nuclear export signal. Hum Mol Genet 12:1393-403.

Yamada M, Iwatsubo T, Mizuno Y, Mochizuki H (2004) Overexpression of alpha-synuclein in rat substantia nigra results in loss of dopaminergic neurons, phosphorylation of alpha-synuclein and activation of caspase-9: resemblance to pathogenetic changes in Parkinson's disease. J Neurochem 91:451-61.

Yamashita K, Takahashi A, Kobayashi S, Hirata H, Mesner PW, Jr., Kaufmann SH, Yonehara S, Yamamoto K, Uchiyama T, Sasada M (1999) Caspases mediate tumor necrosis factor-alpha-induced neutrophil apoptosis and downregulation of reactive oxygen production. Blood 93:674-85.

Yang D, Wang CE, Zhao B, Li W, Ouyang Z, Liu Z, Yang H, Fan P, O'neill A, Gu W, Yi H, Li S, Lai L, Li XJ (2010) Expression of Huntington's disease protein results in apoptotic neurons in the brains of cloned transgenic pigs. Hum Mol Genet 19:3983-94.

Yang M, Lim Y, Li X, Zhong JH, Zhou XF (2011) Precursor of brain-derived neurotrophic factor (proBDNF) forms a complex with Huntingtin-associated protein-1 (HAP1) and sortilin that modulates proBDNF trafficking, degradation, and processing. J Biol Chem 286:16272-84.

Yang XW, Model P, Heintz N (1997) Homologous recombination based modification in Escherichia coli and germline transmission in transgenic mice of a bacterial artificial chromosome. Nat Biotechnol 15:859-65.

Young AB, Penney JB, Starosta-Rubinstein S, Markel DS, Berent S, Giordani B, Ehrenkaufer R, Jewett D, Hichwa R (1986) PET scan investigations of Huntington's disease: cerebral metabolic correlates of neurological features and functional decline. Ann Neurol 20:296-303.

Yu-Taeger L, Petrasch-Parwez E, Osmand AP, Redensek A, Metzger S, Clemens LE, Park L, Howland D, Calaminus C, Gu X, Pichler B, Yang XW, Riess O, Nguyen HP (2012) A Novel BACHD Transgenic Rat Exhibits Characteristic Neuropathological Features of Huntington Disease. J Neurosci 32:15426-38.

Zeitlin S, Liu JP, Chapman DL, Papaioannou VE, Efstratiadis A (1995) Increased apoptosis and early embryonic lethality in mice nullizygous for the Huntington's disease gene homologue. Nat Genet 11:155-63.

Zeron MM, Hansson O, Chen N, Wellington CL, Leavitt BR, Brundin P, Hayden MR, Raymond LA (2002) Increased sensitivity to N-methyl-D-aspartate receptor-mediated excitotoxicity in a mouse model of Huntington's disease. Neuron 33:849-60.

Zhai W, Jeong H, Cui L, Krainc D, Tjian R (2005) In vitro analysis of huntingtin-mediated transcriptional repression reveals multiple transcription factor targets. Cell 123:1241-53.

Zhang H, Li Q, Graham RK, Slow E, Hayden MR, Bezprozvanny I (2008) Full length mutant huntingtin is required for altered Ca2+ signaling and apoptosis of striatal neurons in the YAC mouse model of Huntington's disease. Neurobiol Dis 31:80-8.

Zuccato C, Tartari M, Crotti A, Goffredo D, Valenza M, Conti L, Cataudella T, Leavitt BR, Hayden MR, Timmusk T, Rigamonti D, Cattaneo E (2003) Huntingtin interacts with REST/NRSF to modulate the transcription of NRSE-controlled neuronal genes. Nat Genet 35:76-83.

Zuccato C, Ciammola A, Rigamonti D, Leavitt BR, Goffredo D, Conti L, Macdonald ME, Friedlander RM, Silani V, Hayden MR, Timmusk T, Sipione S, Cattaneo E (2001) Loss of huntingtin-mediated BDNF gene transcription in Huntington's disease. Science 293:493-8.

Zuccato C, Valenza M, Cattaneo E (2010) Molecular mechanisms and potential therapeutical targets in Huntington's disease. Physiol Rev 90:905-81.

Zuccato C, Liber D, Ramos C, Tarditi A, Rigamonti D, Tartari M, Valenza M, Cattaneo E (2005) Progressive loss of BDNF in a mouse model of Huntington's disease and rescue by BDNF delivery. Pharmacol Res 52:133-9.

Zuhlke C, Riess O, Schroder K, Siedlaczck I, Epplen JT, Engel W, Thies U (1993) Expansion of the (CAG)n repeat causing Huntington's disease in 352 patients of German origin. Hum Mol Genet 2:1467-9.